Matrix Cracking and Stress/Strain Behaviour of Continuous Fibre Ceramic Composite Laminates

A. W. Pryce

Submitted for the Degree of Doctor of Philosophy

September 1991

SUMMARY

Matrix damage and its effects on mechanical properties have been examined for SiC (Nicalon[1]) fibre reinforced glass and glass ceramic matrix composites under quasi-static and fatigue loading conditions.

Nicalon/Pyrex laminates of different lay-ups have been tested under quasi-static tension. The elastic moduli have been measured and matrix damage monitored as a function of applied strain. The mechanical properties are strongly influenced by the presence of crystalline regions in the matrix which promote microcracking. Laminated plate theory is used to provide bounds to the moduli of the laminates.

For unidirectional and simple crossply Nicalon/CAS[2] laminates the quasi-static stress/strain behaviour and associated matrix damage accumulation have been examined in detail. The damage development with applied stress was quantified by counts of crack density (in both longitudinal and transverse plies), stiffness loss and cumulative residual strain. The quasi-static stress/strain behaviour during continuous tests (accumulating damage) and discontinuous tests (constant damage) have been modelled using a stress analysis based on Aveston, Cooper and Kelly (ACK) theory. The continuous stress/strain behaviour of (0/90) crossply laminates has been modelled using a shear-lag analysis developed previously to describe the transverse ply cracking behaviour of polymer matrix composites. The analysis is modified to account for longitudinal ply cracking.

Matrix damage development in unidirectional and (0/90) crossply laminates under quasi-static cycling and high frequency fatigue loading have been studied. For unidirectional laminates stable stress/strain hysteresis loops were obtained during quasi-static cycling, corresponding to stable matrix damage states. These and similar loops obtained after high frequency fatigue are modelled using the discontinuous stress/strain analysis. It is suggested that the effect of high frequency fatigue is to decrease the interfacial shear strength.

---

[1] Trade mark of the Nippon Carbon Company

[2] calcium alumino-silicate

ACKNOWLEDGEMENTS

Important contributions have been made by a number of individuals and institutions during the course of this work. The author would like to acknowledge these efforts.

First and foremost I would like to express profound gratitude to my supervisor Dr Paul Smith. Paul's energy, enthusiasm and commitment have been invaluable. Also, I would like to acknowledge Rolls-Royce plc for their financial support and provision of all materials. Special thanks are due to Ms Clara Davies (Rolls-Royce, Bristol) and Dr David Clarke (Rolls-Royce, Derby) and, Dr Lynn Boniface, Dr Julie Yeomans and Dr Steve Ogin (Department of Materials Science and Engineering) for their advice during many helpful disscussions.

The past three years have been made extremely enjoyable due to my many friends and colleagues within the M.S.E. Department and the University as a whole. Help and support have come from many quarters, but, I would particularly like to thank all the members of the Composites Group and the technical and secretarial support staff.

Finally, on a more personal level, a special mention is required for Mark Leaity, Lynn Boniface and Birgir Johannesson for their (a) humour, yes, composites can be fun as well as useful, (b) patience, particularly with my spelling and (c) timely suggestions to quit testing and come for a drink!

For their love and support this thesis is dedicated to my Mother, Father, Sister and Brother-in-law and particularly Katie, who, for three long years, has put up with so much.

CONTENTS

NOTATION

a	flaw radius
A	cross-sectional area
a^*	critical flaw size
b	longitudinal ply thickness
$2d$	transverse ply thickness
e	eccentricity
E	reduced composite modulus
E_1	uncracked longitudinal ply modulus
E_1'	reduced longitudinal ply modulus
E_2	uncracked transverse ply modulus
E_0	uncracked composite modulus
E_0'	reduced composite modulus
E_f	fibre modulus
E_m	matrix modulus
G	strain energy release rate
G_{Ic}	ply toughness
G_{12}	in plane shear modulus
G_{23}	through thickness shear modulus of a transverse ply
I	second moment of area
K	stress intensity factor
K_{Ic}	ply fracture toughness
M	bending moment
P	applied load
r	fibre radius
$2s$	crack spacing
$2s_i$	crack spacing at σ_i
$2\bar{s}_i$	average crack spacing for the ith stress increment
$2\bar{s}_{1(i)}$	average longitudinal ply crack spacing for the ith stress increment
$2\bar{s}_{2(i)}$	average transverse ply crack spacing for the ith stress increment
$2s_f$	saturation crack spacing
x	distance from crack plane
x'	stress transfer length
x'^T	thermal stress transfer length
y	distance from specimen face to neutral axis
V_f	fibre volume fraction
V_m	matrix volume fraction
V_{f0}	volume fraction of 0° plies
α_1	lamina thermal expansion coefficient (parallel to the 0° fibres)
α_2	lamina thermal expansion coefficient (perpendicular to the 0° fibres)
α_f	fibre thermal expansion coefficient
α_m	matrix thermal expansion coefficient
$\bar{\epsilon}$	increase in measured composite strain
$\bar{\epsilon}_f$	mean fibre strain
$d\bar{\epsilon}$	incremental composite strain (constant damage)

$\bar{\epsilon}_{c_T}$	mean composite strain
$\bar{\epsilon}_{f_T}$	mean initial thermal strain in the fibres
ϵ_{u*}	laminate strain to failure
ϵ_{el}	matrix cracking / first ply failure strain
ϵ_{fpf}	first ply failure strain
ϵ_{mu}	matrix failure strain
γ	fracture surface energy of a transverse ply
γ_m	fracture surface energy of the matrix
2Δ	length of exposed fibres
$\Delta\bar{\epsilon}$	incremental strain (change in crack spacing)
$\Delta\bar{\epsilon}_{1(i)}$	incremental strain (change in longitudinal ply crack spacing)
$\Delta\bar{\epsilon}_{2(i)}$	incremental strain (change in transverse ply crack spacing)
ΔT	temperature change
λ	shear-lag parameter
ν_{12}	principal Poisson's ratio
σ	intermediate applied stress
σ'	applied stress for further cracking
σ_c	applied stress
σ_{f_T}	fibre stress
σ_{f_T}	initial thermal stress in the fibres
σ_i	ith increment stress
$d\sigma_c$	stress increment
$\bar{\sigma}_i$	average stress for the ith increment
σ_{u*}	laminate tensile strength
σ_{el}	matrix cracking / first ply failure strength
σ_{mu}	matrix failure strength
σ_1	longitudinal ply stress
$\bar{\sigma}_1$	mean longitudinal ply stress
σ_{2_T}	transverse ply stress
σ_{2_T}	initial thermal stress in a transverse ply
σ_{2u}	transverse ply failure strength
τ	fibre/matrix interfacial shear strength

CHAPTER 1

INTRODUCTION

Although monolithic engineering ceramics possess good wear, corrosion and high temperature resistance concern about their low fracture toughness has severely limited their application. Since the late 1960's efforts have been made to improve the structural reliability of ceramic materials by the provision of a second discontinuous phase to modify crack growth behaviour. These "toughened ceramics" derive their enhanced toughness from a number of mechanisms. Transformation toughening is one such mechanism, where energy is absorbed ahead of an advancing crack via a stress induced transformation to a new crystal structure (e.g. Porter and Heuer 1979). Alternatively, a second phase such as ductile metal particles or ceramic whiskers, platelets or fibres can be incorporated into a ceramic to produce a ceramic matrix composite (CMC). In contrast to transformation toughening, CMCs derive their improved toughness by branching and deflecting advancing cracks. The reinforcing elements are also able to bridge the crack behind the crack tip.

Particulate and whisker reinforced ceramics are considerably tougher than their monolithic counterparts, typically achieving fracture toughness increases of between 200 and 400% (Evans 1990). As a result, today, they are used in applications ranging from cutting tools to processing dies. However, they are still too brittle and variable to be used in structural applications. When the fracture strength is reached, the stored elastic energy is far in excess of that required to fracture the material and thus failure is catastrophic. By reinforcing ceramic matrices with continuous fibres, materials can be produced which exhibit a controlled fracture, some pseudo-plasticity and an increased strain to failure (Davidge 1987).

There is currently a great deal of interest in producing practical continuous fibre reinforced ceramic matrix composites. The driving force of this development is principally by the aerospace and military industries. To quote an example, the British aero engine manufacturer, Rolls-Royce, is undertaking a major programme to investigate new technologies to meet the needs of expected engine developments over the next fifteen years. Their projected use of CMCs as a weight percentage in future engines is shown in Figure 1.1 and illustrates the huge potential for this group of materials. There will also be other applications for less sophisticated components requiring a resistance

to chemical attack, wear and thermal shock.

In order for the potential of ceramic composite materials as a structural engineering material to be exploited fully a broad and detailed understanding is required of their mechanical behaviour under a variety of loading conditions. This can only be achieved by intensive study on a scale which has been/is being conducted for polymer matrix composites. Over the past decade research activity in ceramic composites has accelerated to meet these needs. However, there is still a great deal of work to be done in order to generate a comprehensive data base for and develop a better understanding of these materials before engineers can maximise component performance through innovative design.

One particular area of interest, which is far less advanced than for polymer matrix composites, is the understanding of the development of damage and its effect on mechanical properties. A particular concern with ceramic composites is matrix cracking. In unidirectional ceramic composites, because the failure strain of the fibres is greater than that of the matrix, an array of cracks which span the entire composite cross-section is seen under loading. The damage patterns in ceramic composites of realistic lay-ups are likely to be very complicated. For polymer matrix composites of simple, crossply $(0/90)_s$ construction it is well known (e.g. Reifsnider and Stinchcomb 1986) that damage occurs by multiple cracking of the 90° ply with the cracks spanning the both the width and thickness of the ply.

In the present work the matrix cracking behaviour of unidirectional and simple crossply continuous fibre reinforced glass and glass ceramic matrix laminates is investigated with the aim of developing models to describe their stress/strain behaviour.

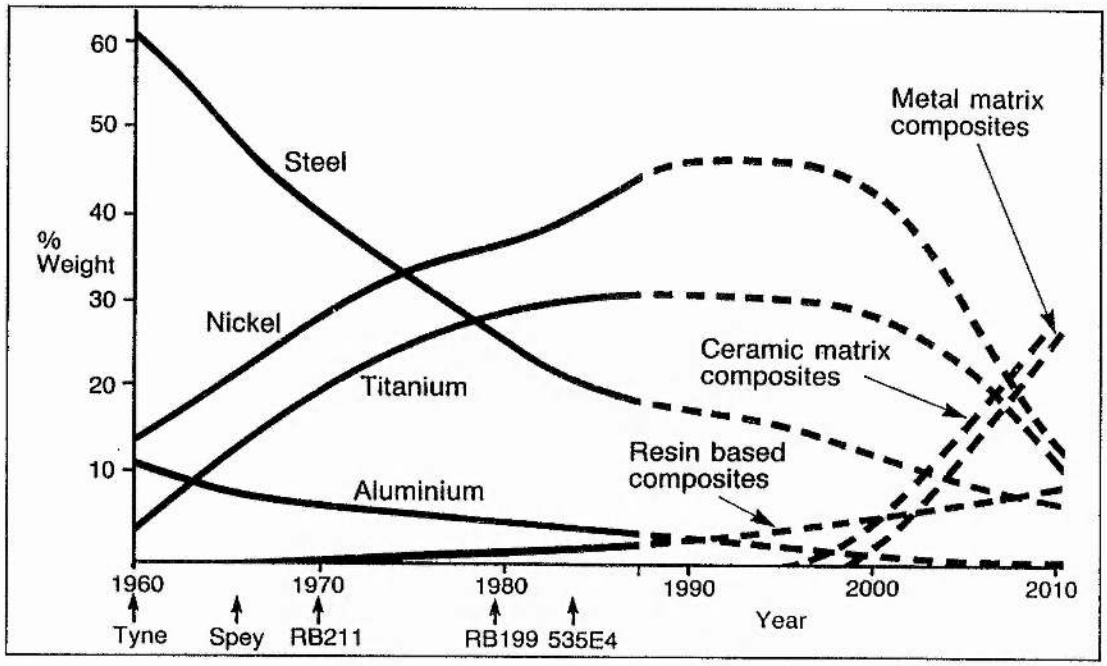

Figure 1.1 Predicted trends in materials usage in jet engines (taken from Jeal 1988).

CHAPTER 2

LITERATURE REVIEW

2.1 INTRODUCTION

Factors that control the mechanical properties of CMCs are many and varied. Such factors include the compatibility of fibre and matrix, processing route and control over the fibre/matrix interface. In the first section of this review the development of the CMCs used in this study is considered. The aim is to show briefly how they have evolved and how, by addressing each factor, optimum properties have been achieved.

The mechanical properties and accumulation of matrix damage under quasi-static loading of Nicalon reinforced glass and glass ceramics are then considered. The limited amount of literature reflects that the area is still very much in its infancy. However, the studies available refer both to unidirectional and crossply laminates.

The fatigue behaviour of monolithic and fibre reinforced ceramics is considered in the following section. The review of monolithic ceramics is by no means comprehensive, the present study is concerned solely with fibre reinforced composite materials. The aim is to present fatigue crack growth mechanisms previously identified in studies of polycrystalline ceramics which may be applicable to ceramic composite laminates. The limited amount of work on the fatigue behaviour of fibre reinforced glass and glass ceramics is then reviewed.

Following literature concerning experimental studies, existing models which predict mechanical property and matrix cracking behaviour are examined. Models concerning brittle matrix unidirectional laminates are considered first. In a later section, those describing the behaviour of crossply laminates are reviewed. In the case of crossply laminates the relevance of models developed previously for resin matrix composites to their CMC counterparts is discussed.

2.2 THE DEVELOPMENT OF FIBRE REINFORCED CMCs

Early studies of fibre reinforced CMCs concentrated on the characterisation of graphite fibre reinforced glass and glass ceramic matrix composites. They dealt with laminate fabrication by hot pressing mixtures of fibre and ceramic powder (e.g. Sambell et al 1972a) or hot pressing pre-preg[3] of fibres and ceramic powder (e.g. Sambell et al 1972b and Levitt 1973). Mechanical properties are discussed in terms of material variables such as fibre volume fraction, fibre orientation and matrix failure strain and also processing variables such as damage during fabrication, matrix porosity and the effect on interface properties (e.g. Phillips et al 1972). The majority of this work was limited to carbon fibre reinforced systems due to the non availability of other suitable fibres.

Little published work concerning CMCs exists from the mid seventies up until the use of alternative reinforcement such as alumina fibres (Bacon and Prewo 1978) in glass and glass ceramic matrices. A resurgence in interest in CMCs was brought about by the commercial availability of a cost-effective SiC fibre produced via a polymer precursor (Yajima et al 1976), reviewed recently by Okamura (1987). Prewo and Brennan (1980) examined the properties of unidirectional laminates of borosilicate glass (Pyrex) reinforced with CVD SiC monofilaments and the new Nicalon SiC fibre in the form of yarn. From a series of flexure tests conducted from room temperature up to 700°C, they concluded that SiC/Pyrex composites in both forms display flexure strengths equivalent to those of graphite/glass composites, with enhanced environmental stability. Further, more detailed studies by Thompson and Prewo (1980) and Prewo and Brennan (1982) have shown that Nicalon/Pyrex and Nicalon/lithium aluminosilicate (LAS) glass ceramic composites display low isotropic thermal expansion coefficients, high strength and stiffness and have a maximum operating temperature of 1100°C which is limited only by the softening point of the matrix. The development of Nicalon reinforced LAS composites is noteworthy for two reasons. Firstly, the thermal expansion mismatch

[3] pre-preg refers to a tape of fibres pre-impregnated with ceramic powder and an organic binder

between Nicalon/LAS is far less than that of graphite/LAS. Consequently, the tendency for thermal cracking of the matrix during laminate processing is reduced. Secondly, oxide glass ceramic matrices of this type may be used in the amorphous state during composite manufacture. This reduces the amount of damage to fibres due to the low viscosity of the glass. After fabrication, the composite may be heat-treated (ceramed) in order to crystallise the matrix and so to achieve high temperature stability (Brennan and Prewo 1982).

Control of the fibre/matrix interface is vital in order to obtain the desired mechanical properties of CMCs. This area is reviewed extensively by Kerans et al (1989) and Kerans and Parthasarathy (1991). Studies using Nicalon reinforced LAS composites (Mah et al 1985b, Prewo 1986) have shown that the fracture behaviour is dependent on both temperature and atmosphere. Brittle failures at temperatures above 1000°C in air were shown to correspond to the removal of a carbon-rich layer associated with the interface. This layer is formed by the degradation of the Nicalon fibres during composite processing. Recently it has been shown that this reaction involves the replacement of carbon by an amorphous silica layer (Bischoff et al 1989) which serves to strengthen the fibre/matrix bond, so adversely affecting material fracture toughness (Thouless et al 1989).

Today the properties of ceramic matrix composites are much better understood in terms of the constituent fibre and matrix properties and the nature of the fibre/matrix interface. In a recent review paper by Evans (1990) the toughness of fibre reinforced ceramic composites is discussed. Optimum toughness is achieved by having a small mismatch in fibre and matrix thermal expansion coefficients to minimise internal stresses. A small interfacial shear strength is also desirable which governs the debonding and frictional sliding events at the fibre/matrix interface and hence fibre pullout behaviour.

2.3 QUASI-STATIC BEHAVIOUR OF FIBRE REINFORCED GLASS AND GLASS CERAMIC COMPOSITE LAMINATES

2.3.1 Unidirectional laminates

Much of the published work concerning Nicalon reinforced glass and glass ceramics, such as the assessment of thermal stability and stress-strain response, has been carried out under flexural loading conditions. This testing method has limitations. Prewo and Brennan (1982) have noted that the viscoelastic deformation of the matrix above its softening temperature invalidates such measurements in this range. In addition, sub-critical damage in the form of matrix cracking during room temperature testing (e.g. Ford et al 1985, Seerat un Nabi and Derby 1988) makes the use of simple beam theory unsuitable for property studies above the matrix cracking strain. A recent study by Davidge and Briggs (1989) has shown that the flexure strength is overestimated (compared to uniaxial measurements) due to movement of the specimen neutral axis (used in the calculation) towards the compressive face. As a result of these limitations, better measurements of stiffness and strength are obtained from parallel sided specimens tested under uniaxial tension. Although these tests are more difficult to perform (due to difficulties associated with specimen gripping and alignment), the results are more straightforward to interpret.

Very few published data exist concerning the tensile mechanical properties and development of damage (principally matrix cracking) of Nicalon reinforced glass and glass ceramic composites. The data that are available show that in recent years the refinement of laminate processing has resulted in the improvement of material properties (e.g. Dawson et al 1987). However, problems associated with laminate processing are still apparent. This has been illustrated by the studies by Murty and Lewis (1989) and Bleay and Scott (1991). They show that for certain processing temperatures and times matrix crystallisation can occur in Nicalon/Pyrex laminates. The thermal expansion mismatch between the crystalline phase and the parent glass results in a heavily microcracked laminate. In the same work Bleay and Scott have studied the fibre/matrix interface of

laminates containing cristobalite associated damage. They explain the measured trends in fibre/matrix interfacial shear strength with interface condition in terms of the diffusion of atomic species and corresponding phase formation at the interface. The fracture behaviour of these laminates is found to be influenced strongly by cristobalite associated damage. However Shin and Knowles (1990) claim that matrix crystallisation does not affect mechanical properties measured in flexure. This needs to be examined carefully. Consideration of the rule of mixtures alone would suggest degraded laminate stiffness properties.

Current optimised mechanical properties are presented in Table 2.1 for Nicalon/Pyrex (Davidge and Briggs 1989) and Nicalon/LAS (Prewo 1986) unidirectional composites. Two studies have examined the stress/strain behaviour of Nicalon/LAS unidirectional laminates under quasi static loading conditions (Mah et al 1985a and Prewo 1986). Both show the existence of a proportional limit. Scanning electron microscopy analysis (Mah et al 1985a) indicates this to be the onset of matrix cracking. A matrix crack spans the entire width and thickness of the coupon and is bridged by fibres. Further matrix cracking occurs with increasing applied load (multiple fracture). Associated with continued cracking is a second linear region on the stress strain curve, the slope of which is less than that of the initial elastic region. By repeatedly loading specimens to progressively higher loads above the observed knee, the longitudinal modulus is seen to decrease. Prewo (1986) has inferred that this is due to continued matrix cracking. Mah and co-workers also identify a third linear region on the stress-strain curve, which, they suggest corresponds to the extension of the fibres alone. They also measure the average crack spacing observed at specimen failure and use this in a model for multiple fracture (see Section 2.5.2) in order to calculate the fibre/matrix shear strength, τ. A similar calculation is made by Ford et al (1985) using the average crack spacing observed on the tensile face of flexure test specimens of Nicalon/Pyrex at failure. The discrepancy between the two values (7 MPa from Mah et al and 27-39 MPa from Ford et al) is perhaps a consequence of the misapplication of simple beam theory.

It has already been indicated that the control of the fibre/matrix interface has a fundamental effect on overall composite properties. Consequently a reliable

experimental technique to measure τ and hence to quantify interfacial behaviour is extremely desirable. A method developed by Marshall (1984) involves the in situ nano-indentation of fibres parallel to their axis and recording the fibre load/displacement behaviour. Several studies employing this method suggest that τ lies in the range 2-10 MPa for Nicalon reinforced glass and glass ceramics (Marshall and Oliver 1987, Kerans and Parthasarathy 1991 and Bleay and Scott 1991). However, Marshall and co-worker do identify limitations to the technique. These are discussed in Chapter 6.

2.3.2 Crossply laminates

So far there have been fewer studies of crossply laminates than of unidirectional laminates. However, the published property data available are shown in Table 2.2. Although comparisons are difficult due to the varying matrix type and condition, some of the data show relatively high moduli compared to those of unidirectional laminates. This suggests that the 90° plies in glass and glass ceramic matrix composites make a significant contribution to overall laminate stiffness properties unlike fibre reinforced resin matrix composites of the same lay-up which are fibre dominated. Studies on $(0/90)_s$ (Sbaizero and Evans 1986), $(0/90)_{2s}$ (Seerat un Nabi and Derby 1988) and $[0(0/90)_2]_s$ laminates (Prewo et al 1989) indicate the existence of two discontinuities in the stress/strain curve. The latter two studies show that the first of these discontinuities occurs at an applied stress of between 25 and 40 MPa and marks the onset of transverse ply cracking where cracks run perpendicular to the applied load, spanning the width and thickness of the 90° ply. Transverse ply cracking of this type has been well documented for resin matrix composites (see Section 2.6). Prewo and co-workers have suggested that the second, more pronounced knee which occurs at an applied stress of about 60 MPa, corresponds to matrix cracking events in 0° plies. However, Sbaizero and co-worker observe the first 90° ply cracks to form at this higher load level (see Table 2.2). These cracks run parallel to the loading direction adjacent to the ply interfaces (delamination cracks). They also report that transverse ply cracking (where cracks run perpendicular to the loading direction) occurs above the second knee at an applied stress of > 130 MPa. Some of these cracks run across several plies. Clearly further work is necessary

to resolve these discrepancies.

It has been reported that the repeated loading of crossply specimens to the first knee leads to a degradation of longitudinal modulus (Seerat un Nabi and Derby 1988). This is a result of continued matrix cracking in the 90° plies. In separate tests the average crack spacing has been measured as a function of applied load (Seerat un Nabi and Derby 1988) and surprisingly follow the trends of a simple progressive cracking model originally developed for resin matrix composites (see Section 2.6).

2.4 FATIGUE BEHAVIOUR OF MONOLITHIC AND FIBRE REINFORCED CERAMICS

2.4.1 Fatigue behaviour of monolithic ceramics

Monolithic ceramics which possess isotropic properties exhibit very limited plasticity at room temperature (McMillan 1979). For this reason fatigue crack growth does not occur by mechanisms involving extensive crack tip plasticity such as those seen in metals due to dislocation movement and in polymers due to viscoelastic effects (e.g. Hertzberg 1989). The experimental observation of fatigue crack growth in polycrystalline ceramics has frequently been reported for a number of years (e.g. Krohn and Hasselman 1972, Evans 1980 and Horibe and Hirahara 1991). A number of mechanisms have been proposed to explain the observed behaviour. Such mechanisms are based either on static fatigue (environmentally assisted cracking) or on the non-reversibility of strain at a crack tip during stress cycling These are discussed briefly below.

Static fatigue effects in monolithic ceramics have been well documented under quasi-static loading (e.g. McMillan 1979) and in particular for glass materials in humid atmospheres (e.g. Wiederhorn et al 1982). In this particular case Si-O bonds at the crack tip are broken by the combined effects of the stress field around the crack tip and the chemical environment. As a result a crack may grow at an applied stress at which it would otherwise (in the absence of an aggressive environment) remain stable. It has reported that the few observations of fatigue crack growth during stress cycling can be explained in terms of static fatigue (e.g. Evans 1980). This is because the amplitude of a cyclic stress has a mean constant value which is analogous to a constant static load. However, findings published within the last couple of years suggest that other mechanisms may also be active.

Recently a number of workers have presented evidence that fatigue crack growth occurs in polycrystalline ceramics in a way that cannot be explained by static fatigue alone. These include studies on silicon carbide, silicon nitride and sialons (Horibe and

Hirahara 1991), alumina (Guiu et al 1991, Reece et al 1989 and Ewart and Suresh 1987) and transformation toughened zirconia (Guiu et al 1991). The fatigue crack growth mechanisms proposed under cyclic tensile loads are based on the non-reversibility of crack tip strains. Horibe and co-worker consider the crack branching and crack deflection which can occur on the loading half of a fatigue cycle. On the unloading half of the cycle, asperity/asperity contacts may cause the crack faces to become "wedged" apart. Crack faces may also become wedged apart by the relaxation of residual stresses (Evans 1980) or by fracture debris caused by grain crushing or grain pullout (Reece et al 1989).

2.4.2 Fatigue behaviour of fibre reinforced glass and glass ceramics

At the present time it is unclear whether the fatigue crack growth mechanisms discussed briefly in the previous section are applicable to fibre reinforced ceramics. This is because there is at present very little published work on this subject. However, studies concerning quasi-static tensile behaviour have already identified matrix cracking and the non-planar form of cracks as they circumvent fibres (e.g. Mah et al 1985a) giving rise to irregular crack surfaces. In addition the thermal expansion mismatch between the fibres and matrix will give rise, after laminate processing, to thermal stresses. It is possible therefore, that mechanisms exist for ceramic composites such as those reviewed by Evans (1990) under quasi-static loading conditions, which give rise to non-reversibility of strain at a crack tip under cyclic loading.

The work published so far on stress cycling of fibre reinforced brittle matrix composites includes flexural fatigue (Prewo 1987), tension/tension fatigue (Prewo 1987) and a study which discusses a possible mechanism giving rise to fatigue damage to fibres during stress cycling (Lewis 1983). Prewo (1987) has conducted fatigue tests on unidirectional Nicalon reinforced LASI and LASII matrix laminates. The two materials display contrasting behaviour under quasi-static loading. The Nicalon/LASI laminates exhibit a linear stress/strain curve to failure, while the Nicalon/LASII material exhibits very non-linear behaviour as a result of extensive matrix cracking prior to failure. Tension/tension

fatigue tests were carried out at room temperature for both materials. Testing was interrupted after 10^3, 10^4 and 10^5 cycles in order to monitor the change in elastic modulus. For a range of maximum stresses below the static laminate fracture stress the Nicalon/LASI specimens displayed no loss in stiffness or residual strength (compared to unfatigued specimens) suggesting that no fatigue damage was being incurred. A similar response was observed for the Nicalon/LASII laminates fatigued at a maximum stress below the static matrix cracking stress.

Nicalon/LASII specimens fatigued at a maximum stress above the static cracking threshold displayed a marked reduction in elastic modulus. The stress/strain loops obtained during fatigue testing narrowed progressively with continued cycling indicative of a reduced hysteresis during unloading and reloading. In addition, the loops showed that below a stress of ~120 MPa (the static matrix cracking stress was ~270 MPa) the measured composite moduli were equal to the original (unfatigued) value. Above this stress the measured moduli progressively decreased with cycling. Prewo attributes the latter observation to a crack closure effect (perhaps of the type discussed in Section 2.4.1). However no mechanistic explanation is offered for the narrowing of the stress/strain loops.

In the same study Prewo reports that the residual laminate strength remains constant after fatigue and equal to the quasi-static value. This behaviour is similar to that of Nicalon/LASII laminates tested in flexure (Prewo 1987) suggesting that no fatigue damage to fibres occurs. However, Minford et al (1985) report a significant decrease in laminate residual strength after fatigue for unidirectional Nicalon/LASII and Nicalon/LASIII laminates tested in flexure and tension/tension fatigue. In the same work they report little or no effect on laminate residual strength for (0/90) crossply laminates. These results do not necessarily contradict each other as a wider range of maximum applied stress is used by Minford and co-worker.

These studies indicate that in order to characterise fully the fatigue behaviour of unidirectional and crossply laminates an investigation is required of laminate mechanical property behaviour together with a microstructural examination of fatigue damage.

2.5 PREDICTIVE MODELS FOR MATRIX CRACKING IN UNIDIRECTIONAL LAMINATES

2.5.1 Introduction

It is well established that one of the important parameters controlling the mechanical properties of ceramic matrix composites is the nature of the bond between fibre and matrix (Kerans et al 1989). Models based on the elastic "shear lag" approach (first described by Aveston and Kelly 1973) are only applicable to well bonded systems. These models are not relevant here and therefore will not be reviewed. Predictive models which are applicable to unidirectional CMC systems are ones in which a weak fibre/matrix bond is considered. In an earlier study, Aveston et al (1971) developed an approach using experimental data from model composites such as glass reinforced plaster. Although these systems have little practical importance, the Aveston, Cooper and Kelly (ACK) model for "multiple fracture" is directly applicable to today's engineering CMCs.

2.5.2 The Aveston, Cooper and Kelly model for multiple fracture

The ACK analysis considers a unidirectional continuous fibre reinforced composite under uniaxial tension. The basic assumptions used during the analysis are that the fibre and matrix have well defined failure strains (and stresses) and that there is no interaction between fibre and matrix elastic displacements in the vicinity of a crack, hence the fibre and matrix will sustain a purely frictional shear stress which remains constant. The main results are discussed in the following three paragraphs.

When the composite is loaded, a crack will form in the matrix if the matrix failure strain is less than that of the fibres and provided there is a sufficiently high volume fraction of fibres to withstand the additional load thrown onto them. The source of the crack and the mechanism of crack growth are not considered; it is assumed that the crack spans the

entire cross section instantaneously. Once a crack forms the matrix adjacent to the crack is relieved of stress and thus cannot crack. However, as a result of the constant interfacial shear stress acting between the fibres and matrix, the stress in the matrix increases linearly with distance away from the crack plane (see Figure 2.1). At a distance x' from the crack the matrix failure strain is again reached. Consequently, cracking continues with no further increase in applied load until there are approximately uniform cracks spanning the width and thickness of the specimen that are spaced between x' and $2x'$ apart, where x' is given by

$$x' = \frac{V_m}{V_f}\left(\frac{\sigma_{mu} r}{2\tau}\right) \qquad (2.1)$$

Aveston and co-workers calculate the strain at which the initial crack forms using a thermodynamic approach in the form of an energy balance. The following terms contribute to the work of fracture matrix crack surface energy, interface debonding energy, frictional work as fibres slide over the matrix (after debonding) and the increase in strain energy of fibres due to load shedding. The energy supplied to the system which balances the work of fracture comprises of; the work done by the externally applied load as the composite extends and the decrease in matrix strain energy over a distance x' either side of the crack. Equating the energy terms leads to an expression for the matrix failure strain

$$\varepsilon_{mu} = \left(\frac{12\tau\gamma_m E_f V_f^2}{E_1 E_m^2 r V_m}\right)^{\frac{1}{3}} \qquad (2.2)$$

It is evident from equation 2.2 that the matrix failure strain can be increased when the fibre diameter is decreased for a constant fibre volume fraction. Cooper and Sillwood (1972) investigated this subsequently and showed that matrix cracking could be suppressed in composites containing very small diameter fibres. Aveston and co-workers suggest that although smaller diameter fibres act as a constraint to matrix cracking, maintaining a constant fibre volume fraction is essential. This is because the additional load which the fibres can withstand after the initial cracking event decreases with

decreasing fibre radius. If the fibre volume fraction is not maintained the material may appear more brittle.

One important feature of the ACK analysis is that stress/strain behaviour for a unidirectional laminate can be evaluated (Figure 2.2a). However, such a curve is only valid for a matrix possessing a single valued strength. When the matrix has a strength distribution they suggest in a qualitative way that the form of the curve will change due to matrix cracking occurring over a range of applied load (Figure 2.2b). Cracking then continues over this range until the matrix takes no further share of the load and fibres slip through the blocks of matrix. The modulus of the laminate when matrix cracking is complete (ignoring any other damage, notably fibre breakage) is given by $E_f V_f$.

In recent years there have been attempts to consider the mechanics and mechanisms of matrix cracking in more detail (Marshall et al 1985, Budiansky et al 1986 and McCartney 1987). These studies have addressed the shortfalls of ACK theory: Firstly, the cracking strengths of glasses and glass ceramics do not have unique values but are sensitive to a distribution of constituent flaws. Secondly, the ACK energy balance only considers the energy change of the system before and after cracking. No consideration is given to the mechanism of crack growth. Budiansky and co-workers develop ACK theory by considering a general class of matrix fractures which vary according to the strength of the fibre/matrix bond. The case where no bond exists is examined (i.e. frictional slippage of fibres) and a fracture mechanics criterion for crack propagation applied. However, many simplifying assumptions are made during their analysis which predicts an incorrect value of zero for the matrix cracking stress when the fibre volume fraction tends to zero. A more consistent method has been developed by the use of continuum models.

2.5.3 Continuum models

Continuum models first proposed by Marshall et al (1985) and developed recently by McCartney (1987) are based on deriving the stress intensity factor for a unidirectional fibre reinforced brittle matrix composite containing "long" and "short" cracks. Long

cracks in these analyses are considered to be greater than a few fibre diameters. Both studies consider first a discrete fibre model as shown in Figure 2.3, where a matrix crack is bridged by fibres which exert tractions on the crack surfaces. By examining the relative displacements of fibres and matrix, the crack opening displacement for a given traction may be determined. A continuum model is then introduced by assuming that the effective traction distribution over the crack surfaces is a smooth, continuous function. This enables an expression to be written for the crack opening displacement distribution over the crack surfaces. The composite (net) stress intensity factor can then be defined. The criterion used for crack propagation is that the composite stress intensity factor equals the fracture toughness ($K = K_{1c}$). Marshall et al assume that the matrix and composite fracture toughnesses scale with stresses in the ratio E_m:E_c. McCartney modifies this relation for plane strain conditions and to account for the changes in stored and frictional energy associated with crack growth.

The analysis of the growth of long cracks is addressed in both works. Marshall and co-workers use a "steady state crack" geometry in order to derive the matrix cracking stress. They show that in the steady state region of the crack (where equilibrium crack opening displacement is obtained) the stress intensity factor is independent of crack length. An energy balance based on ACK theory is performed on their continuum model to produce an expression for the matrix cracking stress. Although the two expressions are similar, the energy balance is too approximate to show the equivalence of their fracture mechanics approach and ACK theory.

McCartney (1987) considers first the discrete fibre model in order to establish the energy changes during fibre/matrix debonding. This takes the form of an extended ACK treatment and results in an identical expression for the matrix cracking strain corrected for plane strain conditions. An energy balance similar to that used by Marshall et al is then performed on the continuum model which accounts for the tractions exerted by the bridging fibres. By setting the two results (modified ACK and continuum energy balance) equal, a different boundary condition for the stress intensity factor approach is defined. The crack geometry used in the McCartney continuum model is shown in Figure 2.4. Regions 1 and 3 have uniform stress and strain fields, unlike region 2 which contains the

crack tip. The matrix cracking stress and strain are obtained using a similar derivation to that used by Marshall and co-workers but with the corrected boundary condition. McCartney's results indicate that for growth of long cracks, the stress intensity factor approach is equivalent to ACK theory corrected for plane strain conditions. This is illustrated in Figure 2.5 where the normalised matrix cracking stress tends to a constant value at long crack lengths.

The analysis of the growth of short cracks by Marshall et al (1985) is hindered by the fact that the expression for the crack opening displacement distribution could not be solved analytically. To overcome this they approximate the crack to a simple mode I crack growing in a semi-infinite plate. By applying their steady state crack boundary condition, the analysis shows a dependence of matrix cracking stress on the length of pre-existing crack (data points in Figure 2.5). McCartney is able to maintain closed form expressions for short cracks by interchanging the crack opening displacement function with a single integral over a fixed range. As a result his continuum model gives a more rigorous dependency (solid line in Figure 2.5). The curve obtained by McCartney is important in two respects. Firstly it is independent of material properties and is therefore applicable to any composite system (where $\epsilon_f > \epsilon_m$). Secondly, the curve is a smooth single valued function. This means that when a crack propagates it will do so until the matrix has completely failed, so long as the applied stress is maintained. As a result stable crack growth is not possible (McCartney 1987).

The main feature of the curve (and to a lesser extent the data points of Marshall et al) is the presence of a threshold level of stress below which matrix cracking is impossible. The threshold corresponds to the stress derived from a pure energetics argument (i.e. ACK theory). It follows, that any applied stress below this level will not result in crack growth as the Griffith failure criterion is not obeyed (McCartney 1987). However, the threshold will vary for a laminate containing a non regular array of fibres as the crack may be blunted in areas of dense fibre packing. In terms of flaw size the threshold corresponds to a pre-existing crack length of a few fibre diameters for Nicalon reinforced LAS. This is of great importance as the inclusion of larger flaws (e.g. during processing) will not significantly decrease the static matrix cracking stress (Marshall et al 1985). For

smaller crack lengths it is evident that although the energy supplied to the system is sufficient to cause matrix cracking, a further increase in applied stress is required before the crack tip stresses are sufficient to propagate the crack (ie $K = K_{1c}$).

2.6 PREDICTIVE MODELS FOR TRANSVERSE PLY CRACKING IN CROSSPLY LAMINATES

2.6.1 Introduction

When a crossply polymer matrix composite (PMC) laminate is loaded under quasi-static or fatigue loading conditions, the first damage to be sustained is cracking of the matrix in the transverse ply (e.g. Hahn and Tsai 1974). The cracks run parallel to the transverse fibres and span the entire width and thickness of the ply. Figure 2.6 shows the configuration of a transverse ply crack and its reference coordinate system. "Sub-critical" damage of this type occurs at lower strains than "critical" longitudinal ply damage (fibre breakage) which leads eventually to laminate failure (Reifsnider et al 1986). Consequently characterising matrix cracking in laminates containing 90° plies is very important, especially when applying damage tolerant design principles. Many design criteria for PMCs are based on "first ply failure", the stress/strain at which 90° ply cracking initiates (Caslini et al 1987). It is anticipated that such design principles may also be applied to CMCs.

Transverse ply cracking in PMCs under quasi-static loading conditions has been studied extensively over the past twenty years. Of particular relevance to this work are those studies which have been used to develop and to verify predictive models. Such models range from elastic analyses of laminates containing transverse ply cracks (e.g. Garrett and Bailey 1977 and Steif 1984), to fracture mechanics approaches (e.g. Ogin and Smith 1987) and statistical-strength based approaches (e.g. Fukanaga et al 1984) predicting transverse ply cracking behaviour.

Recently, studies have shown that transverse ply cracking occurs in ceramic matrix crossply laminates (Seerat un Nabi and Derby 1988 and Prewo et al 1989). These cracks are similar to those found in polymer matrix composites in that they are fully formed (i.e. span the entire ply width and thickness) and increase in number with increasing applied load. It is likely that this occurs as a result of two key factors which are common to both

composite types. Firstly, the central 90° ply is bounded by stiffer longitudinal plies. Secondly, the matrix material is continuous throughout the laminate. As a result the plies can be assumed to be bonded elastically.

In the following sections, transverse ply cracking models previously developed for polymer matrix crossply laminates under quasi-static loading will be reviewed.

2.6.2 Crack initiation

A detailed study using glass reinforced polyester crossply laminates has shown that transverse ply cracks can originate from fibre/matrix debonding (Bailey and Parvizi 1981). In situ scanning electron microscopy of polished coupon edges was used on loaded specimens at different strain levels. Debonds observed at low strains were seen to coalesce at higher strains to form 90° ply cracks with a corresponding small drop in laminate modulus. Similar observations have been made by other workers such as Harrison and Bader (1981). It is believed that transverse ply cracks generally initiate at the laminate edge. This is particularly true for CFRP[4] laminates. However, transverse ply cracks have been observed to initiate away from the free edge in GFRP[5] laminates under fatigue loading conditions (Ogin et al 1984).

Transverse fibres debond from the matrix along their interfaces due to the magnification of strain in the matrix between the stiffer fibres (Kies 1962). A model proposed by Bailey and Parvizi (1981) has used the analysis of Kies in order to predict the 90° ply cracking strain. The model accounts in an approximate way for stress concentrations arising from a non uniform fibre distribution within a ply.

Inherent flaws in laminates also influence the strain in the surrounding matrix. Such flaws, which vary in size and distribution, originate from laminate processing, through incomplete matrix infiltration or by the trapping of air or volatiles between plies during lay-up (Hull 1988).

[4] carbon fibre reinforced polymer

[5] glass fibre reinforced polymer

Based on the above, it is clear that a distribution of flaw sizes exists within composite laminates. These flaws can be present prior to loading (inherent) or be generated under an applied load as a result of fibre/matrix debonding. Multiple cracking of a transverse ply occurs as a result of the initiation and propagation of this distribution of effective flaws and can be modelled using a number of approaches. The propagation of flaws forms the basis of fracture mechanics models, Wang et al (1984), Ogin and Smith (1987), Han et al (1988) and Laws and Dvorak (1988). Alternatively, it can be considered that the presence of flaws in the transverse ply decreases the local ply strength. This approach forms the basis of statistical-strength models such as those proposed by Manders et al (1983), Peters (1984) and Peters and Chou (1987) and Fukanaga et al (1984).

2.6.3 First ply failure

In an early experimental study by Garrett and Bailey (1977) the first ply failure strain of glass reinforced epoxy $(0/90_n)_s$ crossply laminates was shown to be dependent on the thickness of the transverse ply, i.e. the value of n. Their results showed that for a limited range of inner ply thicknesses, as the transverse ply thickness decreased a higher strain was required to form the first crack.

The experimental observations of Garrett and Bailey were taken further by Parvizi, Garrett and Bailey (1978). In this study the first ply failure strain was measured for laminates containing a much larger range of inner ply thicknesses. For all laminates with inner plies of >0.5mm thickness, cracking occurred in a catastrophic manner at a constant value of applied strain near to the failure strain of a unidirectional 90° laminate. Such cracking behaviour was termed "unconstrained cracking" as the cracking process is unaffected by the adjacent 0° plies. In contrast, transverse cracks were seen to grow across the ply width in a stable manner in laminates containing inner plies of <0.5mm thickness. This type of cracking behaviour they termed "constrained cracking" due to the constraining effect of the adjacent longitudinal plies on crack propagation. In the laminate containing the thinnest transverse ply cracking was suppressed completely prior

to overall failure. Similar behaviour was found later in carbon reinforced epoxy laminates Bader et al (1979). Below, predictive models for first ply failure in laminates containing constrained 90° plies and unconstrained 90° plies are discussed.

(a) Constrained cracking

In their work, Parvizi et al (1978) attempted to predict the first ply failure strain of laminates as a function of 90° ply thickness. A thermodynamic criterion for crack formation was used, which was developed originally by Aveston et al (1973) in order to predict crack formation in brittle matrix unidirectional laminates. These fracture mechanics based predictions of Parvizi et al are shown in Figure 2.7 and are in good agreement with experimental data for ply thicknesses (2d) of less than 0.5mm. In addition complete constraint, i.e. where no transverse ply cracking occurred prior to laminate failure, was predicted for $2d<0.1$mm .

More recently other fracture mechanics based models have been proposed in order to describe constrained cracking behaviour. Although these models assume that the growth of a flaw is the mechanism for transverse ply cracking they vary according to how the flaw is situated within the ply. The flaw can extend entirely across the ply thickness and partially through the width (Dvorak and Laws 1987, Ogin and Smith 1987, Han et al 1988 and Caslini et al 1987) or vice versa (e.g. Wang et al 1984). The former case is closer to the experimental observations of Parvizi et al and consequently, has been studied in more detail.

Hahn and co-workers (Hahn and Johannesson 1983, Han et al 1988) consider that when the laminate is loaded, defects coalesce to form a through-thickness flaw. Although the two analyses differ in the form of this initial flaw, both involve calculating the strain energy release rate (G) associated with through-width propagation from the work of crack closure. This represents a balance between the energy supplied to the system and that required to create the new crack surfaces. The condition for crack growth used is that the strain energy release rate is equal to the ply toughness ($G = G_{1c}$). The first ply failure strain is then obtained. The equation shows that G is independent of crack length, indicating that the crack will grow across the ply width in a stable manner, unlike

the extension of an unconstrained crack.

Caslini et al (1987) use a shear lag approach developed by Steif (1984) to describe the change in laminate compliance with increasing crack density (see Section 2.6.4). The first ply failure strain is derived by assuming that any number of cracks can be treated as a single crack of their combined area. Although this assumption is an oversimplification, an expression for the strain energy release rate is obtained via the compliance relation in terms of the crack density. The crack density is then set to zero to describe the onset of matrix cracking. The resulting expression is identical to that obtained by Parvizi et al (1978).

Flaggs and Kural (1982) examined the effect of the transverse ply thickness and the orientation of adjacent plies on the onset of transverse ply cracking for $(\pm\theta/90)_s$ carbon reinforced epoxy laminates, where $\theta=0°$, 30° and 60°. The trends in their data are similar to those obtained by Garrett and co-workers, namely, that decreasing the ply thickness increases the first ply failure strain. The energy based analysis of Parvizi et al (1978) was then used to predict the first ply failure strains which were then compared with their data. Flaggs and Kural suggest that increasing the fibre angle in the adjacent plies is analogous to decreasing the extensional stiffness of longitudinal plies. Their results and analysis indicate that decreasing the modulus of the constraining plies decreases the first ply failure strain.

Wang and co-workers (1980, 1984) considers the propagation of a distribution of effective flaws within a transverse ply. They suggest that the origin of these effective flaws are inherent material microflaws, which cannot be identified physically at the microscopic scale. The flaws are assumed to span the entire ply width but not the thickness and have a size and spacing which can be described by probability functions. A fracture mechanics criterion for propagation across the thickness is then applied. When the strain energy release rate for a flaw of a certain size (calculated using a two dimensional finite element stress analysis) equals the ply toughness ($G = G_{Ic}$), the flaw becomes unstable and propagates across the remainder of the ply thickness. First ply failure corresponds to the propagation of the largest flaw.

(b) Constrained to unconstrained transition

Recently, fracture mechanics based models have been used to examine the transition from constrained to unconstrained cracking behaviour (e.g. Dvorak and Laws 1987 and Ogin and Smith 1987).

The analysis of Dvorak and Laws (1987) considers a partially through-thickness and partially through-width flaw which is located centrally in the transverse ply. This enclosed flaw concept was first proposed by Ogin et al (1984) (see Figure 2.8). The flaw may grow incrementally in the through-width and through-thickness directions with increasing applied load until one of the dimensions reaches a critical size. At this point the flaw will propagate catastrophically. The strain energy release rate for crack propagation is derived from an energy balance. The two cases of thick and thin plies are examined. When the flaw is located in a thin (constrained) ply it is assumed to propagate catastrophically in the through-width direction only. This is because the critical flaw size for through-thickness propagation is greater than the actual ply thickness. When the flaw is located in a thick (unconstrained) ply it is assumed to behave like a slit crack in an infinite orthotropic medium. Deriving the strain energy release rate for through-width and through-thickness propagation shows that first ply failure in thick plies is controlled by through-thickness cracking followed by through-width cracking.

An alternative fracture mechanics analysis has been performed which is based on the stress intensity factor (Ogin and Smith 1987). In a thin (constrained) ply the flaw is assumed to span the ply thickness but not the ply width. Ogin and Smith suggest that load does not build up at the crack tip in a manner dependent on the crack length due to load shedding into the 0° plies. This allows an expression for the stress intensity factor to be derived which is based on the local stress disturbance in the transverse ply. By assuming the ply fracture toughness (K_{1c}) and toughness (G_{1c}) are related, an expression for the first ply failure strain is obtained. The predictions as a function of ply thickness (2d) are shown in Figure 2.7 and compare well with the data of Parvizi et al (1978) for $2d<0.5$mm.

The transition between constrained and unconstrained behaviour was then examined

from this stress intensity factor approach. Using the concept of the enclosed flaw (Figure 2.8) fast fracture in a thick ply occurs through the thickness and width when the smallest flaw dimension (thickness) reaches a critical size. In a thin ply fast fracture occurs at a higher applied strain through the width. This is because only stable growth is possible through the ply thickness. Since, in both cases fast fracture occurs when the stress intensity factor is equal to the fracture toughness, setting the two results equal gives a simple expression for the transition ply thickness in terms of the critical flaw size (a_{crit}). The calculated value of ply thickness is in good agreement with Parvizi and co-workers experimentally observed transition between constrained and unconstrained behaviour.

(c) Unconstrained cracking

The fracture mechanics based predictions of the first ply failure strain for PMC laminates containing inner plies of greater than 0.5mm thickness severely underestimate the experimental data. Parvizi and co-workers (1978) concluded that whilst an energy based criterion is applicable to describe matrix cracking for glass/epoxy laminates with thin (constrained) plies, the propagation of flaws in thick (unconstrained) plies is mechanism controlled. This leads to a variability in the 90° ply strength due to the different stresses required to propagate flaws of different size (Manders et al 1983, Fukanaga 1984 and Peters 1984 and Peters and Chou 1987).

Manders et al (1983) suggest that although fracture events are governed ultimately by thermodynamic considerations, these may be dominated by variations arising from the randomness of the microstructure. As indicated earlier, microstructural features include inherent flaws as well as fibre/matrix debonds which result from a non-uniform fibre distribution. A simple statistical model is used to predict the onset of transverse ply cracking in glass reinforced epoxy laminates (see Section 2.6.4). The single value for the 90° ply failure strength is replaced by a two parameter Weibull distribution to describe the strength variability. Good agreement is found with their experimental results using a fitted value of Weibull modulus. Manders and co-workers show that the degree to which the 90° ply strength varies is dependent on the volume of the ply. The larger the volume (i.e. in a thicker ply) the smaller the magnitude of Weibull modulus and hence the greater the variation.

Fukanaga et al (1984) also use a two parameter Weibull cumulative distribution to describe the 90° ply strength variability. This is used in an expression relating the crack spacing to the applied strain (see Section 2.6.4). By assuming the stress in the ply to be uniform between cracks when the cracks are far apart the first ply failure strain is derived.

Their predictions for the first ply failure strain of $(0/90_n)_s$ laminates are compared with the data of Flaggs and Kural (1982) for CFRP (Figure 2.9a) and Bailey et al (1979) for GFRP laminates (Figure 2.9b). There is excellent agreement for a range of inner ply thicknesses particularly for CFRP laminates. The improvement over the energy based theory of Bailey and co-workers at large ply thicknesses is also shown (Figure 2.9b). It is apparent from these curves that the analysis is extremely sensitive to the value of Weibull modulus. Thicker plies of a lower Weibull modulus (i.e. having a larger strength distribution) crack at lower applied strains. Fukanaga and co-workers suggest that this is the reason why cracks can form in thick plies as a result of thermal stresses. This has been observed by workers such as Peters (1983).

Both Manders et al and Fukanaga et al suggest that a volume effect is responsible for the decrease in first ply failure strain with increasing inner ply thickness. However, it is incorrect to assume that this is the case for thin (constrained) plies. It has already been shown by the many fracture mechanics based approaches that in constrained plies the first ply failure strain increases with decreasing ply thickness due to the greater amounts of energy required to propagate the crack. As a result, statistical-strength based models can only be applied to describe cracking behaviour in thick (unconstrained) plies, where the mechanism of crack propagation is the controlling factor. This should be borne in mind in the following section which discusses fracture mechanics based and statistical-strength based approaches to multiple cracking.

2.6.4 Multiple cracking

When a laminate is loaded to the first ply failure strain the crack that forms in the

transverse ply spans the entire ply width and thickness. In the through-thickness direction the crack is arrested or blunted by the adjacent 0° plies. This permits an increase in applied strain without catastrophic failure of the laminate. Moreover, as the plies remain bonded, load is shed back into the transverse ply away from the crack plane either side of the crack. At a distance a few ply thicknesses away, the 90° ply stress is more or less unaffected by the crack. Consequently, flaws at other locations in the ply may become critical at the higher strain and propagate to form additional cracks. The repeated cracking of the transverse ply with increasing applied strain is termed "multiple cracking".

The redistribution of stress in the transverse and longitudinal plies in the presence of 90° ply cracks and their effect on laminate stiffness properties can be described by shear lag analysis.

(a) Shear lag analysis and stiffness reductions in cracked laminates

Shear lag analysis was used by Aveston and Kelly (1973) to describe the stress strain behaviour of unidirectional brittle matrix laminates containing fully formed matrix cracks. The laminates considered contained fibres which were elastically bonded to the matrix. This analysis was modified by Garrett and Bailey (1977) and later by Steif (1984) amongst others in order to describe the stress distribution in the longitudinal and transverse plies of crossply laminates containing fully formed transverse ply cracks (see Figure 2.10). The approaches of Garrett et al and Steif differ in the form of the longitudinal displacement profile in the 90° ply. Garrett and Bailey assume this to be linear in nature whereas Steif considers the profile to be parabolic. An alternative shear lag analysis by Highsmith and Reifsnider (1982) assumes that the shear between longitudinal and transverse plies is confined to resin rich planes situated at the ply interfaces. This results in a uniform displacement over the majority of the 90° ply.

Shear lag analysis is based on the assumption that the plies remain elastically bonded when the 90° ply is cracked and involves using the 90° ply displacement profile to describe the stress distributions in the longitudinal and transverse plies as a function of distance from the 90° ply crack. The longitudinal plies bear the entire composite load in the plane of the crack. The additional load is then shed back into the transverse ply

with increasing distance from the crack plane via shear at the ply interfaces. When the applied load is increased, further cracking will occur in the 90° ply when its failure strength is again exceeded. From a point of view of modelling multiple cracking, ignoring any statistical variations in transverse ply strength, the location of new cracks is always midway between existing cracks where the transverse ply stress is greatest.

Both Garrett and Bailey and Steif assume the stress profile in the longitudinal plies to be symmetric about a crack. However, Garrett and co-workers model the decay of stress in terms of an exponential function away from a single crack plane. This results in a discontinuity in stress gradient midway between two cracks as only at plus or minus infinity from a crack can the stress gradient equal zero. Clearly the analysis of Garrett and Bailey violates stress equilibrium when the plies are elastically bonded. However, their analysis still shows good agreement with their experimental data for glass/epoxy laminates (Parvizi and Bailey 1978) (Figures 2.11a and 2.11b). The theory takes the form of a stepped curve, because, after cracks have formed, the applied stress must be increased until the criterion for cracking is again satisfied. At this point there is a sudden decrease in crack spacing.

In contrast Steif models the 90° stress profile in terms of a hyperbolic function between two transverse ply cracks. The function is smooth and continuous and predicts the correct value of zero for the stress gradient midway between two cracks. The analysis of Steif may be used to model the progressive cracking of crossply laminates as a function of applied load using the expression

$$\sigma_c = \frac{\sigma_{2u}}{\frac{E_2}{E_0}\left(1 - \frac{1}{\cosh \lambda s}\right)} \qquad (2.3)$$

where σ_c = applied stress

σ_{2u} = 90° ply failure stress

E_0 = uncracked laminate modulus

E_2 = transverse ply modulus

b = longitudinal ply thickness

2d = transverse ply thickness

2s = crack spacing

$$\lambda^2 = \frac{3 G_{23}}{b d^2}\left(\frac{b E_1 + d E_2}{E_1 E_2}\right)$$

where E_1 = longitudinal ply modulus

G_{23} = the through-thickness shear modulus of the transverse ply

When damage is sustained by the transverse ply, its contribution to overall laminate mechanical properties is reduced. One such property is the longitudinal laminate modulus (Hahn and Tsai 1974). Many studies have attempted both to classify and to quantify damage in composite laminates using external stiffness measurements (Highsmith and Reifsnider 1982, Talreja 1985). Since the three principal damage modes, (transverse cracking, delamination and fibre breakage) may all contribute to the degradation of the laminate modulus, no single stiffness measurement will be sufficient. However, the assumption that only transverse ply cracking is operative at low strains enables relationships between crack spacing and longitudinal modulus to be sought.

The shear lag analyses of Garrett and Bailey, Steif, etc, enable expressions to be written for the longitudinal modulus of the laminate (E) in terms of the transverse ply crack spacing (2s). Following Steif

$$E = E_0\left\{1 + \frac{E_0}{E_1}\left[\left(1 + \frac{d}{b}\right) - \frac{E_1}{E_0}\right]\frac{\tanh \lambda s}{\lambda s}\right\}^{-1} \qquad (2.4)$$

The above expression was used by Ogin and Smith (1985) and Smith and Wood (1990) to describe stiffness reduction in GFRP laminates with good agreement. Highsmith and Reifsnider (1982) consider the stiffness changes in glass/epoxy laminates. The effect of cracking on the longitudinal modulus is examined by using a degraded value for the transverse modulus (E_2) in a standard laminate analysis. The reduced value of E_2 for different damage states (crack spacings) is obtained by calculating from shear lag analysis the contribution of the total composite load that is carried by the damaged ply. The transverse ply modulus is then reduced proportionally. The predictions for the stiffness as a function of applied stress show the same trends as their experimentally determined

values. However, the predictions generally overestimate the modulus. This is most noticeable when the transverse modulus is set to zero for a fully cracked ply. Highsmith and co-workers suggest that this is due to the estimated value of shear transfer layer thickness used in their analysis being incorrect.

Talreja (1984, 1985) adopts a completely different approach to describe the reduction in longitudinal modulus with increasing 90° damage. Rather than considering cracks explicitly in terms of their effects on the distribution of stress, they are treated as microstructural features. The presence of cracks is then accounted for by introducing a set of internal state variables in chosen mechanical property functions. Four material constants for an orthotropic laminate are characterised in order to obtain stiffness changes as a function of crack density. The results for glass/epoxy are in good agreement with the experimental data and shear lag predictions of Highsmith et al (1982).

(b) Fracture mechanics approaches to multiple cracking

Using the concept of a distribution of effective flaws as described earlier (see Section 2.6.3), Wang (1984) employs a stochastic simulation procedure to model multiple cracking. This is based on a Monte Carlo random search routine to describe the flaw size and location distributions. The largest flaw propagates first when the strain energy release rate is equal to the ply toughness ($G = G_{1c}$). The routine then searches for the next flaw most likely to form a crack by comparing strain energy release rate values taking into account the presence of the first crack. The applied load associated with the next crack forming (i.e. when $G = G_{1c}$) is then calculated. The routine is then repeated to describe subsequent crack formation. Excellent agreement with experimental data is shown for a range of crossply CFRP laminates.

Han et al (1988) use their fracture mechanics based analysis described earlier to examine the multiple cracking of a transverse ply (see Section 2.6.3). By replacing the boundary condition at infinity with a boundary condition at the midpoint between equally spaced cracks, an expression is obtained for the strain energy release rate per crack. The total energy released for N cracks per unit length is then calculated. Han and co-workers assume that for a given stress in the transverse ply, the crack density increases from N

to N+dN when the increase in energy released equals the energy absorbed. The predicted stress as a function of crack density is compared with the experimental data of Wang et al (1985) for graphite/epoxy laminates. Contrary to the experimental results, the stress remains fairly independent of crack density. This indicates that the strain energy release rate does not increase much until the crack spacing becomes small enough to allow interaction between cracks. Consequently, the model predicts the formation of many cracks almost simultaneously without much increase in the applied stress. Han et al suggest that this is because the fracture energy is not homogeneous. This is shown by plots of fracture energy vs crack density, termed crack growth resistance curves.

Caslini et al (1987) also use the resistance curve concept to describe the multiple cracking of glass/epoxy laminates. As the crack density increases, the strain energy release rate is calculated as a function of total crack area using shear lag analysis (see Section 2.6.3). Their plots of the critical strain energy release rate (toughness) vs crack density show an increase in the resistance to crack formation with increasing crack density. This is attributed to the reduced constraint and load transfer capability of the adjacent 0° plies at small crack spacings.

By way of contrast to the fracture mechanics based models described so far, Laws and Dvorak (1988) suppose that a transverse ply crack will form when it is energetically favourable, but in a location that is associated with a probability density function. This function is proportional to the stress in the transverse ply as determined by shear lag analysis. The analysis is also performed assuming the crack to form midway between two existing cracks (as predicted by deterministic models) and when it is equally likely to form anywhere in the ply. Their predictions of crack density as a function of applied stress are compared with experimental data for glass/epoxy laminates (Highsmith et al 1982) and for carbon/epoxy laminates (Wang et al 1984). Although use of the probability density function yields the better curve, poor agreement is obtained for GFRP even though several values of G_c are used. This is probably due to the large thickness of the transverse ply making the use of fracture mechanics based models inappropriate to describe the transverse ply cracking behaviour. Much better agreement is obtained for CFRP. However, as the authors point out, cracks accumulate in these laminates over a

much smaller range of applied load.

A similar approach combining fracture mechanics and statistics has been taken by Nairn (1989) using a different stress analysis to Laws and Dvorak. Good agreement is obtained for stress/crack spacing data in GFRP laminates.

(c) Statistical-strength approaches to multiple cracking

It has been argued above that fracture mechanics based models predict first ply failure and multiple cracking accurately for thin (constrained) plies. However, these models are unsuitable to describe the cracking behaviour in thick (unconstrained) transverse plies. When the propagation of flaws is mechanism controlled, the presence of a distribution of flaw sizes requires a statistical description of the 90° ply strength. Simple deterministic models such as shear lag analysis are also unsuitable to describe thick ply cracking behaviour. This is because the non-uniformity in ply strength means that cracks do not necessarily form midway between existing cracks. These shortfalls are addressed by statistical-strength based models (Peters 1984, Manders et al 1983 and Fukanaga et al 1984). Such models usually combine shear lag analysis to describe the stress distribution between cracks, with a statistical distribution to describe the variability in ply strength.

In the analysis of Manders et al (1983) 90° ply crack spacing vs applied strain data are obtained for glass reinforced epoxy laminates. A two-parameter Weibull distribution is used to describe the cumulative distribution of crack spacings at each value of applied strain. This they suggest is only possible by assuming the strength of the 90° ply to be statistically distributed due to the presence of effective flaws (inherent and fibre/matrix debonds). In other words, at each value of applied strain the strengths of constituent volumes of the ply can be described by a distribution which is identical to that of the crack spacings. Not only is the validity of this analysis unclear, but the non-linearity of the resultant cumulative distribution vs applied stain curves indicates that this assumption is invalid at high strains (small crack spacings).

By applying a least squares method to the linear sections of each curve an attempt is made to predict the crack spacing as a function of applied strain. This is done using the

shear lag analysis of Parvizi and Bailey (1978) to describe the variation of stress between cracks, together with the cumulative distribution function (cdf) to describe the non-uniformity of strength. An expression for the crack spacing is obtained but remains in terms of failure probability. No solution is offered as this is not in closed analytical form. As a result the equation is simplified by making two assumptions. Firstly, that a constant level of stress exists between cracks. This is valid at low strains when the crack spacing is large. Secondly, the two-parameter Weibull distribution is assumed for the strength of the 90° ply. This gives the expected crack spacing as a function of applied strain, Weibull scale parameter and Weibull shape parameter (Weibull modulus). However, two values for the Weibull shape and scale parameters are obtained from the cdf vs crack spacing relations. Manders and co-workers suggest that this indicates the 90° ply strength becomes more variable at high strains. The equation is solved using the value corresponding to low applied strains. Manders and co-workers claim that there is good agreement between their prediction and the experimental data for a wide range of crack spacings. However, not only is the origin of the Weibull modulus questionable, it is seen to decrease within this range.

The applicability of the statistical model is discussed in terms of the accumulation of cracks. At low strains the region between cracks is relatively uniformly stressed and the position of new cracks are determined by the distribution of weak points. As a result the statistical model is more applicable than the simple shear lag analysis of Parvizi and Bailey (1978). At high strains the opposite is true as the region between cracks is highly non-uniformly stressed. This means that cracks are more likely to form midway between existing cracks, where the stress is greatest.

Peters (1984) considers the 90° ply to be made up from a number of elements connected in series. The length of these elements is determined using the shear lag analysis of Highsmith and Reifsnider (1982) by calculating the distance either side of a crack where 90% of the original load is shed back into the ply. It follows that when each element breaks once, a near constant crack spacing results as is found experimentally (e.g. Garrett and Bailey 1977). Data for the crack spacing as a function of applied strain are obtained experimentally by measuring the load drop (and corresponding increase in laminate

strain) associated with the formation of a crack. Ranking the failure probability using a median ranking technique gives an expression for the survival probability in terms of the Weibull modulus. The data and corresponding Weibull moduli are then modified for each laminate tested. This is to account for the greater probability of an element cracking twice at higher values of applied strain.

The analysis shows that for laminates containing a range of inner ply thicknesses the Weibull modulus increases with decreasing ply thickness. This agrees with the size effect discussed by Manders et al (1983). Peters suggests that the increase in Weibull modulus is due to the propagation of flaws being suppressed in the interface layers of thinner plies. It appears that Peters is describing the transition from unconstrained to constrained cracking behaviour. However, no comment is made on the change in mechanism of crack growth. For laminates containing thick inner plies the data can be described by a constant Weibull modulus which is equal to that of a unidirectional transverse laminate. This is because the influence of the outer longitudinal plies on crack propagation is small.

Fukanaga and co-workers (1984) were able to develop the ideas proposed by Manders et al combining Weibull statistics with shear lag analysis more explicitly. A two parameter Weibull distribution is used for the 90° ply failure probability to describe the variability in ply strength. They consider that when a crack forms, it does so midway between two existing cracks at 50% failure probability. These assumptions are necessary for the final crack spacing vs applied strain expression to remain in closed analytical form. The failure probability is then solved to produce a simple Weibull scaling equation for the stress in the transverse ply for a given crack spacing. This is written in terms of 90° ply stress/crack spacing values for a ply of a different volume (a reference specimen). However, this assumes that the Weibull modulus is independent of volume.

The Weibull scaling equation is then used to produce an expression relating the crack spacing to the applied stress. This is shown to have the correct form for the two boundary conditions; when the crack spacing tends to infinity (an uncracked laminate) and when the crack spacing tends to zero (the crossply is reduced to a longitudinal ply).

The analysis represents a successful attempt to describe the formation of cracks at weak points anywhere between existing cracks in the 90° ply. However, this is only true for individual cracking events. The fact that the shear lag expression contains a crack spacing term implies that any value of applied strain the cracks are equally spaced.

The predictions of crack spacing as a function of applied strain for $(0/90_n)_s$ laminates containing transverse plies of different thicknesses (n=1, 3 and 14) are shown in Figure 2.12. Both the rate at which cracks form and the final crack spacing is extremely sensitive to the value of Weibull modulus. When the thickness of the transverse ply is small (n=1 or 2) the number of cracks is small. As the thickness of the ply becomes large, the crack spacing increases with the thickness of the ply. Fukanaga and co-workers indicate that the analysis predicts this in a qualitative way as the trends follow the experimental observations for glass and carbon reinforced epoxy laminates. However, increasing the value of the Weibull modulus with decreasing 90° ply volume is insufficient to describe the applied stress/crack spacing data for thin (constrained) plies. This is clearly illustrated in Figure 2.12 where n=1.

2.6.5 Crack saturation

The early studies by Garrett and Bailey (1977) and Parvizi and Bailey (1978) showed that the rate at which 90° ply cracks formed decreased with increasing applied stress, approaching zero at high stress. The final or "saturation" crack spacing was found to be approximately equal to the ply thickness.

Reifsnider and co-workers termed the saturation crack pattern in multi-directional laminates the "characteristic damage state", CDS, which they argued could be predicted using shear lag analysis (Masters and Reifsnider 1982, Highsmith and Reifsnider 1982). The CDS consists of a uniform array of cracks in each off axis ply which develops at high static load and remains constant until fracture. The final crack spacing, which they suggest is independent of previous loading history, was found to be dependent on the ply thickness and laminate stacking sequence.

Wang and Crossman (1980), who consider a fracture mechanics approach to multiple cracking, take the saturation crack spacing to be the distance between adjacent cracks at which cracks interact, so reducing the strain energy release rate. Statistical-strength models based on shear lag analysis consider that the probability of cracking close to existing cracks is reduced since the stress in the transverse ply is zero in the plane of a crack. The distance over which the additional load is shed back into the ply is sometimes known as the "unstressed length" and is found to be approximately equal to the ply thickness (Manders et al 1983, Peters 1984. Fukanaga et al 1984).

2.7 CONCLUSIONS

It has been shown in the literature cited that a weak fibre/matrix bond is essential for optimum strength and toughness in unidirectionally reinforced CMCs. As a result, models based on the fibres and matrix being elastically bonded (as used for PMCs) are unsuitable to describe their matrix cracking behaviour. The ACK theory for multiple fracture and continuum approaches seem more suitable as the fibres and matrix are assumed to interact via frictional forces only. The continuum models indicate that at some level of applied stress, although matrix cracking may be energetically favourable (i.e. the ACK approach), the applied stress must be raised in order for crack tip stresses to become large enough for crack propagation. This accounts for the experimental observations of continued cracking with increasing applied stress in unidirectional laminates. However, there is a need for a more complete description of this progressive cracking process and the effect that it has on residual properties, notably stiffness.

The fatigue growth of cracks in polycrystalline ceramics occurs by two distinct mechanisms, static fatigue and as a result of the non reversibility of strain during stress cycling. Although little in the way of published work is available for fibre reinforced ceramics, key observations have been made for unidirectional laminates. These include the degradation of laminate stiffness (and sometimes residual strength) and change in stress/strain hysteresis behaviour with cycling. Further work is necessary to correlate such observations with the relevant damage mechanisms.

The experimental studies cited for crossply laminates indicate that transverse ply cracking behaviour in CMCs is similar to that in PMCs. In both cases the plies can be assumed to be elastically bonded and the central 90° ply is bounded by stiffer longitudinal plies. As a result, some of the models previously developed to describe transverse ply cracking in PMCs should be applicable to their CMC counterparts. The transverse ply cracking models reviewed show that the fracture mechanics based approaches describe accurately the cracking behaviour of PMC laminates containing thin (constrained) plies. However, in CMCs it might be anticipated that transverse ply cracking will occur in a catastrophic

manner even at small ply thicknesses, because the critical flaw size for crack propagation in ceramic materials is small compared to that of polymers. For this reason it is likely that statistical-strength based models are more suitable to describe the cracking behaviour of crossply CMCs. To investigate these ideas more detailed experimental data are required for damage development in crossply ceramic composite laminates than are currently available.

LAMINATE	E_1 (GPa)	σ_f (MPa)	e_f (%)	σ^*_{el} (MPa)	e^*_{el} (%)	V_f
Nicalon/Pyrex [a]	110	600	0.55	500	0.4	0.49
Nicalon/LASII [b] (as pressed)	134	758	0.97	381	0.28	0.44
Nicalon/LASIII [c] (ceramed)	130	664	0.86	439	0.34	0.44

Sources

[a] Davidge and Briggs 1989.

[b] Prewo 1986.

[c] Prewo 1986.

Table 2.1 Current optimised tensile properties of glass and glass ceramic matrix unidirectional laminates.

LAMINATE	E_0 (GPa)	σ_f (MPa)	e_f (%)	σ^*_{el} (MPa)	e^*_{el} (%)	V_f
Nicalon/Pyrex [a] $(0/90)_{2s}$	130	200	0.58	25 60	0.025 0.07	0.4
Nicalon/LASIII [b] $[0(0/90)_2]_s$	76	300	0.8	39 60	0.04	0.4
Nicalon/LASIII [c] $(0/90)_s$	-	180	-	70 130	-	-
Nicalon/LASII [d] ceramed $(0/90)_s$	76	410	0.9	-	-	-

Sources

[a] Seerat un Nabi and Derby 1988.

[b] Prewo 1986.

[c] Sbaizero and Evans 1986.

[d] Prewo 1986.

Table 2.2 Current optimised tensile properties of glass and glass ceramic matrix crossply laminates.

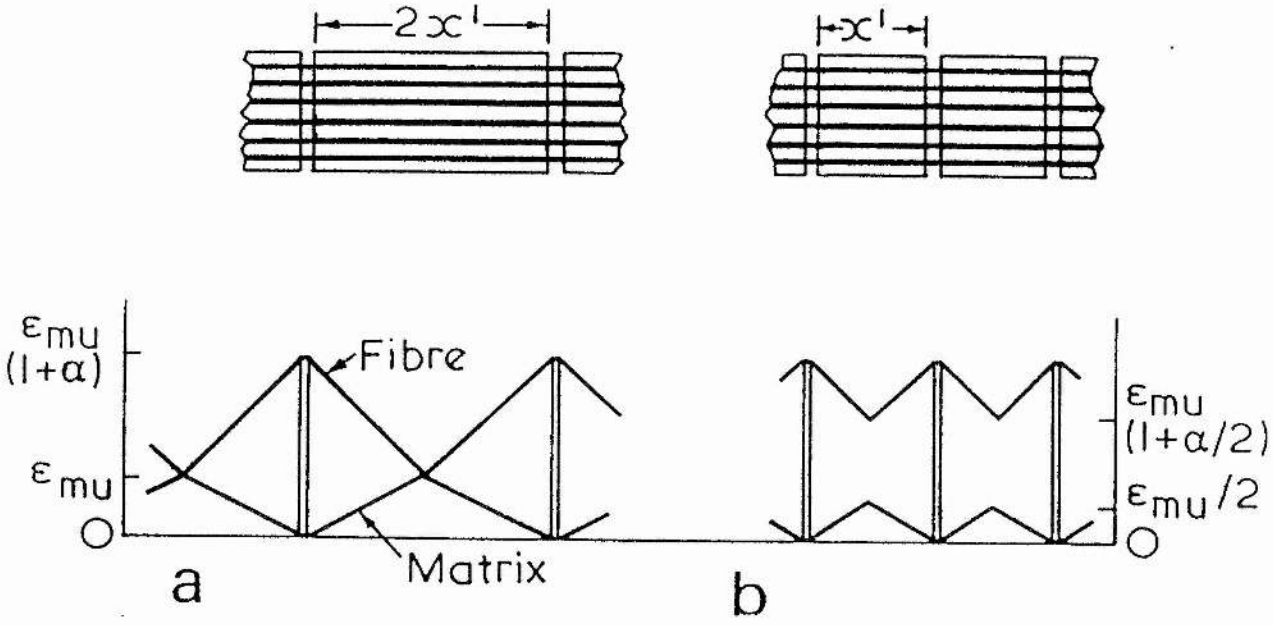

Figure 2.1 Strain profile in the fibres and the matrix of a cracked unidirectional laminate for a crack spacing of (a) $2x'$ and (b) x' (taken from Aveston et al 1971).

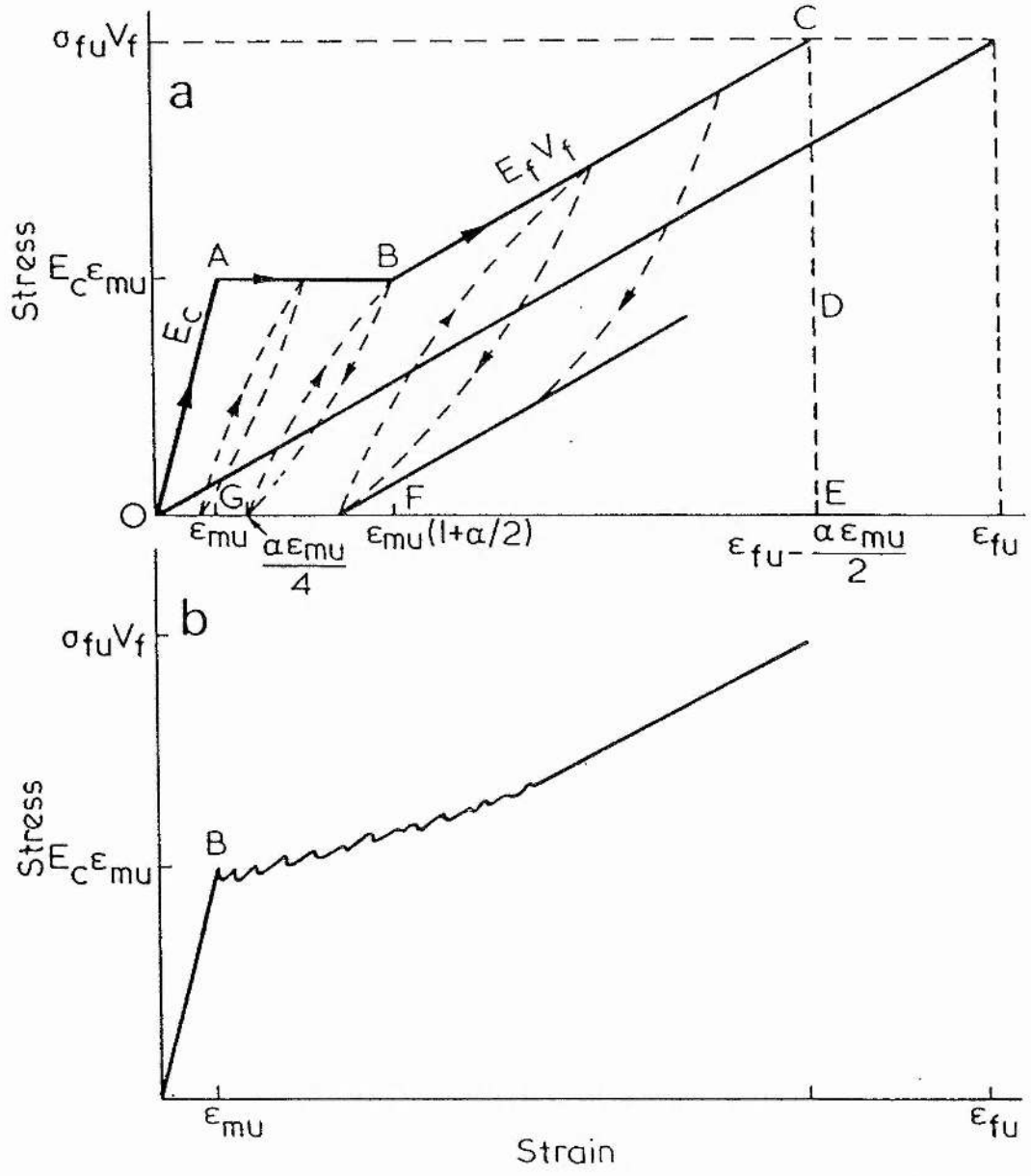

Figure 2.2 Stress/strain curves for a unidirectional laminate (taken from Aveston et al 1971) for (a) a matrix with a single valued failure strength and (b) a matrix of variable strength.

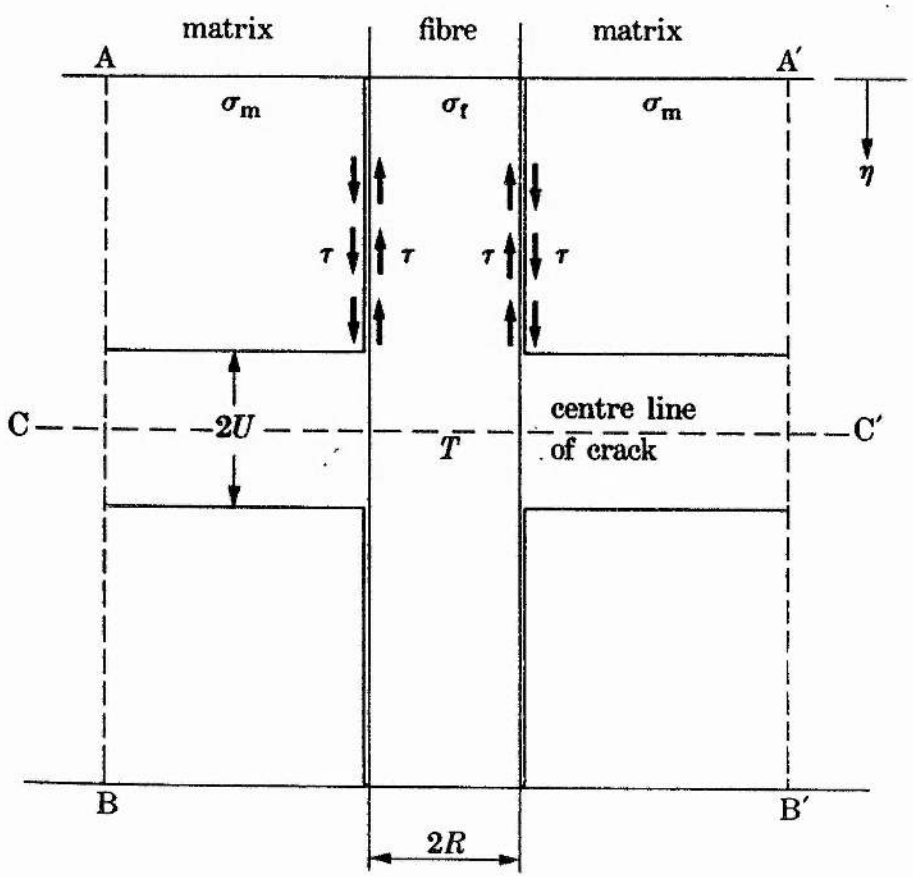

Figure 2.3 Schematic diagram of a discrete fibre used in continuum models which describe matrix cracking in unidirectional laminates (taken from McCartney 1987).

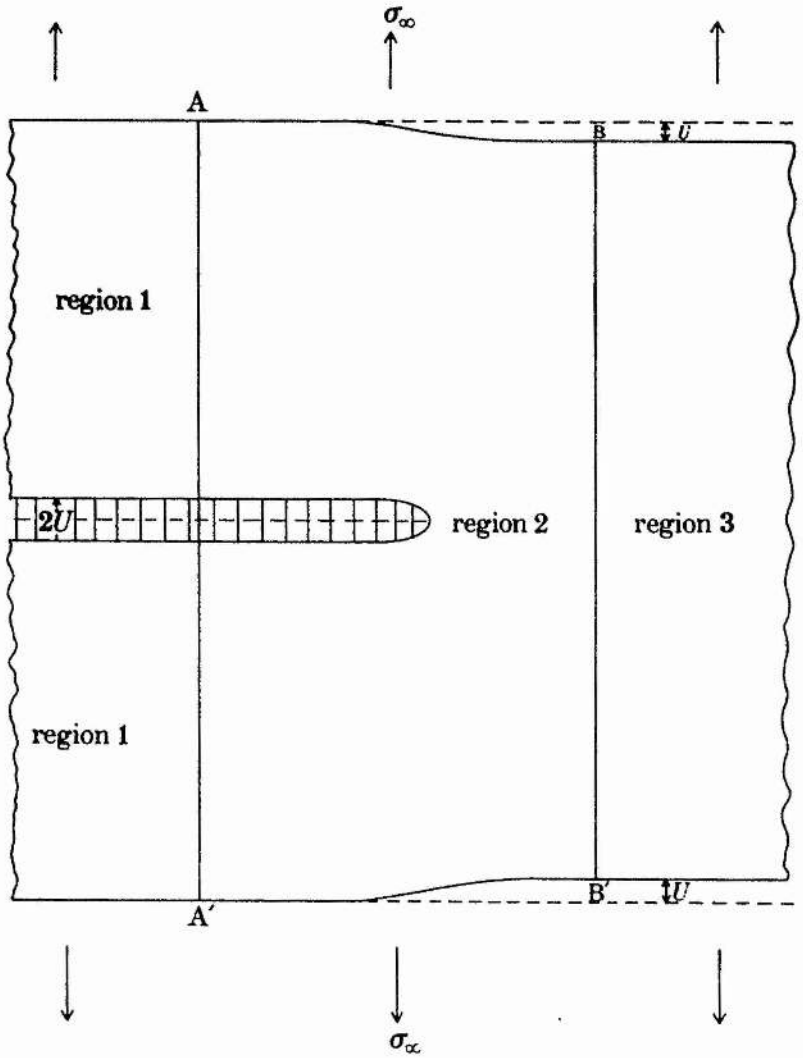

Figure 2.4 Schematic diagram of the crack geometry used in the continuum models which describe matrix cracking in unidirectional laminates (taken from McCartney 1987).

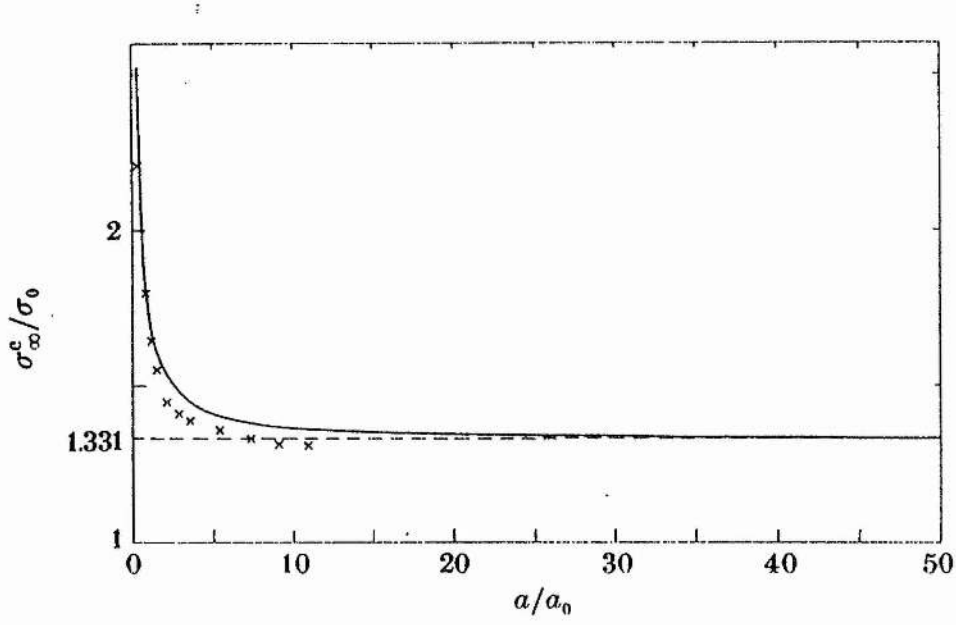

Figure 2.5 Dependence of the matrix cracking stress on the length of pre-existing flaw in unidirectional laminates (taken from McCartney 1987).

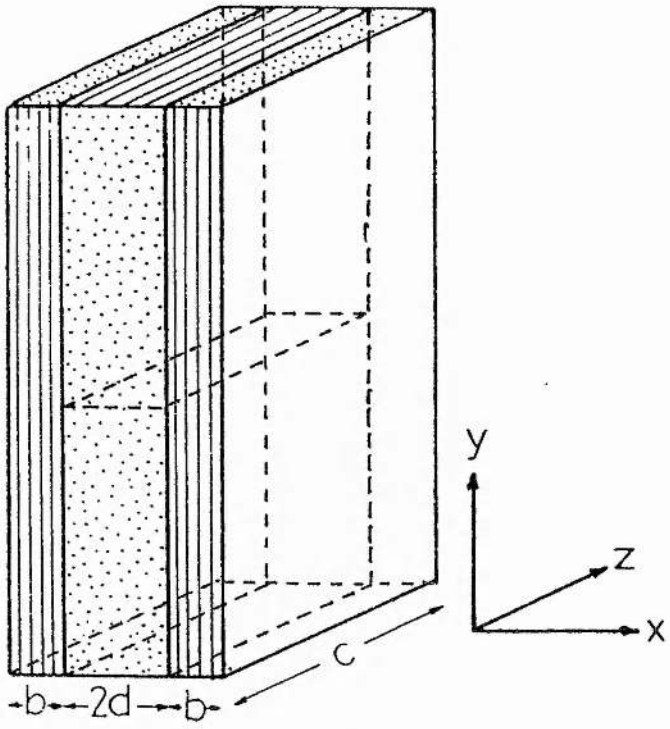

Figure 2.6 Schematic diagram of a crossply laminate containing a transverse ply crack (taken from Parvizi and Bailey 1978).

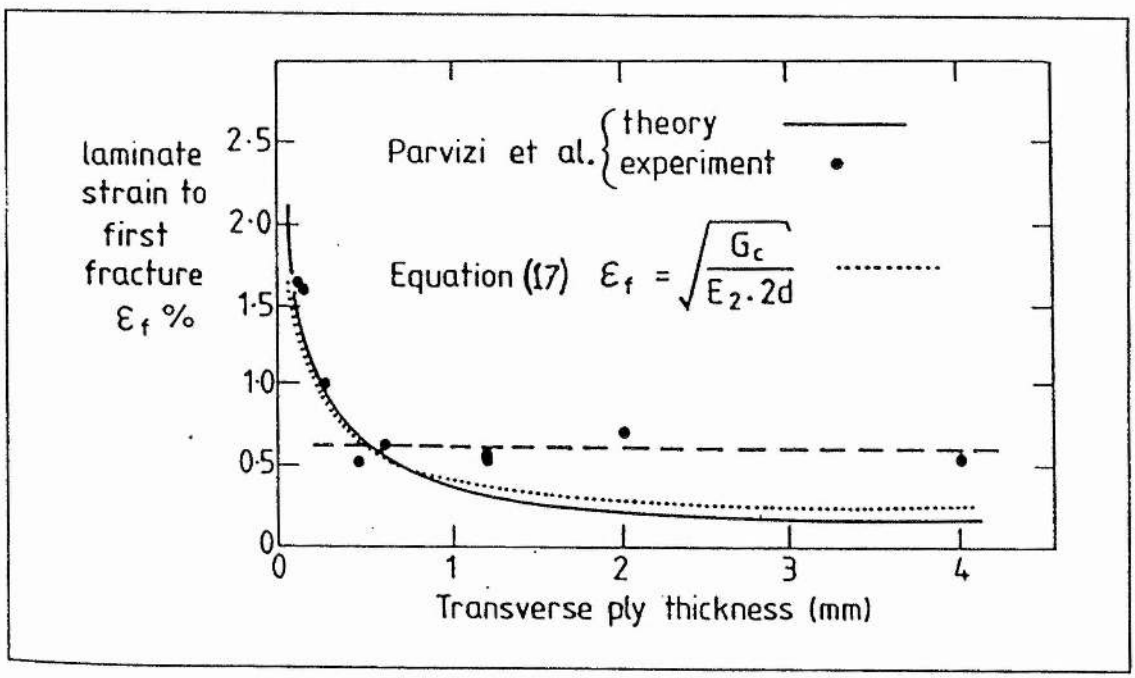

Figure 2.7 Energy based predictions of the first ply failure strain for glass/epoxy crossply laminates, as a function of transverse ply thickness (taken from Ogin and Smith 1987). The broken line represents the failure strain of a 90° laminate tested alone.

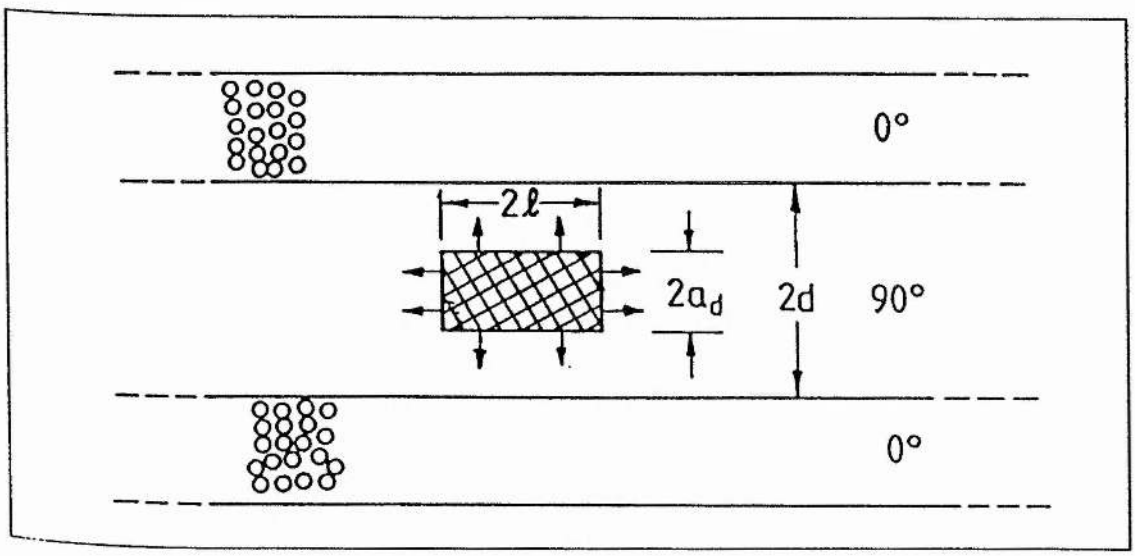

Figure 2.8 Enclosed flaw in a transverse ply (taken from Ogin and Smith 1987).

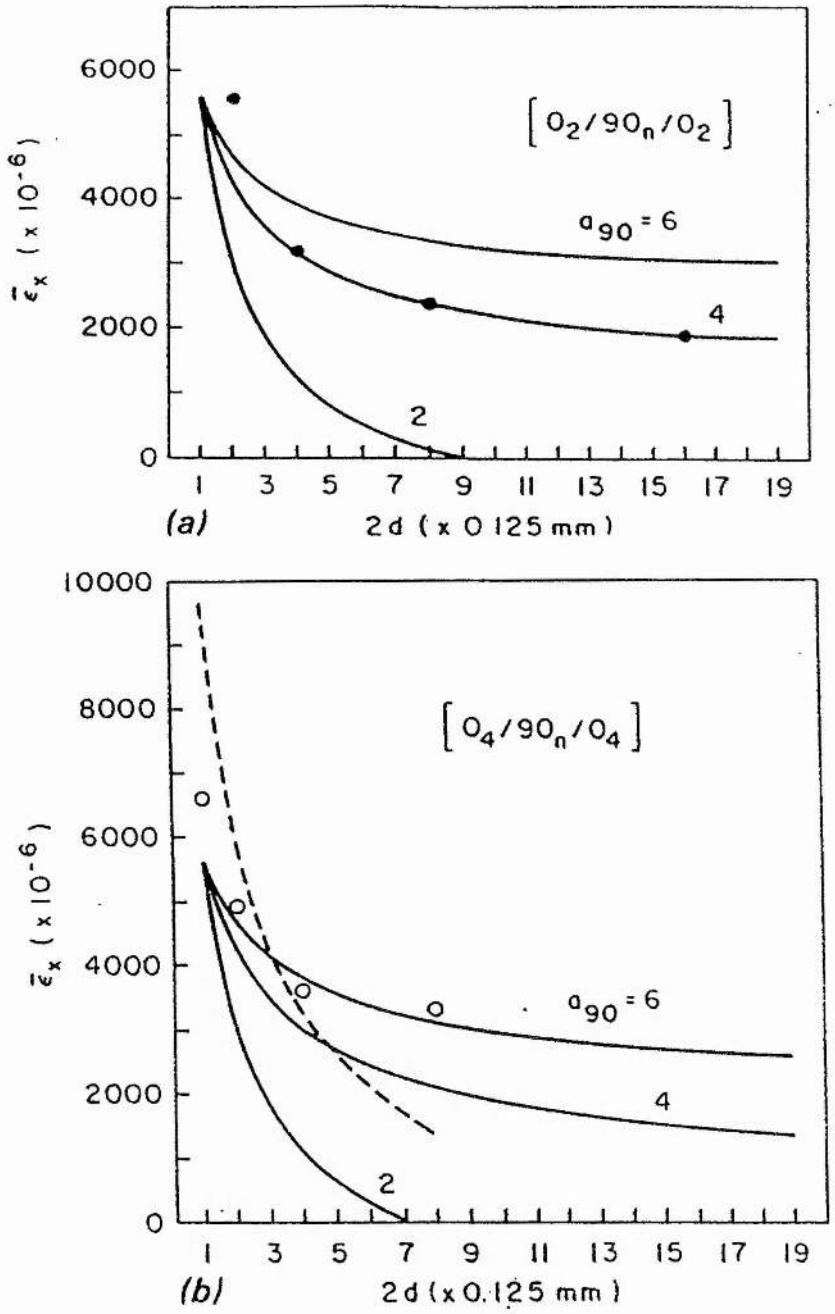

Figure 2.9 Statistical-strength based predictions for the first ply failure strain of crossply laminates as a function of transverse ply thickness.

(a) $(0_2/90_n/0_2)$ carbon/epoxy laminates

——— prediction by Fukanaga et al

• data from Flaggs and Kural (1982).

(b) $(0_4/90_n/0_4)$ glass/epoxy laminates

——— prediction by Fukanaga et al

--------- prediction by Bailey et al (1978)

o data from Bailey et al (1978).

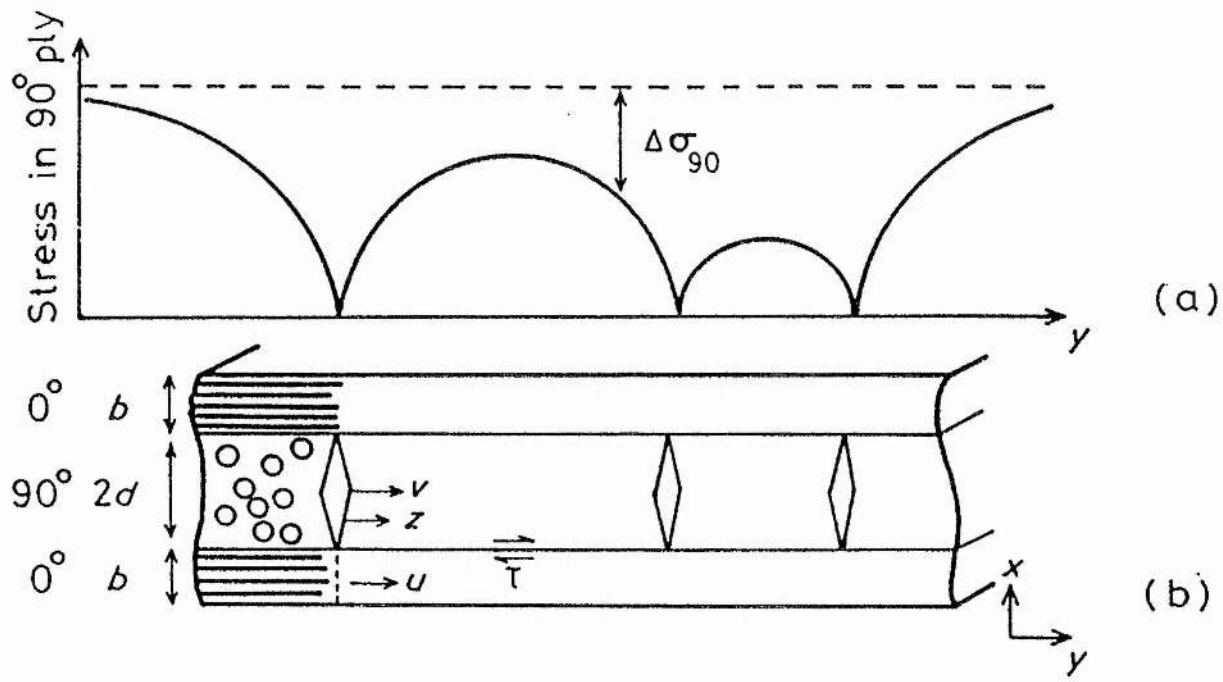

Figure 2.10 (a) Stress distribution in the matrix of a cracked transverse ply (taken from Manders et al 1983).

(b) Cross section of laminate corresponding to (a) showing displacements used in the shear lag analysis.

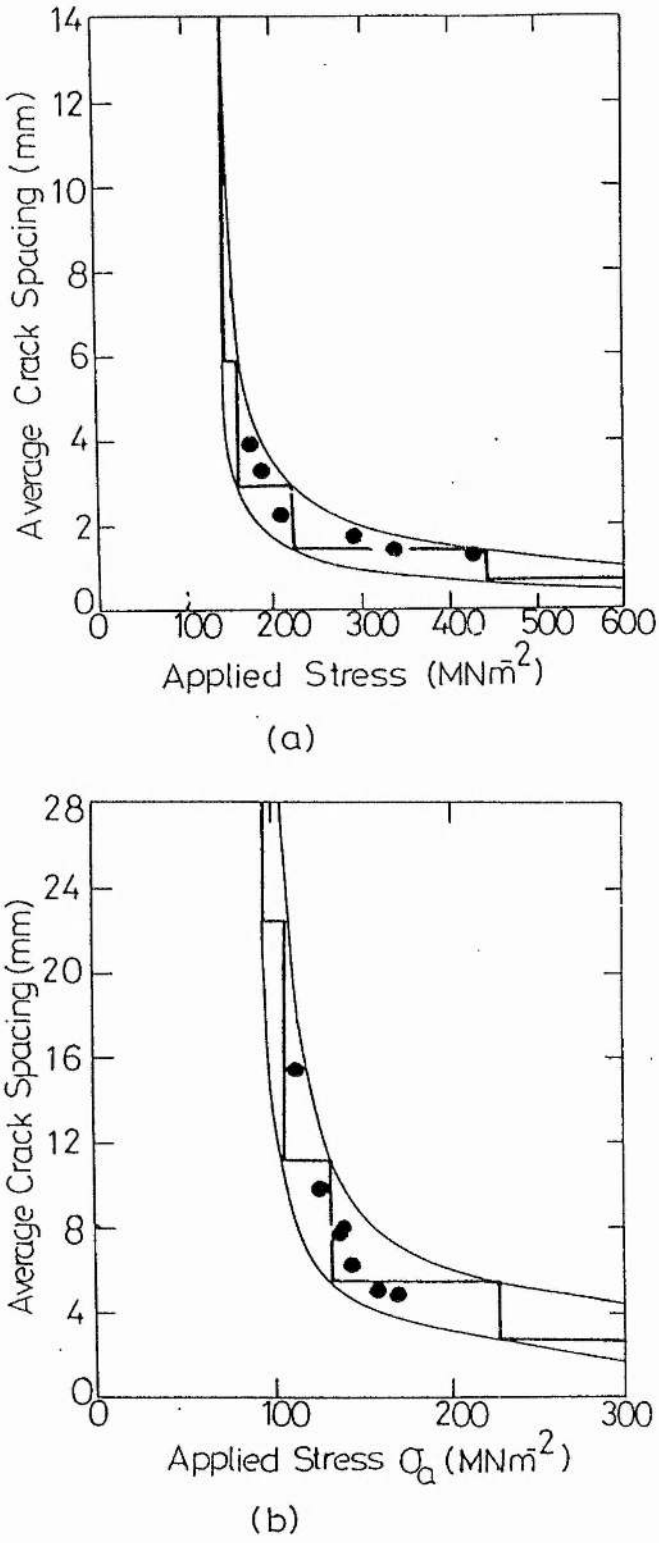

Figure 2.11 Energy based predictions of the transverse ply crack spacing in glass/epoxy crossply laminates as a function of applied stress. The transverse ply is 1.2mm thick in (a) and 4mm in (b).

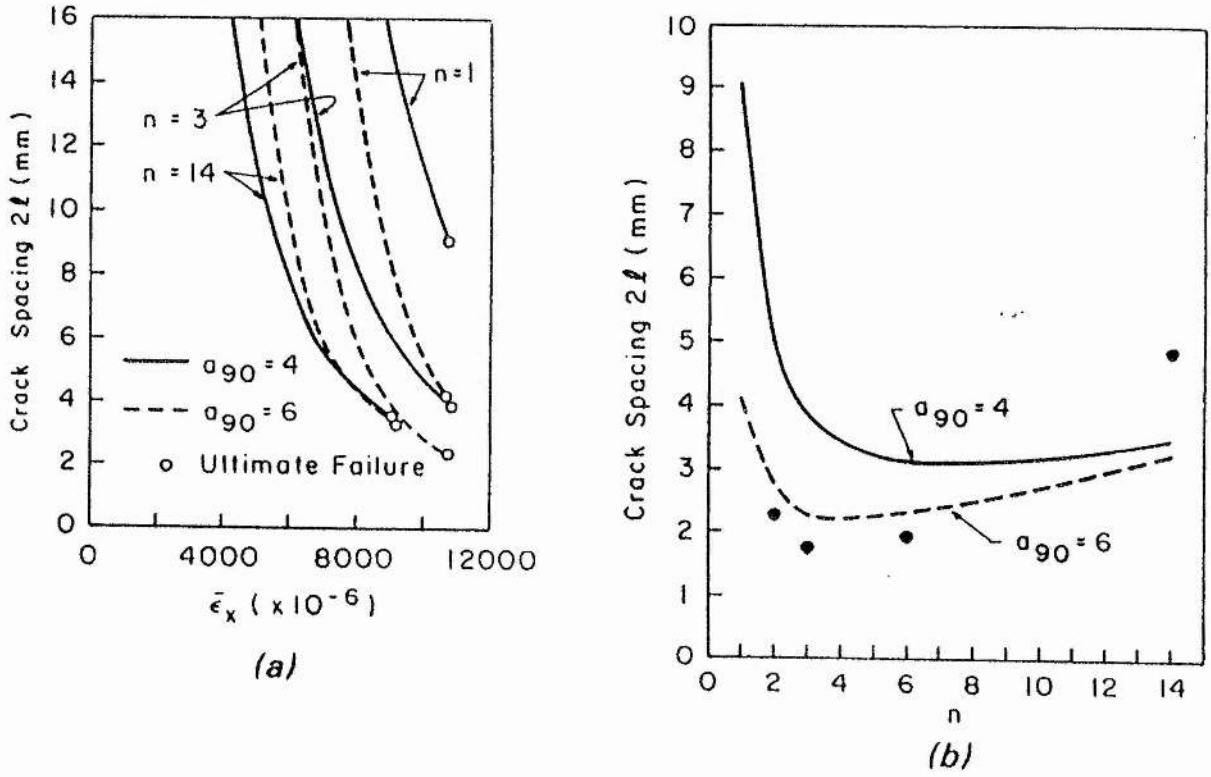

Figure 2.12 Statistical-strength based predictions of the transverse ply crack spacing in $(0_2/90_n)_s$ carbon/epoxy laminates (taken from Fukanaga et al 1984).
(a) Crack spacing as a function of applied strain for different values of transverse ply thickness (n) and Weibull modulus (a_{90}).
(b) Saturation crack spacing as function thickness and Weibull modulus.
---------- predictions by Fukanaga et al
• data from Peters (1983).

CHAPTER 3

MATERIALS AND EXPERIMENTAL METHODS

3.1 SiC/PYREX LAMINATES

3.1.1 Material characterisation

Nicalon SiC fibre reinforced borosilicate (Pyrex) glass laminates all manufactured from pre-preg of thickness ~0.15 mm were provided by Rolls-Royce plc originating from two sources which will be referred to from here on as type I and type II material. A variety of lay-ups were tested; unidirectional, (0/90/0), $(0/90_2)_s$ and $(0/90)_{3s}$ crossplies and several angleply geometries.

Initial microstructures as determined by optical[6] and scanning electron microscopy show the fibre distribution to vary locally in both type I and type II material, i.e. there are large matrix rich regions (Figure 3.1). In addition longitudinal ply fibres are wavy across the ply width (Figure 3.1). A major difference between the two materials is the ease of preparation of polished surfaces. A satisfactory result was achieved for type I samples using a conventional method, unlike type II coupons which exhibited plucked out fibres even though a careful polishing routine based on the Buehler Metlap system was developed (see Appendix 1). This relative ease of polishing is related to the number of inhomogeneities within the matrix of the type II material, which, at higher magnification are visible as discrete crystal type features and are linked by cracks (Figure 3.2). Qualitative x-ray diffractometry (XRD) analysis indicate these features to be the crystalline phase cristobalite, a polymorph of silica, and that a larger volume fraction is present in the type II material. This is discussed in Chapter 4.

3.1.2 Quasi-static tensile testing

Coupon specimens 100 mm long (parallel to the 0° direction) by 15 mm wide were cut from the laminates supplied. Abraded and etched aluminium end tags were bonded onto specimens for ease of gripping in Instron wedge grips. Quasi-static tests were carried out using an Instron 1175 (see Figure 3.3) under displacement control at a crosshead speed

[6] reflected light

of 0.05 mm/min. Longitudinal and transverse strains were measured using strain gauges so that the longitudinal modulus and principal Poisson's ratio could be determined. Some specimens were loaded continuously to failure giving initial tangent values of the modulus and Poisson's ratio. Other specimens were loaded to progressively higher strain levels in order to study damage development. These "discontinuous tests" enabled the progressive change in tangent modulus and principal Poisson's ratio to be determined with applied strain, since in all cases the initial region of the reloading curve was linear.

3.1.3 Compression test method to measure the transverse modulus

An important material parameter when considering the behaviour of laminates is the transverse modulus of a unidirectional lamina E_2. It is not practical to attempt to measure E_2 in tension as failure occurs at very low strains. However, under uniaxial loading conditions the elastic regions of the stress/strain curve in tension and compression are symmetric about the origin (strain) axis for very small strains. As a result a compressive test method has been developed for the measurement of E_2.

Unidirectional tensile coupons 15 mm wide were cut transverse to the fibre direction to prepare samples 15 mm square. Each end was then mounted in a polyester resin block to provide support and to ensure axial loading (Figure 3.4). Strain gauges were bonded onto each face in order to measure longitudinal strain and to assess bending effects. Tests were then carried out at a crosshead speed of 0.05 mm/min and tangent modulus values obtained from the resultant stress/strain data over the range 0 - 0.1% strain. The method of calculation of E_2 is described in Chapter 4.

3.1.4 Damage monitoring techniques

In addition to indirect damage measurements from changes in stiffness and Poisson's ratio as a function of applied strain, direct observations of damage were made using optical and scanning electron microscopy (detecting back scattered electrons) on the

polished edges of tensile coupons. Dye penetrant enhanced (zinc iodide) radiography was also attempted for this purpose but proved unsuccessful due to the crack opening displacements being too small for infiltration to occur readily.

3.2 SiC/CAS LAMINATES

3.2.1 Material characterisation

The materials used for the majority of this study were Nicalon SiC fibre reinforced calcium alumino-silicate (CAS) glass-ceramic matrix laminates manufactured by hot pressing pre-preg. The lay-ups supplied (courtesy of Rolls-Royce plc) were $(0)_{12}$, $(0/90)_s$, $(0_2/90_4)_s$ and $(0/90)_{3s}$ with a nominal ply thickness of 0.18 mm, although this varied by about 10 % from lay-up to lay-up.

Tensile coupons 80 mm by 20 mm were cut from the laminates. Both edges of the coupons were polished carefully (using the Buehler Metlap system - see Appendix 1) and, as can be seen from Figure 3.5, a high grade of finish was obtained. Due to the weak nature of the fibre matrix bond some damage to fibres in longitudinal plies was incurred, but this did not limit the assessment of matrix damage under subsequent mechanical loading. It was observed that the ply thicknesses, fibre diameter and fibre distribution vary considerably. An image analysis technique was used to determine fibre diameter and distribution data in these laminates (see Appendix 2). The results show that the mean fibre diameter is ~16μm and the fibre volume fraction ~34 %. Micro-porosity, in the form of void strings running parallel to the plies, could also be seen, particularly in the $(0_2/90_4)_s$ lay-up. Such voids arise presumably from air and volatiles being trapped between layers of pre-preg during consolidation of the laminate.

3.2.2 Quasi-static tensile testing

Quasi-static tensile testing of the Nicalon/CAS laminates was conducted in a similar way to that for Nicalon/Pyrex laminates, described in section 3.1.2. Abraded and etched aluminium end tags were bonded on to specimens for ease of gripping in wedge grips. Quasi-static tests were carried out using an Instron 1175 under displacement control at a crosshead speed of 0.05 mm/min. Longitudinal and transverse strains were measured

using strain gauges so that the modulus and Poisson's ratio could be determined. Some specimens were loaded continuously to failure giving initial tangent values of modulus and Poisson's ratio. Other specimens were used in "discontinuous tests" in which they were loaded to progressively higher strain levels in order to study damage development. These tests also enabled the progressive changes in secant stiffness properties with applied strain (and extent of damage) to be determined.

3.2.3 Quasi-static cycling and fatigue testing

Quasi-static cycling tests were carried out by cycling laminates between zero and the maximum stress at a crosshead speed (CHS) of 0.05 mm/min using a quasi-static Instron 1175 machine. Stress/strain hysteresis loops were recorded for each loading and unloading cycle. This also allowed a secant stiffness value to be measured as a function of cycles. Periodically specimens were removed from the Instron and crack density measurements made on the polished coupon edges. Specimens were then replaced and cycling continued. This procedure was repeated until the crack density, stress/strain behaviour and associated stiffness loss had stabilised.

After low cycle quasi-static cycling, specimens were placed in a servo-hydraulic Instron 1341 fatigue machine (Figure 3.6) and fatigued at a frequency of 10 Hz. Testing was carried out in a controlled environment of temperature (20°C) and humidity (50%) in order to minimise static fatigue effects that have been reported widely to occur in glasses and glass ceramics (e.g. McMillan, 1979 and Weiderhorn et al 1982). A ratio of minimum to maximum stress of 0.1 was selected to avoid compressive stresses being introduced. Each specimen was removed after 100, 1000, 10 000, 100 000 and 1 000 000 cycles in order to monitor the crack density. A loading and unloading loop was also measured using the static Instron at the slow strain rate (cross-head speed = 0.05 mm/min). This enabled the stress/strain hysteresis and secant stiffness before and after each fatigue interval to be compared.

3.2.4 Damage monitoring techniques

Direct observations of matrix cracking were made using optical and scanning electron microscopy of the polished coupon edges. As the residual opening of the cracks was very small, the coupons were placed in a straining stage after each load cycle and a small strain applied (< 0.05 % for loading cycles > 0.06 %) to open the cracks (Figure 3.7). When placed under the optical microscope, cracks were identified clearly at magnifications of 50 to 100 times. Crack densities were determined by counting the number of cracks in a gauge-length of about 15 mm except for the $(0_2/90_4)_s$ laminate, which has larger crack spacings in the 90_8 plies, where a gauge-length of 50 mm was used.

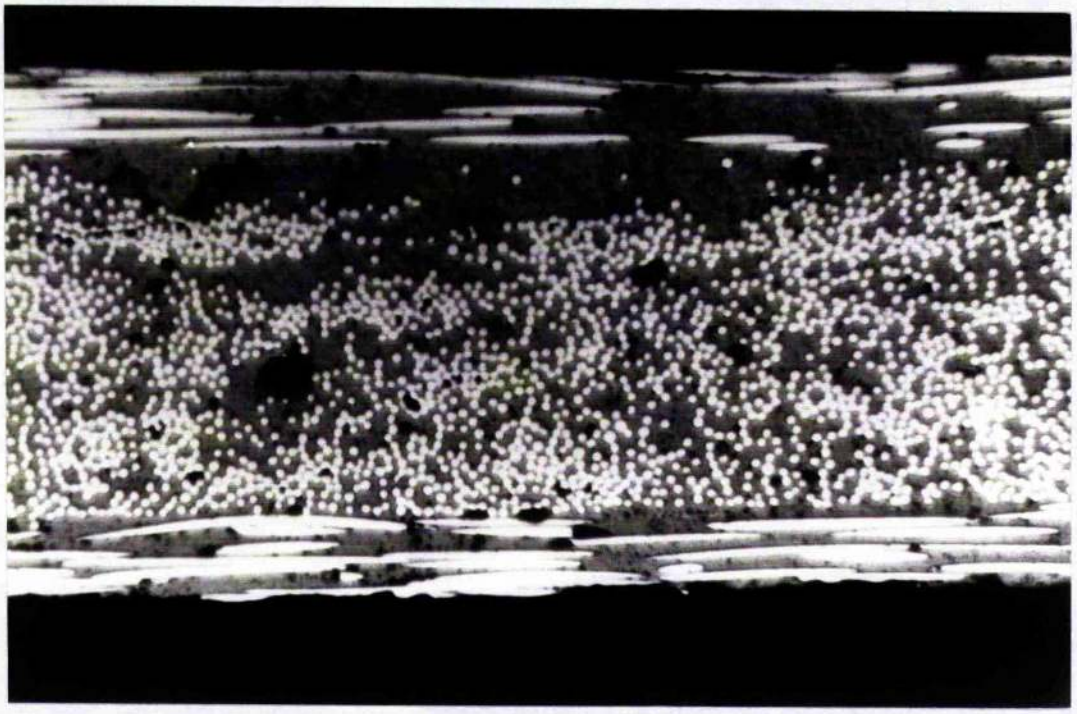

(a)

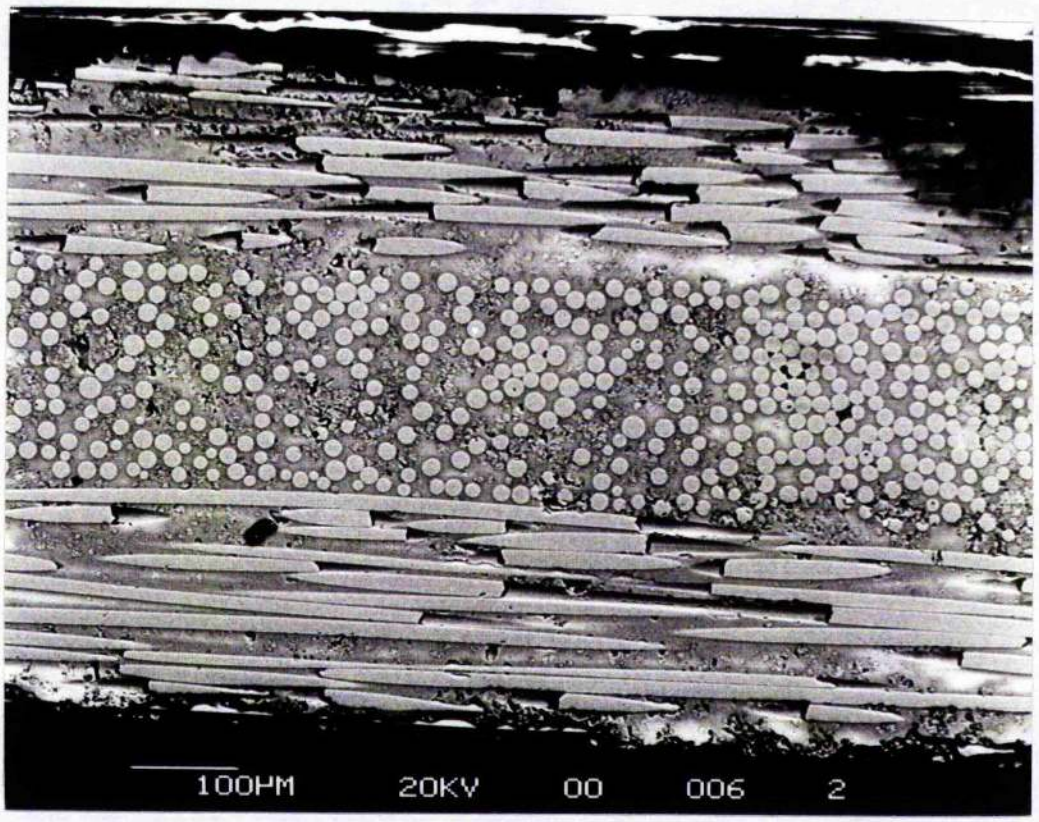

(b)

Figure 3.1 Polished sections of Nicalon/Pyrex reinforced crossply laminates:
(a) Type I
(b) Type II.

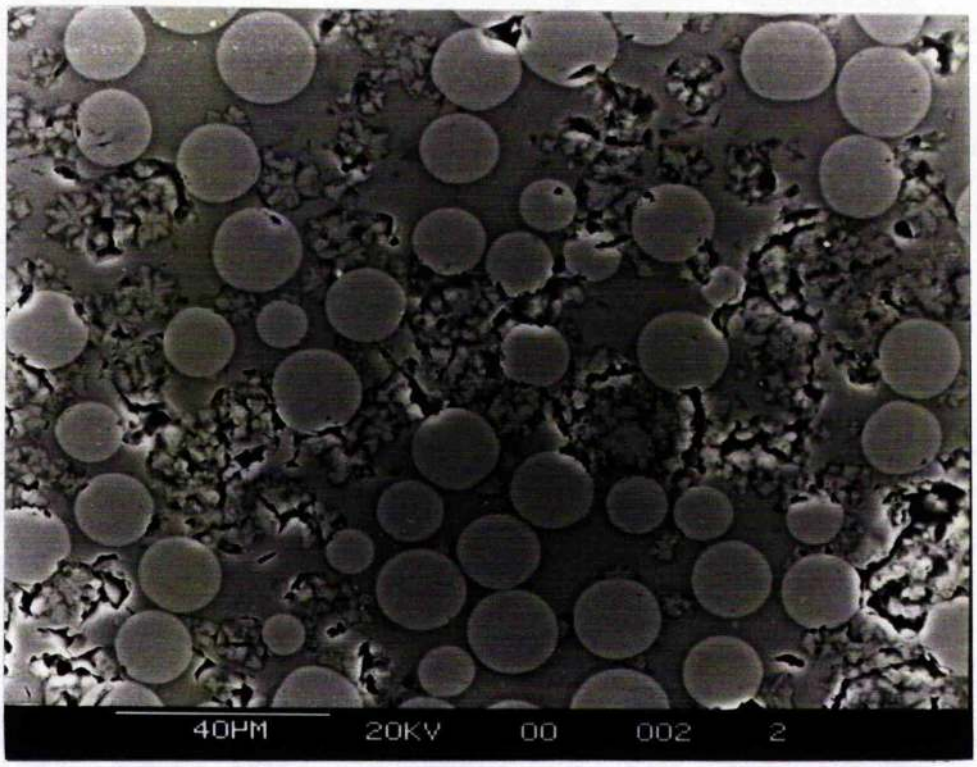

Figure 3.2 Transverse ply of a crossply laminate type II material showing cristobalite regions and the variation in fibre diameter.

Figure 3.3 Quasi-static testing of tensile coupons using an Instron 1175.

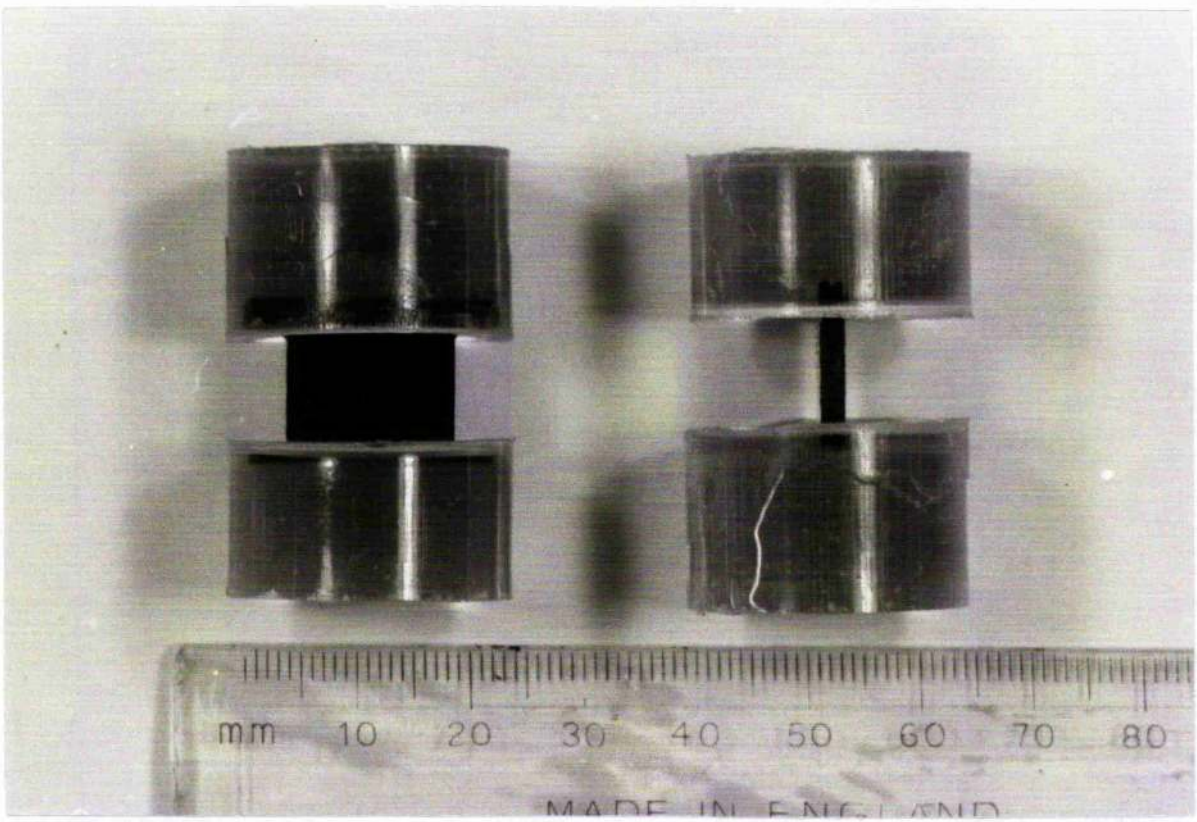

Figure 3.4 Compression test specimen for measuring the transverse modulus E_2.

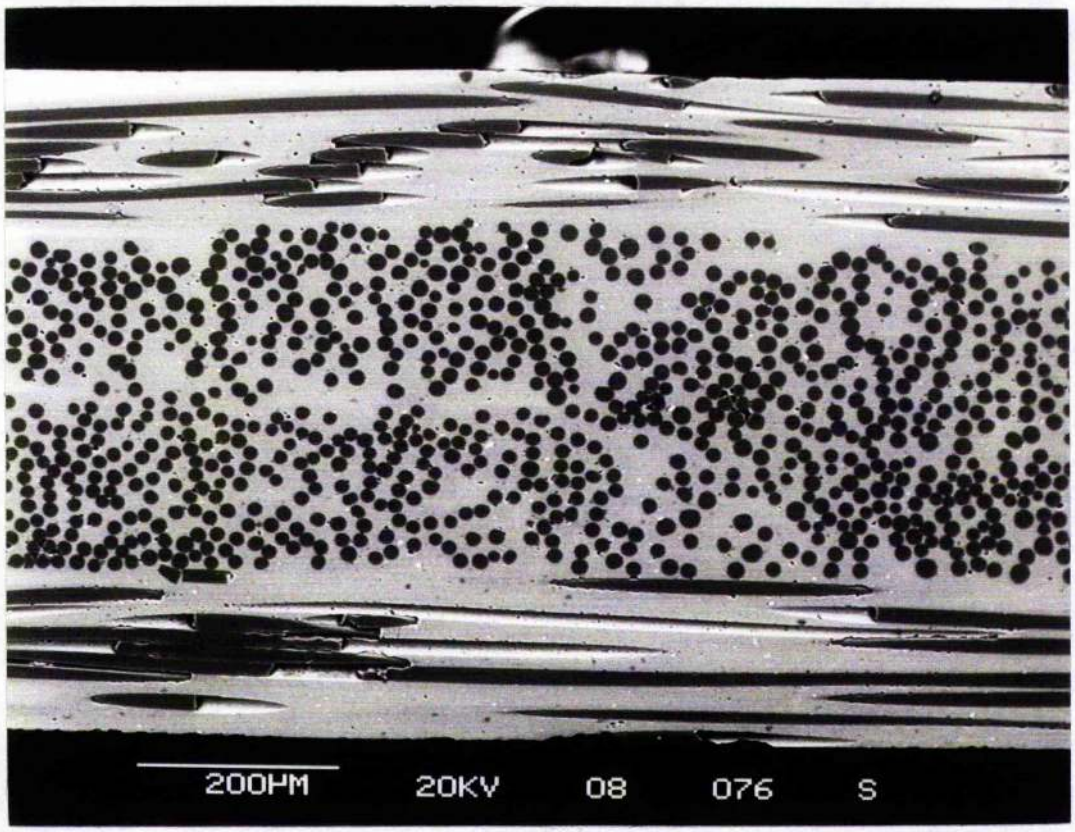

Figure 3.5 Polished edge section of a Nicalon/CAS $(0/90)_s$ laminate showing fibre diameter and distribution variation.

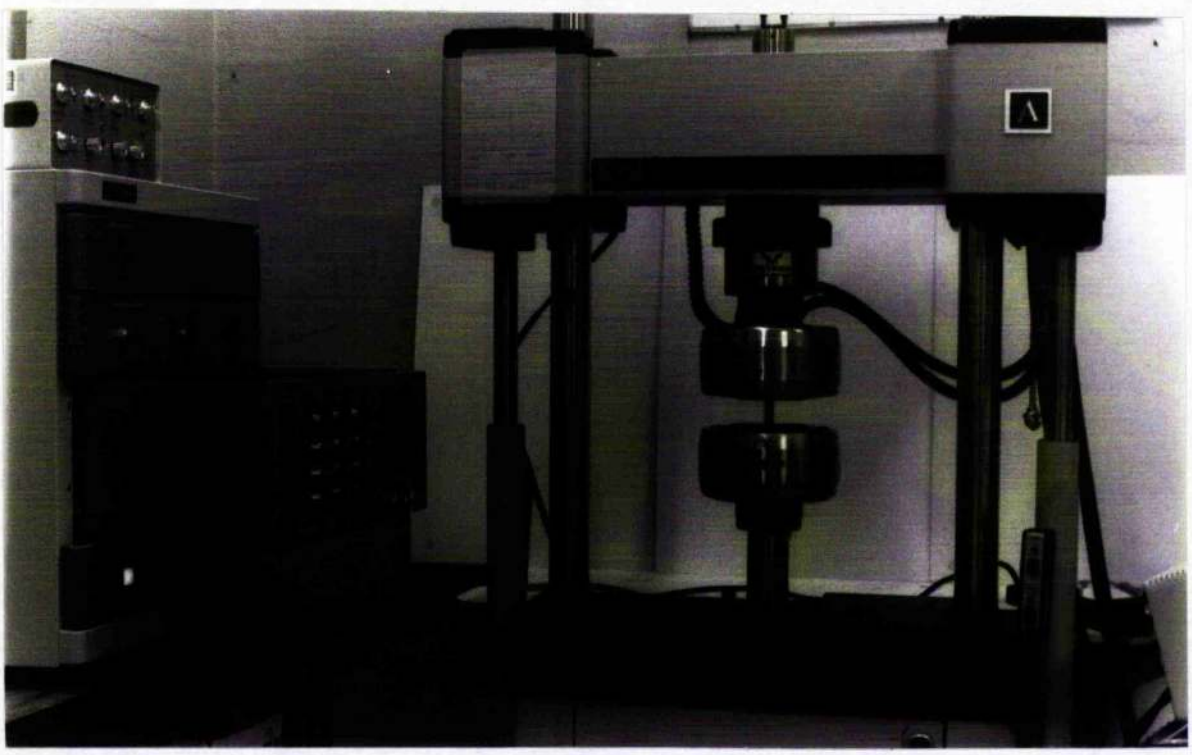

Figure 3.6 Fatigue testing of tensile coupons using an Instron 1341.

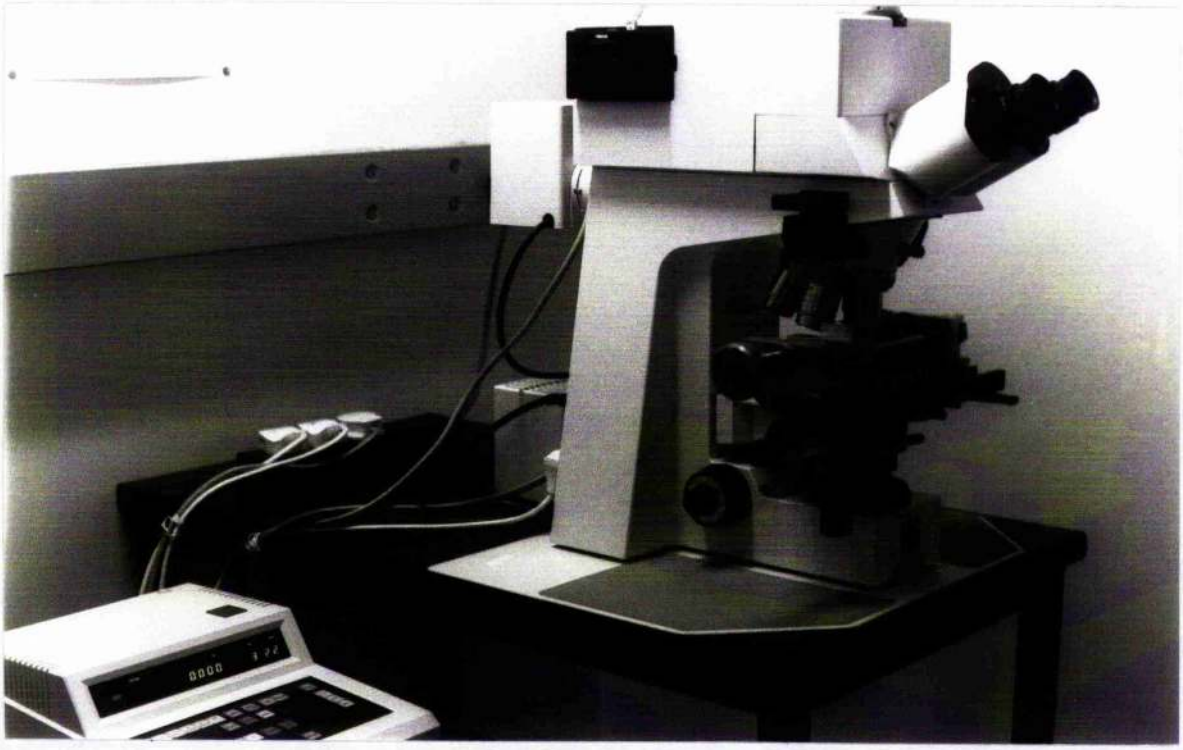

Figure 3.7 Direct observation of damage in Nicalon/CAS laminates using a straining stage in conjunction with an optical microscope.

CHAPTER 4

QUASI-STATIC BEHAVIOUR OF NICALON REINFORCED PYREX LAMINATES

4.1 INTRODUCTION

An increasing amount of literature is now becoming available concerning the mechanical properties of Nicalon/Pyrex laminates (e.g. Ford et al 1987, Dawson et al 1987, Seerat un Nabi and Derby 1988 and Davidge and Briggs 1989). These studies refer to optimised Nicalon/Pyrex properties. Recently a number of studies have highlighted some problems associated with the processing of these laminates, namely, matrix crysallisation (Murty and Lewis 1989 and Bleay and Scott 1991).

In the present chapter the quasi-static tensile behaviour of SiC/Pyrex laminates is reported. Stiffness properties as a function of applied strain are measured and correlated with observed matrix damage. The mechanical properties are found to be strongly influenced by the presence of crystalline regions in the matrix which promote microcracking. Laminated plate theory is used to predict the moduli of the laminates investigated.

4.2 QUASI-STATIC TENSILE BEHAVIOUR

4.2.1 Stress/strain behaviour

The data for the initial longitudinal moduli, principal Poisson's ratio and the failure stresses and strains for all lay-ups tested are shown in Table 4.1. Also shown are the predictions based on laminated plate theory and discounted laminated plate theory which are discussed in Section 4.4. Of particular interest is the difference in properties between type I and type II material of the same lay-up. Unidirectional type II material show a 30% improvement in tensile modulus and an increase of 50% in ultimate strength and failure strain over type I samples. However for the $(0/90_2)$s lay-up it is the type I coupons which have the superior properties.

Type II material was used to assess the effect of lay-up on properties. Typical stress/strain curves for a unidirectional, a crossply and an angleply laminate are shown in Figure 4.1. All three curves are non-linear from zero strain and show no well defined elastic region the limit of which is normally recognised by a knee or discontinuity. In addition both crossply and angleply laminates display low failure strains compared to the unidirectional material. Figures 4.2a and 4.2b show the variation of tangent modulus and principal Poisson's ratio respectively with applied strain for the unidirectional and a number of crossply laminates. At 0.3% strain (for example) the unidirectional material shows a 5% reduction in modulus and a 10% reduction in Poisson's ratio. The elastic properties of crossply specimens are also degraded at this strain with (0/90/0) coupons exhibiting a 30% stiffness loss and over 40% reduction in Poisson's ratio. Similar curves of stiffness and principal Poisson's ratio reductions are shown in Figure 4.3 for the three different 45° angleply laminates tested.

4.2.2 Damage observations

Observations of damage on type II material at various strain levels show that for crossply

and angleply laminates matrix cracking occurs in the off axis plies in a dispersed manner with cracks branching in all directions (Figure 4.4). There is no apparent strain onset for this kind of behaviour, although at low strains it is difficult to distinguish such cracks from polishing damage. Outer longitudinal plies and unidirectional laminates also show dispersed cracking behaviour but only at strains near to or at failure (Figure 4.5).

In only one case was a classical off axis ply cracking pattern (of the sort seen in polymer matrix composites e.g. Highsmith and Reifsnider 1982) observed. This was for a (0/45/0) specimen which developed a region of cracks at a strain of 0.05% that spanned the ply thickness at an angle of ~30° to the longitudinal fibres (Figure 4.6). These cracks did not propagate or increase in density with additional strain, whilst other areas of the same ply developed a dispersed cracking pattern.

Final failure of the crossply laminates was generally planar. By comparison the laminates containing 45° plies failed by a mixture of fibre failure, matrix cracking and delamination.

4.3 E_2 MEASUREMENTS

Load/strain readings from the back to back gauges during a compression test are shown in Figure 4.7. If a state of pure compression had been achieved, these gauges should have given identical values. However, this is clearly not the case with barely any response from the gauge on face B, which is due to specimen bending being superposed onto the applied compression. As a simple approximation we consider the effective loading to be as shown in Figure 4.8.

An expression for the transverse modulus may now be obtained by considering the stresses acting on each face. The stress on face A is given by:

$$\sigma_A = \frac{P}{A} + \frac{My}{I} \qquad (4.1)$$

where P = applied load
A = cross sectional area (= bt)
M = bending moment (= Pe)
y = distance from specimen face to neutral axis
I = second moment of area

or

$$\sigma_A = \sigma_{nom} + \frac{\left(Pe\frac{t}{2}\right)}{\left(\frac{bt^3}{12}\right)} = \sigma_{nom} + \frac{6Pe}{bt^2} \qquad (4.2)$$

where e = eccentricity
σ_{nom} = nominal applied stress

Similarly, the stress on face B is

$$\sigma_B = \sigma_{nom} - \frac{6Pe}{bt^2} \qquad (4.3)$$

Hence

$$\epsilon_A = \frac{1}{E_2}\left(\epsilon_{nom} + \frac{6Pe}{bt^2}\right) \quad (4.4)$$

and

$$\epsilon_B = \frac{1}{E_2}\left(\epsilon_{nom} - \frac{6Pe}{bt^2}\right) \quad (4.5)$$

Adding and rearranging gives

$$E_2 = \frac{2\sigma_{nom}}{\epsilon_A + \epsilon_B} \quad (4.6)$$

Applying equation 4.6 to the test results gives E_2 values in the range 45 to 55 GPa.

4.4 DISCUSSION

4.4.1 Matrix crystallisation

The characterisation of type I and type II materials by microscopy and XRD analysis clearly shows type II material to have a greater cristobalite content. The crystallisation of glass in glass matrix composites is not uncommon as has been demonstrated by Brennan (1986), who found lithium alumino silicate (LAS) and mullite crystals dispersed in the matrix of as-pressed SiC/LAS composites. Such crystals were few and sufficiently small in volume that they did not affect the integrity of the matrix. However, a study by Murty and coworkers (1989) on the present material has highlighted that the difference in thermal expansion coefficients between cristobalite (2.7×10^{-5} C^{-1}) and parent borosilicate glass (3.3×10^{-6} C^{-1}) is an order of magnitude. It therefore appears that during laminate proccessing, on cooling from the consolidation temperature the interface region between parent glass and a cristobalite crystal is flawed if not already cracked as a result of thermal stresses so reducing the integrity of the matrix. A recent study by Bleay and Scott (1991) also suggests that microcracks form in this way. In their work quantitative EDS[7] measurements on type II material indicate that the volume fraction of matrix cristobalite is ~45%. The likely effect on the mechanical properties is discussed below.

4.4.2 Elastic properties of the laminates

We consider first the elastic properties of a unidirectional lamina. The modulus parallel to the fibre direction, E_1, was measured as 106.7 GPa. From the rule of mixtures expression:

$$E_1 = E_f V_f + E_m(1 - V_f) \qquad (4.7)$$

If we take the modulus of the Pyrex glass as 65 GPa, then using the measured E_1 value and the fibre volume fraction as 0.35 we estimate the modulus of the fibre to be

[7] energy-dispersive X-ray spectrometry

184 GPa. This is within the manufacturer's quoted range of 180 - 200 GPa (Prewo 1986). This suggests that at least for type II unidirectional plate, the initial longitudinal modulus is not degraded by any cristobalite present.

The mean transverse modulus of the unidirectional material E_2, measured by the compression technique was 50 GPa. The Reuss approximation is

$$E_2 = \frac{1}{\frac{V_f}{E_f} + \frac{(1 - V_f)}{E_m}} \qquad (4.8)$$

and predicts a value for E_2 of 84 GPa (based on E_m = 65 GPa; E_f = 190 GPa and V_f = 0.35). An alternative approach would be to assume that E_2 is controlled by the matrix [i.e. $E_2 = (1\text{-}V_f)E_m$]. This suggests a value for E_2 of 42 GPa which is much closer to the measured values.

The four elastic constants required for laminated plate theory (LPT) calculations are E_1, E_2, υ_{12} (the principal Poisson's ratio) and G_{12} (the in-plane shear modulus). E_1 and υ_{12} were measured from unidirectional laminates tested in tension (values are shown in Table 4.1) while E_2 was measured using the compression technique. The in-plane shear modulus G_{12} was estimated from the fibre and matrix properties using the Halpin-Tsai equations (see Agarwal and Broutman 1980) to be 33 GPa. The values of the elastic constants were then used in LPT to predict the longitudinal modulus and principal Poisson's ratios of the various type II material lay-ups tested, which are shown in Table 4.1. For all the lay-ups LPT overestimates the modulus, for some laminates by as much as 60%. It is suggested that this is due to the presence of the cristobalite phase, ie the matrix is effectively damaged prior to loading and therefore does not contribute fully to the laminate stiffness.

To investigate this further an approximate "ply discount" analysis was carried out. In this calculation cracked off axis plies are assumed to have zero transverse and shear stiffness as a result of cristobalite associated cracking, whilst the longitudinal plies are assumed to retain those properties measured from the unidirectional plates. Hence the LPT calculation is carried out as before but with the reduced stiffness terms Q_{12}, Q_{22} and Q_{66}

set to zero for the 10°, 45° and 90° plies. The predictions for the longitudinal modulus and principal Poisson's ratio of the various lay-ups using this method are also shown in Table 4.1; note the predictions for the modulus are not very different from those that would be obtained by assuming that the modulus of a laminate is governed solely by the volume fraction of 0° plies. Although some lay-ups show moduli which are in much better agreement with these discounted LPT values, most lay-ups show moduli which lie somewhere between the full LPT and discounted LPT values (the one exception is the (0/10/-10/0) laminate which had a low measured E_L; this may be an anomalous result, though it could be due to stretch/twist coupling which was ignored in the LPT calculation). These results suggest that the amount of cristobalite present varied from laminate to laminate and whilst in some it led to extensive cracking prior to testing, in others it was less significant.

4.4.3 Damage development under tensile loading

Observations of damage in type II material were made in an attempt to correlate the amount of visible damage with reductions of modulus and principal Poisson's ratio. Whilst the contribution due to fibre breaks is unclear, it is evident that matrix cracking is the dominant failure mechanism involved. This is believed to be the cause of the non-linearity of the stress vs strain curves, even for the unidirectional material the behaviour of which may be contrasted with unidirectional SiC/LAS laminates investigated by Prewo (1986). Here two LAS formulations were employed as the matrix in two sets of unidirectional laminates. Results showed one set to be linear elastic to failure with a failure strain of <0.4%. The other set were linear to around 0.3% strain but non-linear thereafter which Prewo attributed to matrix cracking. The type II SiC/Pyrex unidirectional material of the present study gave similar ultimate strength and failure strain values as this second set. However, in contrast no such initial linear response was recorded.

An explanation for the behaviour of the SiC/Pyrex material may be offered by considering the flaws around cristobalite crystals from laminate processing. On loading,

such flaws link to form a network of cracks which results in non-linear behaviour and the absence of an elastic limit, even at small applied loads. The crack network then continues to open with increasing load, although due to its dispersed nature it is difficult to monitor especially for unidirectional material. The effect of this microcracking on the stiffness properties of the unidirectional material can be seen in Figure 4.2. These data are consistent with the results of a recent study by Habib et al (1990) which shows that initial cristobalite associated microcracking results in a lateral expansion of Nicalon/Pyrex unidirectional laminates which counters the normal Poisson contraction.

The microcracking phenomenon also occurs in the off-axis plies of crossply and angleply laminates. In these layers cracking appears to begin at lower applied strains (as shown by the stiffness property degradation curves); this may be because of stress concentrations at the fibre matrix interface, especially if the fibre and matrix are weakly bonded.

As cracking develops both the longitudinal modulus and principal Poisson's ratio decrease markedly for all lay-ups (see Figures 4.2 and 4.3). Referring to Figure 4.2 for the crossply laminate family we see that modulus and Poisson's ratio reductions of up to about 30% and 50% respectively (depending on lay-up) occur prior to failure. For any given lay-up, similar trends for the degradation of either parameter are observed. When comparing two lay-ups it is difficult to draw any conclusions with regard to the relative rates at which the properties degrade with applied strain, since the initial amounts of cristobalite associated damage varies from lay-up to lay-up. Figure 4.3 shows that the stiffness properties of the laminates containing 45° plies are also degraded significantly prior to failure.

It is interesting to note that the stiffness changes are, generally speaking, much larger for SiC/Pyrex laminates than would be the case for their glass or carbon fibre counterparts. The reason for this is that the ratio E_f/E_m is considerably smaller for SiC/Pyrex than for glass or carbon fibre/polymer systems. This means that matrix damage has a greater effect on overall properties. Another difference between polymer systems and the SiC/Pyrex system is that fully formed off-axis ply cracks (i.e. cracks that span the width and thickness of an off-axis ply) are rarely seen in the SiC/Pyrex system. This is because

matrix damage occurs prematurely in a dispersed manner. If the crystalline regions were not present one would anticipate that fully formed off-axis ply cracks would develop.

4.5 CONCLUSIONS

The mechanical properties of SiC/Pyrex composite laminates are influenced strongly by the presence of matrix cristobalite and associated cracks that are formed during laminate processing. As a result stress/strain behaviour is non-linear with cracks linking to form a dispersed network with increasing applied strain. Moduli are degraded by as much as 40% (depending on lay-up) prior to failure.

The transverse modulus of the unidirectional material has been measured using a compression technique. This, together with other unidirectional properties have been used to predict the elastic constants for crossply and angleply laminates by laminated plate theory. These calculations are not straightforward as degraded principal stiffness properties have to be used to allow for the initial damage.

LAY-UP	MEASURED VALUES				LPT		DISCOUNT	
	E_L (GPa)	ν_L	σ_u (MPa)	e_u (%)	E_L (GPa)	ν_L (%)	E_L (GPa)	ν_L (%)
Type I $(0)_8$	84.7	0.20	450.4	0.68	-	-	-	-
$(0/90_2)_s$	52.2	0.10	109	0.30	-	-	-	-
Type II $(0)_8$	106.7	0.17	706.2	1.04	-	-	-	-
(0/90/0)	70.2	0.12	133.9	0.25	89	0.13	72	0.09
$(0/90_2)_s$	45.7	0.03	77.9	0.23	72	0.10	36	0.03
$(0/90)_{3s}$	69.6	0.09	271.8	0.75	81	0.11	54	0.06
(0/45/0)	79.9	0.22	180.3	0.25	96	0.16	75	0.29
$(0/45)_s$	83.2	0.15	173.4	0.31	91	0.15	57	0.35
(0/45/-45/0)	81.3	0.19	158.3	0.25	92	0.16	60	0.44
(45/0/45)	64.2	0.15	71.4	0.12	85	0.13	39	0.40
(0/10/-10/0)	84.2	0.09	303.7	0.34	106	0.17	104	0.23
$(0/10)_s$	102.5	0.15	267.3	0.41	106	0.17	100	0.22

Table 4.1 Tensile data and LPT predictions for all Nicalon/Pyrex laminates tested.

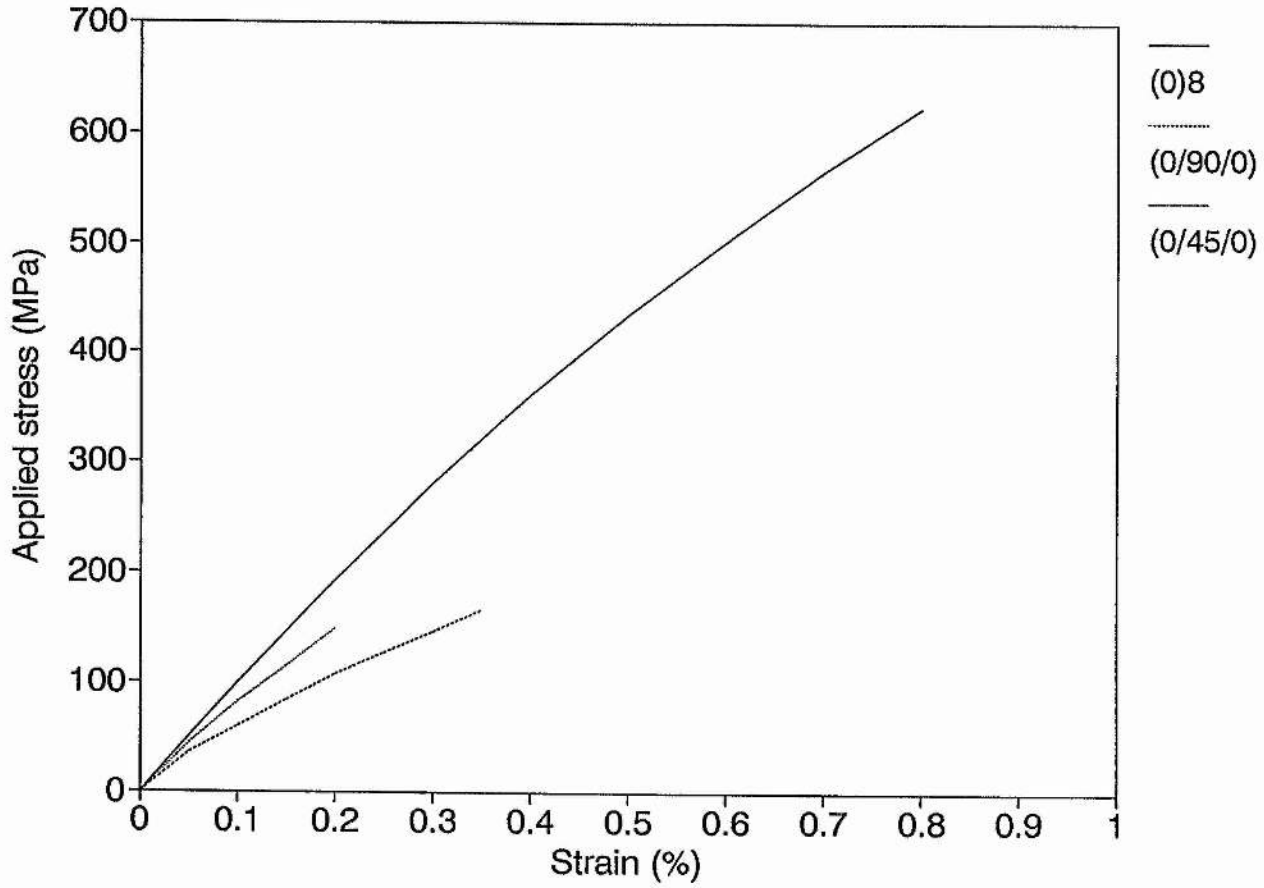

Figure 4.1 Typical stress/strain curves for unidirectional, crossply and angleply type II material.

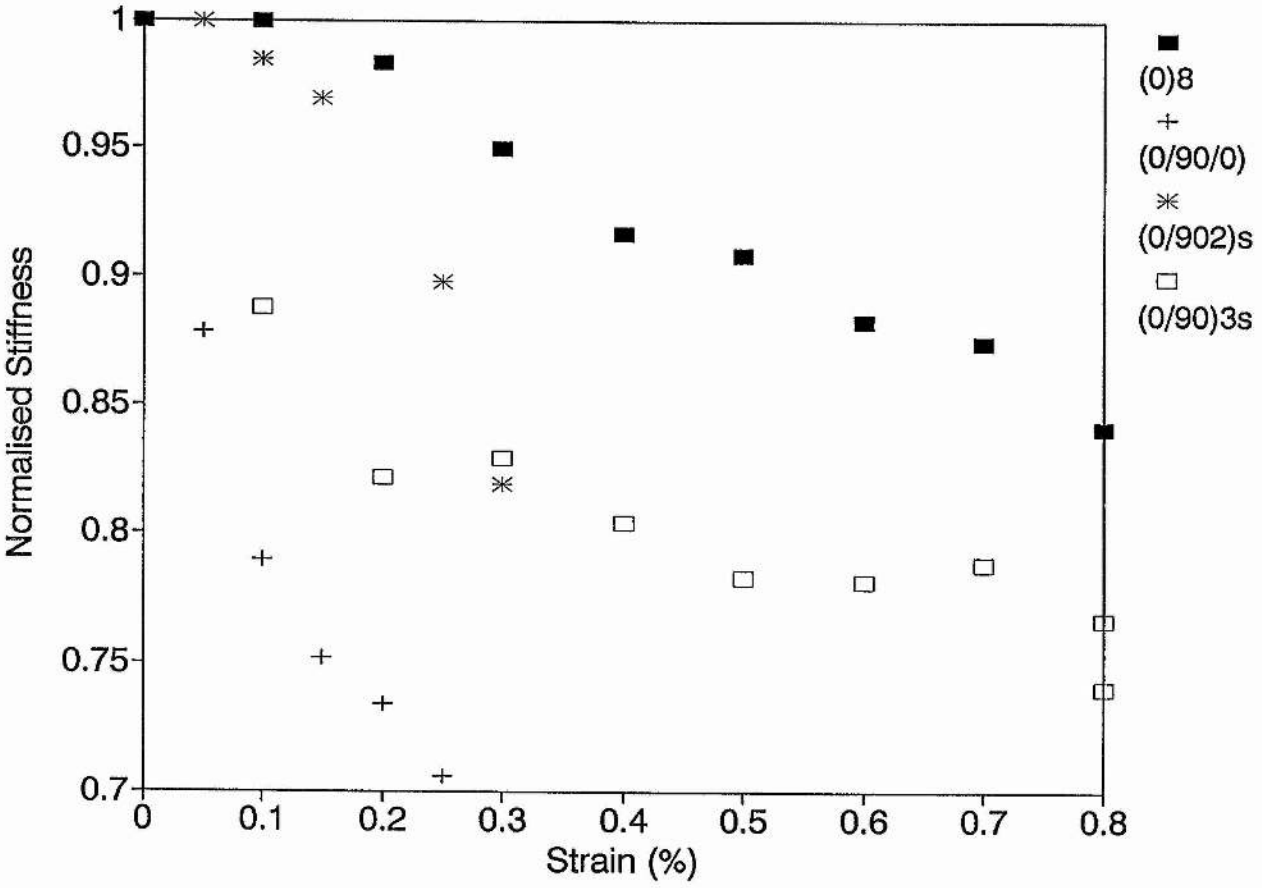

Figure 4.2 Reduction in elastic properties of unidirectional and crossply type II material (a) longitudinal modulus

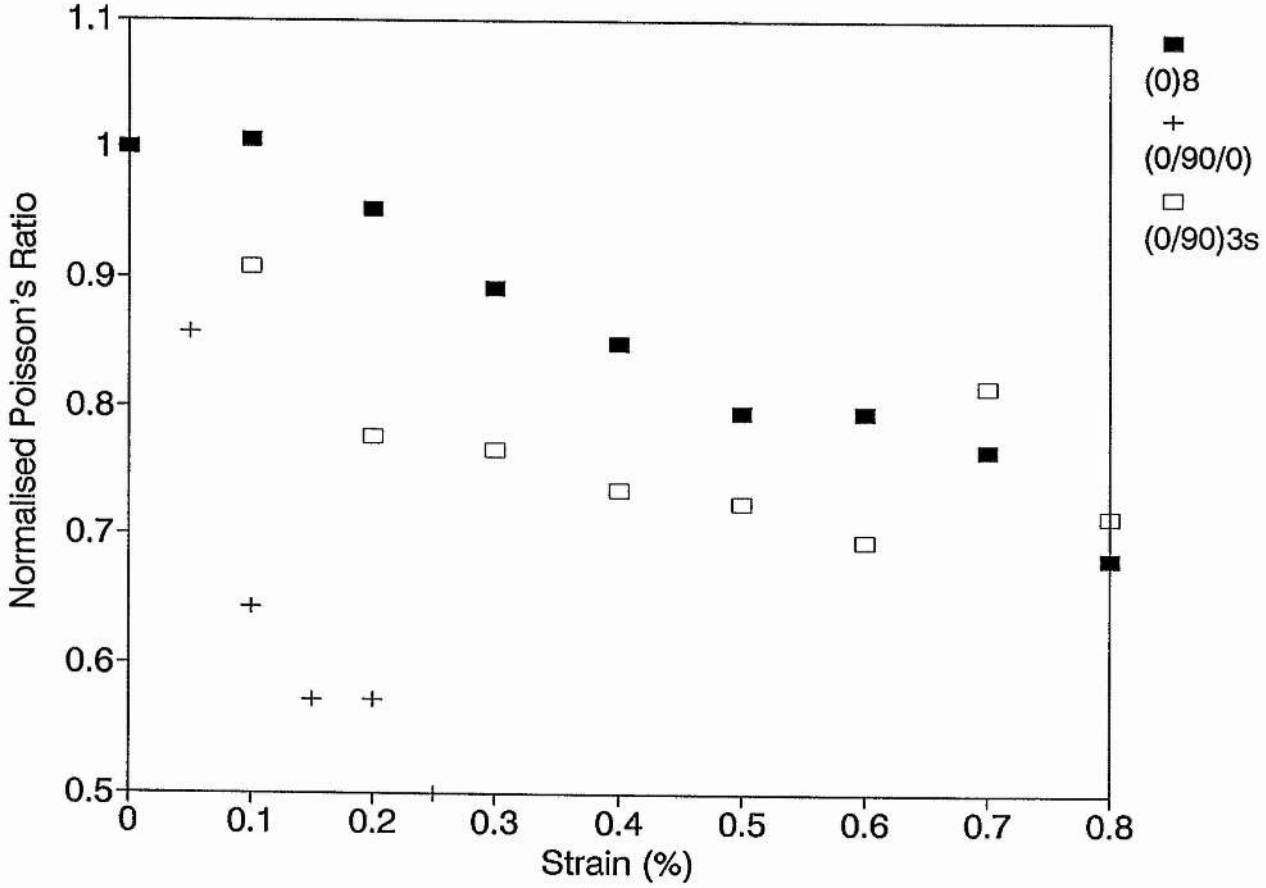

(b) Poisson's ratio.

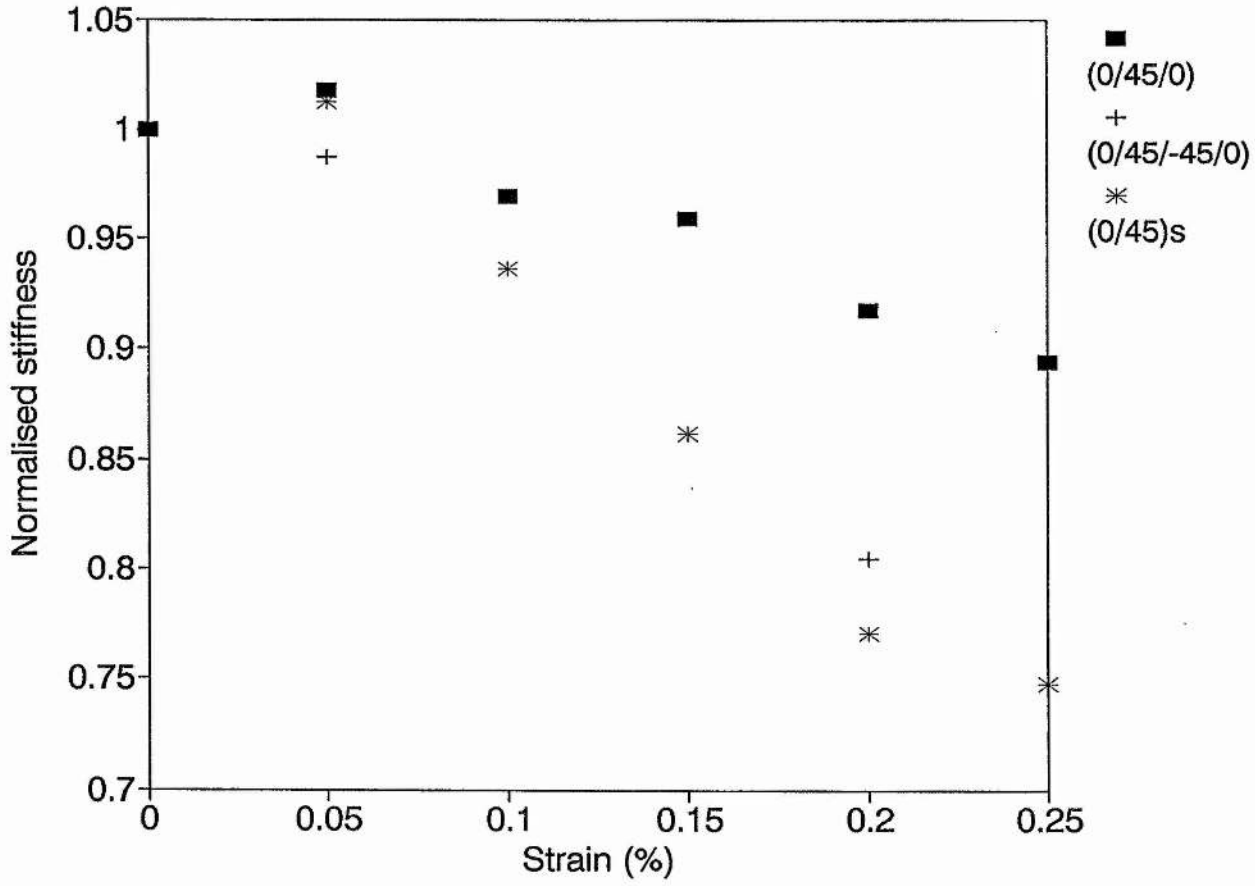

Figure 4.3 Reduction in elastic properties of angleply type II material
(a) longitudinal modulus

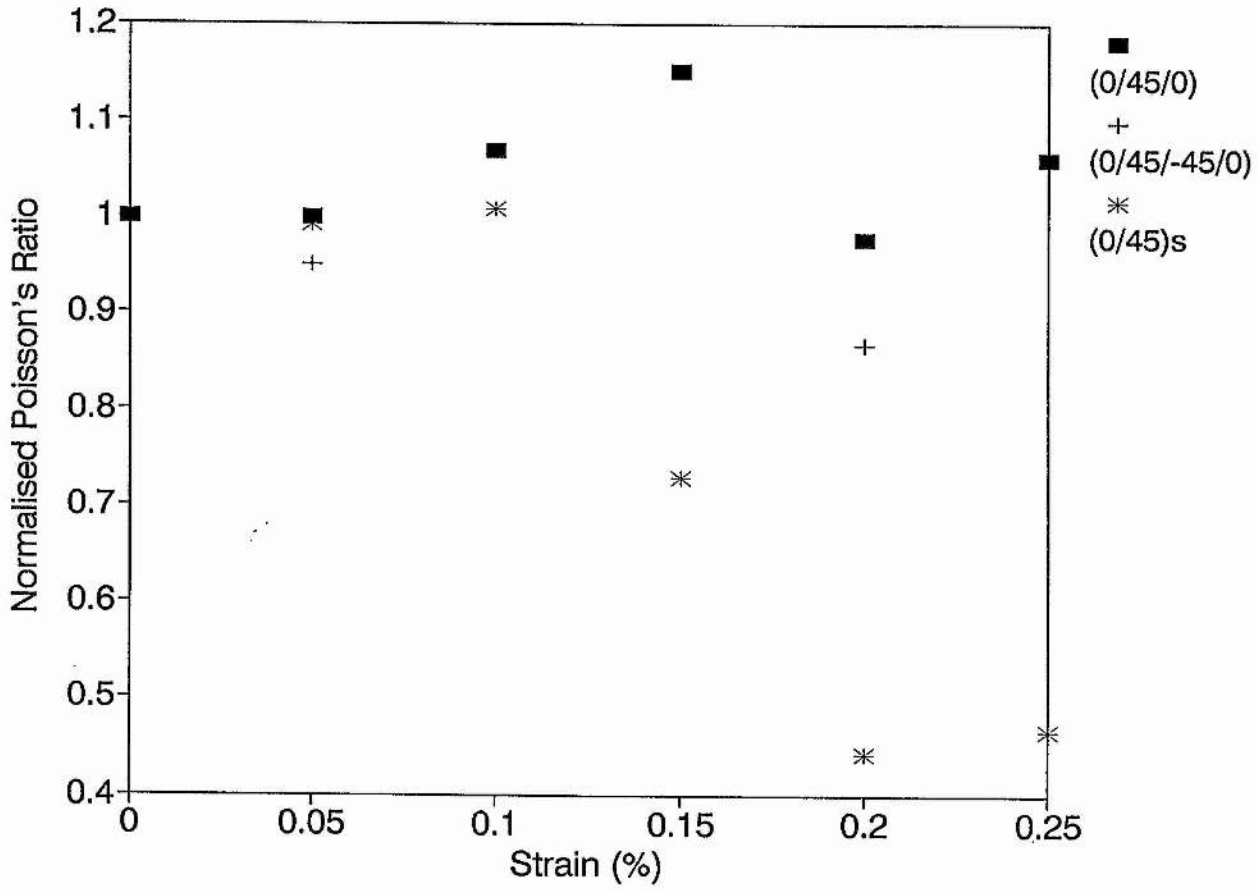

(b) Poisson's ratio.

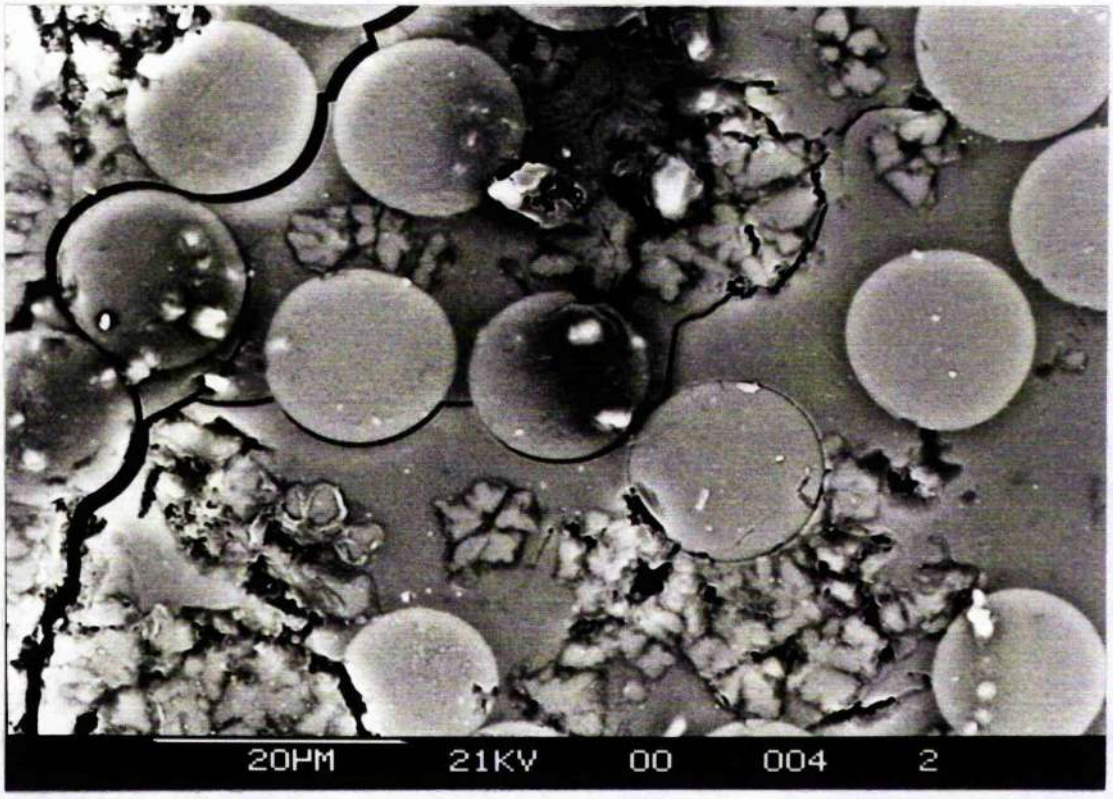

Figure 4.4 Damage in the transverse ply of a (0/90/0) type II laminate showing dispersed cracking.

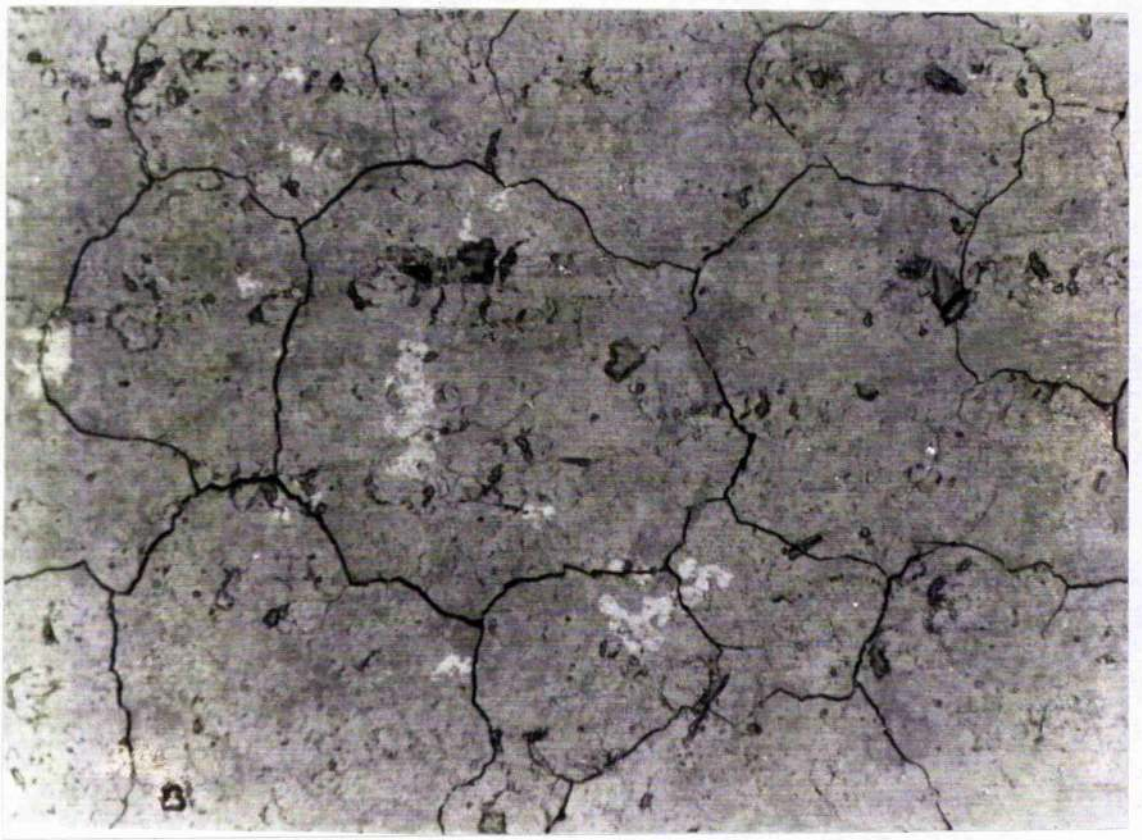

Figure 4.5 Crack network on the surface of the 0° ply of the (0/90/0) laminate after failure.

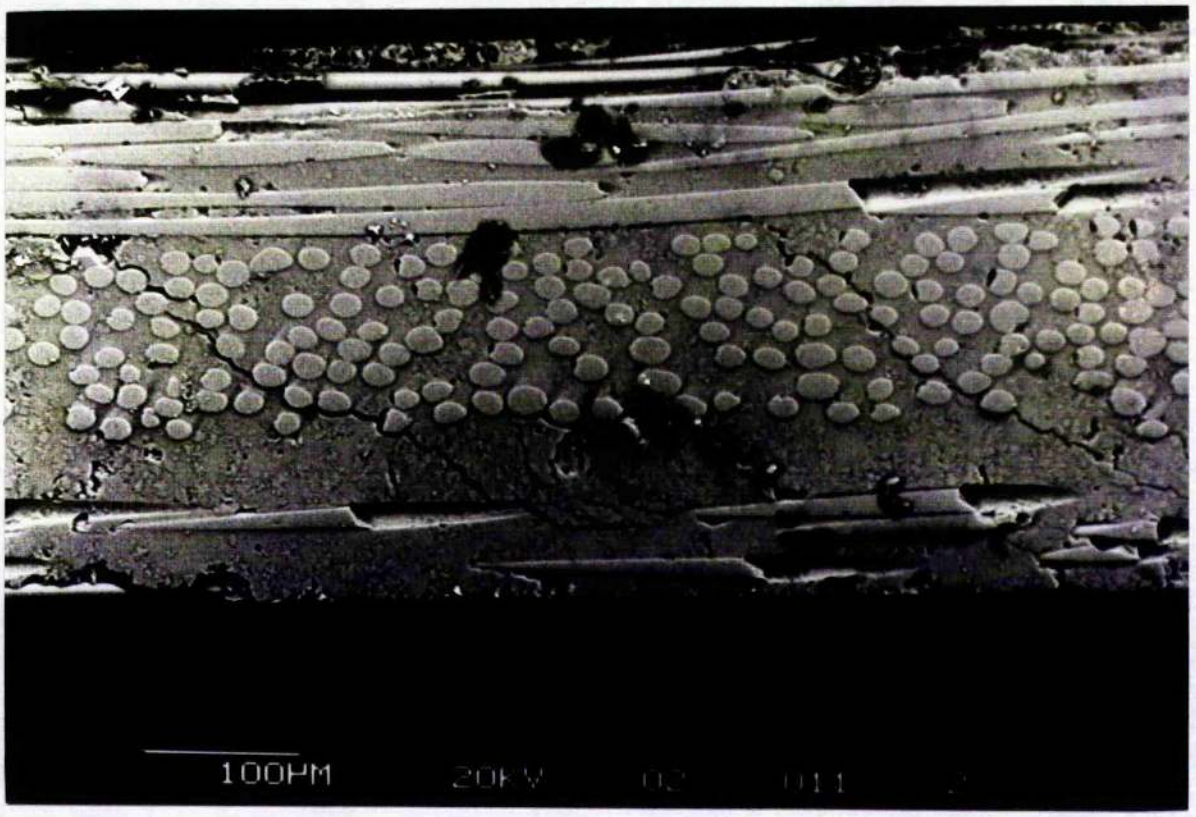

Figure 4.6 Full thickness off-axis cracks in a (0/45/0) laminate at 0.05% strain.

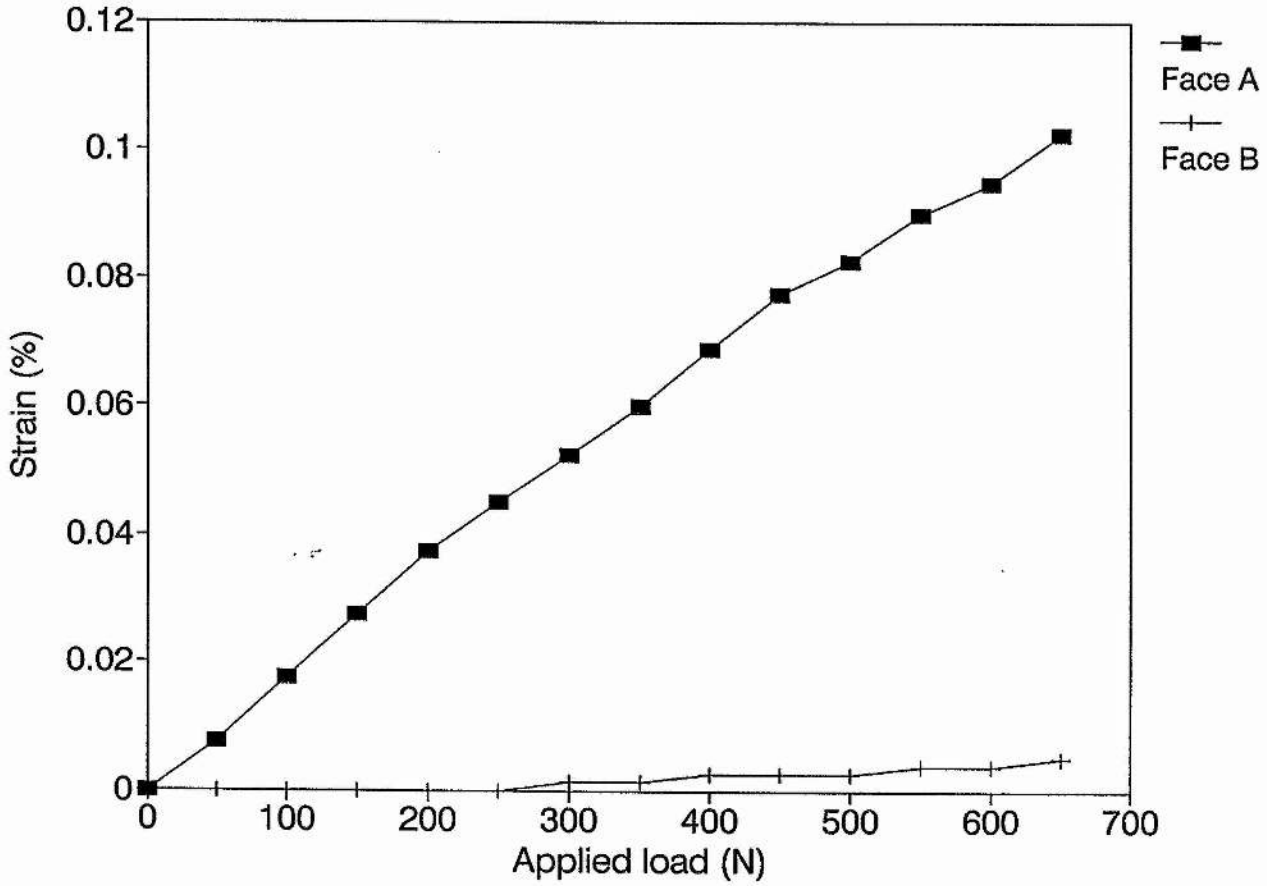

Figure 4.7 Load/strain curves for the measurement of E_2.

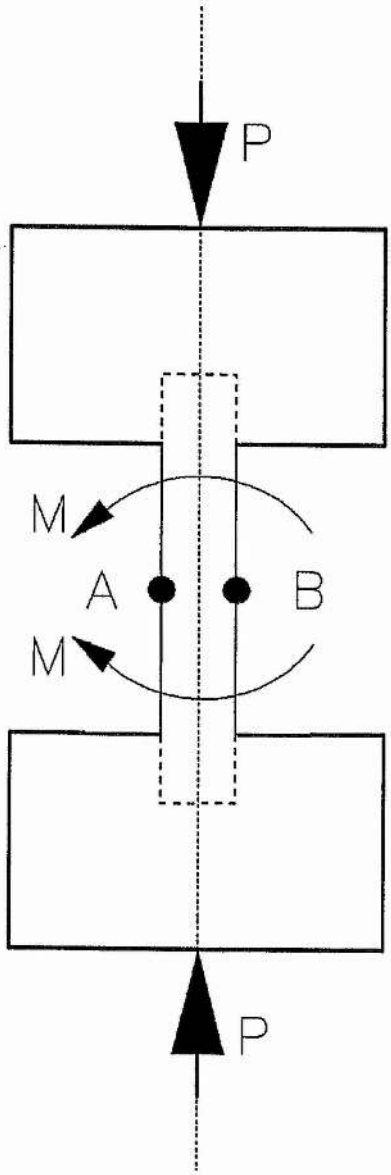

Figure 4.8 Schematic diagram of a loaded E_2 specimen.

CHAPTER 5

QUASI-STATIC BEHAVIOUR OF NICALON REINFORCED CAS LAMINATES

5.1 INTRODUCTION

For continuous fibre ceramic matrix composites (CMC) to be used in engineering applications a knowledge of and capability to model their mechanical behaviour are obviously of great importance. As outlined in Chapter 2, there are already in the literature a number of models which consider the cracking behaviour of unidirectional fibre reinforced brittle matrix materials loaded parallel to the fibre direction, Aveston et al (1971), Marshall et al (1985), Budiansky et al (1986), McCartney (1987) and Evans et al (1989). To model transverse ply cracking in crossply (i.e. 0/90 type) ceramic composites it should be possible to make use of some of the existing models developed for polymer matrix composites.

Experimental data in the literature enabling such models to be tested are limited, although there are a number of studies which describe and interpret the basic mechanical behaviour e.g. Prewo (1986), Sbaizero and Evans (1986), Ford et al (1987), Seerat-un-Nabi and Derby (1988) and Prewo et al (1989). In the present chapter detailed experimental observations are presented on the quasi-static behaviour of unidirectional and a range of crossply Nicalon reinforced CAS laminates. Stress/strain data and damage observations made during continuous tests are shown first. Later crack density and modulus reduction data are given. Two models are then applied to interpret the observed behaviour.

5.2 STRESS/STRAIN BEHAVIOUR AND DAMAGE OBSERVATIONS

5.2.1 Unidirectional laminates

The basic mechanical properties for the $(0)_{12}$ laminates are summarised in Tables 5.1 and 5.2. A typical stress-strain curve, Figure 5.1, displays a well-defined "knee" at about 0.08 % applied strain, which corresponds to the onset of matrix damage. This type of discontinuity and the general shape of the stress-strain curve have been observed for other CMC systems (Prewo 1986 and Mah et al 1985a). The matrix damage is in the form of an array of cracks spanning the width and thickness of the laminate, see Figure 5.2, and the density of these cracks (i.e the number of cracks per unit length) increases with increasing applied strain. The stress/strain curve becomes linear again at about 0.3 %, suggesting that matrix cracking has saturated (become constant) by this stage and this was confirmed by crack counting (see next section). Final fracture of the laminate (involving fibre failure) occurs at a strain of about 0.8 %.

5.2.2 (0/90) crossply laminates

Figure 5.3 shows stress/strain curves for the various crossply laminates tested and Table 5.2 gives the basic mechanical properties. These laminates show an initial knee at between 0.02 and 0.04 %, corresponding to matrix cracking in the 90° plies. From results for polymer matrix composites (or by applying simple strength/volume arguments) we would expect the crossply laminates with the thickest 90° plies to show the lowest knee. This is shown by the experimental results with the knee for the $(0_2/90_4)_s$ laminate at about 0.02 % compared to those for the other laminates at greater than 0.03 %. Cracking in the 90° plies continues with increasing strain, Figure 5.4. At higher strains the matrix in the longitudinal plies also cracks. Sometimes the longitudinal ply cracks occur as a result of extension of existing 90° ply cracks into neighbouring 0° plies (Figure 5.5); they are also seen to form independently (Figure 5.6). The crack density in both transverse and longitudinal plies continues to increase with increasing applied

strain until eventually saturation crack spacings are observed. Final fracture of all the crossply laminates occurs at strains of 0.63 - 0.65 %, compared to the value of 0.8 % for the $(0)_{12}$ lay-up.

5.3 CRACK DENSITY AND MODULUS REDUCTION DATA

The development of cracking and the associated degradation in laminate stiffness properties were studied in detail during discontinuous testing. As indicated earlier the crack density was determined by counting the number of cracks visible on a polished edge within a known gauge length. Both edges of a coupon were examined periodically in order to check that the cracks counted extended across the ply width as well as the ply thickness. For specimens where the cracks spanned a ply in a direction more or less perpendicular to the applied load, crack counting was straightforward. However, for the thickest 90° plies (in the $(0_2/90_4)_s$ lay-up) the cracks were distinctly non-planar. In this case a systematic method of crack counting had to be used, as indicated in Figure 5.7.

In a previous study of polymer matrix composites (Smith and Wood 1990) it was found, while performing discontinuous tests, that on reloading cracked specimens the stress-strain curves were linear until the stage where further cracking occurred, at which point the curves became non-linear. This was not so for the ceramic composites. Both unidirectional and crossply CMC lay-ups displayed non-linear stress-strain curves when previously cracked (see Figure 5.8 for an illustration of this in the unidirectional material). This is a result of fibre matrix sliding in the unidirectional material (Aveston et al 1971). In the crossply material there is additionally the possibility of crack closure arising from frictional effects across the faces of any transverse ply cracks which are not perpendicular to the applied load, consequently these cracks will not open unless a certain stress is applied. Because of these effects the values of reduced moduli as a function of applied strain presented in this chapter are secant values, measured at 0.05% applied strain for the unidirectional laminate and 0.02% for the crossply laminates.

5.3.1 Unidirectional laminates

Figure 5.9 shows the crack density as a function of applied stress in the $(0)_{12}$ laminate while Figure 5.10 shows the same crack density data plotted as a function of applied

strain, in which form it may be compared with the cracking data for the unidirectional plies of the various crossply laminates. Figure 5.11 shows the normalised stiffness as a function of applied strain. The overall stiffness reductions are large, reflecting the significant contribution made by the matrix to the laminate modulus. There may also be a contribution to the stiffness reduction in both the unidirectional and the crossplies from fibre breakage particularly at high stresses. This is reflected in the cumulative residual strain as a function of applied stress data (Figure 5.12) which continue increasing at stresses where there is no further increase in crack density.

5.3.2 (0/90) crossply laminates

The results for the crossply laminates are presented in Figures 5.10 and 5.13 to 5.20. Considering first the $(0/90)_s$ laminate, Figure 5.13 shows the crack density as a function of applied stress for the 90_2 plies (in which form the data may be compared with a simple shear-lag model, see Section 5.4.4). Figure 5.14 shows the same crack density data plotted as a function of applied strain; in this form the data may be compared with the results obtained from the 90_2 plies in the $(0/90)_{3s}$ laminate. Figure 5.15 shows the normalised stiffness of the $(0/90)_s$ laminate as a function of applied strain; note that this stiffness reduction is a result of the combined effects of the 90_2 ply cracking (Figure 5.14) and the 0° plies cracking (Figure 5.10).

Figure 5.16 shows the crack density in the 90_8 plies of the $(0_2/90_4)_s$ as a function of applied stress (also compared with the shear-lag prediction, see Section 5.4.4) and Figure 5.17 shows the same data plotted against applied strain. Figure 5.18 shows the normalised stiffness as a function of applied strain, again reflecting longitudinal ply cracking (Figure 5.10) as well as the 90_8 cracking (Figure 5.17).

For the $(0/90)_{3s}$ laminate, Figure 5.19 shows the crack density in the single 90° ply as a function of applied strain. Figure 5.20 shows the normalised stiffness as a function of strain and represents the combined effects of the single 90° plies cracking (Figure 5.19), the central 90_2 cracking (Figure 5.13) and the 0° plies cracking (Figure 5.10).

5.3.3 Stress cycling

Stress cycling tests were carried out on unidirectional laminates only. Tests were conducted by repeatedly cycling specimens at progressively higher stress levels. Each specimen was cycled for a maximum number of five cycles or until laminate stress/strain hysteresis loops were closed and identical, i.e. stabilised (see Figure 5.21 for an example). Analysis of the hysteresis loops allowed laminate stiffness (0.05% secant values) and residual strain (the strain offset at zero stress) to be monitored as a function of cycles at each maximum stress (Figures 5.22 and 5.23). Reference to Figures 5.22 and 5.23 show that on the first cycle at each maximum stress there is a large increase in residual strain and a reduction in laminate stiffness. At low stresses (and hence damage) between 1 and 2 additional cycles to the same maximum stress are required in order for stress/strain loading and unloading to stabilise. At higher stresses up to 5 additional cycles are required.

5.4 DISCUSSION

5.4.1 Residual thermal stresses

In any modelling of the crack development in the laminates it is necessary to take account of the stresses generated in the laminates as a result of mismatch in thermal expansion co-efficients between the fibres and matrix, during cooling from the final processing stage. Suppliers data give the principle co-efficients of thermal expansion of unidirectional material, α_1 and α_2 (parallel and perpendicular to the fibre direction respectively), as 4.3 x 10^{-6} and 4.5 x 10^{-6} K^{-1} while the values for the Nicalon fibre and CAS matrix are α_f = 3.2 x 10^{-6} and α_m = 4.6 x 10^{-6} K^{-1}. For a temperature change of 1200 K (the material is "ceramed" at about 1500 K), the initial residual (tensile) thermal strain in the matrix of a unidirectional laminate parallel to the fibres is simply $(\alpha_m - \alpha_1)\Delta T$ i.e. ~0.036 %. For crossply laminates the thermal strain in the transverse ply (taken as being the matrix thermal strain) can be found using laminated plate theory (LPT, e.g. Jones 1975) for any particular laminate lay-up and elastic constants. LPT gives the thermal strains in the transverse plies as 0.011 % in the $(0/90)_s$ and $(0/90)_{3s}$ laminates and 0.009 % in the $(0_2/90_4)_s$ laminate. The thermal strains in the matrix of the longitudinal plies in each laminate were estimated by inferring the effective composite laminate expansion co-efficient from LPT and calculating the mismatch between this value and the expansion co-efficient of the unrestrained matrix α_m. Proceeding in this way, the thermal strains in the matrices of the 0° plies were estimated at 0.025 % in the $(0/90)_s$ and $(0/90)_{3s}$ laminates and 0.022 % in the $(0_2/90_4)_s$ laminate. However, it should be recognised that these values represent the maximum thermal stresses possible. This is because the maximum temperature difference (1200 K) is considered.

5.4.2 Initial elastic moduli of the laminates

The initial elastic moduli of the laminates are shown in Table 5.2. The data show some variation which could be a result of cracks being present in the matrix as received,

although nothing was seen on micrographs to support this. The matrix makes a substantial contribution to the overall modulus of the laminate so that the moduli of the (0/90) laminates approach the modulus of the $(0)_{12}$ laminate. Although the modulus of a lamina perpendicular to the fibre direction (E_2) was not measured independently, it can be inferred from the crossply moduli by using laminated plate theory (or, to a good approximation, the rule-of-mixtures). Proceeding this way suggests that E_2 lies in the range 85 - 110 GPa, showing the CMC to be more isotropic than its polymer matrix counterpart. The lower end of this range is inferred from the $(0_2/90_4)_s$ laminate, perhaps suggesting that the quality of the (thick) 90_8 plies is not as good as that of the (thinner) transverse plies in the other laminates, certainly polished sections from the $(0_2/90_4)_s$ laminates show more porosity than any of the other lay-ups. In all calculations for a particular lay-up (including the thermal stress calculations above) where a value of E_2 is needed, the inferred in situ value for that lay-up is used. Although the Poisson's ratios for the laminates show more scatter than the moduli (perhaps because a transverse gauge samples over a smaller volume than a longitudinal gauge), the trends are sensible. The value of E_2 inferred from the $(0/90)_s$ laminate is close to the E_1 value, hence the two principle Poisson's ratios of a 0° lamina (ν_{12} and ν_{21}) are almost equal. Consequently we would expect the Poisson's ratio of the $(0/90)_s$ laminate to be very close to that of the $(0)_{12}$ laminate and this was found experimentally. For the $(0/90)_{3s}$ laminate the inferred E_2 (and hence ν_{21}) is lower than for the $(0/90)_s$ laminate and so the Poisson's ratio is lower for the $(0/90)_{3s}$ laminate. Finally, the $(0_2/90_4)_s$ laminate has the lowest E_2 value and also the greatest fraction of 90° plies; hence the Poisson's ratio value is the lowest of all the crossply laminates.

5.4.3 Cracking in unidirectional laminates

Many studies in the literature have attempted to model matrix cracking processes in unidirectional CMCs. The classic paper by Aveston et al (ACK) (1971) employs an overall energy balance to obtain an expression for the matrix cracking strain, ϵ_{mu}:
where E_m, E_f and E_1 are the modulus of the matrix, the fibre and the composite respectively; V_f is the volume fraction of fibre and V_m (= 1 - V_f) is the volume fraction

$$\epsilon_{mu} = \left(\frac{12 \tau \gamma_m E_f V_f^2}{E_1 E_m^2 r V_m} \right)^{\frac{1}{3}} \qquad (5.1)$$

of the matrix; r is the fibre radius. The quantity γ_m is the fracture surface energy of the matrix and τ is the (assumed constant) interfacial shear stress between the fibre and matrix. Once a crack forms, then at the plane of that crack all the load on the composite is taken by the fibres. However, as a result of the interfacial shear stress (τ) acting between the fibres and the matrix, the stress in the matrix increases linearly (from zero) with distance away from the crack plane. At a distance x' from the crack the matrix failure strain is reached again. Consequently cracking continues with no further increase in applied load until there are approximately uniform cracks, spanning the width and thickness of the specimen, spaced between x' and $2x'$ apart, where

$$x' = \frac{V_m}{V_f} \left(\frac{\sigma_{mu} r}{2 \tau} \right) \qquad (5.2)$$

and σ_{mu} ($= E_m \epsilon_{mu}$) is the fracture stress of the matrix.

Subsequent studies (including Marshall et al 1985 and McCartney 1987) have considered the mechanics of crack growth in more detail and have shown that Equation 5.1 is a valid description for the propagation of large flaws (calculations show to be of greater than a few fibre diameters). Due to the range of initial (processing) defects and the non-uniform stress distribution due to microstructural variations (local volume fraction and fibre diameter variations etc) it is likely that a range of flaw sizes exists in the matrix. As a result the approach described by Aveston et al will represent a lower bound for crack propagation illustrated by the plateau in Figure 2.5. In this region of the curve the composite stress intensity factor (determined by the continuum models of Marshall et al and McCartney) is independent of flaw size and large (ACK) flaws will propagate according to the energy based criterion (equation 5.1). In the case of smaller flaws (less than a few fibre diameters) applied strains are required in excess of that described by equation 5.1 in order for them to propagate. For these flaws the composite stress intensity factor is not independent of flaw size as indicated by the curved region of Figure 2.5; the stress field around the flaw tip must be sufficiently large to cause the flaw

to become unstable.

As a first approximation we can use the ACK analyses to interpret the crack density vs applied stress data for the unidirectional lay-up (Figure 5.9). These data indicate that matrix cracking occurs over a range of applied stress and is consistent with a range of initial flaw sizes which lead to cracks (analyzed by Marshall et al and McCartney) . The first cracks to go in (at about 0.08 % strain applied i.e. a stress of about 96 MPa) may occur due to the propagation of large pre-existing flaws, while those which occur at progressively higher strains could propagate from smaller flaws. The final (or "saturation") crack spacing in the 0° laminates, $2s_f$, was 0.14 mm. Following Kimber and Keer (1982)

$$2s_f = 1.33x' \quad (5.3)$$

From equations 5.1, 5.2 and 5.3 using the experimentally determined value of ϵ_{mu} (0.12 %, including thermal strain) and taking 8 μm as a representative value for the fibre radius (determined by image analysis techniques, see Appendix 2), the inferred values of τ and $2\gamma_m$ are 10 MPa and 6 J m^{-2} respectively. The value of τ is perhaps high while the value of $2\gamma_m$ is reasonable for a ceramic matrix (Cao et al 1990). These calculated values of $2\gamma_m$ and τ enable a "prediction" to be made for the data of Figure 5.9, based on the ACK model. The plot shows clearly that the ACK model is an oversimplification as outlined above. The matrix cracks propagate over a range of applied stress.

The flaw size distribution in the matrix, although unknown here, can be interpreted qualitatively given the data in Figure 5.9 and the subsequent analysis using the ACK theory. The absence of an initial vertical portion to the crack density vs applied stress data suggests that the largest matrix flaws are too small to lie on the plateau region of Figure 2.5 and hence to propagate according to the energy based criterion (equation 5.1). It is likely therefore that the composite stress intensity factor will be described by the continuum analyses of Marshall et al and McCartney over the range of applied stress where matrix cracking is the dominant damage mechanism. Clearly if material processing and microstructural uniformity were improved then it may be possible to eliminate the

largest flaws. As a result the stress at which the first and largest flaw propagates would be pushed further up the curve in Figure 2.5 as a higher stress would be required to form the first crack. This is illustrated in Figure 5.24 (a schematic diagram of Figure 5.9) which shows the crack density as a function of applied stress according to ACK theory (broken line), the form of the experimental data (dotted line) and the trends one might expect for distributions of progressively smaller flaws in the matrix (solid lines). Improving the matrix cracking threshold is a fundamental requirement (given the data presented in this chapter) for the commercial use of this kind of ceramic matrix composite in structural applications.

5.4.4 Cracking in (0/90) crossply laminates

First we consider the cracking thresholds of the 90° plies in the various laminates. These can be estimated in a consistent way by extrapolating the crack density/applied strain curves to the point where they cross the strain axis. The data found in this way were consistent with the strain at which there is the first discontinuity in the stress/strain curves from the continuous tests. Data for the 90_8 plies crack density in the $(0_2/90_4)_s$ laminate could not be extrapolated reliably because the first strain interval in the discontinuous tests exceeded the cracking threshold, so for this laminate the threshold was taken from the first discontinuity in the stress/strain curves from continuous tests. For all laminates, the cracking strains obtained are then added to the calculated thermal strains to give the cracking thresholds shown in Table 5.3. These data confirm that the lowest cracking strain occurs in the laminate with the thickest transverse ply. In polymer composites the trend of increasing strain for first cracking in the transverse plies of crossply laminates of progressively smaller transverse ply thicknesses has been explained in two different ways. Using fracture mechanics arguments e.g. Parvizi and Bailey (1978), Ogin and Smith (1985) and Laws and Dvorak (1988) it can be shown that for thin transverse plies the strain required to propagate a microcrack spanning the thickness of the ply across the width of the laminate is, to a first order approximation, inversely proportional to the square root of the transverse ply thickness. This is the so-called "constrained cracking" situation. Alternatively, in a thick transverse ply the microcracks are smaller than the transverse

ply thickness and the strength of the ply can be imagined to show a Weibull-type statistical distribution of strengths (corresponding to the stress levels at which the different size microcracks propagate), in which case the thicker the ply the lower the expected mean strength e.g. Manders et al (1983), Fukanaga et al (1984) and Peters (1984). This is known as "unconstrained" transverse ply cracking and is the situation which we might expect to apply to CMCs.

To investigate this further, we use simple fracture mechanics methods to estimate the critical flaw size in the 90° plies of the crossply laminates in the following way. For a penny-shaped crack of radius, a, in an infinite isotropic body, the stress intensity factor, K, is given by Knott (1973):

$$K = \frac{2}{\sqrt{\pi}} \sigma \sqrt{a} \qquad (5.4)$$

Hence, for a transverse ply which cracks at a strain, ϵ_{fpf}, by setting $K = K_{1C} = \sqrt{(E_2.2\gamma)}$ where γ is the fracture surface energy of the transverse ply and taking $\sigma = E_2\epsilon_{fpf}$, the critical flaw size, a^*, can be estimated from

$$a^* = \frac{\pi 2\gamma}{4 E_2 \epsilon_{fpf}^2} \qquad (5.5)$$

We can estimate 2γ very simply as $(1 - V_f).2\gamma_m$ (this is a mean toughness as a crack passes through a representative cross section, if the bulk of the fracture path is at fibre-matrix interfaces we expect the toughness to be considerably lower). Using values for the different crossply laminates in equation 5.5 suggests that the initial flaw diameter, $2a^*$, is about 0.23 mm in the 90_2 plies of the $(0/90)_{3s}$ and $(0/90)_s$ laminates and 1.06 mm in the 90_8 plies of the $(0_2/90_4)_s$ laminate. In each laminate the inferred flaw size is less than the transverse ply thickness and the flaw size is larger in the laminate with the largest transverse ply volume. It is probable that the true flaw sizes are all smaller than calculated due to the value of 2γ used being too high. Given these small critical flaw sizes, it would appear that crossply ceramic matrix composite laminates will exhibit unconstrained cracking for practical ply thicknesses.

Transverse ply cracks increase in density with further loading beyond the initiation strain

in a very similar manner to polymer matrix composites. If we assume that the plies of the composite remain bonded and that the response is elastic then we can describe the stress distributions in a cracked (0/90) composite using shear-lag analysis (see e.g. Laws and Dvorak 1988, Garrett and Bailey 1977 and Ogin et al 1984). For a $(0/90)_s$ laminate of longitudinal ply thickness, b, and transverse ply thickness, 2d, containing a regular array of transverse cracks spaced 2s apart the longitudinal stress distribution in the transverse ply as a function of distance y (measured along the length of the specimen from a coordinate origin midway between two cracks) is

$$\sigma_2 = \left(\sigma \frac{E_2}{E_0} + \sigma_2^T\right)\left(1 - \frac{\cosh\lambda y}{\cosh\lambda s}\right) \qquad (5.6)$$

where E_0 is the rule-of-mixtures modulus of the laminate ($=[bE_1 + dE_2]/[b + d]$), σ is the applied stress, $\sigma_2{}^T$ is the initial thermal stress in the transverse ply and

$$\lambda^2 = \frac{3 G_{23} (b + d) E_0}{d^2 b E_1 E_2} \qquad (5.7)$$

Following the Steif analysis (see Ogin et al 1984), equation 5.6 can be used to predict progressive matrix cracking in a very simplistic way by assuming that the next set of cracks form midway between existing cracks (i.e. at y = 0) when the stress at that point reaches the transverse ply strength, σ_{2u}, (assumed constant, which is not correct given that there will be a distribution of initial flaw sizes present). The necessary applied stress for further cracking, σ', is then given by

$$\sigma' = \left[\frac{\sigma_{2u}}{\left(1 - \frac{1}{\cosh\lambda s}\right)} - \sigma_2^T\right]\frac{E_0}{E_2} \qquad (5.8)$$

The prediction of equation 5.8 is compared with the experimental data for 90° cracking in the $(0/90)_s$ and $(0_2/90_4)_s$ laminates in Figures 5.13 and 5.16 respectively. Agreement with the trends of the data is reasonable. However, there are two main factors which need to be incorporated to improve this type of model. Firstly the statistical nature of

the 90° failure processes needs to be incorporated (perhaps using an approach along the lines of that of Fukanaga et al (1984) for polymer composites). Secondly at high strains the effect of the degradation of the stiffness of the constraining plies (E_1) as a result of their cracking must be considered.

Figure 5.14 enables crack development in the 90_2 plies of two different laminates as a function of applied strain to be compared. The behaviour is similar as might be expected, given that both plies demonstrate unconstrained cracking.

The "saturation" crack spacings for the 90° plies are summarised in Table 5.3. For polymer matrix composites it is well established that "saturation" matrix cracking corresponds to an average crack spacing of the order of the ply thickness e.g. Masters and Reifsnider (1982). From Table 5.3 it is clear that saturation crack spacing in the 90_8 plies (0.9 mm) is greater than in the other plies and substantially less than their thickness (1.39 mm). The 90_2 plies saturate at a crack spacing (0.25-0.33 mm) about equal to their thickness (0.35 mm) while the single 90 ply saturates at a spacing (0.25 mm) rather larger than the ply thickness (0.18 mm). Overall there is an effect of transverse ply thickness on saturation crack spacing, as would be expected given that the transverse ply thickness influences the rate at which stress is shed back from the 0's into the 90's, but the trend is not well defined for the thinner plies. It is interesting that the saturation crack spacings in the crossply CMCs (especially for the 90_8 plies) are smaller (as a multiple of the ply thickness) than for their polymer matrix counterparts. An explanation may be that in crossply polymer composites a limiting factor is the shear stress that can be sustained by the resin at the (0/90) interface, which in term limits the transfer of load back into the 90° plies at small crack spacings making additional cracking less likely. In the glass matrix CMCs the interface will remain elastic at much higher loads, efficiently transferring stress back into the 90° plies by shear, even at small crack spacings, making further cracking possible.

As the transverse ply crack and longitudinal ply crack arrays develop in the laminates the moduli fall dramatically (as shown by the secant plots of Figures 5.11, 5.15, 5.18 and 5.20 and the tangent data of Table 5.2. Shear-lag relations such as equation 5.8 enable

expressions for the normalised stiffness as a function of transverse ply crack density to be written; however, such expressions would need to be modified to account for the effect of 0° plies cracking. The limiting value for the modulus of a laminate where the matrix is fully discounted is simply $V_{f0}V_fE_f$, where V_{f0} is the volume fraction of 0° plies in the laminate. The tangent data of Table 5.2 are much lower than the discount value for all four laminates. There are two probable reasons for this: firstly fibre breakage will occur before failure, reducing the modulus below the matrix discount value; secondly, there will be permanent strains associated with the damage which will not affect the true elastic modulus but will have been included in a value measured from a continuous stress-strain curve.

It is interesting to compare the cracking behaviour of the unidirectional plies in the cross-ply laminates with the cracking behaviour of the unidirectional laminate. In general the strain at which cracks initiate is similar (Figure 5.10 and Table 5.3). However, in some specimens, notably of the $(0/90)_{3s}$, longitudinal cracks occurred at lower strains than in the unidirectional material; when this happened, the cracks seemed to arise from the propagation of 90° cracks into the constraining 0° plies. The "saturation" crack spacing in the 0° plies of all the laminates seems to tend to the same value, independent of the 0° ply thickness. This is consistent with the model of stress transfer used in the ACK shear-lag analysis i.e. that each fibre interacts with a cylinder of matrix in which it is contained, consequently it is the fibre radius which is the dimension governing stress transfer between fibre and matrix (equation 5.2) and the ply thickness has no influence.

5.4.5 Stress cycling

The stress cycling results shown in Figure 5.21 and 5.22 indicate that on the first cycle for each maximum stress level the amount of damage increases giving a non-zero residual strain and a decrease in laminate stiffness. Up to five additional cycles are required in order for stress/strain hysteresis to stabilise. This could be due to either (a) stabilisation of the slippage process occurring at the fibre/matrix interface, or, (b) continued cracking during cycling.

The results presented here are insufficient to indicate which of these mechanisms are active. This is because at no stage during testing were specimens removed from the Instron and matrix damaged quantified (by crack counting). In Chapter 6 the fibre/matrix slippage process is analyzed and a model proposed to predict the stress/strain behaviour of a cracked unidirectional laminate. In Chapter 7 quasi-static stress cycling and high frequency fatigue are examined and matrix damage quantified as a function of cycles.

5.5 CONCLUSIONS

The work presented in this chapter has identified and quantified matrix cracking in unidirectional and crossply Nicalon reinforced CAS laminates. The unidirectional material cracks at an applied strain of about 0.08% (~0.12% including thermal strain). Crack development on further straining is consistent with that seen by other workers and can be described approximately using the ACK model. A more complete description of the stress/crack spacing behaviour could be obtained by using the models of Marshall et al (1985) and McCartney (1987) in conjunction with a known toughness to deduce the flaw size distribution which develop into fully formed cracks over a range of applied stress.

The progressive cracking of the longitudinal plies in crossply laminates is reasonably similar to that seen in unidirectional laminates; there is a similar threshold strain and saturation spacing. Transverse ply cracking in the crossply laminates initiates at low applied strains (0.02 - 0.04%) and is unconstrained in that the critical flaw sizes are estimated to be much smaller than the ply thickness. A simple shear-lag model, which assumes elastic bonding between the plies, describes the trend of the crack multiplication as a function of applied stress. However, such a shear-lag model needs to be modified to account for (a) the statistical nature of the failure process and (b) the effect of the simultaneous cracking of the 0° plies.

E_f	Fibre modulus	190 GPa
α_f	Fibre thermal expansion co-efficient	3.3×10^{-6} K^{-1}
E_m	Matrix modulus	90 GPa
α_m	Matrix thermal expansion co-efficient	4.6×10^{-6} K^{-1}
E_1	Lamina modulus (parallel to fibres)	128 GPa
E_2	Lamina modulus (perpendicular to fibres)	85-110 GPa*
ν_{12}	Lamina principle Poisson's ratio	0.24
G_{23}	Lamina shear modulus (through-thickness)	36 GPa#
α_1	Lamina expansion co-efficient (parallel to fibres)	4.3×10^{-6} K^{-1}
α_2	Lamina expansion co-efficient (perpendicular to fibres)	4.5×10^{-6} K^{-1}

* Range of values estimated from (0/90) data using laminated plate theory

\# Estimated assuming 2-3 plane is isotropic and using $G_{23} = E_2/2(1 + \nu_{23})$, taking $\nu_{23} = 0.25$.

Table 5.1 Summary of the main matrix, fibre and unidirectional lamina properties (for $V_f = 0.34$)

LAY-UP	INITIAL MODULUS* (GPa)	POISSON'S RATIO*	ϵ_f+ (%)	σ_u+ (MPa)	FINAL TANGENT MODULUS (GPa)
$(0)_{12}$	128±7	0.45±0.03	0.78	400	39
$(0/90)_s$	120±20	0.24±0.07	0.63	173	13
$(0_2/90_4)_s$	101±16	0.20±0.03	0.65	107	8
$(0/90)_{3s}$	110±5	0.22±0.05	0.63	146	12

* Mean of at least five specimens

\+ One specimen only

Table 5.2 Initial moduli, moduli at failure, failure strengths and failure strains for $(0)_{12}$, $(0/90)_s$, $(0/90)_{3s}$ and $(0_2/90_4)_s$ laminates.

LAY-UP	PLY	THICKNESS (mm)	THRESHOLD CRACKING STRAIN (%)	SATURATION CRACK SPACING (mm)
$(0)_{12}$	0_{12}	2.10	0.12	0.14
$(0_2/90_4)_s$	0_2	0.43	0.10	0.15
$(0/90)_s$	0	0.16	0.14	0.16
$(0/90)_{3s}$	0	0.17	0.08	0.18
$(0_2/90_4)_s$	90_8	1.39	0.03	0.9
$(0/90)_s$	90_2	0.35	0.05	0.25
$(0/90)_{3s}$	90_2	0.36	0.05	0.33
$(0/90)_{3s}$	90	0.18	0.05	0.25

Table 5.3 Summary of cracking thresholds (from extrapolating crack density/applied strain curves and adding the calculated thermal strain) and saturation crack spacings for laminates tested.

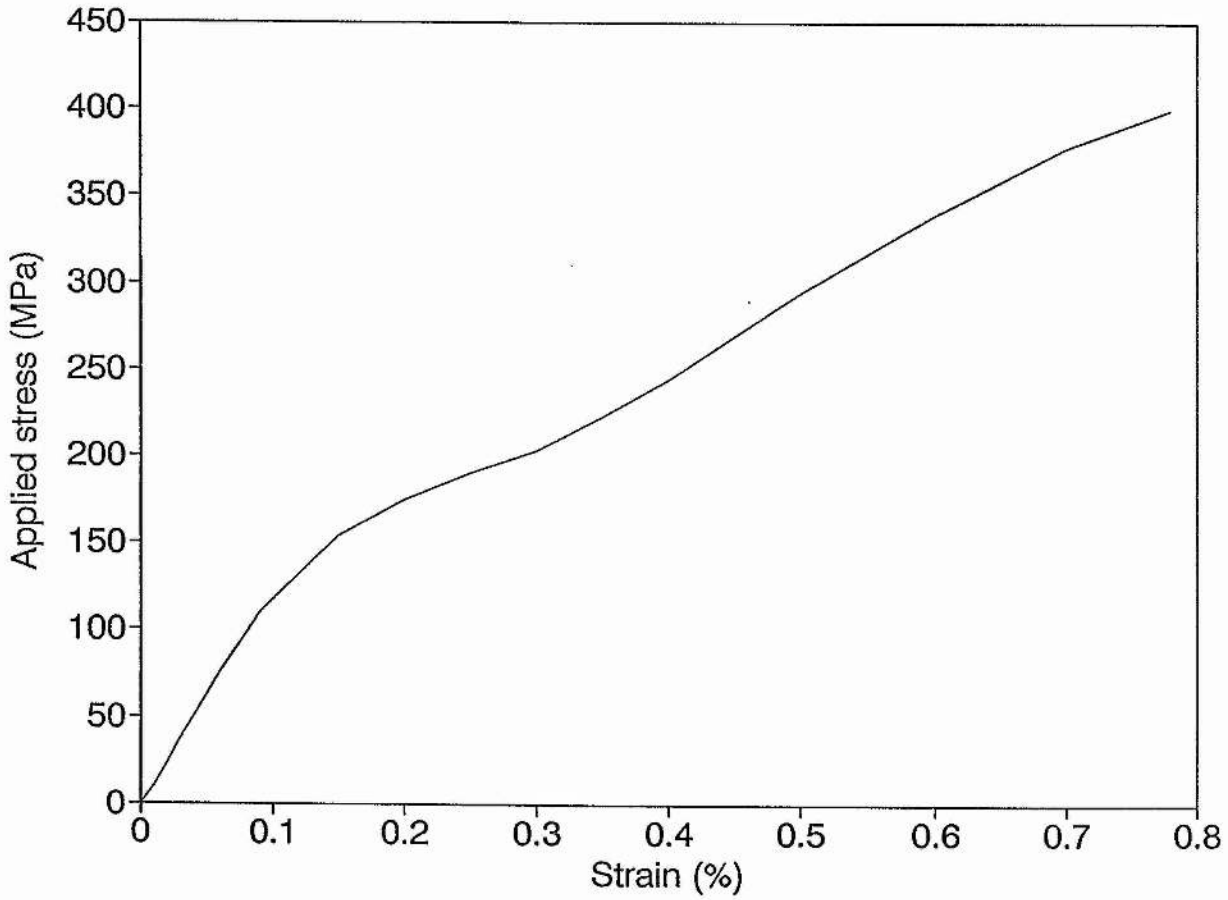

Figure 5.1 Stress/strain curve for a $(0)_{12}$ laminate.

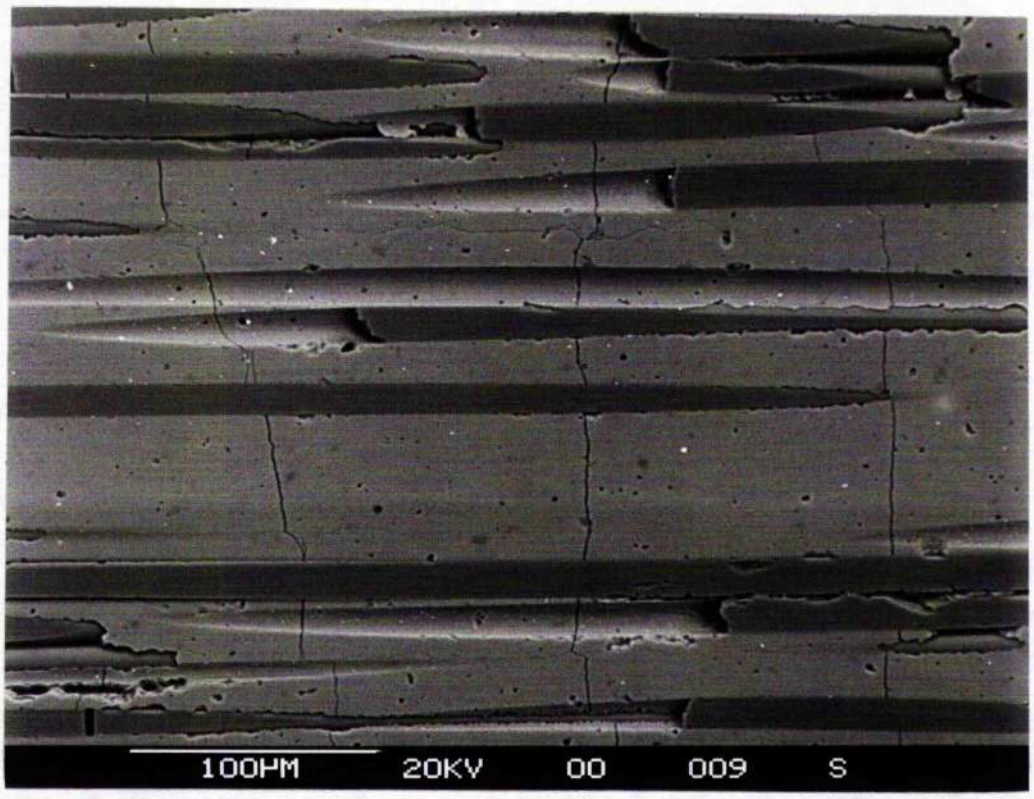

Figure 5.2 Typical matrix cracking damage in a $(0)_{12}$ laminate.

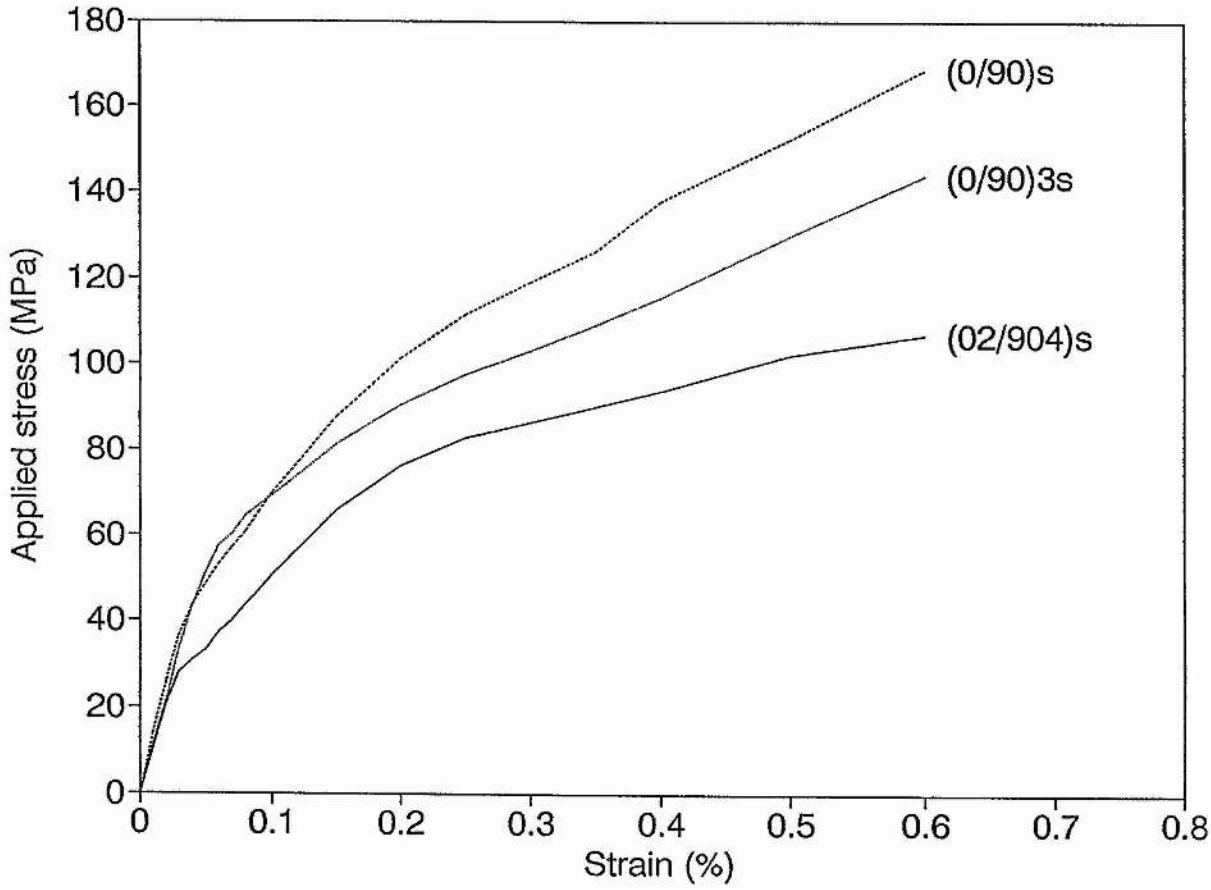

Figure 5.3 Stress/strain curves for $(0/90)_s$, $(0_2/90_4)_s$ and $(0/90)_{3s}$ laminates.

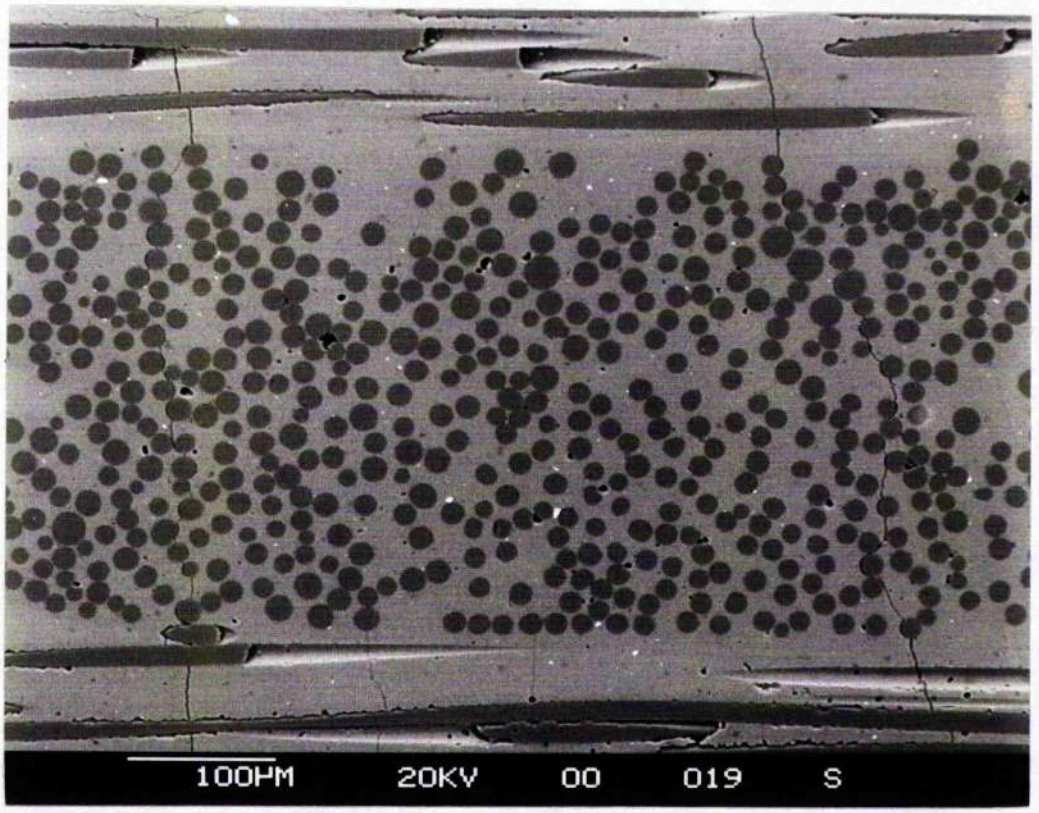

Figure 5.4 Typical transverse ply damage in $(0/90)_s$ laminates.

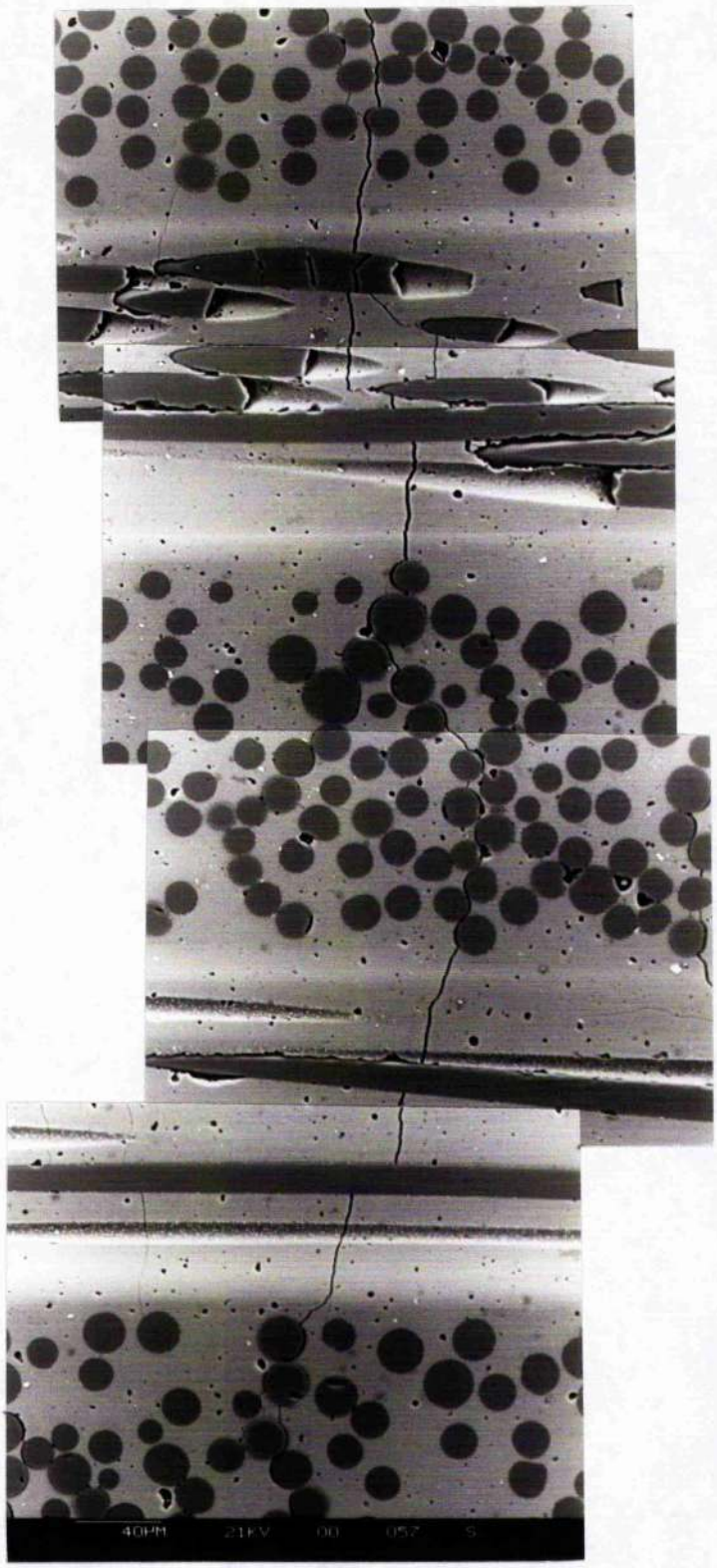

Figure 5.5 Damage in a $(0/90)_{3s}$ laminate showing a matrix crack running through both 0° and 90° plies.

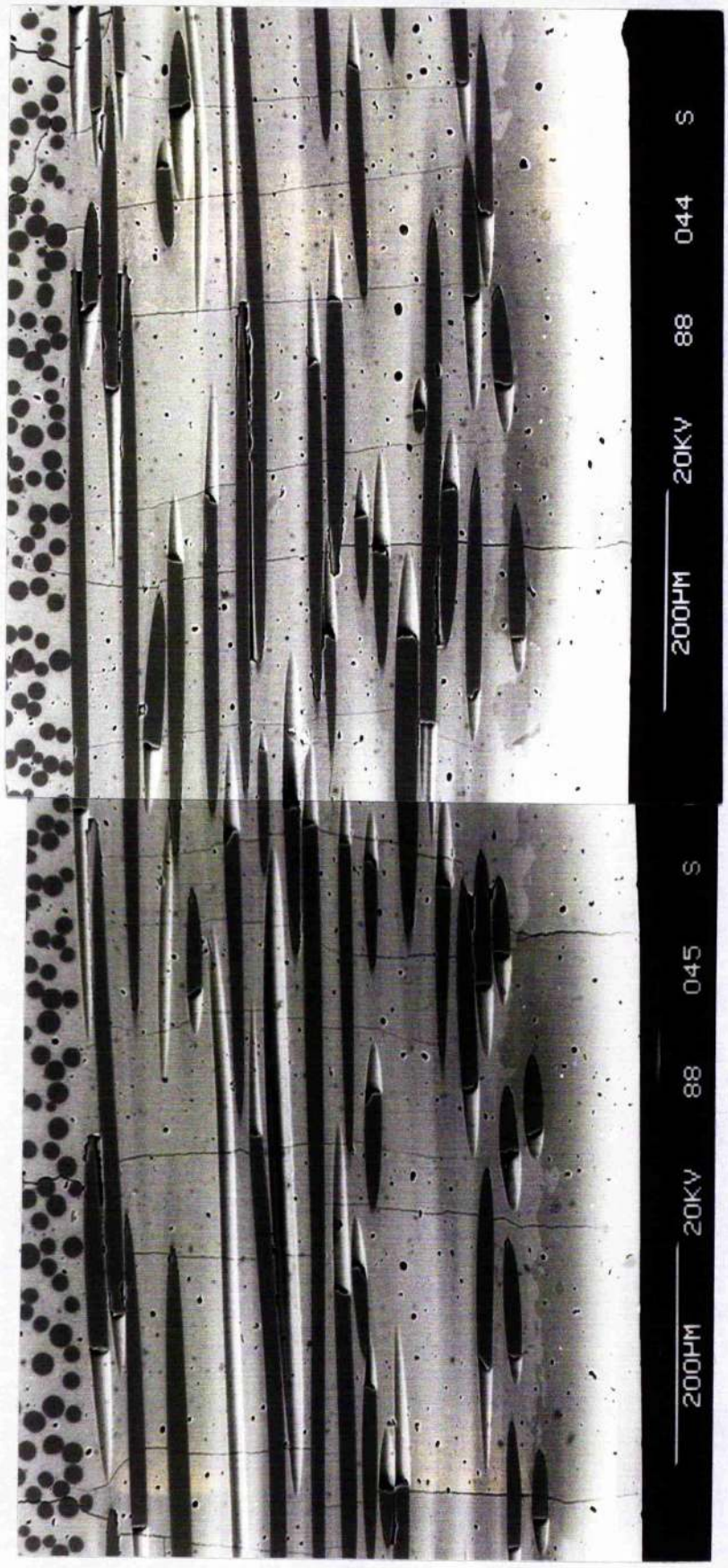

Figure 5.6 Longitudinal ply cracks in a $(0_2/90_4)_s$ laminate.

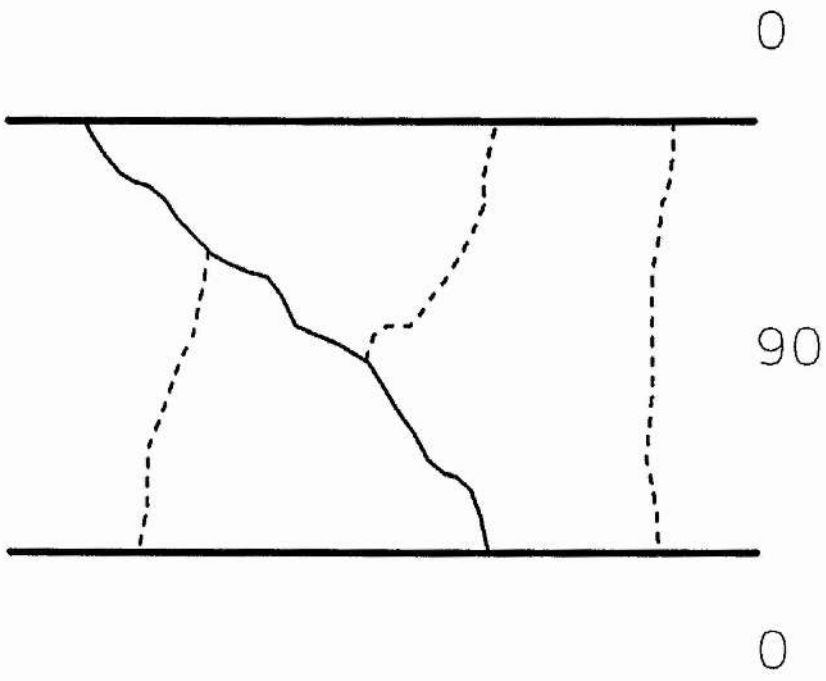

Figure 5.7 Illustration of the transverse ply crack counting technique for $(0_2/90_4)_s$ laminates.

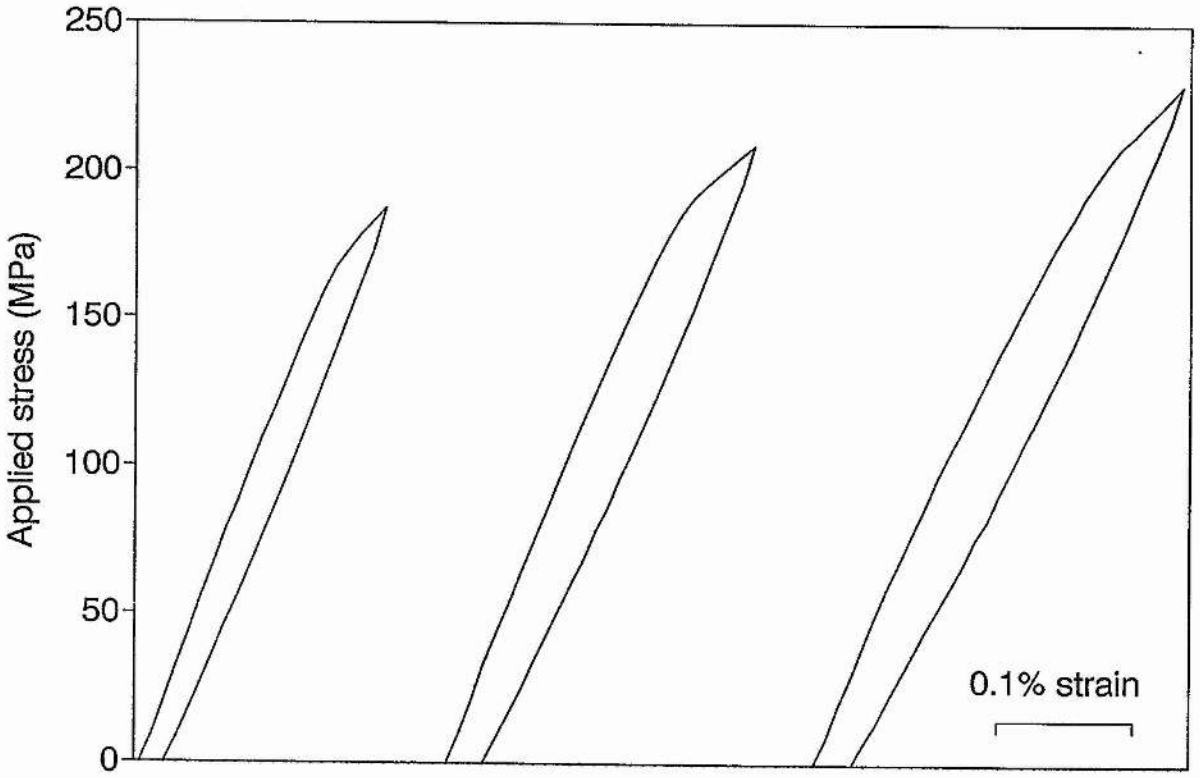

Figure 5.8 Non-linearity of stress/strain behaviour in discontinuous tests on $(0)_{12}$ laminates.

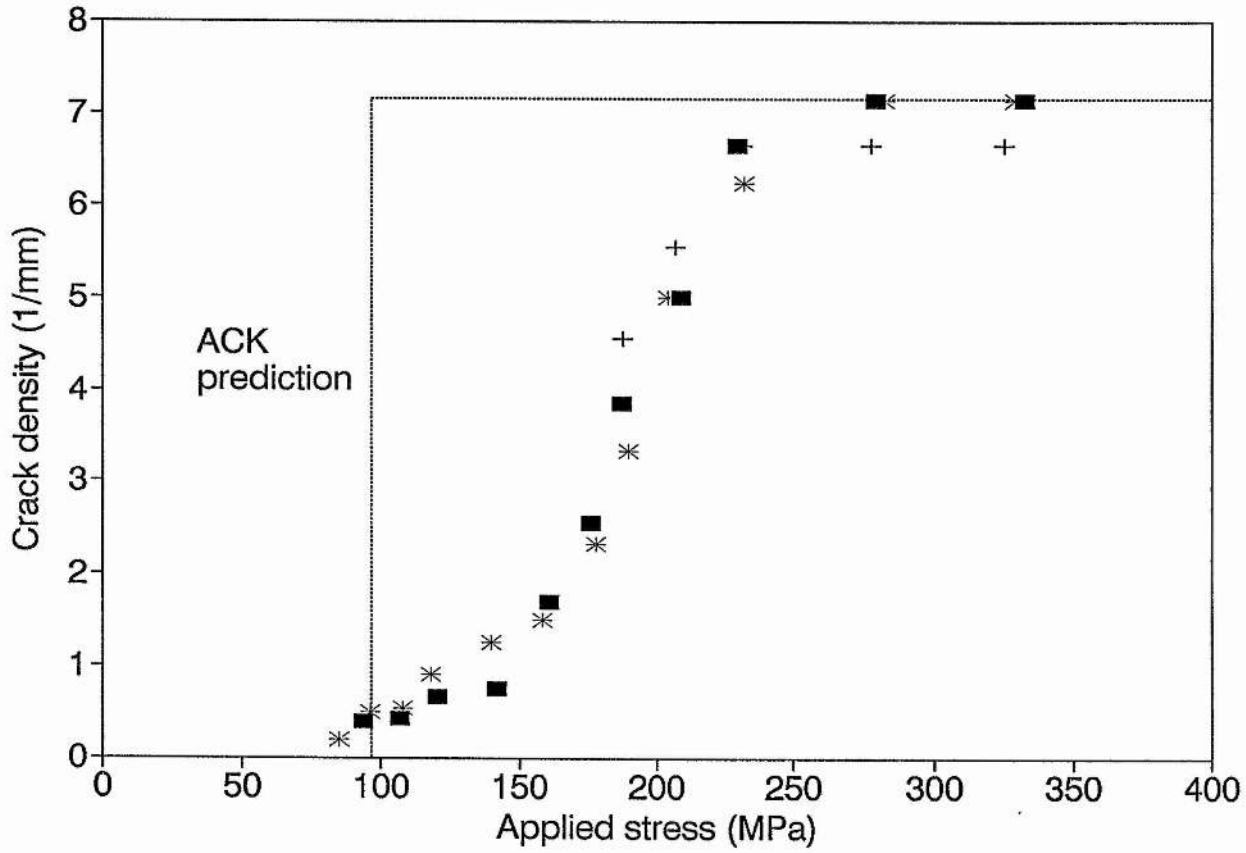

Figure 5.9 Crack density as a function of applied stress in $(0)_{12}$ laminates and prediction of ACK model with τ = 10 MPa and $2\gamma_m$ = 6 Jm^{-2}.

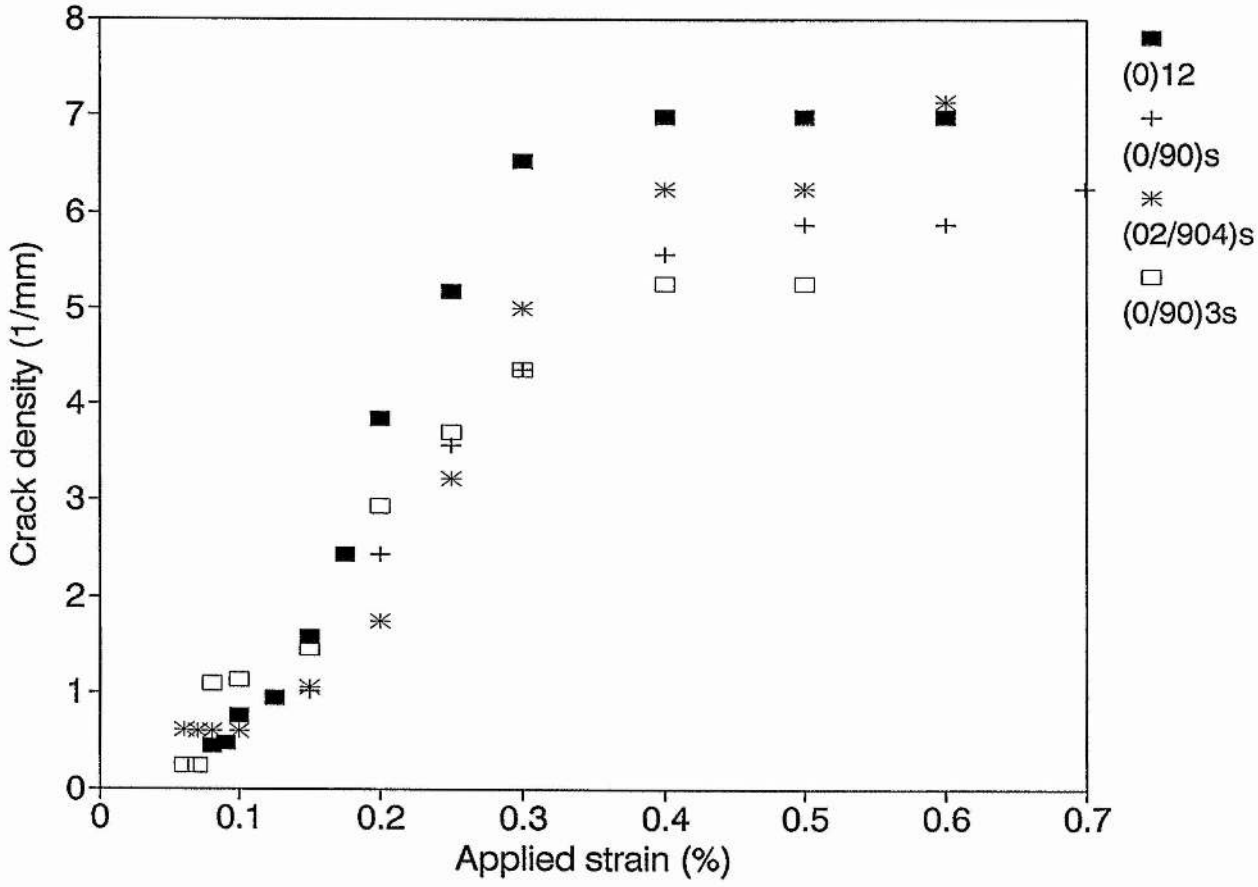

Figure 5.10 Crack density as a function of applied strain in the 0° plies of $(0)_{12}$, $(0/90)_s$, $(0_2/90_4)_s$ and $(0/90)_{3s}$ laminates.

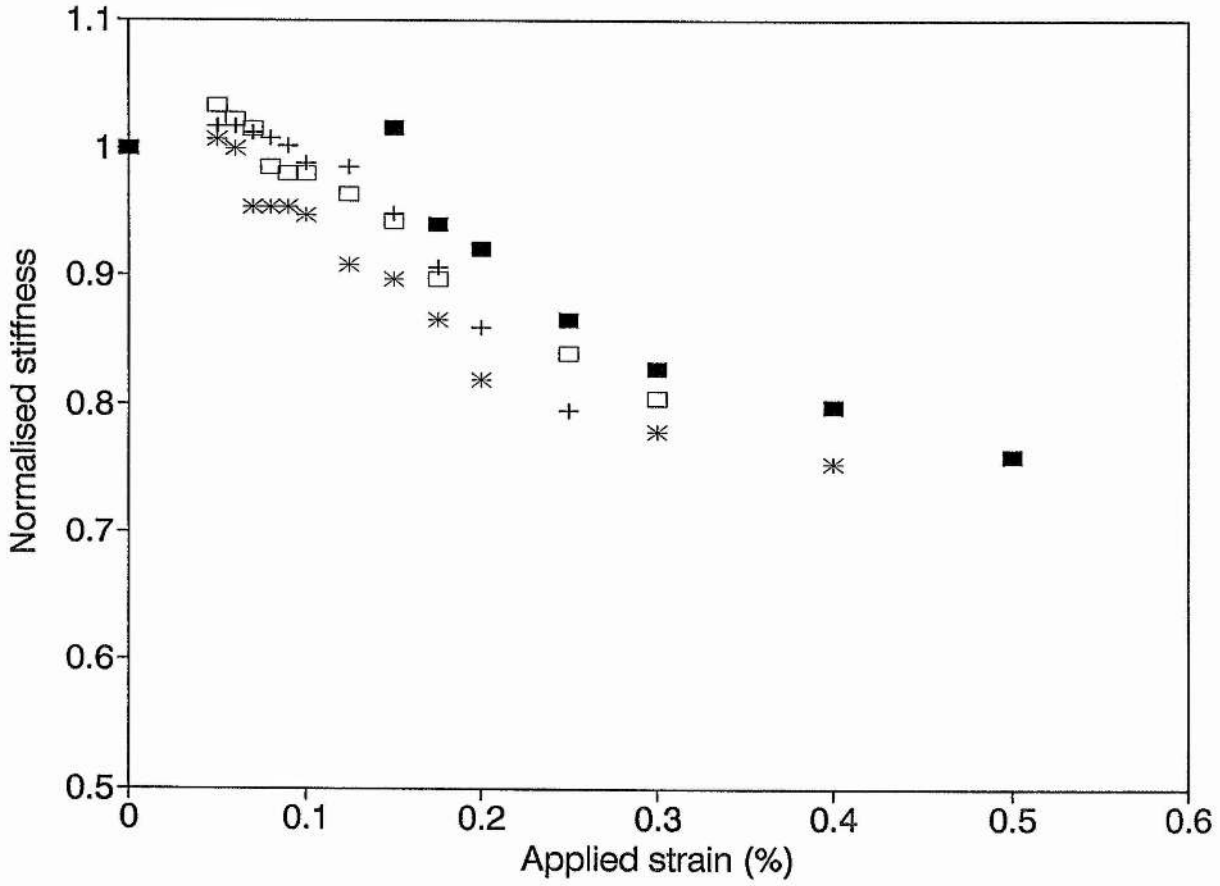

Figure 5.11 Normalised stiffness as a function of applied strain in $(0)_{12}$ laminates.

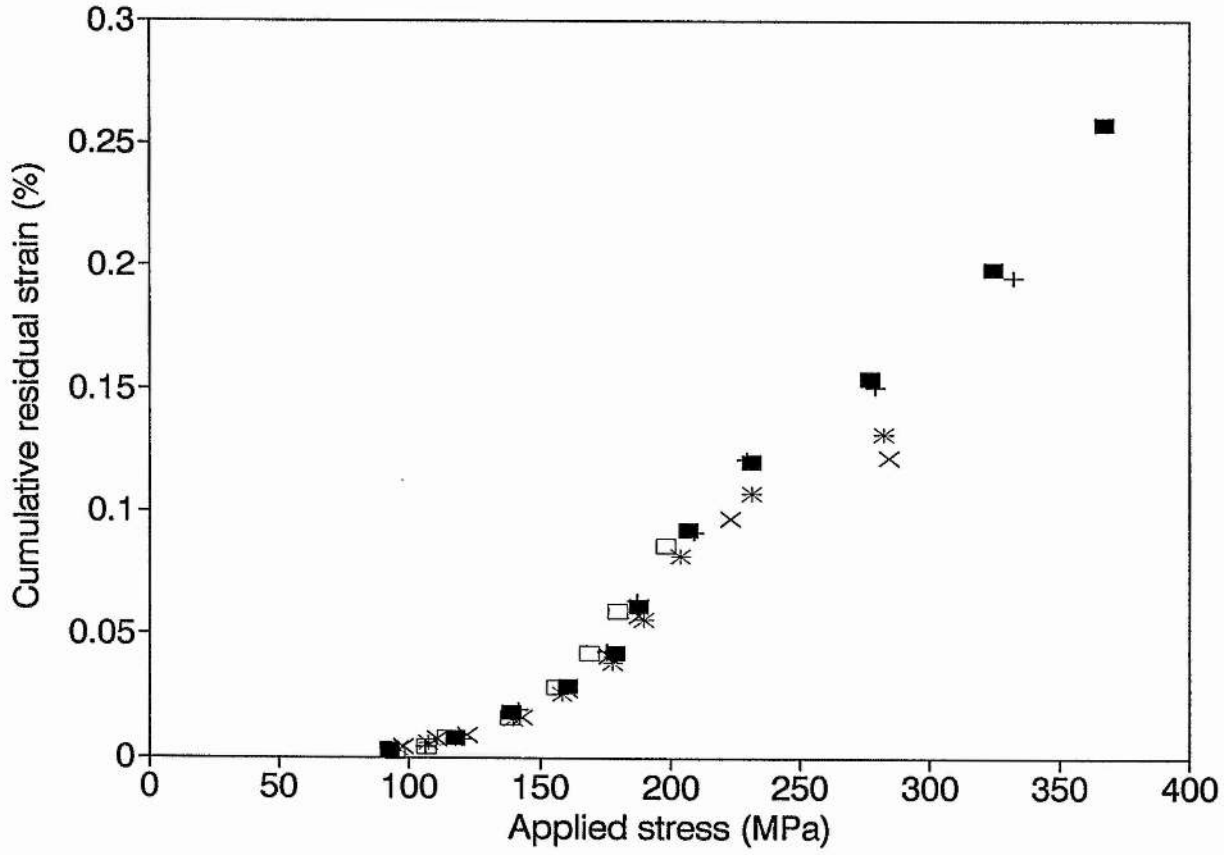

Figure 5.12 Cumulative residual strain as a function of applied stress in $(0)_{12}$ laminates.

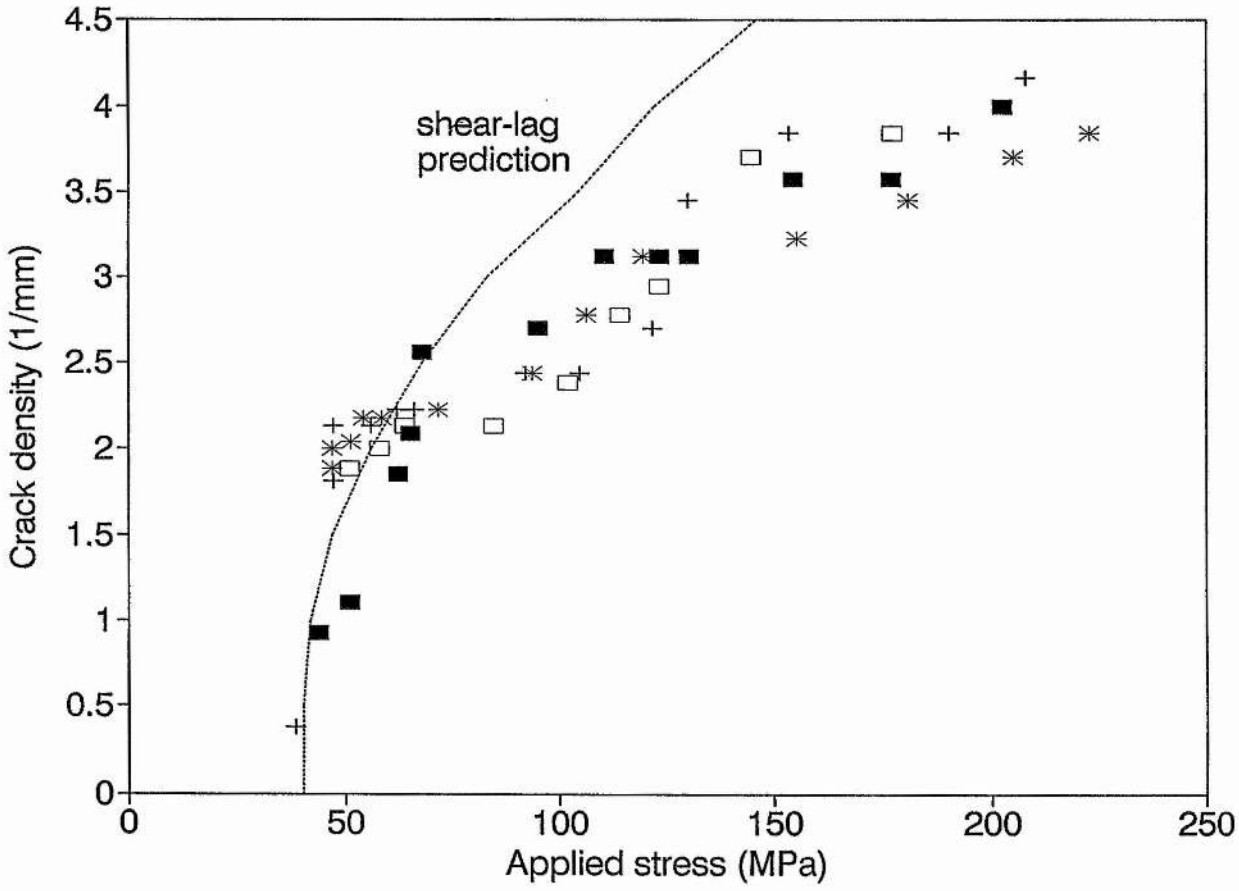

Figure 5.13 Crack density as a function of applied stress for the 90_2 (0.35 mm thick) ply in $(0/90)_s$ laminates along with a prediction of a simple shear-lag model (equation 5.8).

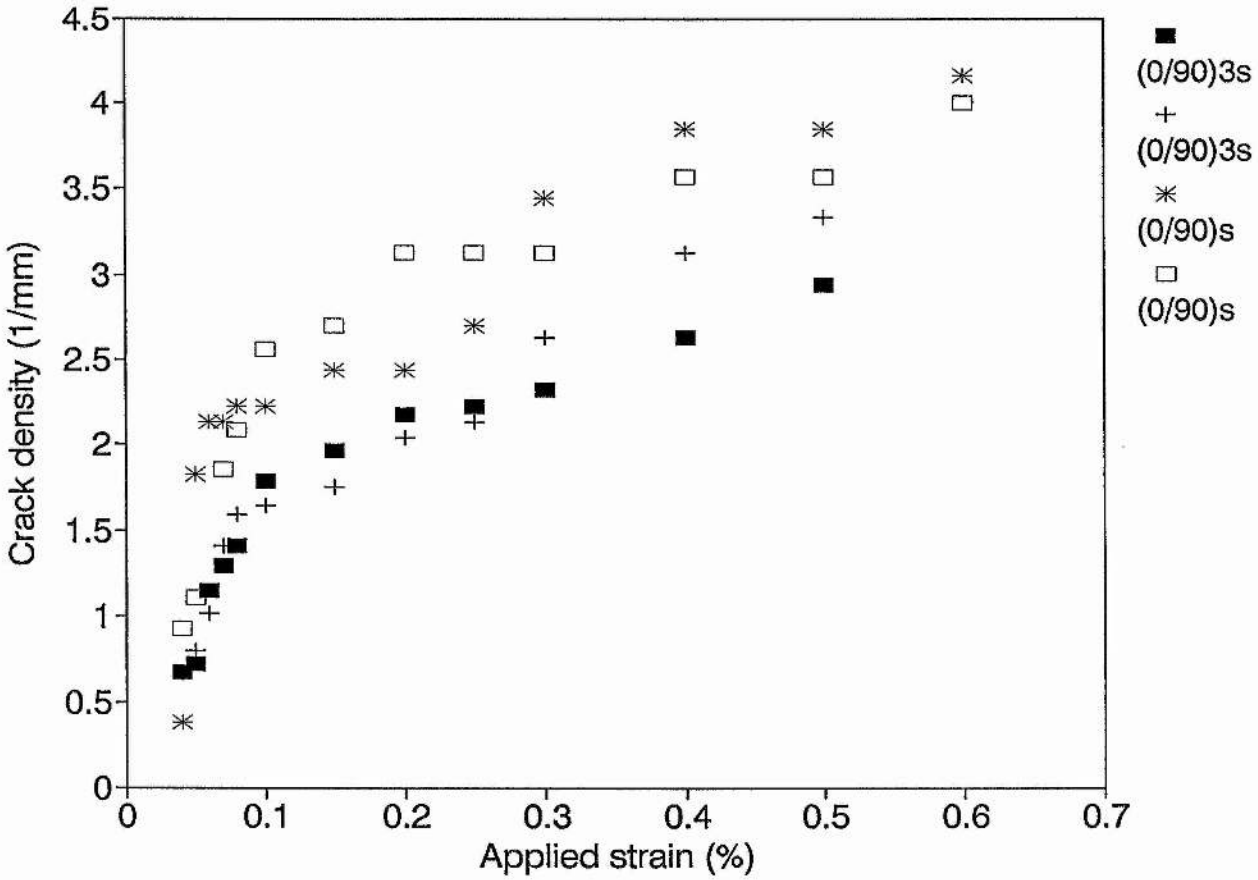

Figure 5.14 Crack density as a function of applied strain for the 90_2 (0.35 mm thick) ply in $(0/90)_s$ and $(0/90)_{3s}$ laminates.

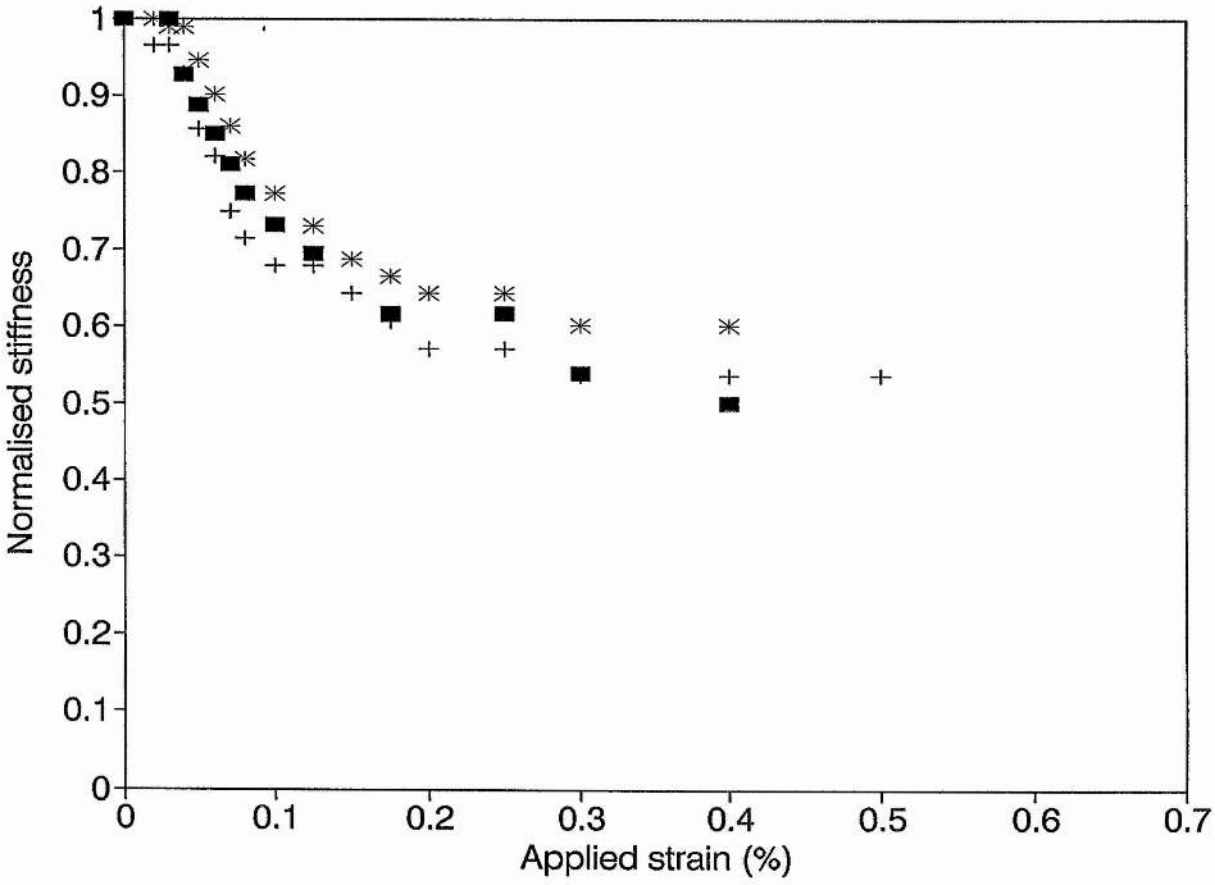

Figure 5.15 Normalised stiffness as a function of applied strain in $(0/90)_s$ laminates.

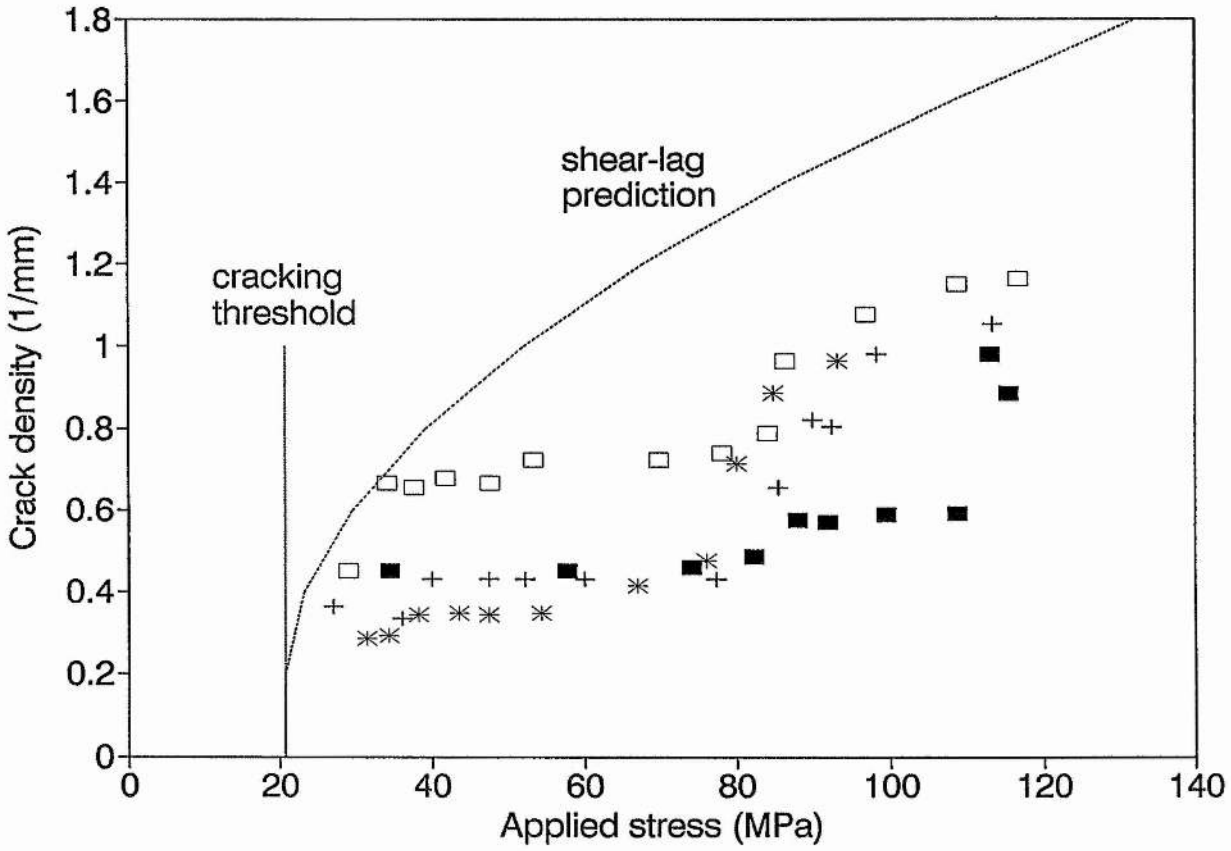

Figure 5.16 Crack density as a function of applied stress for the 90_8 (1.39 mm thick) ply in $(0_2/90_4)_s$ laminates along with a prediction of a simple shear-lag model (equation 5.8).

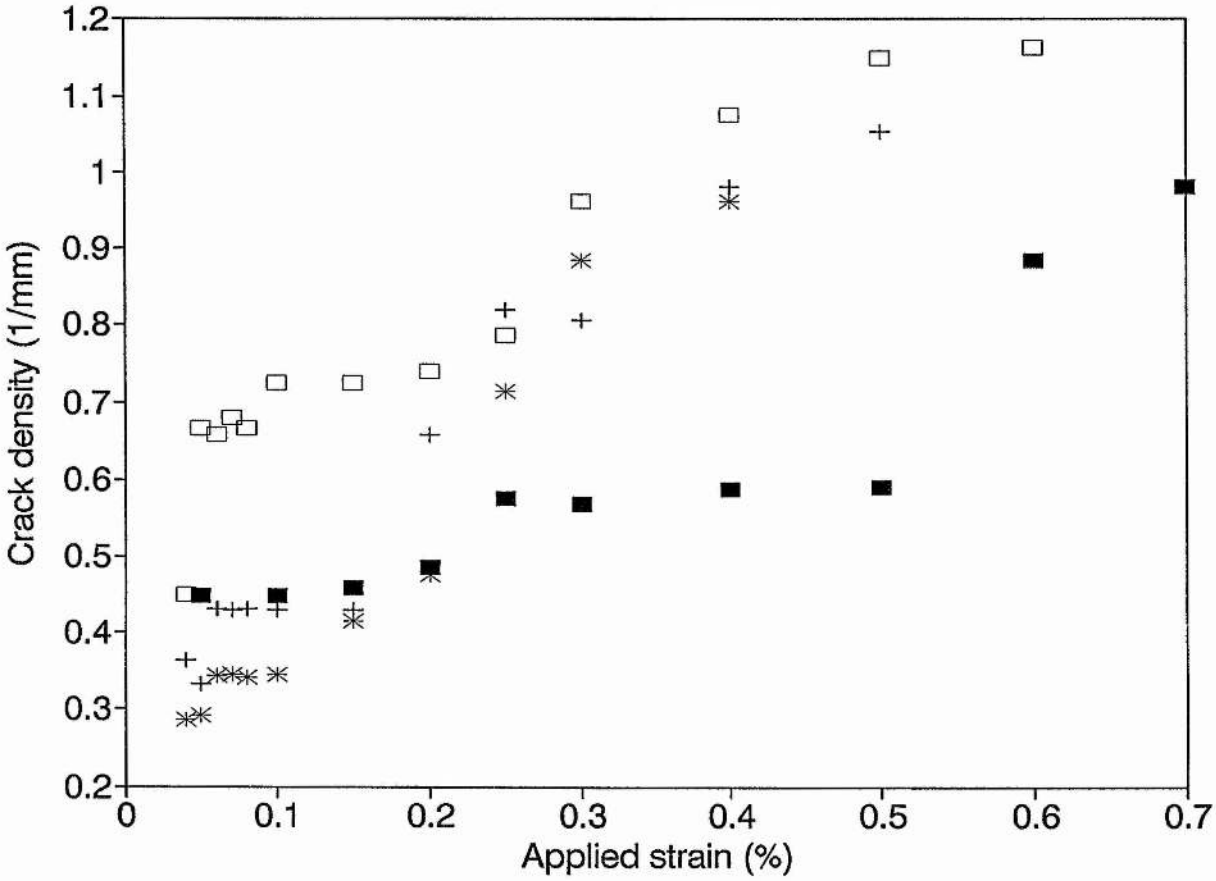

Figure 5.17 Crack density as a function of applied strain for the 90_8 (1.39 mm thick) ply in $(0_2/90_4)_s$ laminates.

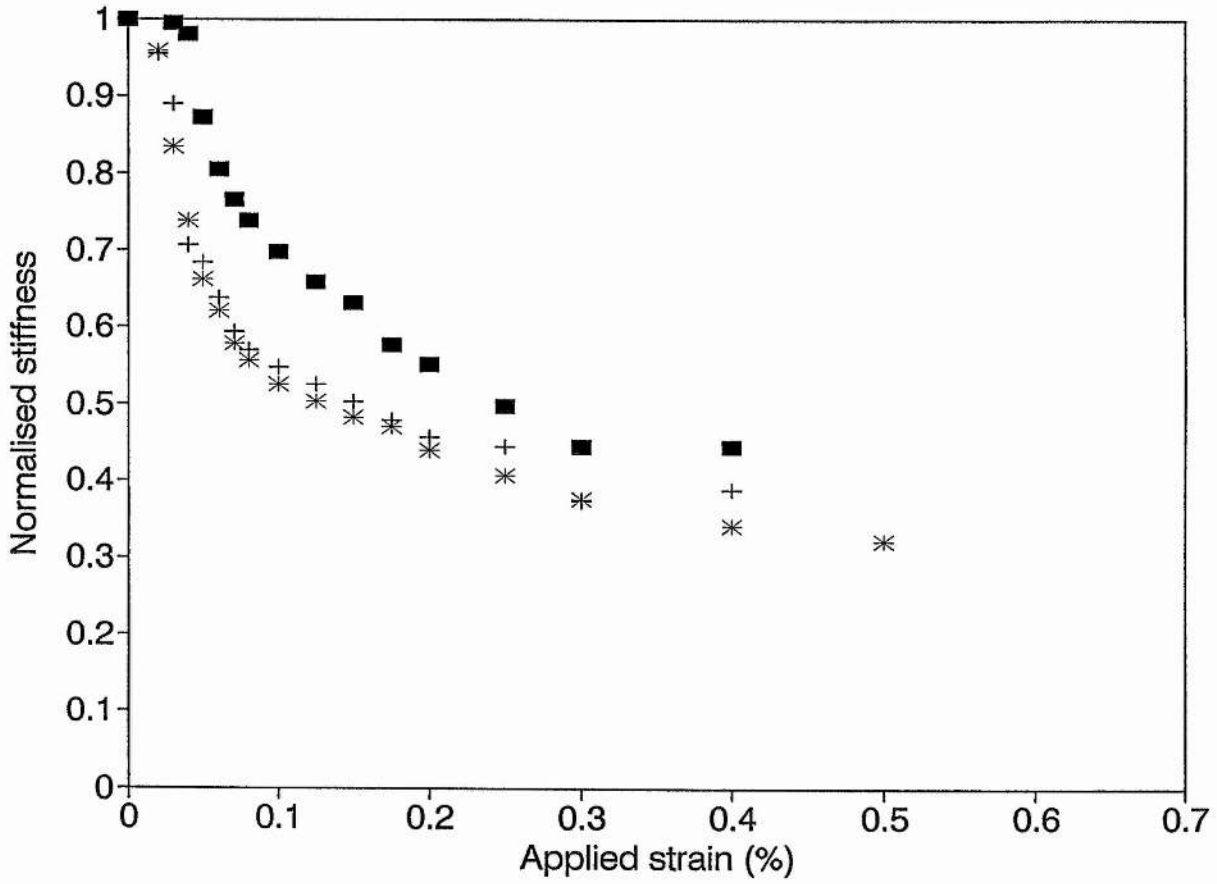

Figure 5.18 Normalised stiffness as a function of applied strain in $(0_2/90_4)_s$ laminates.

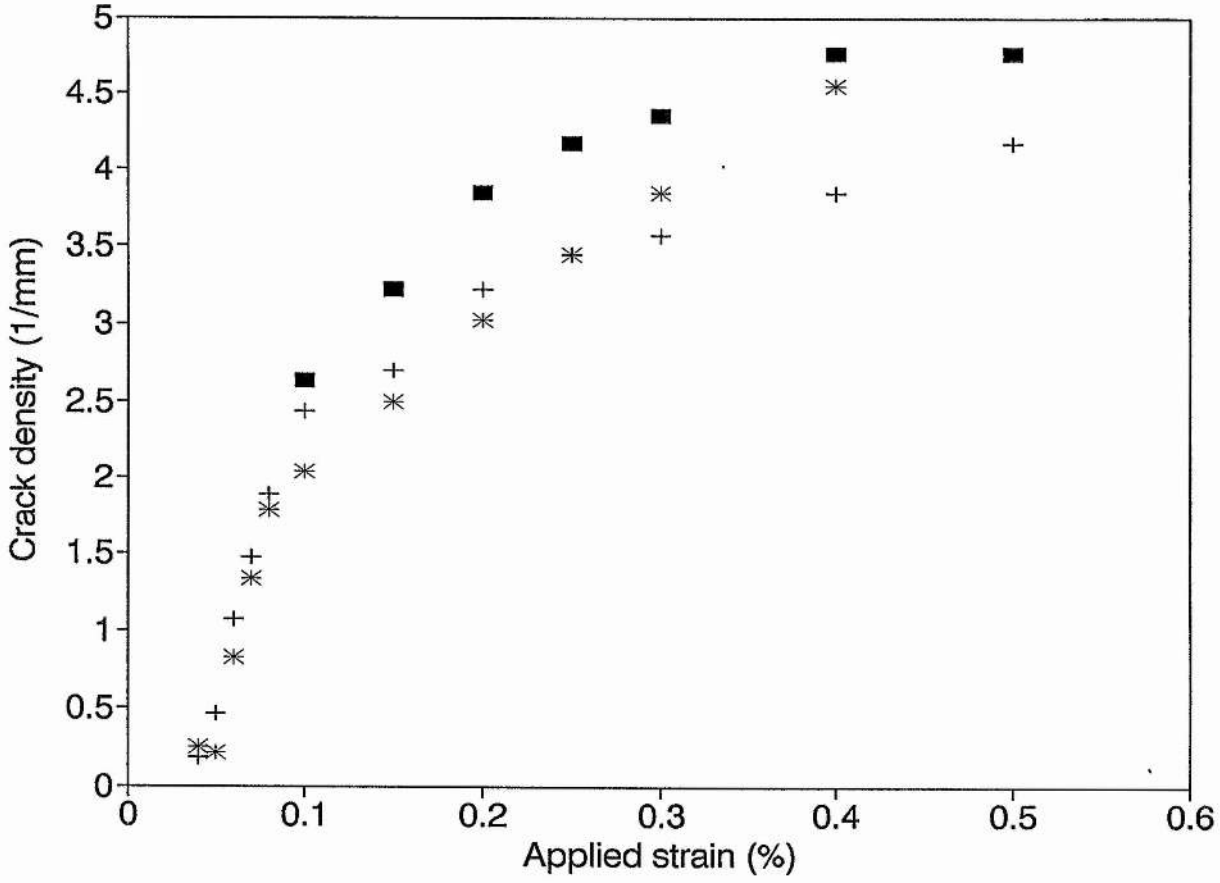

Figure 5.19 Crack density as a function of applied strain for the 90 (0.18 mm thick) ply in $(0/90)_{3s}$ laminates.

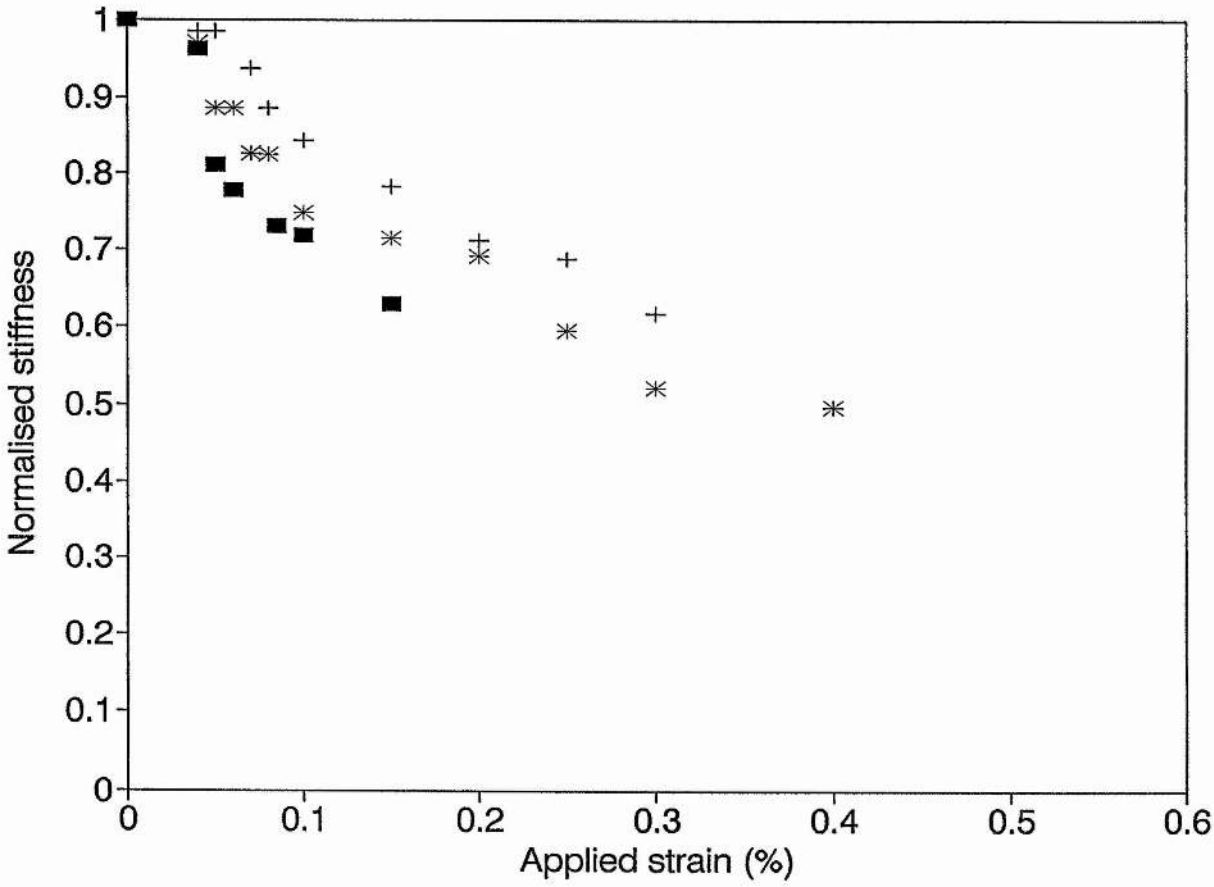

Figure 5.20 Normalised stiffness as a function of applied strain in $(0/90)_{3s}$ laminates.

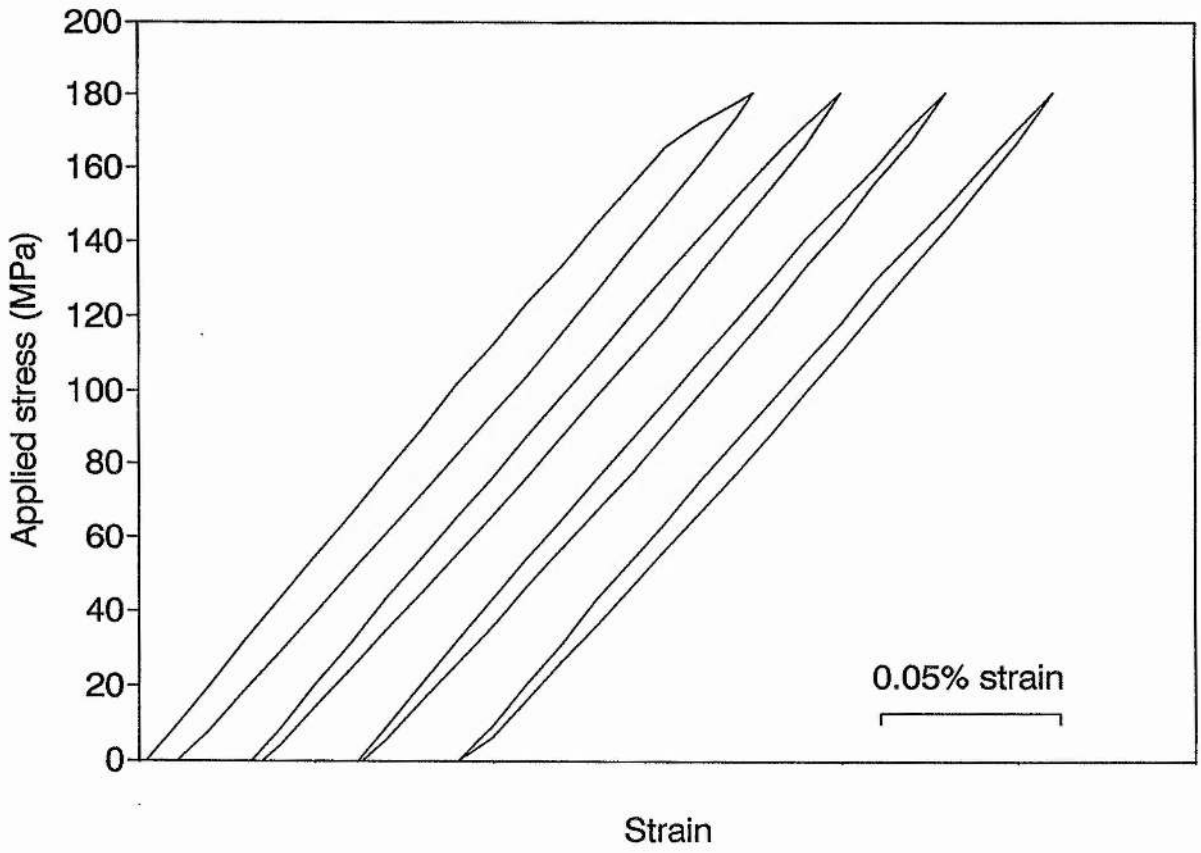

Figure 5.21 Stress/strain hysteresis loops obtained by cycling a unidirectional laminate to a maximum stress of 190 MPa for 4 cycles showing the stabilisation of unloading and reloading behaviour.

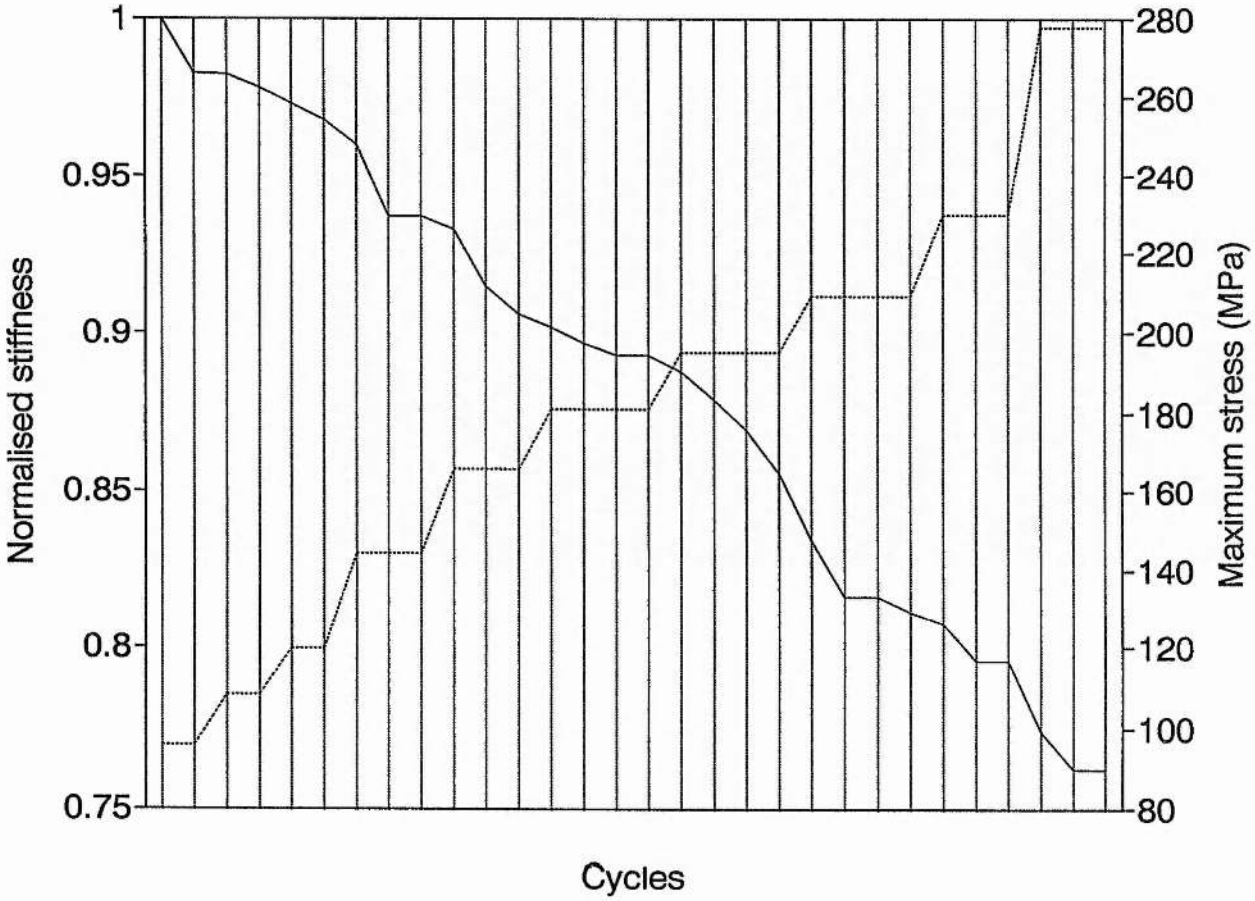

Figure 5.22 Normalised stiffness as a function of cycles at each maximum stress level during the quasi-static stress cycling of unidirectional laminates.

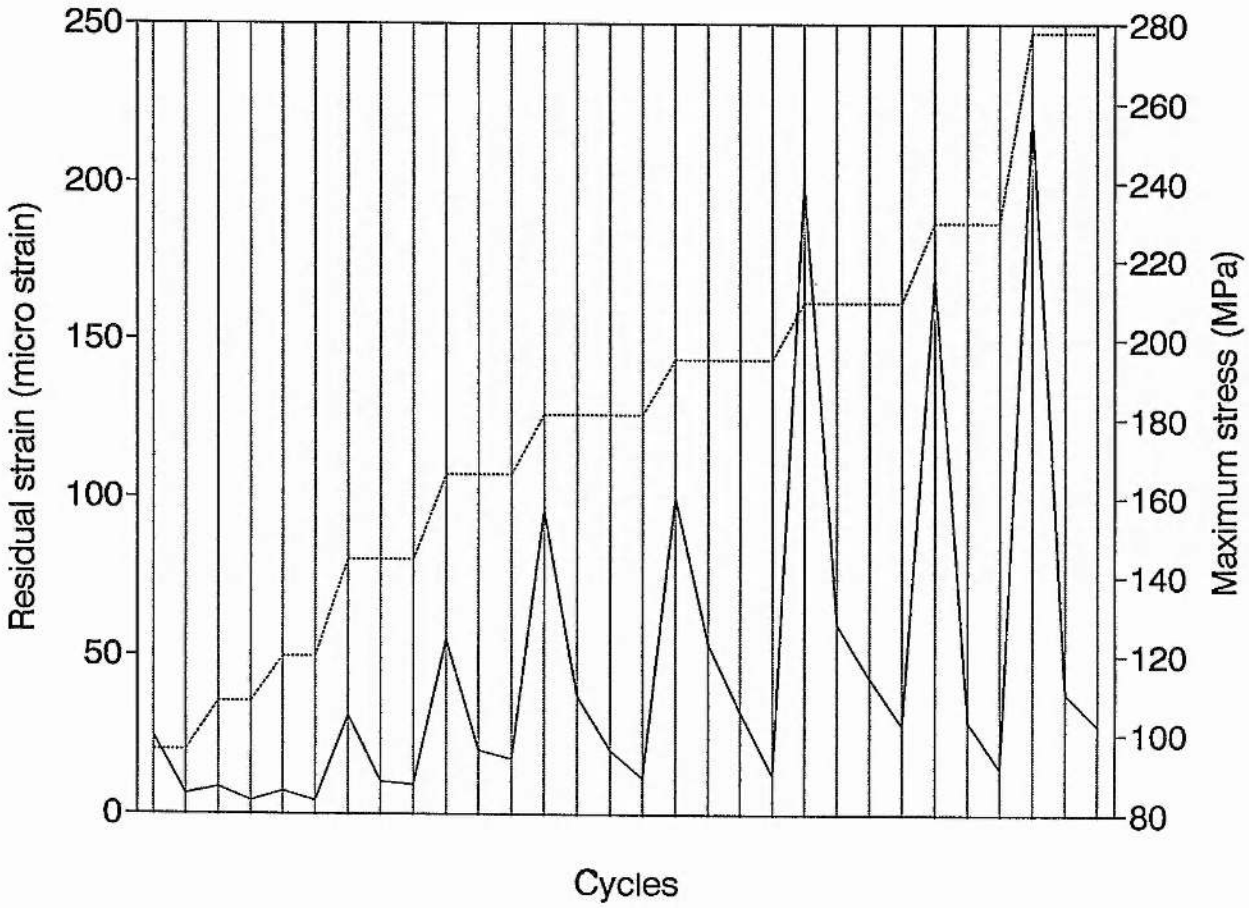

Figure 5.23 Residual strain as a function of cycles at each maximum stress level during the quasi-static stress cycling of unidirectional laminates.

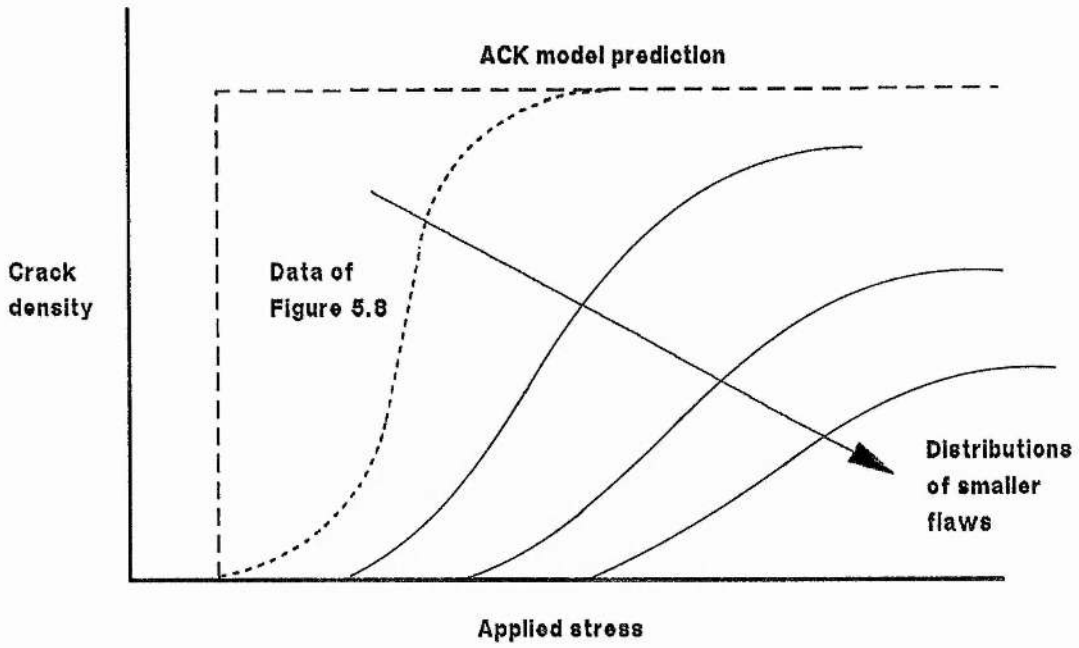

Figure 5.24 Schematic crack density as a function of applied stress diagram for $(0)_{12}$ laminates showing the form of the ACK prediction (broken line), the data shown in Figure 5.9 (dotted line) and the trends for distributions of progressively smaller flaws (solid lines).

CHAPTER 6

MODELLING THE QUASI-STATIC STRESS/STRAIN BEHAVIOUR OF NICALON REINFORCED CAS LAMINATES

6.1 INTRODUCTION

In Chapter 5 experimental data were presented describing the development of cracking in the 0° and 90° plies of unidirectional and crossply CMC laminates. The progressive cracking behaviour was discussed in the light of various fracture mechanics/stress based models.

An important consequence of matrix cracking is the reduction in laminate stiffness. This was seen on the continuous stress/strain curves for unidirectional and crossply laminates, the stable hysteresis loops developed during the quasi-static cycling of unidirectional material and the residual secant stiffness. In the present chapter the continuous and discontinuous stress/strain behaviour is modelled using an extended stress analysis based on ACK theory which incorporates the cracking data presented in Chapter 5.

To describe the continuous stress/strain behaviour of (0/90) crossply laminates a model is proposed which is based on the shear-lag analysis of Steif (see Ogin et al 1984). The analysis is modified to account for longitudinal ply cracking which occurs at high strains.

6.2 UNIDIRECTIONAL LAMINATES

6.2.1 Continuous stress/strain behaviour

To model the continuous stress-strain behaviour of a unidirectional laminate, within the range over which matrix cracking is the dominant damage event, we divide the stress/strain curve into a number of stress intervals (see Figure 6.1). Each interval is characterised by values of stress and crack density at the beginning and end of the interval. It is assumed that the number of cracks at any stress level in the continuous test is the same as in the discontinuous tests and that new cracks form only at the mean stress in any interval. To describe the stress/strain behaviour based on these assumptions and the data for the crack density/applied stress (obtained in the discontinuous tests) we proceed in the following way. Consider pairs of values of stress and average crack spacing $(\sigma_0,2s_0)$, $(\sigma_1,2s_1)$,..$(\sigma_{i-1},2s_{i-1})$, $(\sigma_i,2s_i)$, $(\sigma_{i+1},2s_{i+1})$, ...$(\sigma_n,2s_n)$ for a total of n stress increments. The ith increment can be characterised by an average crack spacing $2\bar{s}_i$ which is obtained from the crack spacing vs applied stress data (discontinuous tests) at the mean stress in the increment $\bar{\sigma}_i$, where $\bar{\sigma}_i = (\sigma_{i-1} + \sigma_i)/2$. This means that the crack spacing remains constant over the stress interval defined by σ_{i-1} and σ_i. At σ_i the crack spacing will then decrease from $2\bar{s}_i$ to $2\bar{s}_{i+1}$. In the following paragraphs, expressions describing the strains associated with these events are developed.

For a cracked laminate under an applied stress σ_c, we assume that at any stage the crack spacing is uniform. In the plane of the matrix cracks the matrix carries no load. Away from the crack plane the additional load shed onto the fibres is transferred back into the matrix by a constant interfacial shear stress, τ, in accordance with the ACK model. As long as the length over which the additional stress is transferred, x', is less than or equal to the half crack spacing, s, then the stress distribution in the fibres, shown schematically in Figure 6.2, can be described by:

$$\sigma_f = \frac{\sigma_c}{V_f} - \frac{2\tau x}{r} \quad (6.1)$$

where V_f is the fibre volume fraction, r is the fibre radius and x is the distance from the crack plane. Equation 6.1 can be used to find the transfer distance x', the point at which slippage no longer occurs and the fibre and matrix extend compatibly. At this point the fibre stress is given by

$$\sigma_f = \sigma_c \frac{E_f}{E_c} + \sigma_f^T \quad (6.2)$$

In equation 6.2 σ_c and σ_f^T are the stress on the composite and the thermal stress in the fibre (in the absence of mechanical load); E_f is the fibre modulus and E_c (= $V_f E_f + V_m E_m$, where E_m is the matrix modulus and V_m the matrix volume fraction) is the modulus of the uncracked composite. Equating equations 6.1 and 6.2 leads to an expression for x':

$$x' = \frac{r}{2\tau}\left[\sigma_c \frac{V_m E_m}{V_f E_c} - \sigma_f^T\right] \quad (6.3)$$

We can now calculate the mean strain in the fibres, which is the same as the mean strain on the composite. Over the portion AB (Figure 6.2) of the fibre stress profile the mean strain is given by

$$\epsilon_{AB} = \frac{1}{2E_f}\left[\frac{\sigma_c}{V_f} + \sigma_c \frac{E_f}{E_c} + \sigma_f^T\right] \quad (6.4)$$

Between B and C the composite strain is

$$\epsilon_{BC} = \frac{\sigma_c}{E_c} + \frac{\sigma_f^T}{E_f} \quad (6.5)$$

Hence the mean composite strain can be written as

$$\bar{\epsilon}_c = \left(\frac{2x'}{2s}\right)\left[\frac{\sigma_c(2V_f E_f + V_m E_m)}{2V_f E_f E_c} + \frac{\sigma_f^T}{2E_f}\right] + \left(\frac{2s - 2x'}{2s}\right)\left[\frac{\sigma_c}{E_c} + \frac{\sigma_f^T}{E_f}\right] \quad (6.6)$$

Equation 6.6 does not include the contribution to the mean composite strain by the exposed fibres between the faces of matrix cracks. In Appendix 3 the mean composite strain is calculated which includes the contribution by the exposed fibres (equation A3.1). This is compared with the value determined from equation 6.6. The calculation shows that because the maximum length of the exposed fibres (the crack opening displacement) within the valid stress range is only ~20μm, a maximum error of <1% is generated. As a result the contribution to the mean composite strain by the exposed fibres is neglected.

The mean strain on the fibre in the initially unloaded (and uncracked) composite is as a result of thermal stresses alone. This is

$$\bar{\epsilon}_f^T = \frac{\sigma_f^T}{E_f} \qquad (6.7)$$

The difference between equations 6.6 and 6.7 gives, after rearrangement, the increase in measured strain as a function of applied stress and crack spacing as:

$$\bar{\epsilon} = \frac{\sigma_c}{E_c} + \frac{r}{4s\tau E_f}\left[\sigma_c \frac{E_m V_m}{E_c V_f} - \sigma_f^T\right]^2 \qquad (6.8)$$

By differentiating equation 6.8, an expression may be obtained for the incremental strain, $d\bar{\epsilon}$, associated with a (small) stress increment, $d\sigma_c$, at constant crack spacing:

$$d\bar{\epsilon} = \left[\frac{1}{E_c} + \frac{r}{2s\tau E_f}\frac{E_m V_m}{E_c V_f}\left(\sigma_c \frac{E_m V_m}{E_c V_f} - \sigma_f^T\right)\right] d\sigma_c \qquad (6.9)$$

Note that equation 6.9 has sensible limits. For an uncracked laminate the crack spacing tends to infinity and the stress and strain increments are related via the initial modulus. Moreover, for a cracked laminate once x' (given by equation 6.3) is equal to half the crack spacing, $x' = s$, then the matrix can sustain no further load in which case the fibres slip through the broken blocks of matrix and the effective modulus of the composite is given by $E_f V_f$.

The incremental strain, $\Delta\bar{\epsilon}$ resulting from a change in crack spacing from $2\bar{s}_{i-1}$ to $2\bar{s}_i$ at constant stress, σ_c, may be calculated from writing equation 6.8 at the two different

values of the crack spacing and subtracting the former from the latter. On simplification we find:

$$\Delta\bar{\epsilon} = \frac{r}{4\tau E_f}\left[\sigma_c \frac{E_m V_m}{E_c V_f} - \sigma_f^T\right]^2 \left[\frac{1}{\bar{s}_i} - \frac{1}{\bar{s}_{i-1}}\right] \quad (6.10)$$

As indicated earlier, equations 6.8 to 6.10 are valid for applied stresses where $x' \leq s$. At values of σ_c where $x' > s$, the stress distribution along the fibres between two matrix cracks is as illustrated in Figure 6.3. The additional stress thrown onto the fibres adjacent to a matrix crack cannot be fully transferred back into the matrix. As a result the increase in measured strain is

$$\bar{\epsilon} = \frac{1}{E_f}\left[\frac{\sigma_c}{V_f} - \frac{\tau s}{r} - \sigma_f^T\right] \quad (6.11)$$

The strain increment $d\bar{\epsilon}$ associated with a small increment of stress $d\sigma_c$ is

$$d\bar{\epsilon} = \frac{1}{E_f V_f} d\sigma_c \quad (6.12)$$

Hence with increasing applied stress the stress profiles for the fibres and the matrix (Figure 6.3) diverge as the matrix can take no further share of the load and the composite continues to deform with an effective modulus given by $E_f V_f$.

The increment of strain associated with a change in crack spacing from $\bar{s}_{i-1}$ to $\bar{s}_i$ at constant stress σ_c is found in the same way as for equation 6.10 but writing equation 6.11 at the two values of crack spacing and subtracting one from the other. This gives

$$\Delta\bar{\epsilon} = \frac{\tau}{E_f r}(\bar{s}_{i-1} - \bar{s}_i) \quad (6.13)$$

Stress/strain predictions are based on stress intervals of 10 MPa defined from the measured elastic limit, 96 MPa. The increment of strain, $\Delta\bar{\epsilon}$, associated with a change in crack spacing at constant stress (given by equation 6.10 when $x' \leq s$ and by equation 6.13 when $x' > s$) is plotted as a horizontal line at the beginning of each stress

increment. The total strain for any stress increment is the sum of the contributions $\Delta\bar{\varepsilon}$ and $d\bar{\varepsilon}$. As a result the strain $d\bar{\varepsilon}$ associated with a stress increment $d\sigma_c$ at constant crack spacing (given by equation 6.9 when $x' \leq s$ and by equation 6.12 when $x' > s$) is plotted from the new origin defined by $\Delta\bar{\varepsilon}$. This gives the stepped form to the schematic stress/strain prediction shown in Figure 6.4. Actual stress/strain predictions shown in Figure 6.5 and Figure 6.6 illustrate the sensitivity of the values of τ and σ_f^T used in equations 6.1 to 6.13. Two values of τ are considered, 5 MPa (Figure 6.5) and 10 MPa (Figure 6.6) for σ_f^T = 0, -50, -100 and -200 MPa (where the negative sign indicates a compressive stress). Examination of these figures also show that the magnitude of one parameter counters the other. As a result there is no unique solution to these equations to describe the continuous stress/strain behaviour. In order to determine the values or τ and σ_f^T accurately the unloading and subsequent reloading behaviour of a cracked laminate must be considered (see Section 6.2.2). Using the values of 8 MPa and 50 MPa (compressive) for τ and σ_f^T respectively, obtained from the analysis of Section 6.2.2, the range of applied stress can be determined for which equations 6.8 to 6.10 and equations 6.11 to 6.13 are valid (Figure 6.7). Hence a stress/strain prediction obtained (Figure 6.8). The prediction shows good agreement with the data over the matrix cracking region of the continuous stress/strain curve.

6.2.2 Unloading and reloading stress/strain behaviour

Our starting point is a laminate loaded from zero to a stress σ_c (in the matrix cracking region) which produces an array of cracks spaced 2s apart. The length over which the additional load shed onto the fibres is transferred back into the matrix, x', is assumed to be less than the half crack spacing, s. The stress profile in the fibres from a crack plane to the midpoint between two cracks is illustrated in Figure 6.9 (broken line). The mean composite strain is described by equation 6.8.

If the laminate is unloaded by some small amount, a volume of matrix adjacent to the crack plane will slip relative to the fibres as the matrix in the plane of the crack is unable to sustain a stress. With continued unloading further slippage will occur in such a way

that the slippage distance varies linearly with stress. This assumption is reasonable as slippage is controlled by the (constant) interfacial shear strength τ. The stress profile in the fibres when the applied stress is at some intermediate level σ (between σ_c and zero) is illustrated in Figure 6.9 (dotted line). The mean composite strain corresponding to this profile cannot be described by equation 6.6. This is because of the slippage occurring over the distance y from the crack plane. In addition between x' and x'- y from the crack plane the mismatch in fibre and matrix strains can be sustained by the interface. This means that the transfer length x' remains constant during unloading (and subsequent reloading to σ_c). It follows that determining average strain in the fibres (in the same way as for equations 6.4 and 6.5) and deducting the initial thermal strain gives the measured mean composite strain as

$$\bar{\epsilon} = \frac{x'}{s}\bar{\epsilon}_f + \left(1 - \frac{x'}{s}\right)\frac{1}{E_f}\left[\sigma\frac{E_f}{E_c} + \sigma_f^T\right] - \frac{\sigma_f^T}{E_f} \qquad (6.14)$$

In equation 6.14 $\bar{\epsilon}_f$ is the mean strain in the fibres between zero and x' from the crack plane. On substituting and rearranging

$$\bar{\epsilon} = \frac{\sigma}{E_c} + \frac{r}{8s\tau E_f}\left[\left(\frac{E_m V_m}{E_c V_f}\right)^2\left(\sigma_c^2 - \sigma^2 + 2\sigma\sigma_c\right) - 4\sigma_c\sigma_f^T\frac{E_m V_m}{E_c V_f} + 2\left(\sigma_f^T\right)^2\right] \qquad (6.15)$$

When the laminate is fully unloaded the matrix will have slipped a distance $(x' + x'^T)/2$ producing the residual stress profile in the fibres shown in Figure 6.9 (solid line). The mean residual composite strain $\bar{\epsilon}_{res}$ (permanent set) is given by equation 6.15 by setting $\sigma = 0$. This gives

$$\bar{\epsilon}_{res} = \frac{r}{8s\tau E_f}\left[\left(\sigma_c\frac{E_m V_m}{E_c V_f}\right)^2 - 4\sigma_c\sigma_f^T\frac{E_m V_m}{E_c V_f} + 2\left(\sigma_f^T\right)^2\right] \qquad (6.16)$$

Equation 6.16 is a general expression for $\bar{\epsilon}_{res}$. If the thermal stress is zero and the transfer length x' is equal to half the crack spacing, s, it reduces to the expression given by Aveston et al (1971).

If the laminate is now reloaded from this residual strain, the slippage distance will again

vary linearly with stress between zero and σ_c. This is because the shear stress between fibres and matrix will always act in the direction which opposes the loading. At some intermediate stress σ the stress profile in the fibres is as shown in Figure 6.10 (dotted line). The measured composite strain is given by equation 6.14 when the appropriate expression for $\bar{e}_f$ is substituted. On rearranging

$$\bar{e} = \frac{\sigma}{E_c} + \frac{r}{8s\tau E_f}\left[\left(\sigma^2 + \sigma_c^2\right)\left(\frac{E_m V_m}{E_c V_f}\right)^2 - 4\sigma_c\sigma_f^T\frac{E_m V_m}{E_c V_f} + 2\left(\sigma_f^T\right)^2\right] \quad (6.17)$$

Equations 6.15 and 6.17 can be shown to be consistent with their expected limits. When the applied stress is zero ($\sigma = 0$) they both reduce to equation 6.16. When the applied stress is equal to the previous maximum value ($\sigma = \sigma_c$) they both predict the strain given by equation 6.8.

In order to obtain the values for the interfacial shear strength, τ, and initial thermal stress in the fibres, σ_f^T, used in equations 6.15, 6.16 and 6.17 a computer program was written. The program was able to converge on a unique solution for τ and σ_f^T by determining the best fit with the experimental unloading and reloading data (see discontinuous test results in Chapter 5). This is because the strain at zero applied stress (the cumulative residual strain) is calculated (equation 6.16) as well as the hysteresis during unloading (equation 6.15) and reloading (equation 6.17). Unloading and reloading predictions using values of 8 MPa for the interfacial shear strength and 50 MPa (compression) for the initial thermal stress in the fibres are shown in Figures 6.11a, 6.11b and 6.11c for the complete range of maximum applied stress. Good agreement is found with the discontinuous stress/strain data for maximum applied stresses of less than 190 MPa (and hence $x'<s$) for which the model is valid (Figures 6.11a and 6.11b). The model becomes invalid for maximum applied stresses in excess of 190 MPa (where $x'>s$) as the assumptions regarding the transfer of stress between the fibres and the matrix are violated (see Figure 6.7). In accordance, when $\sigma_c>190$ MPa the (invalid) model predictions no longer describe the experimental data (Figure 6.11c).

The cumulative residual strain calculated using equation 6.16 is also shown as a function of maximum applied stress in Figure 6.12. The data previously shown in Figure 5.12 is

also plotted. Good agreement is found once again using the values of τ = 8 MPa and σ_f^T 50 MPa (compressive) up to an a maximum stress of 190 MPa, the limit of validity for equation 6.16.

6.3 (0/90) CROSSPLY LAMINATES

6.3.1 Continuous stress/strain behaviour

To model the continuous stress/strain behaviour of a crossply laminate within the range where transverse and longitudinal ply cracking are the dominant damage mechanisms we adopt a similar approach to that used for the unidirectional laminates described in Section 6.2. We divide the stress/strain curve into a number of stress intervals. The beginning and end of each interval are characterised by values of stress, transverse ply crack density and longitudinal ply crack density. It is assumed that the number of transverse ply cracks and longitudinal ply cracks at any stress level in the continuous test are the same as in the discontinuous tests (see Chapter 5) and that new cracks form only at the mean stress in any interval. In addition it is assumed that the crack spacings in the 90° ply and in the 0° plies are uniform and that cracks terminate at the ply interface. The ith increment can be characterised by an average transverse ply crack spacing $2\bar{s}_{2(i)}$ and longitudinal ply crack spacing $2\bar{s}_{1(i)}$ which are obtained from the crack spacing vs applied stress data (see Chapter 5) at the mean applied stress in the increment $\bar{\sigma}_{c(i)}$ where $\bar{\sigma}_{c(i)} = (\sigma_{c(i-1)} + \sigma_{c(i)})/2$. This means that the crack spacing in both plies remains constant over the increment defined by $\sigma_{c(i-1)}$ and $\sigma_{c(i)}$. At $\sigma_{c(i)}$ the transverse ply crack spacing decreases from $2\bar{s}_{2(i)}$ to $2\bar{s}_{2(i+1)}$ and the longitudinal crack spacing decreases from $2\bar{s}_{1(i)}$ to $2\bar{s}_{1(i+1)}$. In the following paragraphs expressions describing the strains associated with theses events are developed.

Following the shear-lag analysis of Steif (1984) for a crossply laminate under an applied stress σ_c the stress in the longitudinal plies at a distance y from a co-ordinate origin midway between two transverse ply crack cracks (spaced $2s_2$ apart) is, ignoring thermal stresses

$$\sigma_1 = \sigma_c\left[\left(1 + \frac{d}{b}\right) - \frac{E_1}{E_0}\right]\frac{\cosh\lambda y}{\cosh\lambda s_2} + \sigma_c\frac{E_1}{E_0} \qquad (6.18)$$

where

$$\lambda^2 = \frac{3G_{23}}{bd^2}\left(\frac{bE_1 + dE_2}{E_1E_2}\right) \qquad (6.19)$$

with the notation:

E_1 = uncracked longitudinal ply modulus

E_2 = uncracked transverse ply modulus

E_0 = composite modulus (= $[bE_1+dE_2]/[b+d]$)

G_{23} = through-thickness shear modulus of the transverse ply

b = longitudinal ply thickness

2d = transverse ply thickness

Integrating equation 6.18 over the distance between two transverse ply cracks gives the average longitudinal ply stress $\bar{\sigma}_1$ as

$$\bar{\sigma}_1 = \frac{1}{2s_2}\int_{-s_2}^{s_2}\sigma_1\,dy = \frac{\sigma_c}{\lambda s_2}\tanh\lambda s_2\left[\left(1 + \frac{d}{b}\right) - \frac{E_1}{E_0}\right] + \sigma_c\frac{E_1}{E_0} \qquad (6.20)$$

When damage occurs in the longitudinal plies in the form of 0° ply cracks the values of the longitudinal ply modulus E_1 and the composite modulus E_0 (which are related by the rule of mixtures) used in equation 6.20 are no longer constant. The accumulation of longitudinal ply cracks in both $(0/90)_s$ and $(0_2/90_4)_s$ laminates as a function of applied strain is to a first approximation the same as that of the unidirectional material (Figure 5.10). If it is assumed that the constraint on the longitudinal plies by the central transverse ply does not affect the distribution of stress adjacent to cracks in the longitudinal plies then the model proposed in Section 6.2.1 can be used to describe the 0° ply cracking process and its effect on E_1 (and hence E_0). In the case of the unidirectional material it was shown that at applied stresses in excess of 190 MPa (for τ=8 MPa and σ_f^T=-50 MPa) the additional stress thrown onto the fibres (as a result of a matrix crack) could not be fully transferred back into the matrix. As a result two different expressions for the increase in measured composite strain $\bar{\epsilon}$ were developed (equations 6.8 and 6.11) when $\sigma_c \leq 190$ MPa (and $x' \leq s$) and when $\sigma_c > 190$ MPa (and $x' > s$) respectively. In order to describe accurately the contribution by 0° ply cracking

to the overall composite strain in crossply laminates the two cases when $x' \leq s$ and when $x' > s$ must again be considered.

(a) $x' \leq s_1$

When the average stress in the longitudinal plies $\bar{\sigma}_1$ is less than 190 MPa then the transfer length, x', is less than the half crack spacing, s_1. As a result the stress distribution along the fibres in the longitudinal plies is as shown in Figure 6.2 and the average longitudinal ply strain is described by equation 6.6. Ignoring thermal stresses in the fibres and matrix the degraded longitudinal ply modulus as a function of average longitudinal ply stress $\bar{\sigma}_1$ and crack spacing $2s_1$ can be obtained from equation 6.6. After substitution (noting $E_c \equiv E_1$) and rearrangement this gives

$$E_1' = \frac{d\bar{\sigma}_1}{d\bar{\epsilon}_1} = \left(\frac{1}{E_1} + \frac{\bar{\sigma}_1 r (E_m V_m)^2}{2 s_1 \tau (E_1 V_f)^2 E_f} \right)^{-1} \qquad (6.21)$$

The degraded composite modulus can be determined using the rule of mixtures:

$$E_0' = \frac{b E_1' + d E_2}{b + d} \qquad (6.22)$$

Substituting the values of E_1' from equation 6.21 and E_c' from equation 6.22 into equation 6.20 allows the measured composite strain to be determined as a function of applied stress, transverse ply crack density and longitudinal ply crack density since $\bar{\epsilon} = \bar{\sigma}_1 / E_1'$. This gives

$$\bar{\epsilon} = \frac{\sigma_c}{E_1' \lambda' s_2} \tanh \lambda' s_2 \left[\left(1 + \frac{d}{b} \right) - \frac{E_1'}{E_0'} \right] + \frac{\sigma_c}{E_0'} \qquad (6.23)$$

where

$$\lambda'^2 = \frac{3 G_{23}}{b d^2} \left(\frac{b E_1' + d E_2}{E_1' E_2} \right) \qquad (6.24)$$

For the ith stress increment (of average stress $\bar{\sigma}_{c(i)}$) the average stress in the longitudinal plies $\bar{\sigma}_{1(i)}$ is calculated from equation 6.20 using the previous increment values $E'_{1(i-1)}$,

$E'_{0(i-1)}$ and $\lambda'_{(i-1)}$ for E_1, E_0 and λ respectively. Physically this means that the increase in transverse ply crack density determines the additional stress thrown onto the longitudinal plies. $E'_{1(i)}$, $E'_{0(i)}$ and $\lambda'_{(i)}$ are subsequently calculated (equations 6.21, 6.22 and 6.24) to account for the new longitudinal ply damage and are used in equation 6.23 in order to determine $\bar{\varepsilon}_{(i)}$. The process is iterated for subsequent increments so that $\bar{\sigma}_{1(i+1)}$ may be calculated and hence $\bar{\varepsilon}_{(i+1)}$ obtained.

By differentiating equation 6.23 an expression may be obtained for the incremental strain $d\bar{\varepsilon}_{(i)}$ associated with a (small) increment of stress $d\sigma_{c(i)}$ at constant transverse and longitudinal ply crack spacings:

$$d\bar{\varepsilon}_{(i)} = \left\{ \frac{\tanh \lambda'_{(i)} \bar{s}_{2(i)}}{E'_{1(i)} \lambda'_{(i)} \bar{s}_{2(i)}} \left[\left(1 + \frac{d}{b}\right) - \frac{E'_{1(i)}}{E'_{0(i)}} \right] + \frac{1}{E'_{0(i)}} \right\} d\sigma_{c(i)} \qquad (6.25)$$

Note that on appropriate substitution equation 6.25 has sensible limits in terms of the transverse ply crack spacing, $2s_2$. When $s_2 \to 0$ the effective composite modulus is $bE_1'/(b+d)$. Moreover, if the longitudinal plies are undamaged when $\bar{\sigma}_{1(i)}$ is below the longitudinal ply cracking threshold then $E'_{0(i)} = bE'_{1(i)}/(b+d) = bE_1/(b+d)$. When $s_2 \to \infty$ the composite modulus is given simply by the rule of mixtures (equation 6.22).

At constant stress $\bar{\sigma}_{1(i)}$ there will be an incremental strain from a change in transverse ply crack density and from a change in longitudinal ply crack density. The incremental strain $\Delta\bar{\varepsilon}_{2(i)}$ resulting from a change in transverse ply crack spacing from $2\bar{s}_{2(i-1)}$ to $2\bar{s}_{2(i)}$ can be calculated by writing equation 6.23 at the two different values of crack spacing and subtracting the former from the latter. This gives

$$\Delta\bar{\varepsilon}_{2(i)} = \frac{\bar{\sigma}_{c(i)}}{E'_{1(i)} \lambda'_{(i)}} \left[\left(1 + \frac{d}{b}\right) - \frac{E'_{1(i)}}{E'_{0(i)}} \right] \left[\frac{\tanh \lambda'_{(i)} \bar{s}_{2(i)}}{\bar{s}_{2(i)}} - \frac{\tanh \lambda'_{(i-1)} \bar{s}_{2(i-1)}}{\bar{s}_{2(i-1)}} \right] \qquad (6.26)$$

The incremental strain $\Delta\bar{\varepsilon}_{1(i)}$ associated with a change in longitudinal crack spacing from $2\bar{s}_{1(i-1)}$ to $2\bar{s}_{1(i)}$ can be calculated in a similar way and is described in Section 6.2. Writing equation 6.8 at constant 0° ply stress at the two values of crack spacing (ignoring

thermal stresses in the fibres and matrix) and subtracting one from the other gives

$$\Delta\bar{\varepsilon}_{1(i)} = \frac{\bar{\sigma}_{1(i)}^2 r (E_m V_m)^2}{4\tau E_f (E_1 V_f)^2}\left[\frac{1}{\bar{s}_{1(i)}} - \frac{1}{\bar{s}_{1(i-1)}}\right] \quad (6.27)$$

(b) $x'>s_1$

For the stress increments where $\bar{\sigma}_{1(i)}>190$ MPa and hence $x'>s_{1(i)}$ the stress distribution along the fibres in the longitudinal plies is as shown in Figure 6.3. The average longitudinal ply strain $\bar{\varepsilon}_{1(i)}$ is described by equation 6.11. Consequently the strain increments $d\bar{\varepsilon}_{(i)}$ and $\Delta\bar{\varepsilon}_{2(i)}$ are given by equation 6.25 and 6.26 (respectively) where the degraded longitudinal ply modulus E'_1 is equal to the limiting value of $E_f V_f$. The strain increment $\Delta\bar{\varepsilon}_{1(i)}$ associated with a change in longitudinal crack spacing from $2\bar{s}_{1(i-1)}$ to $2\bar{s}_{1(i)}$ is given by rewriting equation 6.13 as

$$\Delta\bar{\varepsilon}_{1(i)} = \frac{\tau}{E_f r}(\bar{s}_{1(i-1)} - \bar{s}_{1(i)}) \quad (6.28)$$

For both $(0/90)_s$ and $(0_2/90_4)_s$ lay-ups stress increments of 10 MPa were used from the transverse ply cracking threshold. This occurs at an applied stress of 40 MPa for the $(0/90)_s$ laminates and at 17 MPa for the $(0_2/90_4)_s$ laminates. For each stress increment the total strain is equal to the sum of the contributions $\Delta\bar{\varepsilon}_{2(i)}$, $\Delta\bar{\varepsilon}_{1(i)}$ and $d\bar{\varepsilon}_{(i)}$. The contributions $\Delta\bar{\varepsilon}_{2(i)}$ (given by equation 6.26) and $\Delta\bar{\varepsilon}_{1(i)}$ (given by equation 6.27 when $x'\leq s_1$ and by equation 6.28 when $x'>s_1$) are plotted as horizontal lines at the beginning of the increment. The contribution $d\bar{\varepsilon}_{(i)}$ associated with the stress increment $d\sigma_{c(i)}$ at constant transverse and longitudinal ply crack spacings (given by equation 6.25) is plotted at the new origin defined by $\Delta\bar{\varepsilon}_{2(i)} + \Delta\bar{\varepsilon}_{1(i)}$. This gives the stepped form to the predicted stress/strain response shown schematically in Figure 6.13. Actual predictions for the $(0/90)_s$ and $(0_2/90_4)_s$ laminates are shown in Figures 6.14 and 6.15 respectively. Also shown in each figure is experimental stress/strain data and the prediction obtained using equation 6.23, the case when the longitudinal plies remain undamaged, i.e. the original Steif shear-lag model. Using a value of 8 MPa for the fibre/matrix interfacial shear strength (determined in Section 6.2) reasonable agreement is found between the modified shear-lag model and the experimental data. Although with increasing applied

stress the error in the model predictions increases (~40% for the $(0_2/90_4)_s$ lay-up at 100 MPa) there is a significant improvement in the predicted stress/strain behaviour over the unmodified Steif shear-lag model in both cases.

6.4 DISCUSSION

6.4.1 Unidirectional laminates

The stress/strain behaviour of laminates containing an array of matrix cracks has been modelled by extending the stress analysis of Aveston et al (1971). Values of 8 MPa for the interfacial shear strength and 50 MPa (compression) for the initial thermal stress in the fibres give good agreement with the continuous and discontinuous stress/strain data. The value of τ seems reasonable given that the fibre/matrix bond in this type of composite is extremely weak (Prewo et al 1989), assumed here to be purely frictional in nature. Two approaches to measure τ for Nicalon reinforced lithium aluminosilicate laminates have recently been reviewed by Evans and Marshall (1989). Firstly an indentation method is described where load/unload cycles are measured for the nano-indentation of single fibres. According to previous work (Marshall and Oliver 1987) the method appears to be valid when τ is small ($\leq$ 10 MPa). However, as the authors point out when fibres are loaded in compression the interface will be compressed. This could give a substantial error in the measured τ value. The second method described uses measurements of the hysteresis in crack opening displacement when a laminate is stress cycled. The calculation of τ necessitates knowing the stress at which individual cracks have formed. It is clear from Figure 5.9 that for Nicalon reinforced CAS laminates this stress has a range of values. The approach taken in Section 6.2 avoids many of the problems outlined above. This is because the model uses uniaxial stress/strain data for known crack densities. Stiffness parameters of this type are associated with the bulk where the stress state is uniform and an average fibre volume fraction can be used. As a result the values of τ and σ_f^T that have been determined are perhaps more reliable.

The initial thermal stress in the fibres is generated by the difference in the displacements between the fibres and matrix when the laminate is cooled from the processing temperature. A simple estimate for this value has been made in Section 5.4.1 by considering the thermal expansion coefficient mismatch between the unreinforced matrix

and the composite in the longitudinal direction over the maximum temperature range (from the processing temperature to room temperature). For stress equilibrium the thermal stress in the fibres is given by $\sigma_m{}^T V_m = \sigma_f{}^T V_f$. Although the magnitude of the resultant stress, 65 MPa, is a little higher, both it and the value of $\sigma_f{}^T$ used in the models (50 MPa) are compressive in nature. In addition the calculation described in Section 5.4.1 represents an upper bound for $\sigma_f{}^T$ because the temperature range used is the largest possible. Clearly elastic stresses will only begin to build up at some temperature beneath the processing temperature (when the matrix no longer flows and grain boundaries interlock). Hence the predicted value of $\sigma_f{}^T$ would seem reasonable.

The model used to describe the discontinuous stress/strain behaviour is limited to maximum applied stresses of less than or equal to 190 MPa. This is because the assumptions regarding the distribution of stress between the fibres and the matrix require that $x' \leq s$ i.e. the additional load shed onto the fibres as a result of a matrix crack is fully transferred back into the matrix over the transfer length x'. The model used to describe the continuous stress/strain behaviour does not suffer from this restriction. Figure 6.3 shows that when $\sigma_c > 190$ MPa the stress profiles for the fibres and the matrix diverge as the matrix can take no further share of the load. As a result the average composite strain, given by the average strain in the fibres, is dependent on the amount of load carried by the fibres which can be transferred back into the matrix over the half crack spacing, s (equation 6.11). Consequently the strain $\Delta\bar{e}$ associated with a change in crack spacing from $2\bar{s}_{(i-1)}$ to $2\bar{s}_{(i)}$ (for $\sigma_c > 190$ MPa) is dependent on τ but independent of applied stress (equation 6.13). With increasing stress above 190 MPa the fibres slip through the broken blocks of matrix and the effective composite modulus (equation 6.12) is given by $E_f V_f$.

During stress cycling tests after the initial damage had been put into the laminate (on the first cycle), between 1 and 5 further cycles to the same maximum stress were required in order to generate closed hysteresis loops (see Section 5.4.5). For a constant damage state the model gives a closed hysteresis loop on the second cycle to the same maximum stress. The disparity between the experimental observations and the predicted response can be explained if additional matrix cracking occurs during cycling. However, the fact

that the predictions for the continuous and discontinuous stress/strain behaviour (which use the same crack density vs applied stress data) are consistent with the data would seem to rule this out. Instead, it is suggested that slippage between the fibres and matrix (occurring adjacent to the crack plane) is responsible for the residual strain obtained on the second and subsequent cycles at each damage state. The model presented in this chapter assumes that slippage is perfectly reversible on loading and unloading. Consequently all the residual strain predicted is derived from the first cycle (when the initial damage was put in). In reality asperities at the fibre/matrix interface for instance may inhibit the slippage process. As a result the laminate may require a certain number of additional cycles to shakedown to the reversible slippage system.

6.4.2 (0/90) crossply laminates

The continuous stress/strain behaviour of Nicalon reinforced CAS $(0/90)_s$ and $(0_2/90_4)_s$ crossply laminates have been modelled using the analysis of Section 6.2 (to account for the longitudinal ply cracking) in conjunction with the Steif shear-lag analysis (to account for the transverse ply cracking). Reasonable agreement with experimental data is obtained for each lay-up using the value of 8 MPa for the fibre/matrix interfacial shear strength (determined in Section 6.2). Although in both cases the model predictions appear to underestimate the laminate strain for a given applied stress, it represents a significant improvement over that of the unmodified shear-lag analysis where the longitudinal plies are assumed to retain their original (uncracked) stiffness.

The fact that the model predictions shown in Figures 6.14 and 6.15 underestimate the stress/strain behaviour is perhaps more reassuring than if the opposite were observed. This is because two key assumptions are made in the analysis which make the calculated strain at any applied stress an underestimate. The first of these assumptions is that laminate thermal stresses are zero. Thermal stresses are generated in the longitudinal and transverse plies as a result of the mismatch in thermal expansion between the fibres and matrix during laminate processing. The laminate plate theory calculations of Section 5.4.1 show that in both lay-ups the thermal stress is tensile in nature in the

central transverse ply and compressive in the longitudinal plies. When the laminate is under load and the transverse and longitudinal plies are cracked thermal stresses can be relieved adjacent to the crack planes. Due to the relaxation of the stiffer longitudinal plies a net increase in laminate strain results. In order to describe accurately the experimental stress/strain data it would be necessary to include laminate thermal stresses. This is not attempted in Section 6.3 due to the extremely complex interaction between stress fields adjacent to transverse and longitudinal ply cracks even when the cracks are assumed to be in model arrays. The problem is compounded given the experimental observations of irregular crack arrays and the presence of cracks traversing several plies or even the entire composite cross section. Nonetheless the model proposed in Section 6.3 attempts to describe with reasonable accuracy the stress transfer between plies which are elastically bonded where the intrinsic fibre/matrix bond is purely frictional in nature.

The second key assumption in the modified shear-lag model which gives rise to an underestimate of laminate stress/strain behaviour is that the fibres in the longitudinal plies remain intact over the entire stress range. From the evidence of Chapter 5 fibre breakages do occur at higher stresses and must therefore be taken into account. It is difficult to speculate as to the value of applied stress at which fibres begin to fail given the complexity of the stress distribution between cracked longitudinal and transverse plies and the statistical variations of fibre strength data as indicated by Prewo (1986) and Bleay (private communication). The continuous stress/strain prediction for the unidirectional lay-up using the model of Section 6.2 (Figure 6.8) indicates that fibre breakages could begin to occur at an applied strain of ~0.35%, where the theory and the experimental data diverge. An experimental investigation is required in order to clarify this. However, it is interesting to note that effect of fibre breakages occurring in the unidirectional lay-up and in the longitudinal plies of crossply laminates could be incorporated into the models proposed in Sections 6.2 and 6.3 (respectively) by modification of the fibre volume fraction term V_f.

In Section 5.4.4 it was shown by approximate critical flaw size calculations that the transverse ply cracks in both $(0/90)_s$ and $(0_2/90_4)_s$ lay-ups form in an unconstrained

manner. As a result the strength of a transverse ply can be described by a statistical distribution (e.g. Weibull) which corresponds to flaws of different size propagating over a range of transverse ply stresses. In several analyses for polymer matrix composites a shear-lag analysis is used containing a weibull distribution for the transverse ply strength in order to describe transverse ply crack multiplication (e.g. Manders et al, 1983, Fukanaga et al, 1984 and Peters, 1984). If transverse ply crack multiplication were to be investigated for the CMC laminates considered here, a similar approach may be necessary. However, the model proposed in Section 6.3 does not require the use of Weibull statistics and the subsequent fitting of the characteristic strength and Weibull exponent. This is because it is based on a stress analysis of the transverse and longitudinal plies when they contain arrays of cracks. Consequently the model assumptions pertain to the arrangement of the cracks and the nature of the ply and fibre/matrix interfaces.

6.5 CONCLUSIONS

The continuous and discontinuous stress/strain behaviour of unidirectional Nicalon/CAS laminates have been modelled over the region where matrix cracking is the dominant damage mechanism using an extended ACK analysis. The (assumed constant) interfacial shear strength τ is 8 MPa which is good agreement with values obtained for similar systems using alternative techniques. The initial thermal stress in the fibres σ_f^T is 50 MPa (compression). This value seems reasonable when the thermal expansion mismatch between the fibres and the matrix is considered.

The continuous stress/strain behaviour of (0/90) crossply Nicalon/CAS laminates has been modelled using a modified shear-lag analysis. The model accounts for longitudinal ply cracking and is a significant improvement over the Steif shear-lag analysis which assumes the longitudinal plies to remain undamaged.

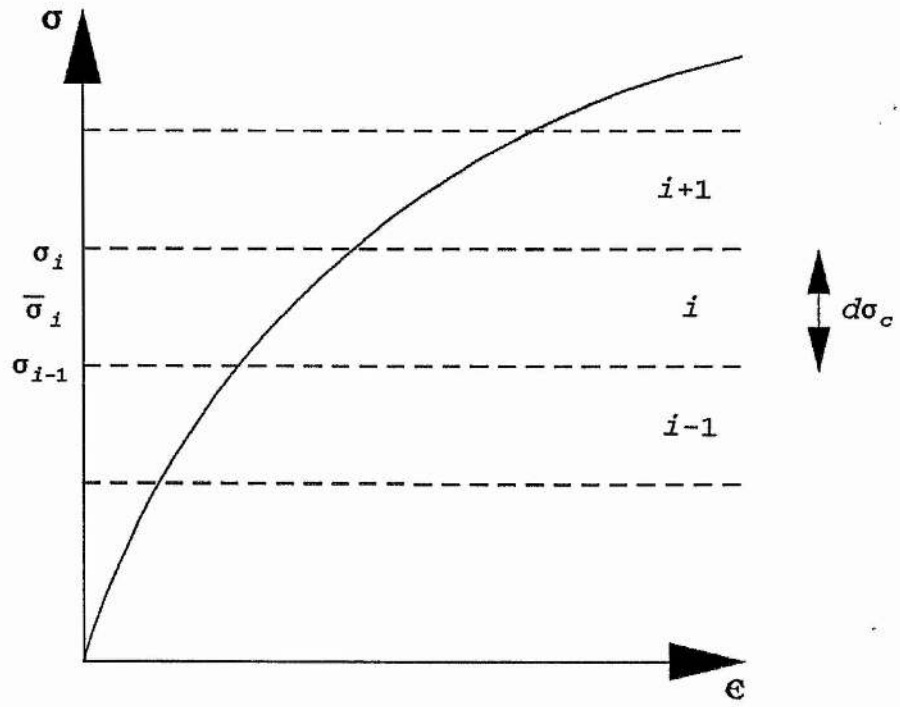

Figure 6.1 Schematic illustration of a continuous stress/strain curve divided into stress increments.

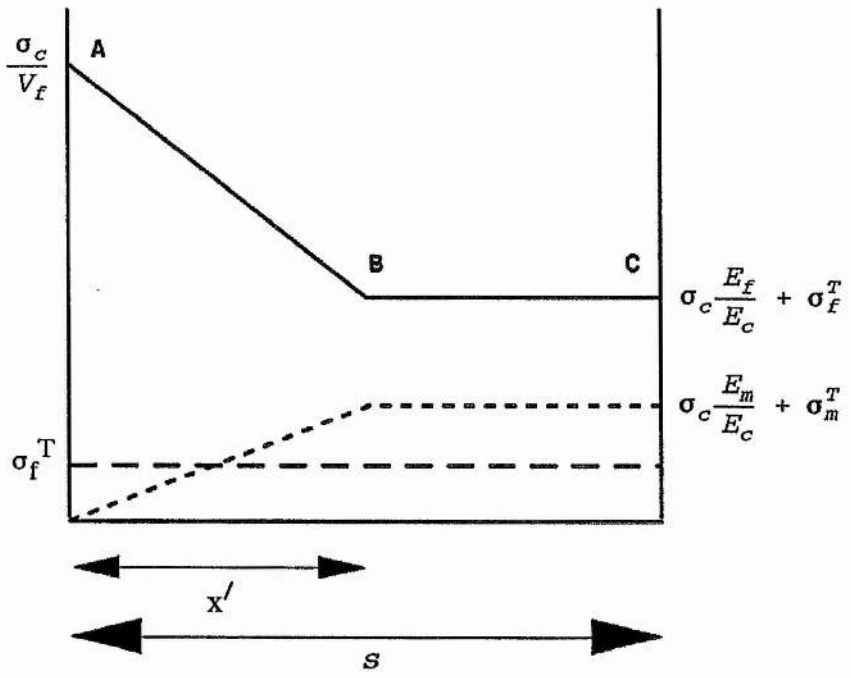

Figure 6.2 Stress profile in the fibres (solid line) and the matrix (dotted line) for a cracked unidirectional laminate at an applied stress σ_c where σ_c<190 MPa.

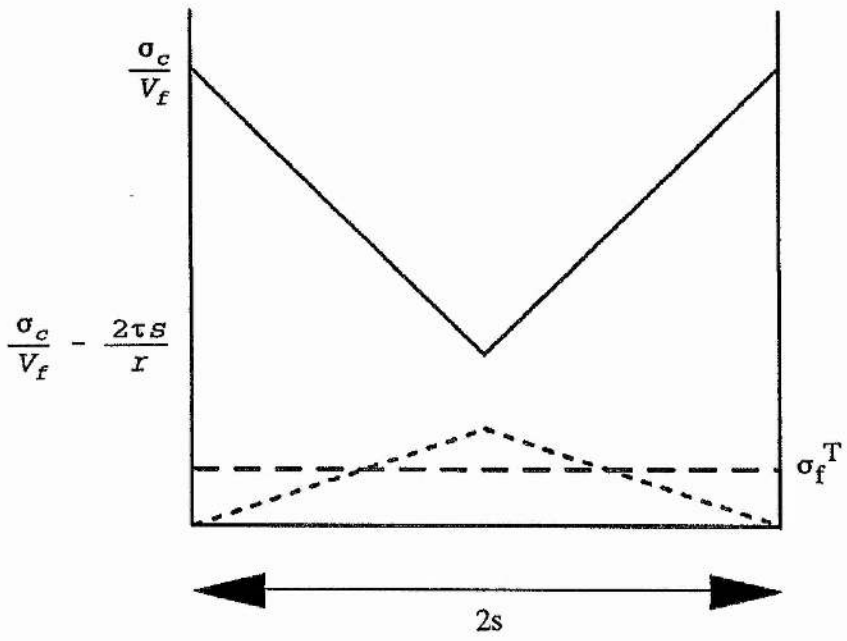

Figure 6.3 Stress profile in the fibres (solid line) and the matrix (dotted line) for a cracked unidirectional laminate at an applied stress σ_c where σ_c>190 MPa.

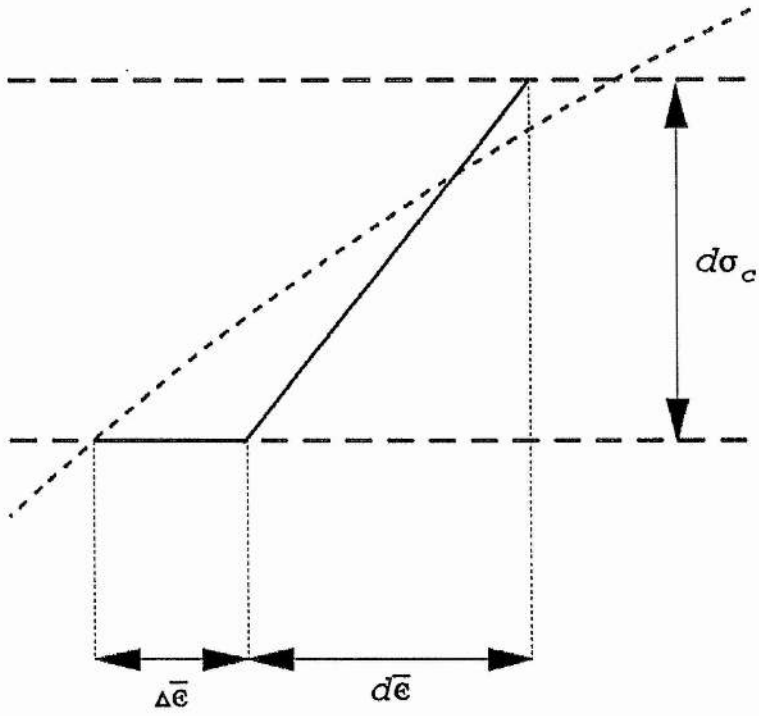

Figure 6.4 Schematic illustration of the continuous stress/strain prediction for the unidirectional lay-up over a single stress increment (dotted lines mark increment limits).

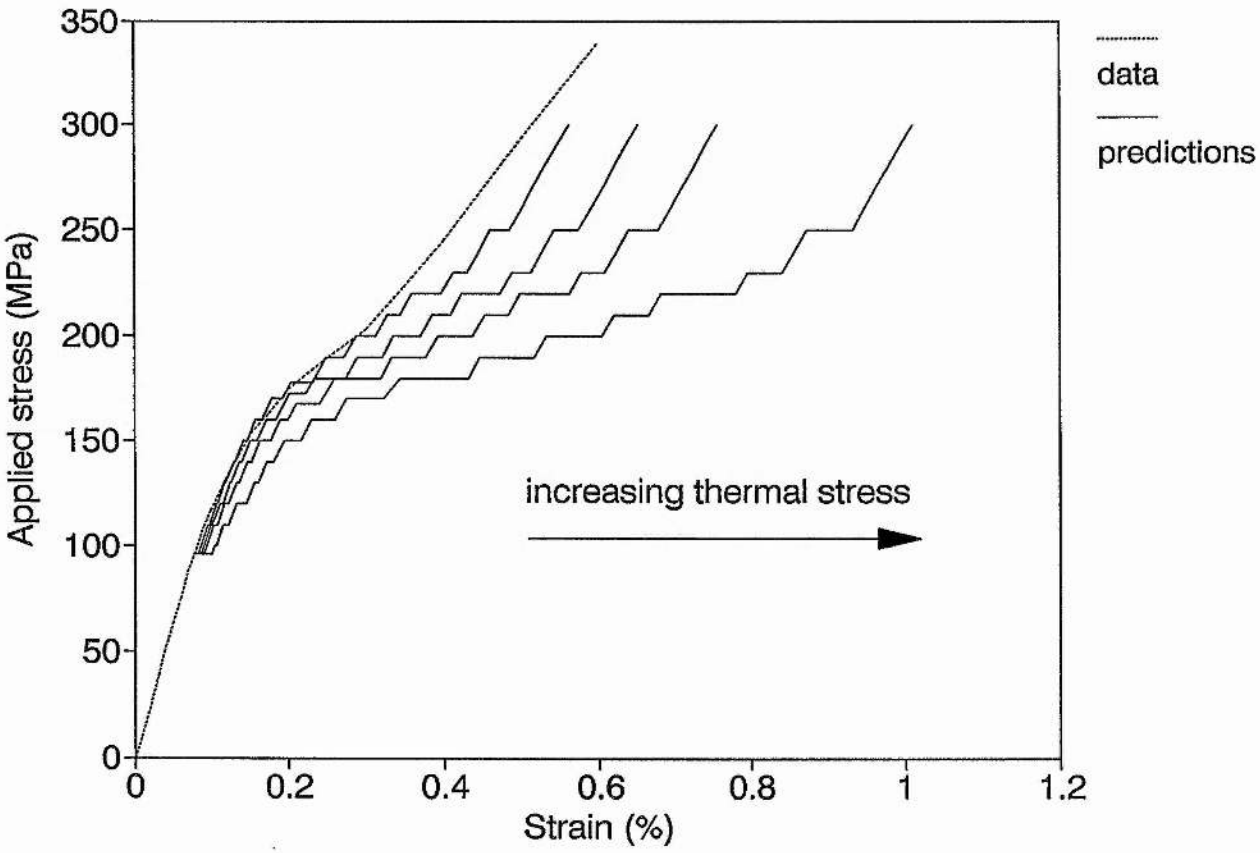

Figure 6.5 Continuous stress/strain data for the unidirectional lay-up (broken line) compared with model predictions using a constant value of 5 MPa for τ and varying values of 0, 50, 100 and 200 MPa (compression) for σ_f^T (solid lines).

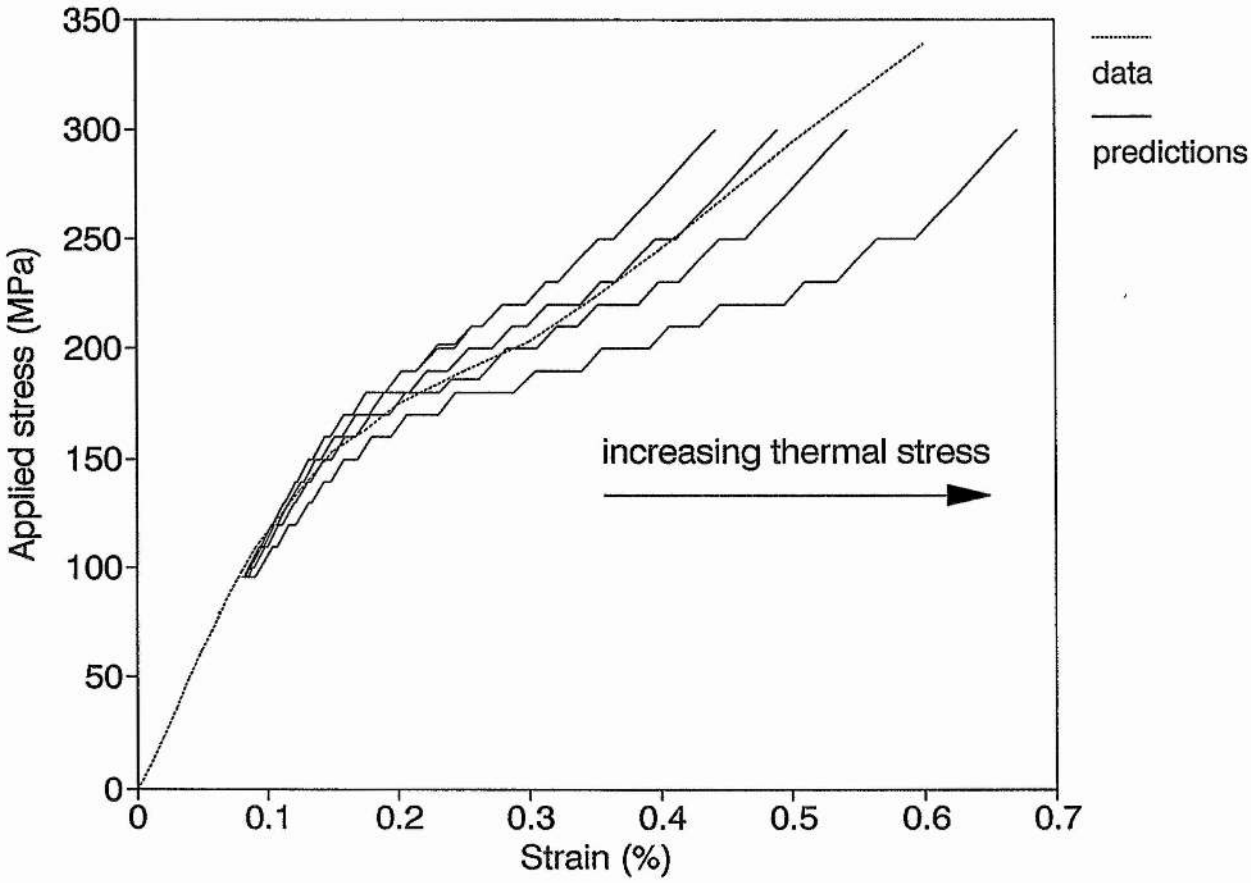

Figure 6.6 Continuous stress/strain data for the unidirectional lay-up (broken line) compared with model predictions using a constant value of 10 MPa for τ and varying values of 0, 50, 100 and 200 MPa (compression) for σ_f^T (solid lines).

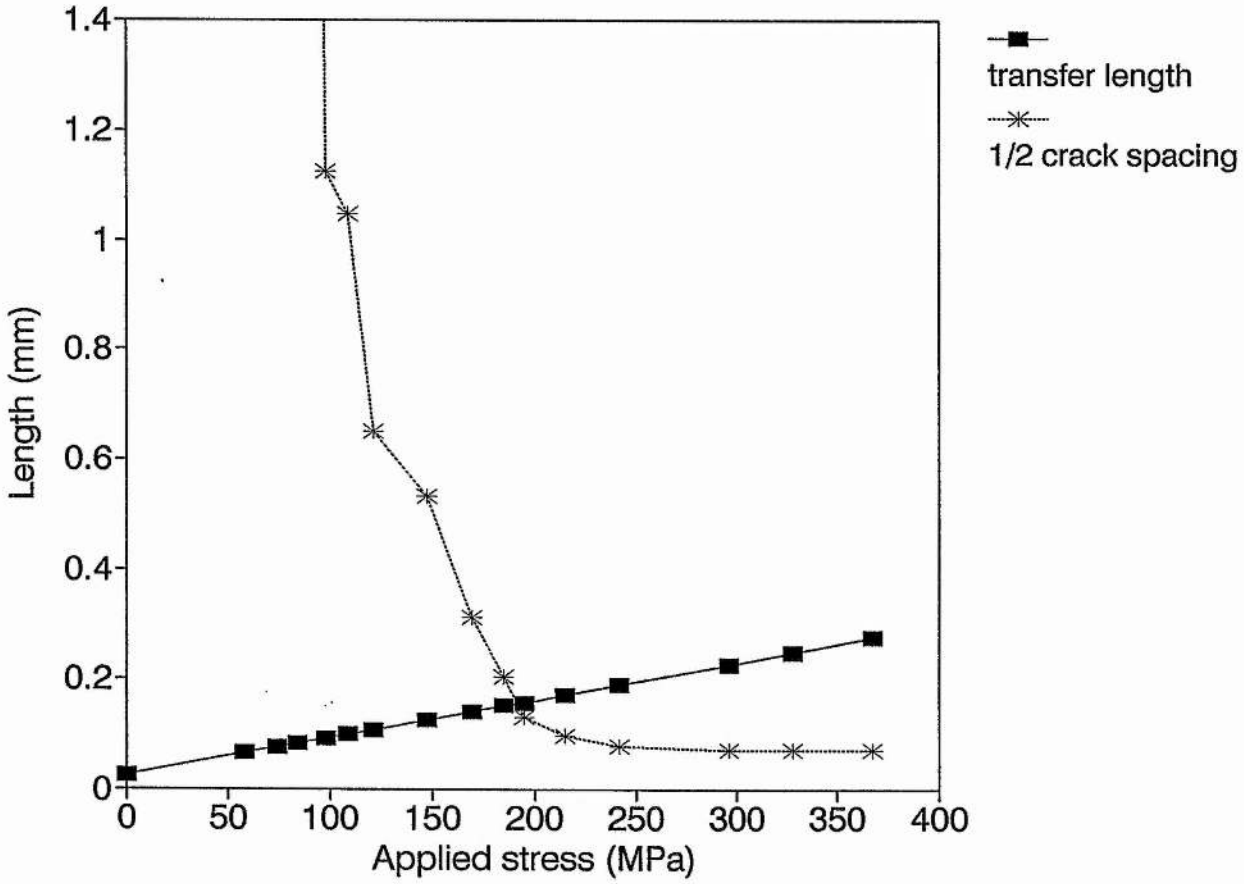

Figure 6.7 Relationship between the transfer length x' and the half crack spacing s as a function of applied stress.

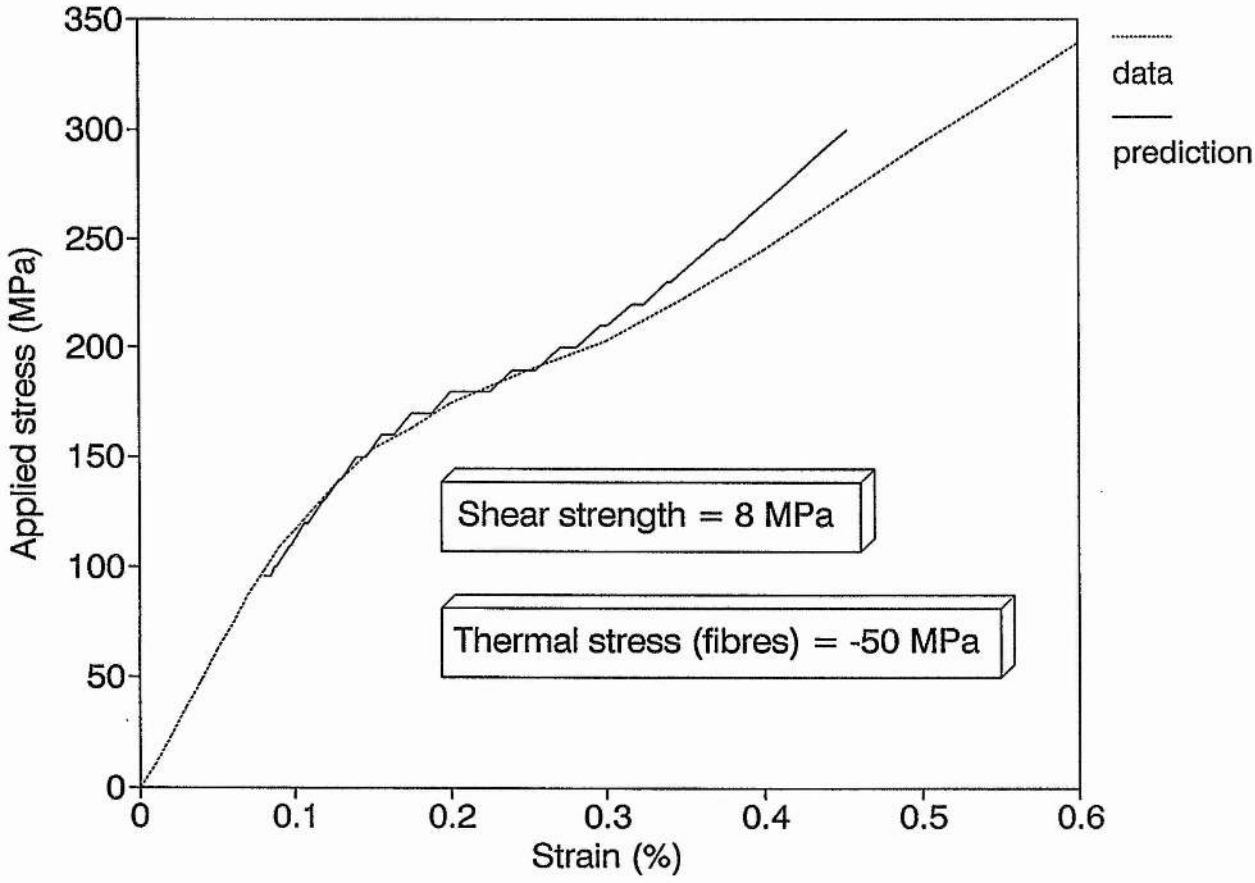

Figure 6.8 Continuous stress/strain data for the unidirectional lay-up (broken line) compared with the model prediction using a value of 8 MPa for τ and 50 MPa (compression) for σ_f^T (solid line).

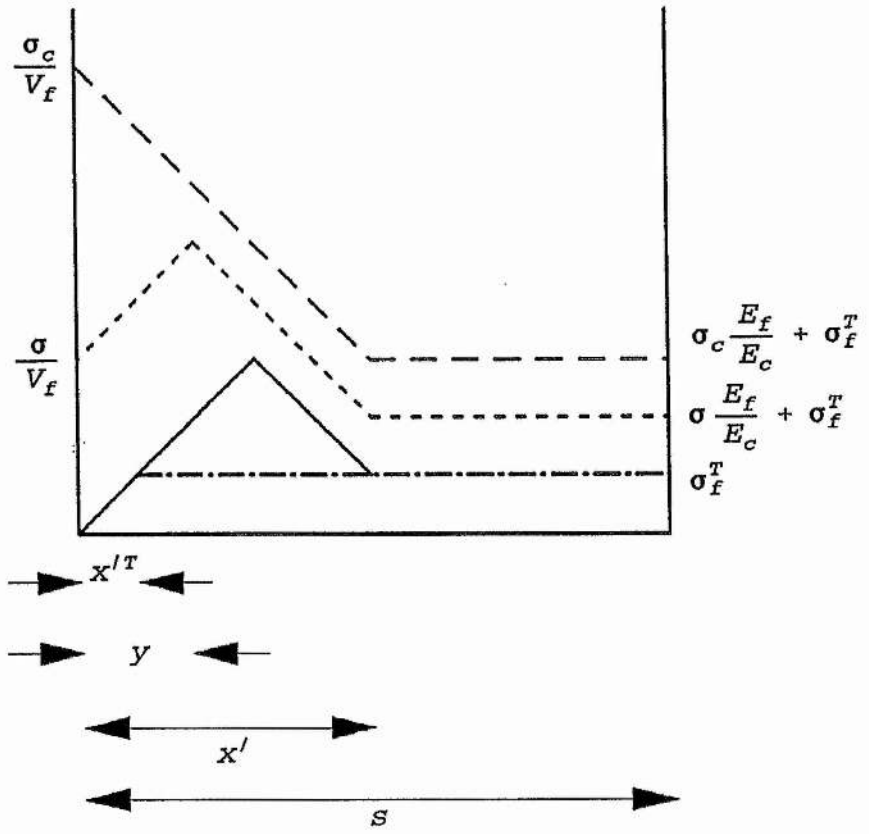

Figure 6.9 Stress profile in the fibres for a cracked unidirectional laminate during unloading from an applied stress σ_c to zero.

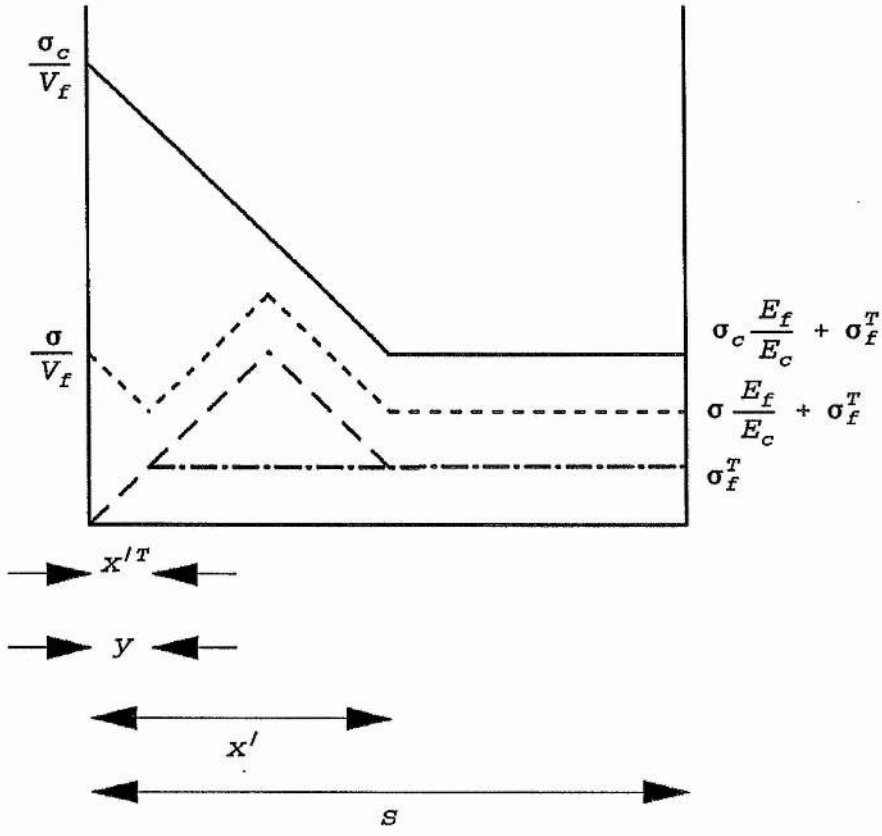

Figure 6.10 Stress profile in the fibres for a cracked unidirectional laminate during reloading from zero to an applied stress σ_c.

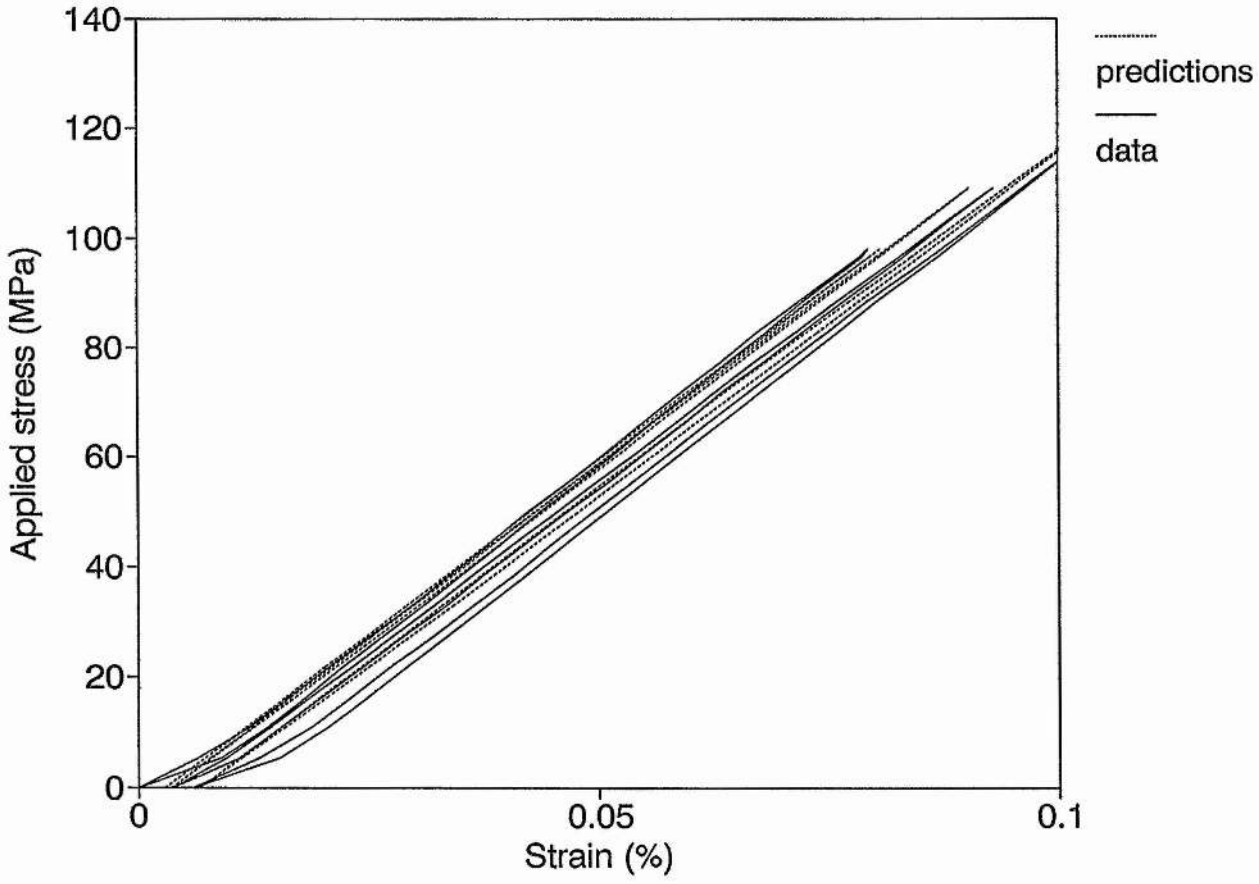

Figure 11a Unloading and reloading model predictions (broken lines) for the unidirectional lay-up compared with discontinuous data (solid lines) for maximum applied stresses of 98, 110 and 122 MPa.

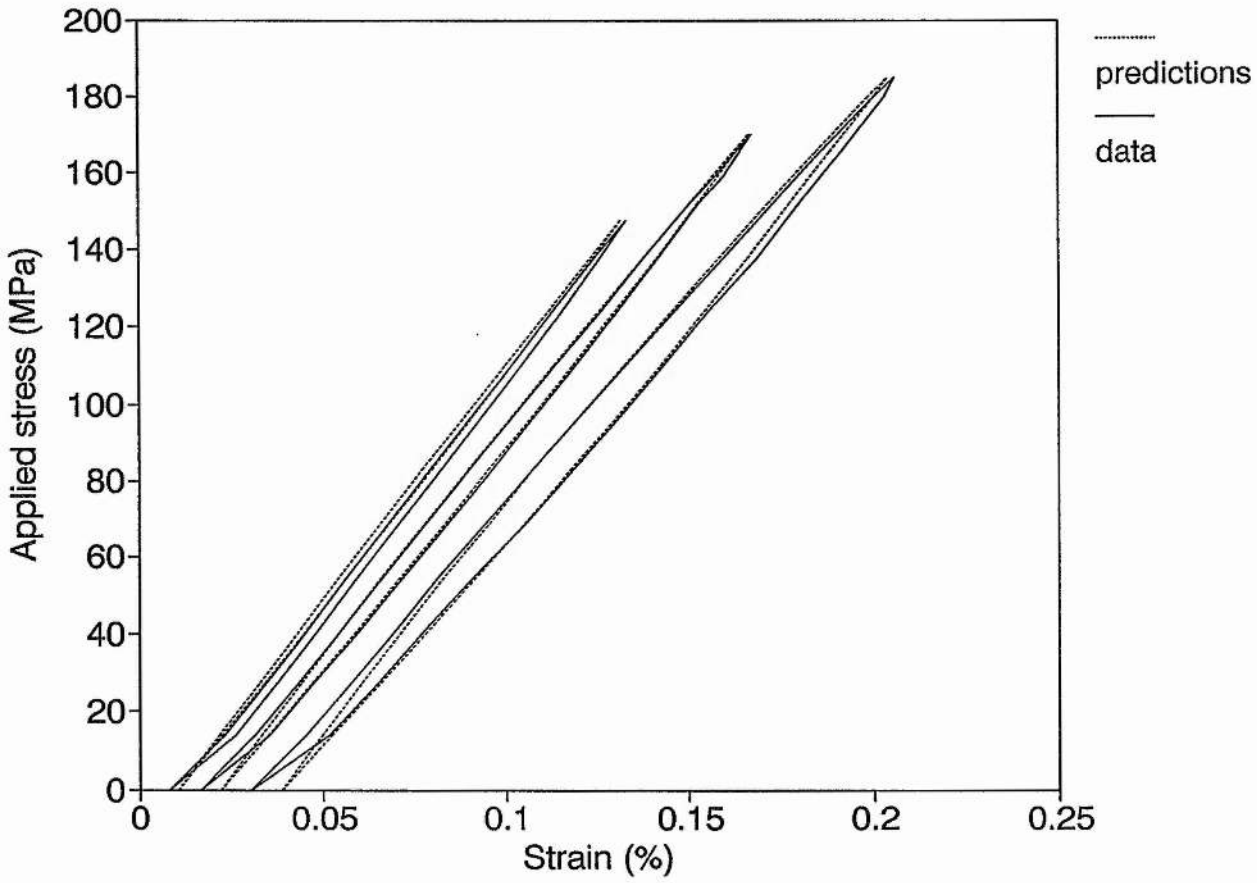

Figure 11b Unloading and reloading model predictions (broken lines) for the unidirectional lay-up compared with discontinuous data (solid lines) for maximum applied stresses of 148, 170 and 185 MPa.

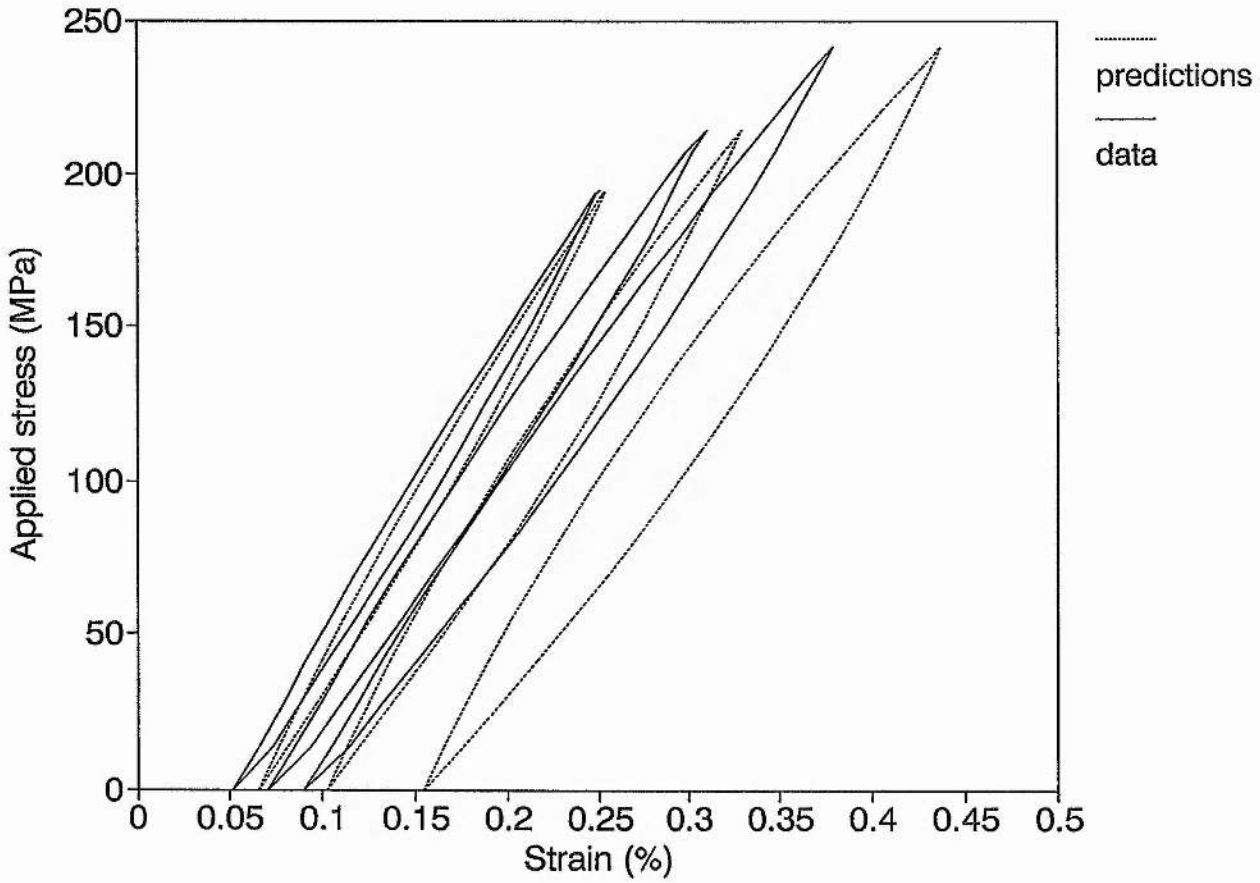

Figure 11c Unloading and reloading model predictions (broken lines) for the unidirectional lay-up compared with discontinuous data (solid lines) for maximum applied stresses of 195, 210 and 242 MPa.

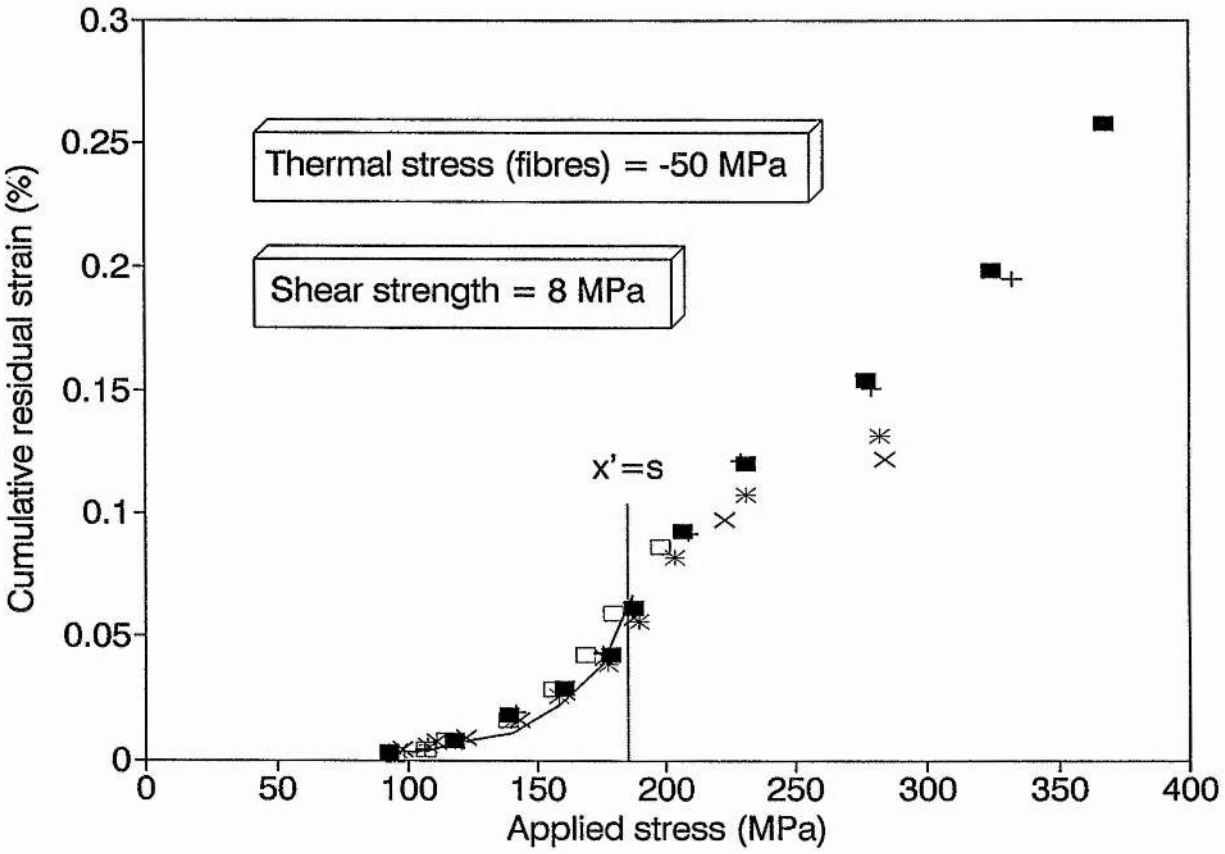

Figure 6.12 Cumulative residual strain vs applied stress data for the unidirectional lay-up compared with model predictions using a value of 8 MPa for τ and 50 MPa (compression) for σ_f^T.

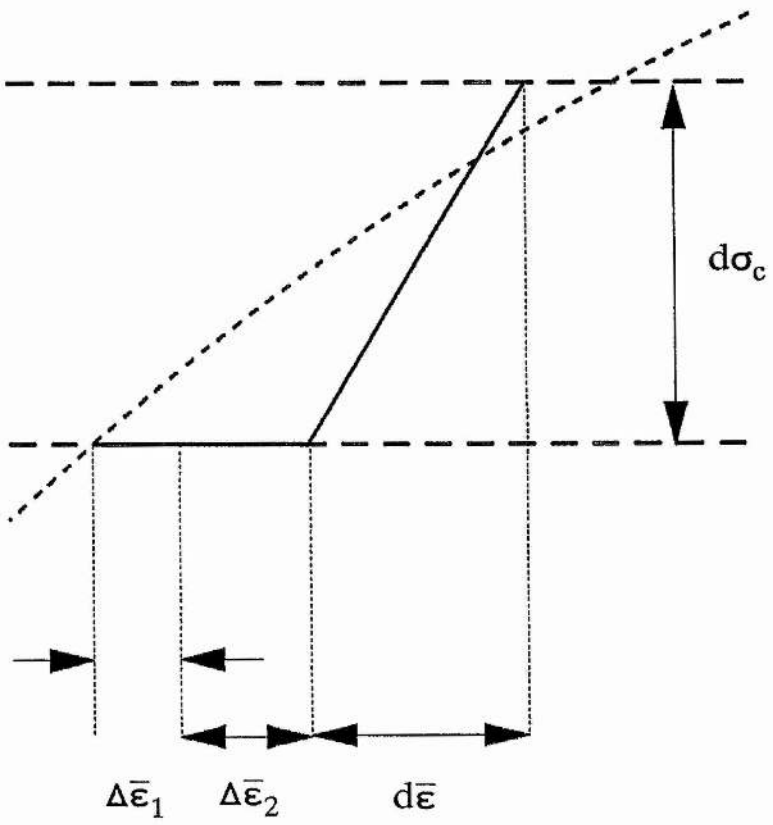

Figure 6.13 Schematic illustration of the continuous stress/strain prediction for a crossply laminate over a single stress increment.

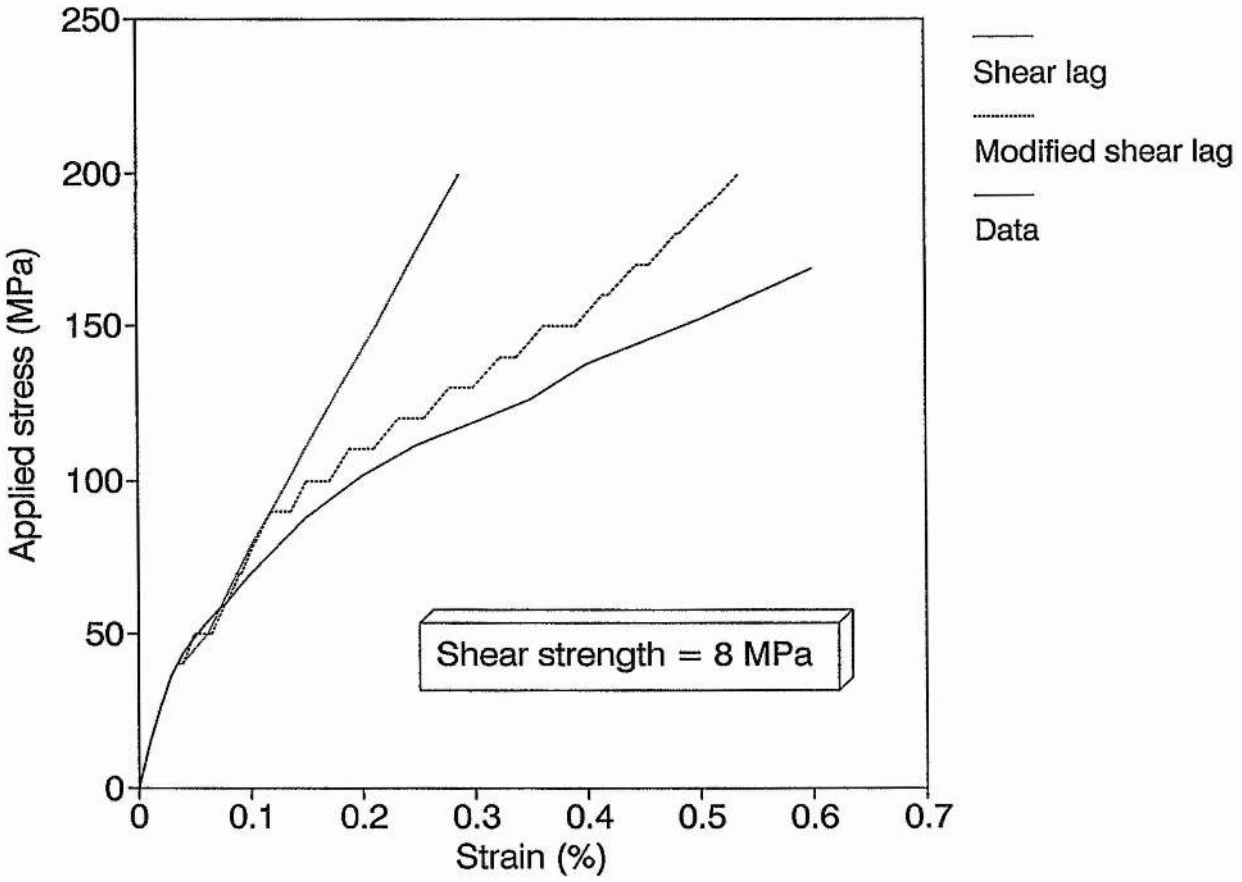

Figure 6.14 Continuous stress/strain prediction using the modified shear-lag analysis for the $(0/90)_s$ lay-up (broken line) compared with experimental data (solid line) and the shear-lag analysis of Steif (1984) (dotted line).

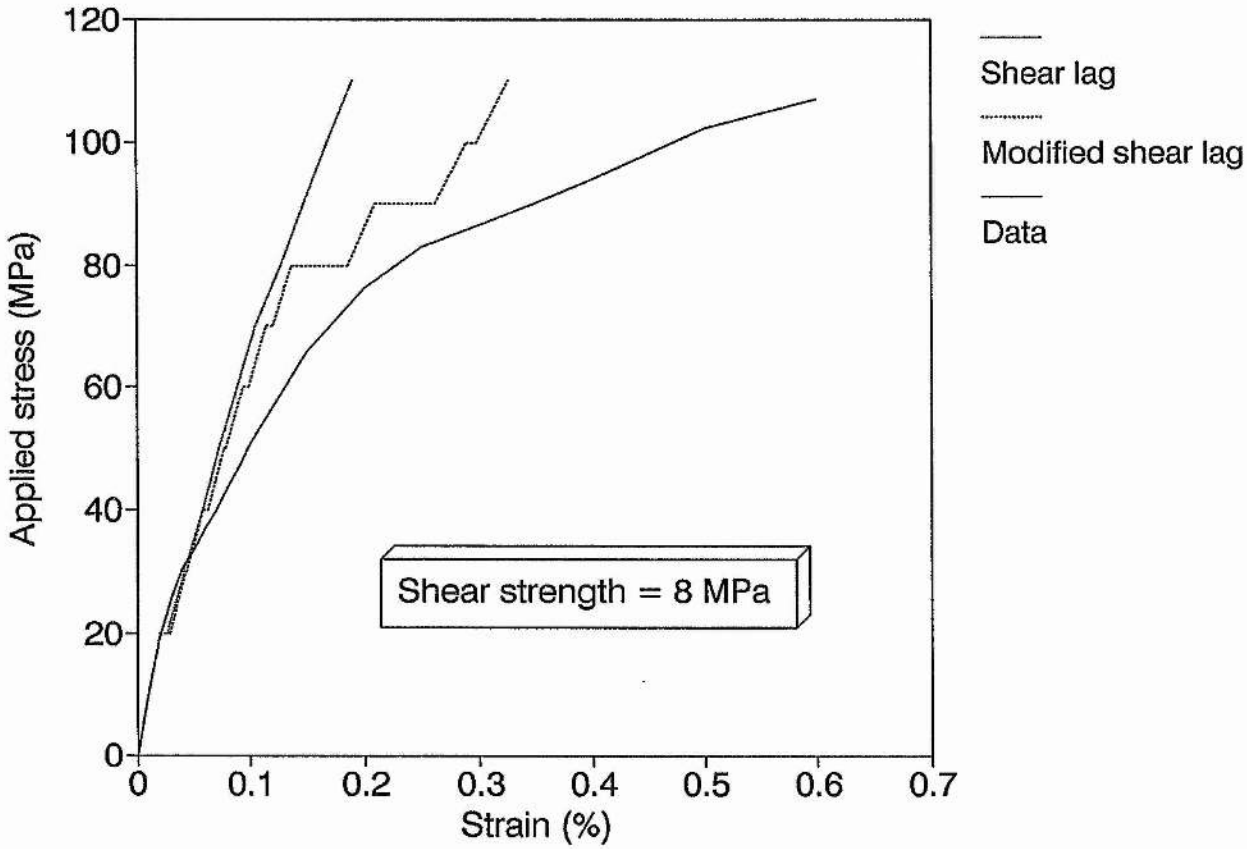

Figure 6.15 Continuous stress/strain prediction using the modified shear-lag analysis for the $(0_2/90_4)_s$ lay-up (broken line) compared with experimental data (solid line) and the shear-lag analysis of Steif (1984) (dotted line).

CHAPTER 7

FATIGUE BEHAVIOUR OF NICALON REINFORCED CAS LAMINATES

7.1 INTRODUCTION

The fatigue behaviour of monolithic ceramics has been studied extensively in recent years. It has been shown that in a range of materials crack growth occurs under cyclic loading conditions that cannot be associated with static fatigue (environmentally assisted crack growth) mechanisms alone (e.g. Krohn and Hasselman 1972, Evans 1980 and Horibe and Hirahara 1991). In contrast, as was shown in the literature review, there is as yet very little understanding concerning the fatigue behaviour of ceramic matrix composites. Minford and Prewo (1985) and Prewo (1987) have made some preliminary studies on matrix damage and mechanical behaviour of Nicalon fibre reinforced glass ceramic matrix laminates and Lewis (1983) has suggested a damage mechanism based on the buckling of fibres.

The aim of the work presented in this chapter has been to elucidate the cracking behaviour of unidirectional and crossply Nicalon reinforced CAS laminates. A specific objective was to examine if the stable stress/strain hysteresis loops obtained by quasi-static cycling (presented in Chapter 5 and analyzed in Chapter 6) correspond to stable matrix damage states and if they are unaffected by further cycling. Quasi-static cycling and high frequency fatigue tests were carried out and matrix damage accumulation monitored. The stress/strain behaviour as a function of cracking is examined using the model proposed in Chapter 6.

7.2 UNIDIRECTIONAL LAMINATES

7.2.1 Fatigue stress levels

Fatigue tests were carried out by cycling unidirectional specimens at three maximum stress levels. These stress levels, shown in Table 7.1 were 75 MPa (below the static matrix cracking threshold), 150 MPa and 200 MPa (above the cracking threshold). The latter two values correspond to situations where (according to the stress transfer model of Chapter 6) fibre/matrix slippage occurs partially between two cracks ($x'<s$) and along the entire length of the broken matrix ($x'>s$) respectively.

7.2.2 Quasi-static cycling

Crack density results for the unidirectional material show that for the 150 MPa and 200 MPa specimens cycled at the low strain rate, the amount of matrix damage rises to a maximum over the first 10 cycles. The crack density remains constant thereafter (Figure 7.1). A maximum number of 20 low strain rate cycles was applied to each specimen. In all cases the cracks were fully formed and traversed both the specimen width and thickness. The associated stiffness losses reflect the stabilisation in crack density for both the 150 MPa and 200 MPa specimens (Figure 7.2). The specimen cycled at a maximum stress below the static cracking threshold (75 MPa) showed no evidence of matrix cracking and as a result retained its original stiffness over the 20 cycles.

Figure 7.3 shows that the cumulative residual strain increases gradually with continued cycling up to the maximum 20 quasi-static cycles at each of the three stress levels. As no cracking was observed for the 75 MPa specimen it is evident that this increase is not due solely to damage. Subsequent experiments have shown that thermal effects due to the soldered strain gauge terminals cooling gives rise to a drift in the strain readout over a fifteen to twenty minute period. The cycling experiments described here were performed before the gauging system had time to reach equilibrium and as a result

contain a residual strain error due to thermal drift. This error is more or less constant for all the specimens. Consequently if the residual strain for the 75 MPa specimen is deducted after each cycle from the measurements made for the specimens cycled above the cracking threshold the residual strain as a result of thermal drift and matrix cracking/shakedown can be separated. Analysis of Figure 7.3 also shows that there is sometimes a sharp increase in residual strain occurring on the first cycle after specimens were replaced in the Instron (after crack density measurements). These increases of between 30 and 50$\mu\varepsilon$ are not due to matrix cracking. It can however be explained by considering the initial misalignment of the Instron wedge grips. With the grips misaligned slightly a small compressive strain can be introduced as a result of regripping the specimen. However, reference to Figure 7.4 shows that on the loading half of the first cycle after regripping this strain is reduced to zero. At the maximum stress when the grips are fully aligned the maximum tensile strain is identical to that of the previous (and subsequent) cycles for constant damage. In addition because the grips maintain alignment until the specimen is removed once more, subsequent unloading and reloading stress/strain loops (corrected for thermal drift) are closed and identical. The cumulative residual strain as a function of low strain rate cycles corrected for thermal drift and grip misalignment where necessary is shown in Figure 7.5. The trends observed reflect more accurately the effect of the accumulation of matrix damage than the measurements shown in Figure 7.3.

The corrected data shows that both the 150 MPa and 200 MPa specimens experience a rapid increase in residual strain over the first 10 cycles partially as a result of increasing matrix damage. However, in each case the increases in residual strain cannot be accounted for by matrix cracking alone, additional cycles are required for a constant crack density before the residual strain reduces to zero. This shakedown effect is similar to the data obtained by cycling unidirectional specimens in an identical way in Chapter 5 and analyzed in Chapter 6.

7.2.3 High frequency fatigue

Fatiguing at the high frequency of 10 Hz appears to have little affect on the crack density and associated stiffness losses for the unidirectional laminates. Only the specimen fatigued at a maximum stress of 200 MPa showed any signs of continued cracking (Figure 7.1). A corresponding rise in cumulative residual strain (corrected for thermal drift and grip misalignment) was measured (Figure 7.6). However, after 100 000 cycles the increase in crack density was not large enough to affect the measured 0.05% secant stiffness value (Figure 7.2). Due to experimental error the specimen cycled below the cracking threshold experienced a stress overload after 1000 cycles. A stiffness loss of around 5% was measured subsequently. However, both the crack density and 0.05% secant stiffness remained constant up to 1 million cycles. These observations are consistent with those of Prewo (1987) for Nicalon reinforced LASII laminates. He found that fatiguing specimens below the static cracking threshold did not result in any matrix damage or degradation in laminate stiffness.

Areas of the polished coupon edges used for crack density measurements after 100 000 cycles are shown in Figure 7.7 and 7.8 for the 150 MPa and 200 MPa specimens respectively. It can be seen that all matrix cracks are fully formed and that no visible fatigue damage has been incurred to either matrix or fibres by fatiguing at the high strain rate. Stress/strain hysteresis loops obtained during fatigue cycling are shown in Figures 7.9 and 7.10 for the 150 MPa and 200 MPa specimens respectively. It is evident from these plots, particularly for the higher stress series (Figure 7.10), that the amount of hysteresis during loading and unloading decreases with an increasing number of cycles. This is discussed further in Section 7.4.1.

Both specimens fatigued above the cracking threshold failed between 100 000 and 1 million cycles, the 150 MPa specimen after 325 000 cycles and the 200 MPa specimen after 168 000 cycles. In each case the failure occurred outside the Instron grips and was fibrous in nature. The crack responsible for the failure had propagated from one edge and extended partially across the specimen width with extensive longitudinal splitting apparent adjacent to the fracture. Such observations were made possible due to the

displacement limits disabling the fatigue machine before the specimens were broken into two pieces. The failures described here are consistent with ideas regarding sequential fibre failures in polymer matrix composites reported by Batdorf et al (1982a and b). The mechanism known as the "critical i-plet theory" describes how fibres fail as a result of the additional load thrown onto them by neighbouring fibre failures. The process continues until a critical number of fibre failures have occurred and catastrophic failure of the specimen follows.

7.3 (0/90) CROSSPLY LAMINATES

7.3.1 Fatigue stress levels

Three stress levels were selected for the $(0/90)_s$ and $(0_2/90_4)_s$ crossply laminates. The lowest, 30 MPa and 10 MPa for the $(0/90)_s$ and $(0_2/90_4)_s$ respectively, are below their transverse ply cracking thresholds. The intermediate stress levels, 50 MPa and 30 MPa are above their respective 90° ply cracking thresholds but below their 0° ply cracking thresholds. The highest, 100 MPa and 70 MPa are greater than both their 90° ply and 0° ply cracking thresholds (see Table 7.1).

7.3.2 Quasi-static cycling

Low strain rate fatigue results for the $(0/90)_s$ and $(0_2/90_4)_s$ crossply laminates are shown in Figures 7.11 to 7.28. No matrix cracks were observed in either lay-up cycled below their respective 90° ply cracking thresholds (Figures 7.11 and 7.12). As a result no loss in 0.02% secant stiffness was observed (Figures 7.13 and 7.14). However gradual increases in cumulative residual strain were measured. These were similar in magnitude to the strains associated with thermal drift in the strain gauge terminals discussed in the previous section for the unidirectional laminates. In addition similar sharp increases in residual strain were observed after specimens were replaced in the Instron grips (after crack density measurements). As a result the same analysis as described in the previous section for the unidirectional laminates was performed on Figures 7.15 and 7.16 for the $(0/90)_s$ and $(0_2/90_4)_s$ respectively to produce the cumulative residual strain as a function of cycles relations corrected for thermal drift and grip misalignment (Figures 7.17 and 7.18). The trends for each specimen reflect more accurately the changes in 0° ply and 90° ply crack densities.

Crack density results for both lay-ups cycled above the 90° ply but below the 0° ply cracking thresholds show that the transverse ply crack density stabilised after a single

cycle and did not change over the 20 quasi-static cycles (Figure 7.11 and 7.12). In the case of the $(0/90)_s$ specimen transverse ply cracks terminated at the ply interfaces with the longitudinal plies. No longitudinal ply cracks were observed (Figure 7.19). The change in 0.02% secant stiffness over the 20 cycles is shown in Figure 7.13. It indicates that from 5 to 20 cycles stiffness values remain constant. This reflects the stabilisation in the transverse ply crack density. In contrast crack arrays in the $(0_2/90_4)_s$ laminate after 5 cycles consisted of some transverse ply cracks bounded by longitudinal plies. Others however had grown across the longitudinal plies to span the entire laminate cross section. After the maximum 20 quasi-static cycles all transverse ply cracks had propagated across the neighbouring longitudinal plies (Figure 7.20). The extension of the transverse ply cracks into the longitudinal plies is reflected by the continued stiffness loss between 5 and 20 cycles (Figure 7.14).

The transverse ply cracking behaviour of specimens cycled above the 90° and 0° ply cracking thresholds were very similar to that of the intermediate stress specimens. Results show that in both lay-ups the transverse ply crack density stabilised almost immediately with little or no change in the number of cracks over the 20 quasi-static cycles (Figures 7.11 and 7.12). However, over the first 10 quasi-static cycles there was a rapid rise in the number of longitudinal ply cracks. This is reflected by the stiffness losses of 45% for the $(0_2/90_4)_s$ and 30% for the $(0/90)_s$ during this interval (Figures 7.13 and 7.14). After 20 quasi-static cycles all of the transverse ply cracks had extended across the longitudinal plies (Figures 7.21 and 7.22). In many cases for the $(0_2/90_4)_s$ lay-up a number of longitudinal ply cracks emanated from a single transverse ply crack and were angled at roughly between 45° and 90° to the loading axis.

7.3.3 High frequency fatigue

After low strain rate cycling all crossply laminates were fatigued at a frequency of 10 Hz. Specimens cycled below the 90° ply cracking threshold continued to show no evidence of transverse or longitudinal ply cracking. The laminate 0.02% secant stiffness and cumulative residual strain (corrected for thermal drift and grip misalignment) remained

constant (Figures 7.13, 7.14 and 7.23 and 7.24).

The $(0_2/90_4)_s$ specimen fatigued at a maximum stress between the 90° ply and 0° ply cracking thresholds experienced very little change. After one million cycles the crack density in both longitudinal and transverse plies had not altered appreciably (Figure 7.25 as compared to Figure 7.20). As a result there was little change in 0.02% secant stiffness and cumulative residual strain (corrected for thermal drift and grip misalignment). In contrast the crack density in the 0° plies of the $(0/90)_s$ specimen increased gradually with increasing cycles. Optical microscopy revealed that this was due to the extension of transverse ply cracks into the longitudinal plies (Figure 7.26 as compared to Figure 7.19). After one million cycles all transverse ply cracks spanned the entire laminate cross section and the crack density in both 0° and 90° plies was approximately equal (Figure 7.11). However, the extension of 90° ply cracks appears too small to have had an effect on the 0.02% secant stiffness and cumulative residual strain (Figures 7.13 and 7.23).

Specimens of both lay-ups fatigued above their 90° and 0° ply cracking thresholds experienced significant increases in longitudinal and transverse ply crack density over the maximum million cycles. These increases corresponded to new transverse ply cracks extending across neighbouring 0° plies, additional 0° ply cracks running at ≈45° (to the loading axis) and an increase in the number of discrete longitudinal ply cracks (see Figures 7.27 and 7.28). These increases gave rise to large reductions in 0.02% secant stiffness and increases in cumulative residual strain.

7.4 DISCUSSION

7.4.1 Unidirectional Material

(a) Quasi-static fatigue

The crack density vs cycles data for the unidirectional material is shown in Figure 7.1. The specimen cycled below the static matrix cracking threshold showed no evidence of matrix cracking after 20 cycles. Crack density measurements for the specimens cycled above the cracking threshold were seen to stabilise within the first 10 cycles. Consistent with the data from Chapter 5, with increasing stress above the matrix cracking threshold and hence increasing fibre/matrix slippage, a greater number of cycles is required to obtain a stable matrix damage state and hysteresis loop. In the case of the 150 MPa specimen (where slippage occurs partially between two cracks) stability was almost immediate compared to the 200 MPa specimen (where slippage occurs throughout the matrix) which required 10 cycles before a stable crack density measurement was recorded. The slippage process itself could cause the initial increase in crack density due to the surface roughness between the fibres and matrix. This is discussed at length by Kerans (1991). Asperity contacts sliding over each other could result in localised stress concentrations and cause pre-existing matrix flaws to propagate.

The stabilisation in crack density and fibre/matrix sliding behaviour for the 150 and 200 MPa specimens are reflected by the 0.05% secant stiffness and corrected cumulative residual strain measurements approaching constant values. In Chapter 5 the 0.05% secant stiffness and cumulative residual strain values were measured as a function of applied stress (Figures 5.11 and 5.12). Specimens used in these tests were not removed from the Instron at any stage (crack density measurements were not made) or their strain gauge terminals disconnected. Comparing the secant stiffness and cumulative residual strain data of the present tests (Figures 7.2 and 7.6) with the discontinuous test data (Figures 5.11 and 5.12 respectively) shows excellent agreement. As a result it can be confirmed that the stable stress/strain hysteresis loops obtained by stress cycling above the matrix cracking threshold (presented in Chapter 5 and analyzed in Chapter 6)

correspond to stable matrix damage states.

(b) High frequency fatigue

After 100 000 fatigue cycles at a frequency of 10 Hz the specimens cycled above the matrix cracking threshold showed only very small increases in crack density with the higher maximum stress specimen (200 MPa) showing the larger increase. As a result little or no increase in 0.05% secant stiffness was observed for these specimens. In fact only when the specimen fatigued below the cracking threshold experienced a stress overload after 1000 cycles was there any substantial change in the crack density. A corresponding decrease in 0.05% secant stiffness was measured. However, the damage state remained unchanged thereafter up to one million cycles. In all cases the slight increases in crack density corresponded to the formation of new full width and thickness cracks as viewed on the specimen edge. Using the polished edge method to quantify the number of cracks it is difficult to speculate as to the mechanism of crack growth. Fatigue crack growth may occur in the bulk of the specimen and not be detected. However, a qualitative explanation is offered below.

The crack density vs quasi-static stress data of Figure 5.9 suggest that above the matrix cracking threshold the composite stress intensity factor is described by the continuum analyses of Marshall et al (1985) and McCartney (1987); cracks propagate over a range of applied stress. During high frequency fatigue it appears that for both maximum stress levels above the static matrix cracking threshold there is very little fatigue crack growth. The slight increases in crack density observed probably correspond to flaws of near critical size (for the maximum applied stress) either, propagating catastrophically as a result of the non-uniform stress distribution in the matrix (due to microstructural irregularities etc), or, growing a small amount with fatigue cycling until they reach the critical size at which point they propagate catastrophically. In each case full width and thickness cracks will form rapidly and not by steady growth across the specimen. Rapid crack growth rates are associated with materials which display limited plasticity and has in recent years been quantified for a variety of polycrystalline ceramics e.g. Fett et al (1991). This hypothesis is also supported by the absence of matrix cracks in the specimen cycled below the static cracking threshold (until the specimen was overloaded),

an experimental observation also made by Prewo (1987). The first crack to form will do so only when the largest matrix flaw (perhaps enlarged initially by fatigue growth) becomes unstable.

If a limited amount of fatigue crack growth in the matrix does occur, it is possible that the mechanisms discussed in Chapter 2 maybe relevant. These are classified as either static fatigue or based on the non reversibility of strain during stress cycling.

During the present work it was attempted to minimise the effect of static fatigue by careful control of the testing environment, particularly the humidity which is well known to be detrimental to glass and glass ceramics (McMillan, 1979 and Weiderhorn et al, 1982). However, the role of static fatigue in ceramic composite laminates is far from understood. One suspects it may be very important given the observations of Bleay and Scott (1991) when carbon reinforced pyrex laminates were heated in air. Bleay and co-worker report that the fibre/matrix interface appears to act as a transport channel for hot gases. As a result evidence of oxidation was detected away from the specimen surface. The fibre/matrix interface may also provide channels for the transport of humid and other aggressive atmospheres which promote static fatigue.

Fatigue crack growth may also occur due to the non reversibility of strain during stress cycling. Mechanisms proposed for polycrystalline ceramics consider the wedging open of cracks due to asperity/asperity contacts on the unloading half of the fatigue cycle. This can occur by crack branching and deflection (Horibe and Hirahara 1991) and by the relief of residual stresses through microcracking (Evans 1980). The non planar form of the matrix cracks shown (e.g. when circumventing fibres) and the residual thermal stresses calculated in the present work indicate that such mechanisms may be active. Crack wedging may also occur by the mechanism described for unidirectional laminates by Lewis (1983). Pulled out fibres on the tensile half of a cycle may be unable to slide back into their matrix sockets and therefore buckle on the compressive half of the cycle. Although during the present study no evidence of debris (broken fibres or pieces of matrix) was observed between crack faces this mechanism can not be overlooked; during quasi-static testing the stress/strain response at high stresses suggests that fibres do fail

before the catastrophic failure of the laminate.

(c) Changes in stress/strain hysteresis during fatigue

Consistent with the trends of crack density and stiffness parameters there is no significant change in stress/strain hysteresis behaviour for the specimen fatigued at a frequency of 10 Hz to a maximum stress of 150 MPa (Figure 7.9). However, an increase in cumulative residual strain was observed (Figure 7.6). Inspection of Figure 7.10 shows that for the 200 MPa specimen the hysteresis loop width decreases with cycles in addition to an increase in cumulative residual strain. The maximum applied stress of 200 MPa corresponds to the situation where fibre/matrix slippage occurs over the entire length between two matrix cracks. It is likely that the increases in cumulative residual strain and the change in loading and unloading behaviour is as a result of a change in the nature of the fibre/matrix interface. Such changes could include progressive decreases in interfacial shear strength τ and initial thermal stresses. If this is the case then their effects can be studied using the loading and unloading model proposed in Chapter 6 for the 150 MPa specimen (for which the model is valid since at the maximum applied stress $x'<s$). Figure 7.29 shows the stress/strain loop for the 150 MPa specimen measured after 100 000 cycles (solid line). Also shown are predicted loops (broken lines) obtained using equations 6.15 and 6.17 for a constant thermal stress (in the fibres) of -50 MPa and varying values of interfacial shear strength of 8,6,4,2 and 1 MPa. Figure 7.30 shows the same measured loop together with predictions for a constant interfacial shear strength of 8 MPa and varying values of initial thermal stress (in the fibres) of -50, -40, -30, -20 and 0 MPa. Comparison of these figures indicates that the model predictions are extremely sensitive to the value of interfacial shear strength but are relatively insensitive to the initial thermal stresses. A degraded value of 2 MPa for τ gives reasonable agreement with the measured loop, particularly at the starting point, the cumulative residual strain. A decrease in interfacial shear strength is likely to be as a result of a decrease in the surface roughness between fibres and matrix with increasing fatigue cycles. This could occur by the wearing down of asperities which are in contact with each other during fatigue cycling. However, the predictions show the loop width to increase with decreasing interfacial shear strength. No visible difference was observed in the stress/strain behaviour of the 150 MPa specimen and the opposite trend was observed

experimentally for the 200 MPa specimen. This suggests that the model cannot be used in its present form to predict the loop for reasons which are discussed below along with a more qualitative explanation of the observed behaviour.

A fundamental assumption of the model is that the transfer length x' is always less than or equal to the half crack spacing, s. When fibre/matrix sliding has occurred over the entire length between two cracks (i.e. $x'>s$), any further composite strain is due solely to the elastic extension of the fibres. The corresponding stress/strain response is linear with gradient equal to $E_f V_f$. It is likely therefore that the effect of high frequency fatigue is to reduce the stress at which fibre/matrix sliding occurs over the entire length between two matrix cracks via a decrease in the interfacial shear strength τ in accordance with relation derived in Chapter 6;

$$x' = \frac{r}{2\tau}\left[\sigma_c \frac{V_m E_m}{V_f E_c} - \sigma_f^T\right] \qquad (7.1)$$

This is illustrated in Figure 7.31 and 7.32 which compare schematically the stress/strain behaviour during loading to and unloading from the same maximum stress σ_c for the two cases when $x'<s$ (Figure 7.31) and $x'>s$ (Figure 7.32). When $x'<s$ slippage occurs only partially between two cracks (Figure 7.31b). The resultant stress/strain behaviour is non-linear (Figure 7.31a) and is described by equations 6.15 and 6.17. When $x'>s$ the initial stress/strain response during loading is as a result of slippage occurring progressively throughout the matrix (Figure 7.32a). With increasing slippage a decrease in laminate stiffness occurs. At a higher stress during loading when slippage has occurred throughout the entire matrix (Figure 7.32b) the stress/strain response is linear with gradient $E_f V_f$. When the specimen is unloaded the shear stress at the fibre/matrix interface acts to oppose reverse slippage (in the reverse direction to loading). As a result the initial strain to be recovered is due to reverse slippage followed by the linear elastic strain of the fibres. This loading and unloading behaviour gives rise to a decrease in the amount of stress/strain hysteresis.

The two effects of increasing loop width due to a decrease in τ (when $x'<s$) and

decreasing loop width due to the elastic deformation of fibres when $x'>s$ serve to oppose each other. In the case of the 150 MPa specimen, after low strain rate fatigue cycling the stress/strain behaviour is described by equations 6.15 and 6.17 suggesting that x' is still less than s. It would appear that further fatigue cycling causes a decrease in τ which is large enough such that x' becomes greater than s. With no further increase in crack density any increase in loop width (due to τ decreasing) is offset by the elastic deformation of the fibres dominating the stress/strain loop. This would account for the experimentally observed increase in cumulative residual strain with very little change in loop width. In the case of the 200 MPa specimen although decreases in τ serve to increase the loop width when $x'<s$, fatigue cycling at this high maximum stress causes the transfer length to become greater than the half crack spacing at a very early stage, probably within the first few low frequency cycles. High frequency fatigue causes further increases in x' (via further decreases in τ) and a small increase in crack density. Hence the amount of fibre/matrix sliding reduces still further. As a result the portion of the stress/strain loop which is hysteretic decreases and the majority of the curve is dominated by the elastic deformation of the fibres. This gives rise to the reductions in loop width with continued high frequency fatigue.

In both cases the gradients of the stress/strain curves (100 GPa for the 150 MPa specimen and 80 GPa for the 200 MPa specimen) which represent the elastic deformation of fibres are greater than E_fV_f (65 GPa). The fact that they both overestimate E_fV_f is not necessarily inconsistent with the model. This is because the model assumes that the crack spacing is uniform. In reality when making a crack density measurement a distribution of crack spacings was observed and an average value calculated. As a result although the half average crack spacing may equal or become less than the transfer length the stress/strain behaviour in the regions between two cracks spaced further apart than average may still be influenced by the matrix. As a result the actual stress/strain gradient (the stiffness) will be greater than that predicted by the model. The greater error occurring in the specimen experiencing the lower maximum stress would also appear to support this. Manders et al (1983) and Peters et al (1987) have shown in their studies on GFRP crossply laminates that there is a greater statistical variation in transverse ply crack density (described by an unstressed length) when cracks

are spaced wide apart (low applied stress). This variation decreases as the applied stress is increased and the crack spacing becomes smaller. Such a statistical analysis could perhaps be applied to matrix cracks in unidirectional CMC laminates and account for the observed behaviour.

7.4.2 (0/90) crossply laminates

(a) Quasi-static cycling

The $(0/90)_s$ and $(0_2/90_4)_s$ crossply specimens cycled for 20 quasi-static cycles below the 90° ply cracking threshold showed no evidence of cracking in either transverse or longitudinal plies. In addition the $(0/90)_s$ specimen cycled between the 90° and 0° ply cracking thresholds only incurred cracks in the transverse ply. No cracks were observed in the longitudinal plies after the 20 cycles. However, 0° ply cracks in addition to 90° ply cracks were seen to form in the $(0_2/90_4)_s$ cycled between the transverse and longitudinal ply cracking thresholds. It is likely that these longitudinal ply cracks form as a result of a larger redistribution of stress due to transverse ply cracking because the 90° plies of the $(0_2/90_4)_s$ laminate constitute a larger area fraction of a specimen than that of the $(0/90)_s$ specimens. This hypothesis would seem to explain the experimentally observed behaviour of the $(0/90)_s$ and $(0_2/90_4)_s$ specimens cycled for 20 quasi-static cycles above their 0° and 90° ply cracking thresholds. In both cases a high stress exists in the 0° plies generated by the higher applied stress and the additional stress thrown onto the 0° plies due to 90° ply cracks. As a result it is likely that a range of flaw sizes will become critical in these plies assisted perhaps by fibre/matrix slippage as described in Chapter 6. This would account for the formation of discrete longitudinal ply cracks as well as all transverse ply cracks extending across the longitudinal plies.

Changes in 0.02% secant stiffness and cumulative residual strain (corrected for thermal drift and grip misalignment) are shown in Figures 7.13 to 7.28. These data give little insight into the shakedown effects for a constant damage state which are understood to occur in unidirectional laminates. This is because the transfer of stress between 0° and 90° plies is much more complex as a result of longitudinal and transverse ply cracking.

When a transverse ply crack forms the resultant stress redistribution throws additional stress onto the neighbouring longitudinal plies. Likewise, the presence of longitudinal ply cracks throws additional stress onto the central transverse ply. How the stress states in individual plies interact is extremely complex and difficult to model (see Chapter 6). However, the observed trends in stiffness and residual strain reflect the increases in 0° and 90° ply crack density in both lay-ups.

An interesting observation concerning the $(0_2/90_4)_s$ specimen cycled at the highest stress (70 MPa) was the occurrence of 0° ply cracks running at 45° as well as perpendicular to the loading axis (Figure 7.28). It is believed that such cracks form as a result of the fibre/matrix slippage which occurs adjacent to existing perpendicular 0° ply cracks. Reference to Figure 7.33 shows that the slippage is constrained by the central transverse ply near the 0°/90° ply interface. This is possible due to the fact that the transverse ply stress is reduced adjacent to transverse ply cracks (via load shedding onto the longitudinal plies). As a result the length of the exposed fibres (the crack opening displacement) will be greater toward the outer edge of the longitudinal ply where fibre/matrix slippage is less inhibited. This causes the matrix adjacent to an existing 0° ply crack to be in a state of shear, illustrated by the stress element in Figure 7.33. If a flaw becomes critical in this region (following the stress redistribution from transverse ply cracking) a 0° ply crack will propagate in the direction of maximum resolved stress, at ~45° to the loading axis.

(b) High frequency fatigue

Fatiguing the $(0/90)_s$ and $(0_2/90_4)_s$ crossply laminates below the 90° ply cracking threshold at a frequency of 10 Hz appears to have no effect on their cracking behaviour. No 90° or 0° ply cracks were observed after one million cycles (Figures 7.11 and 7.12). In contrast the high frequency fatigue of crossply specimens above the 90° ply cracking threshold had a profound effect on 90° and 0° ply cracking. All transverse ply cracks in the $(0/90)_s$ specimen fatigued at an intermediate stress ($90°_{onset} < \sigma < 0°_{onset}$) were seen to extend across neighbouring 0° plies. At both maximum stress levels no slow growth of cracks across 0° plies was seen. As was the case with the unidirectional material it was new fully formed cracks appearing after each fatigue interval that gave rise to the increases in crack density. The cracking data for the $(0/90)_s$ and $(0_2/90_4)_s$ crossply

laminates fatigued at a maximum stress in excess of 90° and 0° ply cracking thresholds showed continued cracking in both plies with increasing cycles. These data are consistent with the crack propagation mechanisms discussed in Section 7.4.1 given the stress redistribution in the 90° and 0° plies when they become cracked.

7.5 CONCLUSIONS

Cracking in the matrix of unidirectional laminates and in the 0° and 90° plies of (0/90) crossply laminates has been quantified for the Nicalon/CAS system under quasi-static cycling and high frequency fatigue. Cracks do not form in unidirectional or crossply laminates when the maximum stress is below the matrix/transverse ply cracking threshold; the laminate stiffness is not degraded. Above the cracking thresholds all cracks form rapidly, slow crack growth is not observed.

The stable stress/strain hysteresis loops obtained by cycling unidirectional laminates at a slow strain rate correspond to a stable damage state; the unloading and reloading hysteresis is generated by fibre/matrix slippage. The hysteresis loops obtained after high frequency fatigue have been modelled by the analysis presented in Chapter 6 using a value of 2 MPa for τ suggesting that high frequency fatigue reduces the interfacial shear strength.

Transverse ply and longitudinal ply cracking occurs in crossply laminates during quasi-static cycling and high frequency fatigue above their respective cracking thresholds. Longitudinal ply crack formation below the 0° ply cracking threshold in $(0_2/90_4)_s$ laminates is explained in terms of the complex stress distribution between the plies. The formation of longitudinal ply cracks running ~45° to the fibre direction is examined by considering the constraint on the 0° ply by the central 90° ply adjacent to an existing 0° ply crack.

LAY-UP	MAXIMUM STRESS	CRACKING THRESHOLD
$(0)_{12}$	75 MPa	σ < MATRIX
$(0)_{12}$	150 MPa	σ > MATRIX (PARTIAL SLIPPAGE)
$(0)_{12}$	200 MPa	σ > MATRIX (TOTAL SLIPPAGE)
$(0/90)_s$	30 MPa	σ < 90° PLY
$(0/90)_s$	50 MPa	90° PLY < σ < 0° PLY
$(0/90)_s$	100 MPa	σ > 0° PLY >> 90° PLY
$(0_2/90_4)_s$	10 MPa	σ < 90° PLY
$(0_2/90_4)_s$	30 MPa	90° PLY < σ < 0° PLY
$(0_2/90_4)_s$	70 MPa	σ > 0° PLY >> 90° PLY

Table 7.1 Stress levels used in the fatigue testing of unidirectional and crossply laminates.

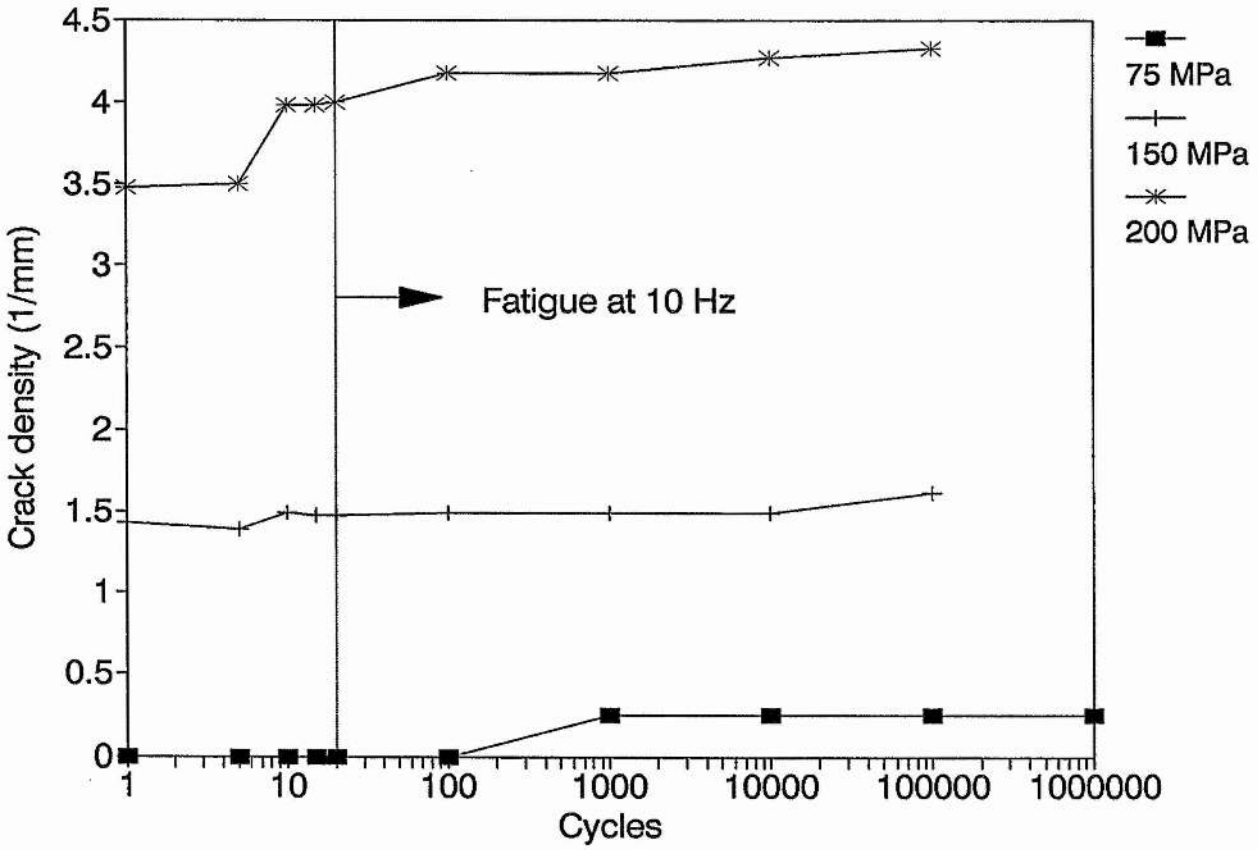

Figure 7.1 Crack density vs cycles for the unidirectional laminates.

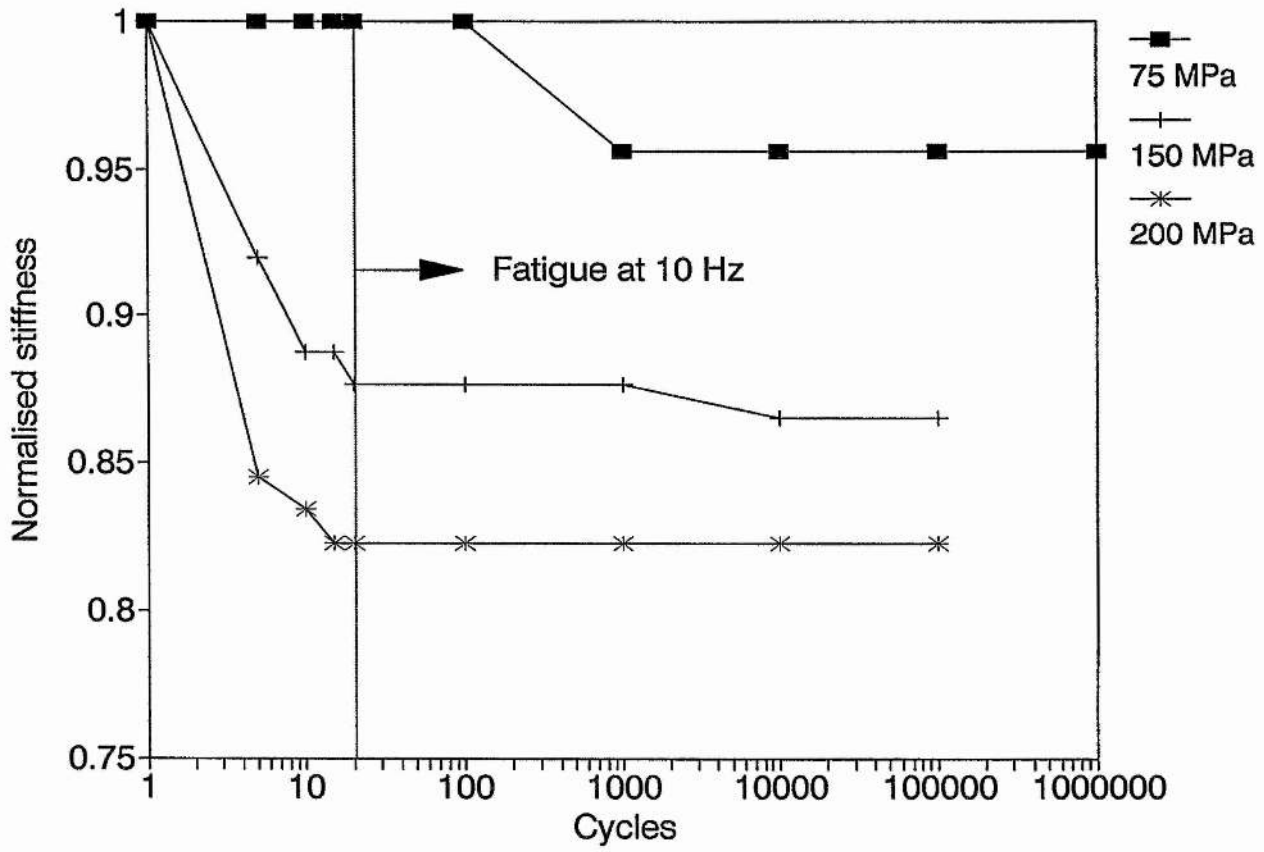

Figure 7.2 Normalised 0.05% secant stiffness vs cycles for the unidirectional laminates.

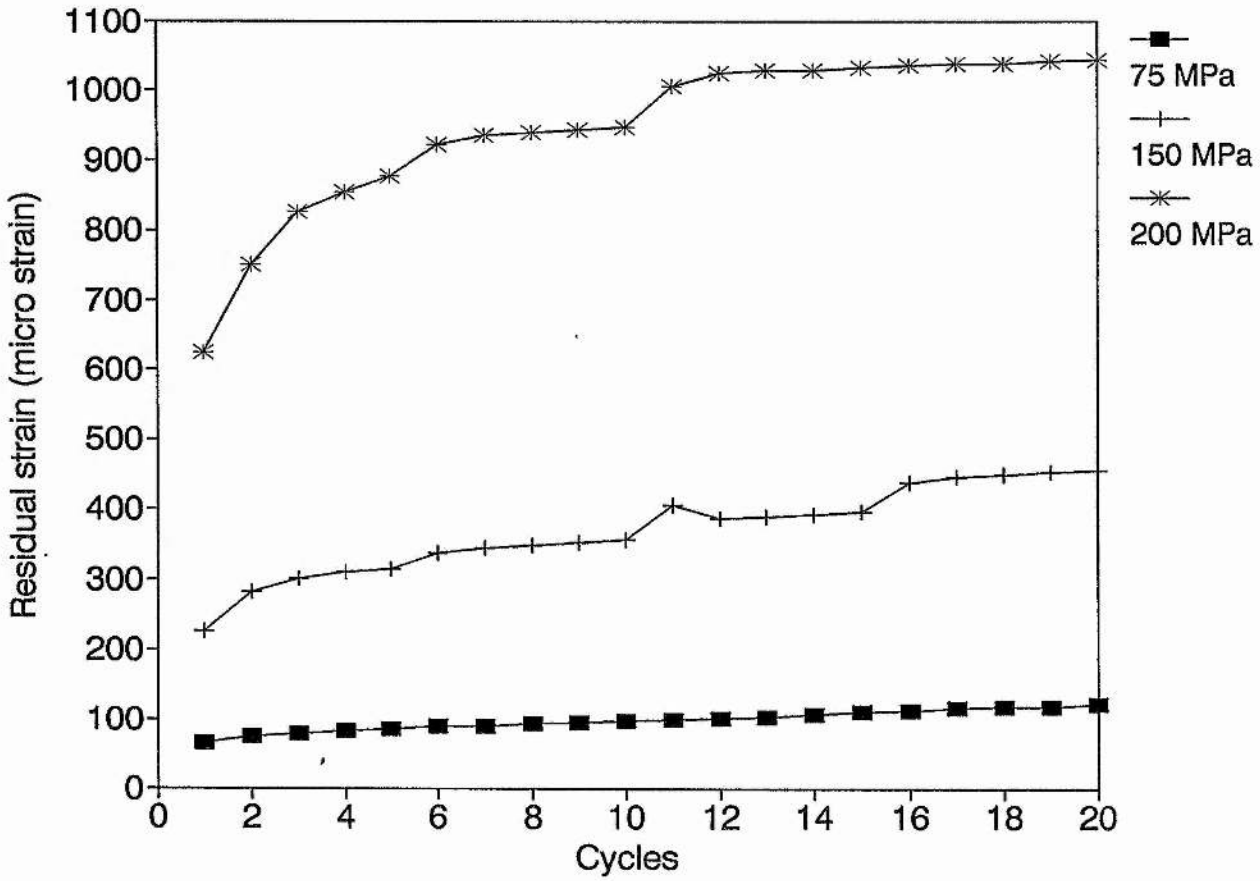

Figure 7.3 Cumulative residual strain vs low strain rate cycles for the unidirectional laminates.

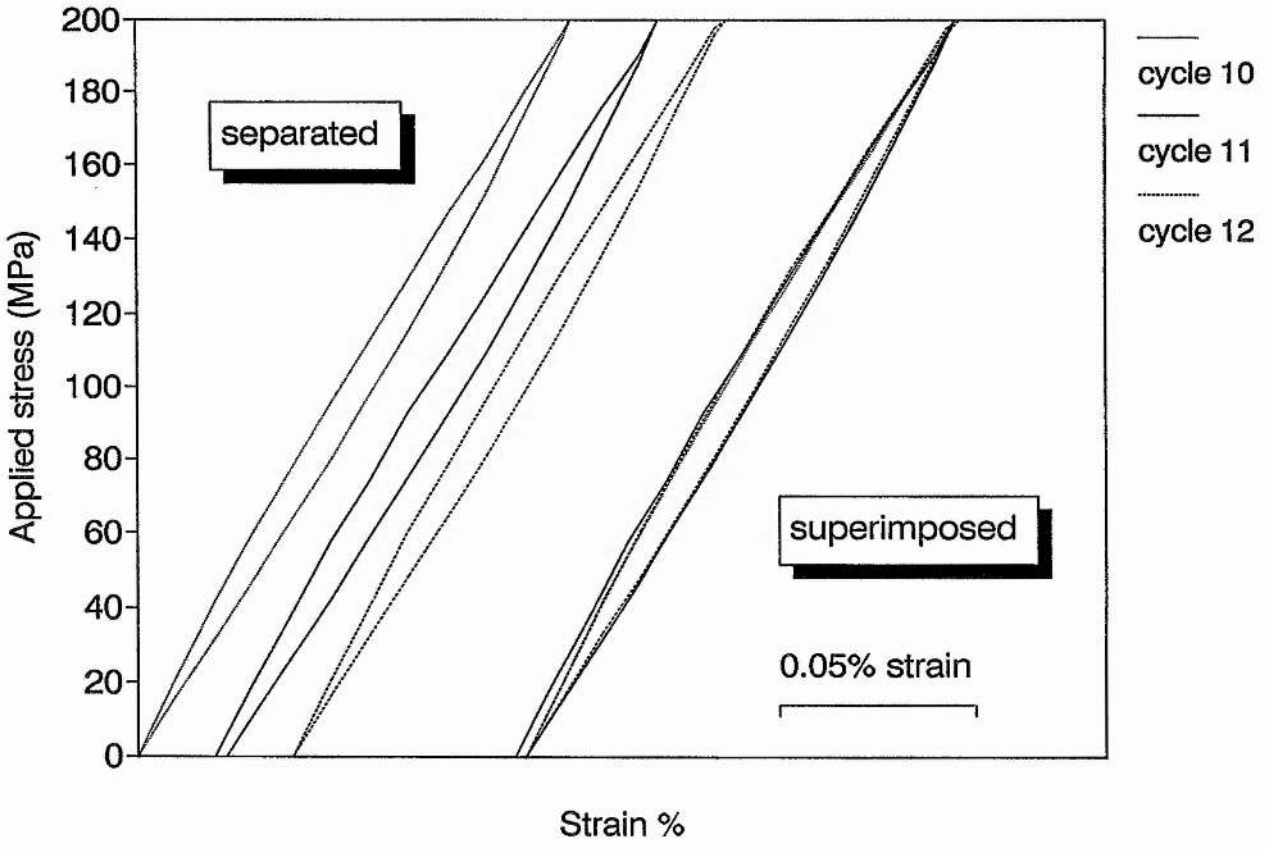

Figure 7.4 Comparison of loading and unloading curves for the specimen subjected to the highest maximum stress (200 MPa) showing grip misalignment (specimen removed from Instron after cycle 10).

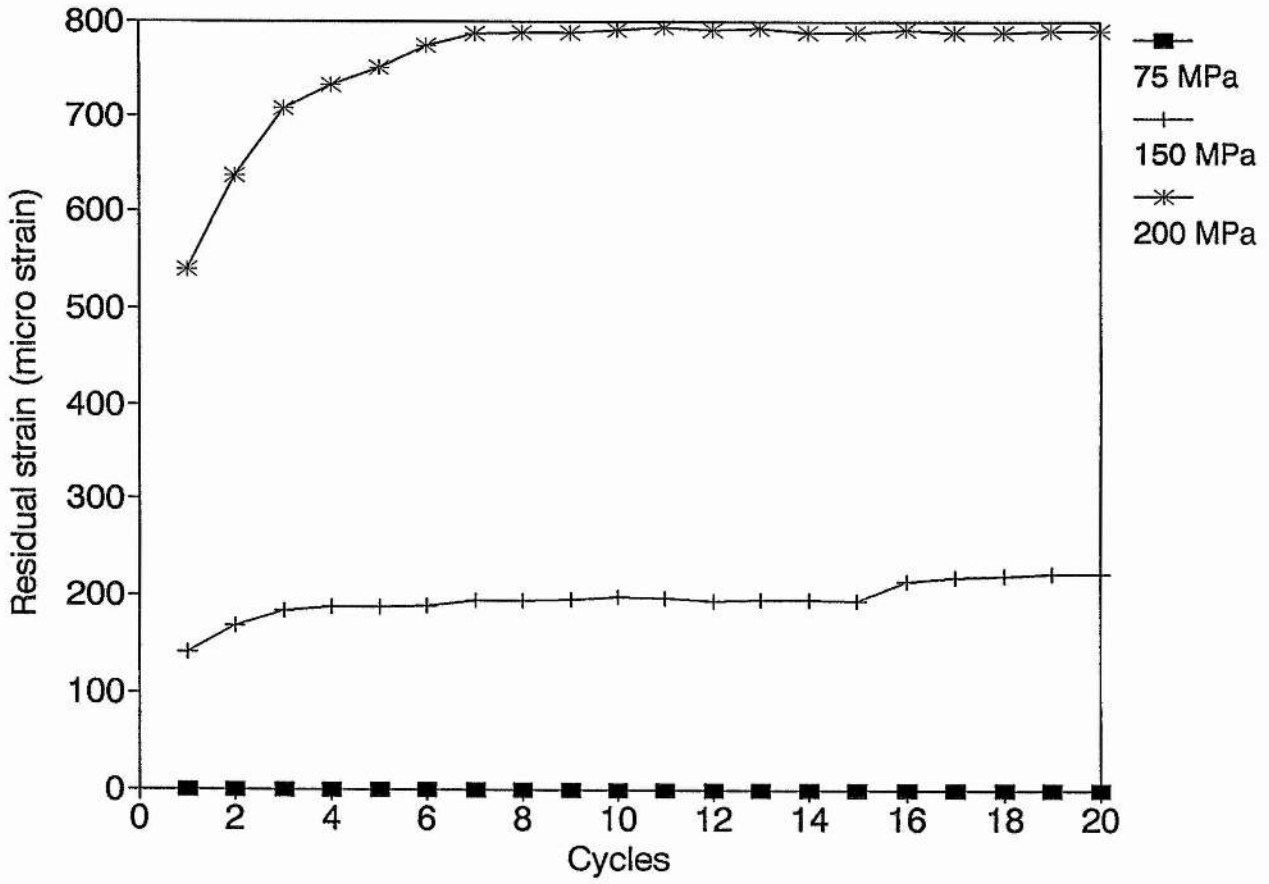

Figure 7.5 Cumulative residual strain vs low strain rate cycles for the unidirectional laminates corrected for thermal drift and grip misalignment.

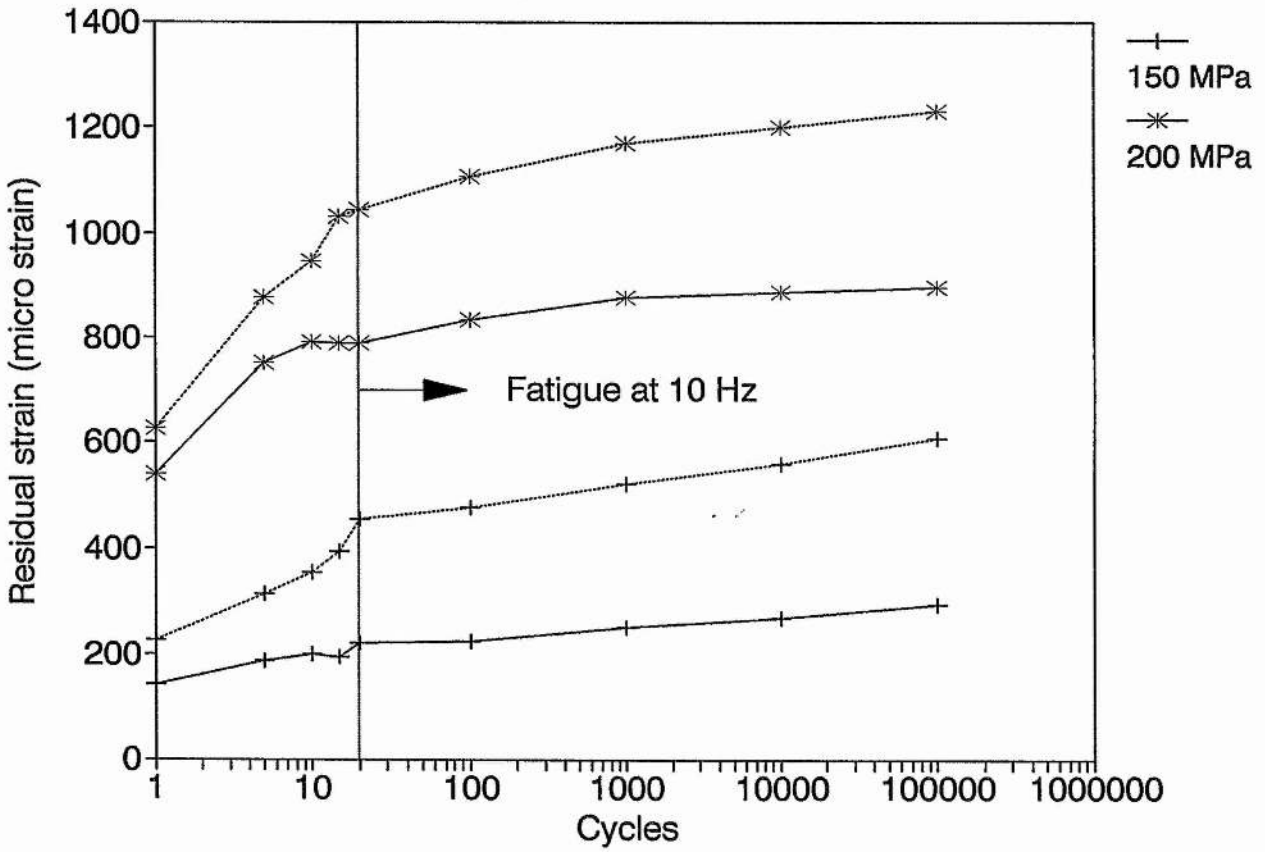

Figure 7.6 Cumulative residual strain vs cycles data for the unidirectional laminates.
Original data - broken lines.
Data corrected for thermal drift and grip misalignment - solid lines.

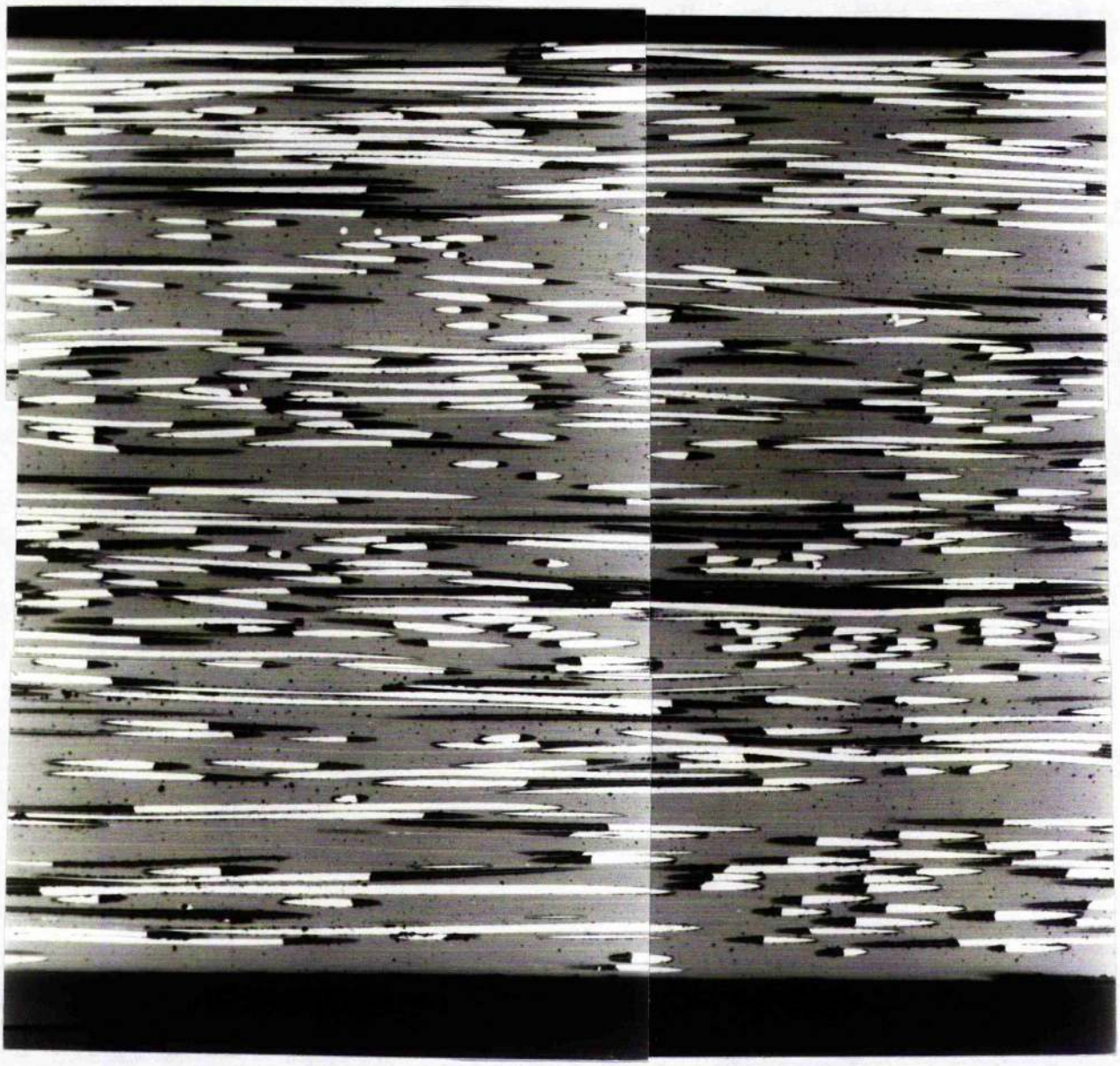

Figure 7.7 Optical micrograph of the unidirectional 150 MPa specimen after 100 000 cycles at 10 Hz.

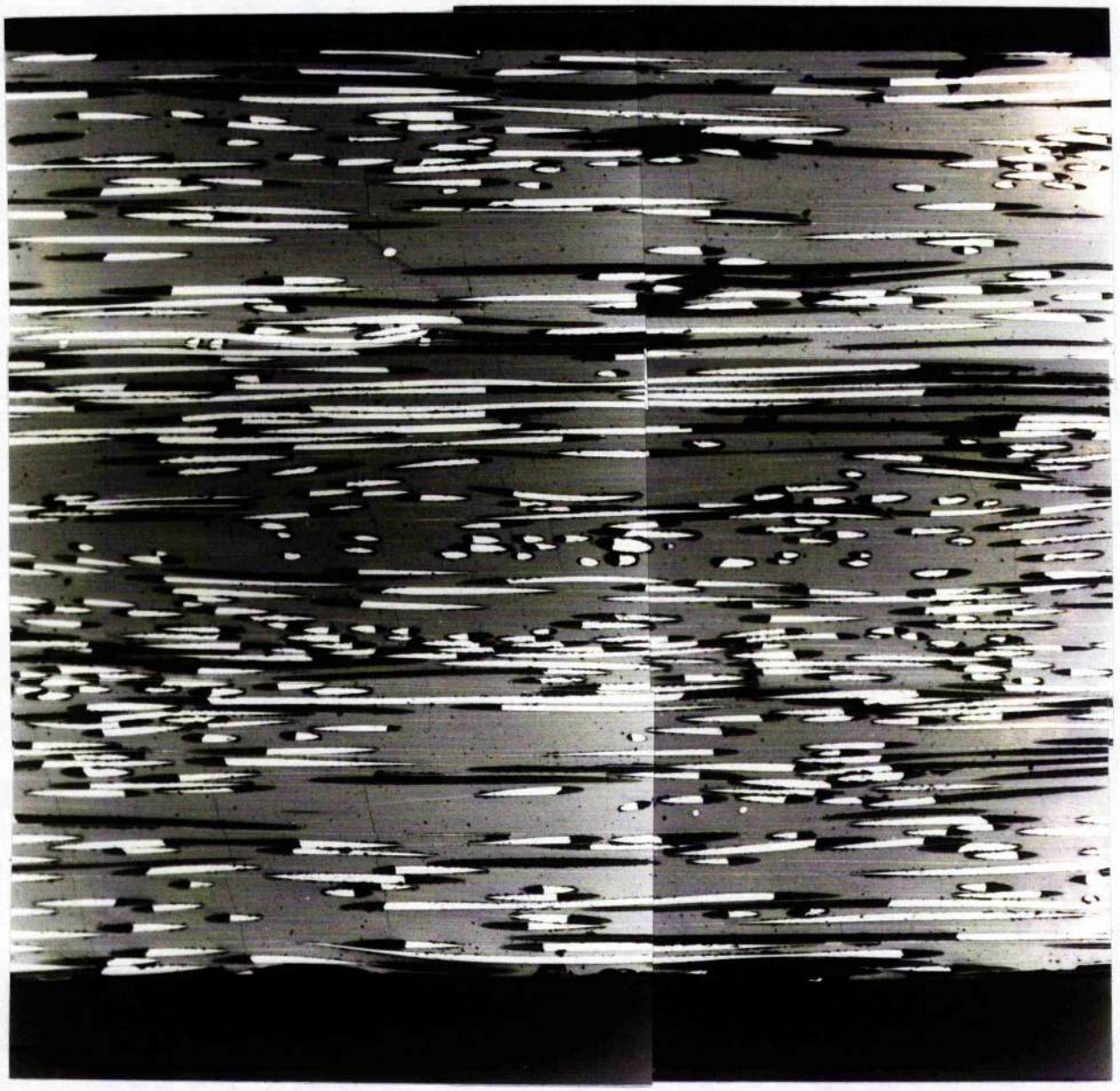

Figure 7.8 Optical micrograph of the unidirectional 200 MPa specimen after 100 000 cycles at 10 Hz.

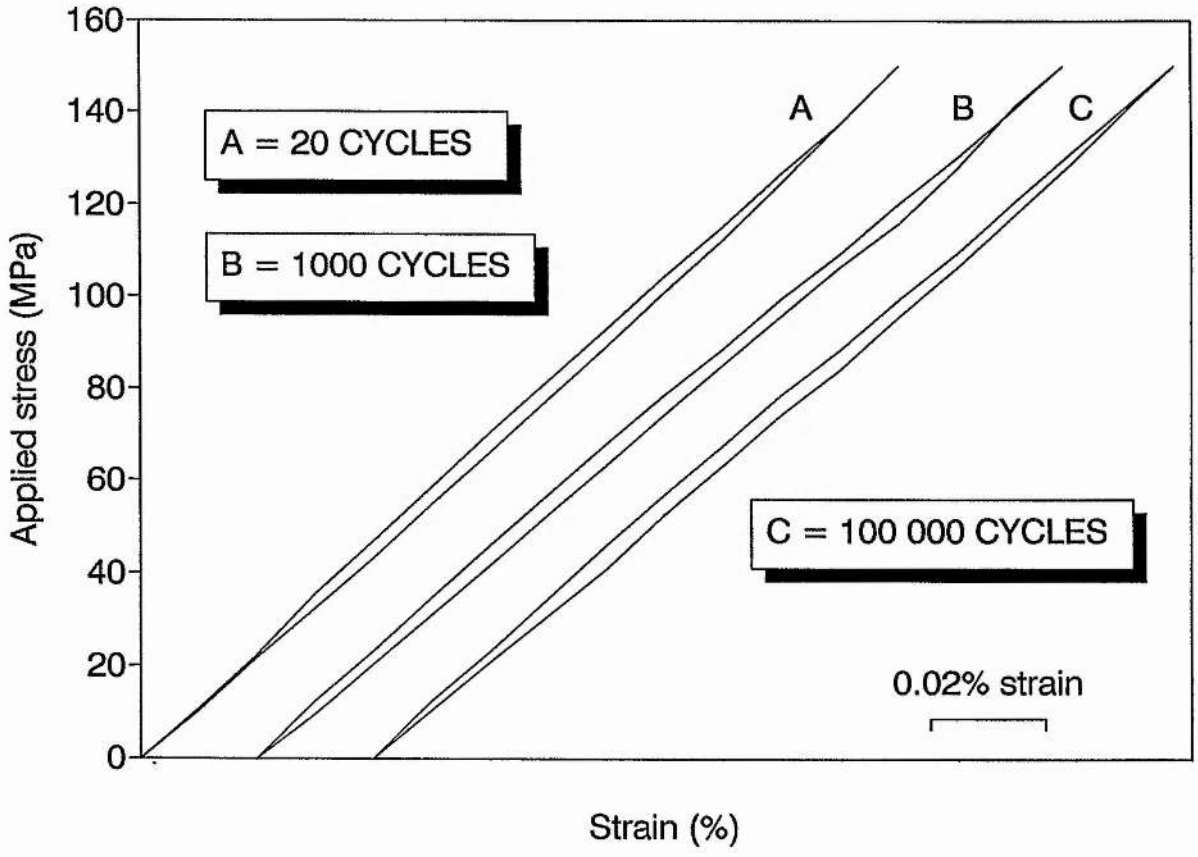

Figure 7.9 Stress/strain hysteresis loops for the 150 MPa unidirectional specimen.

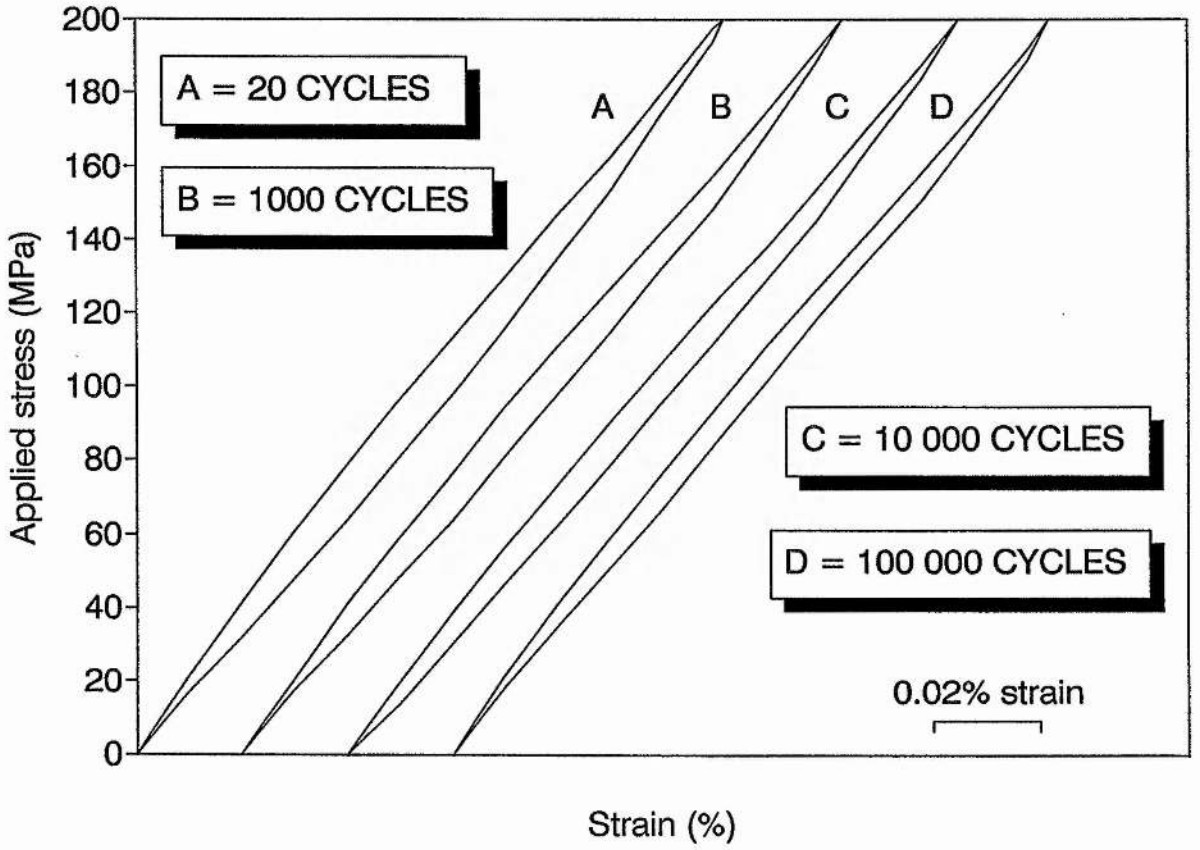

Figure 7.10 Stress/strain hysteresis loops for the 200 MPa unidirectional specimen.

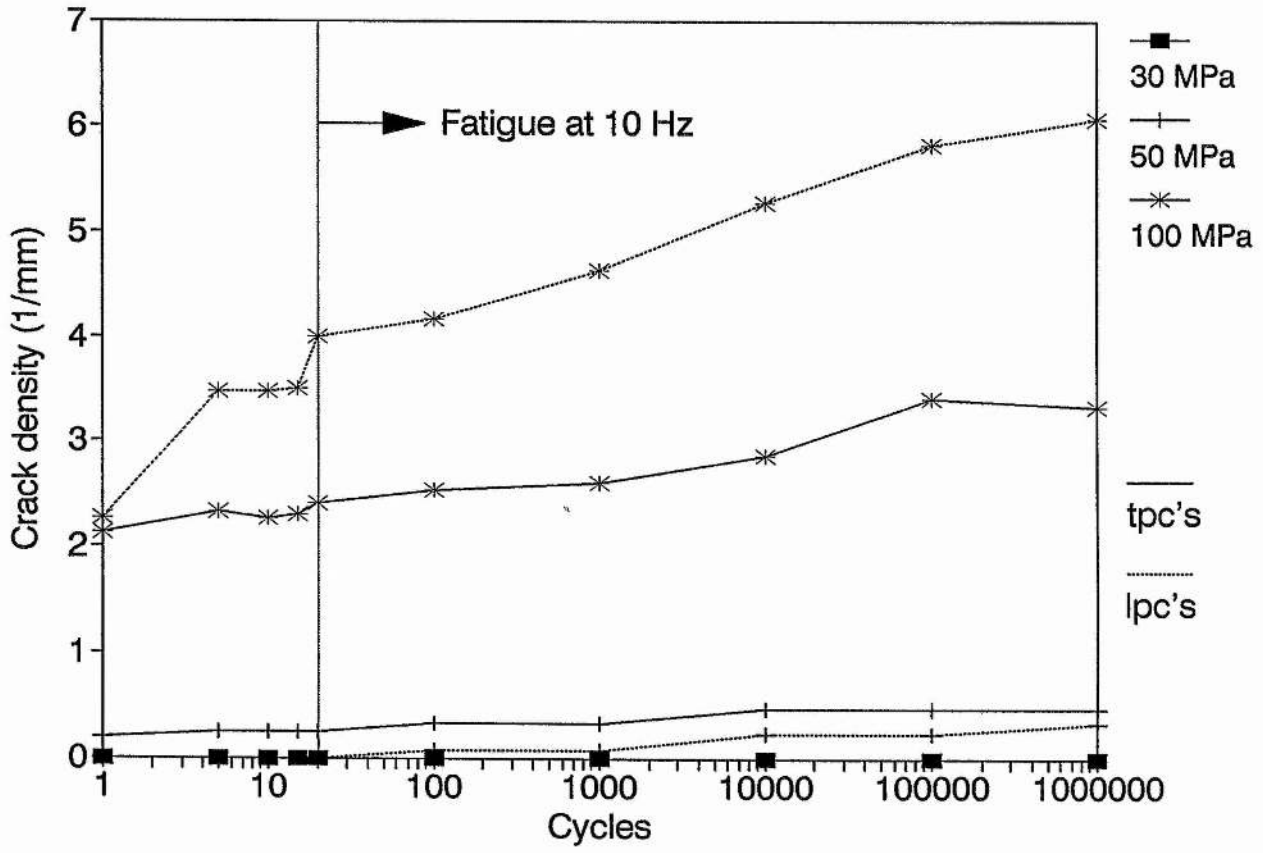

Figure 7.11 Transverse and longitudinal ply crack densities as a function of fatigue cycles for $(0/90)_s$ laminates at three different maximum stress levels.

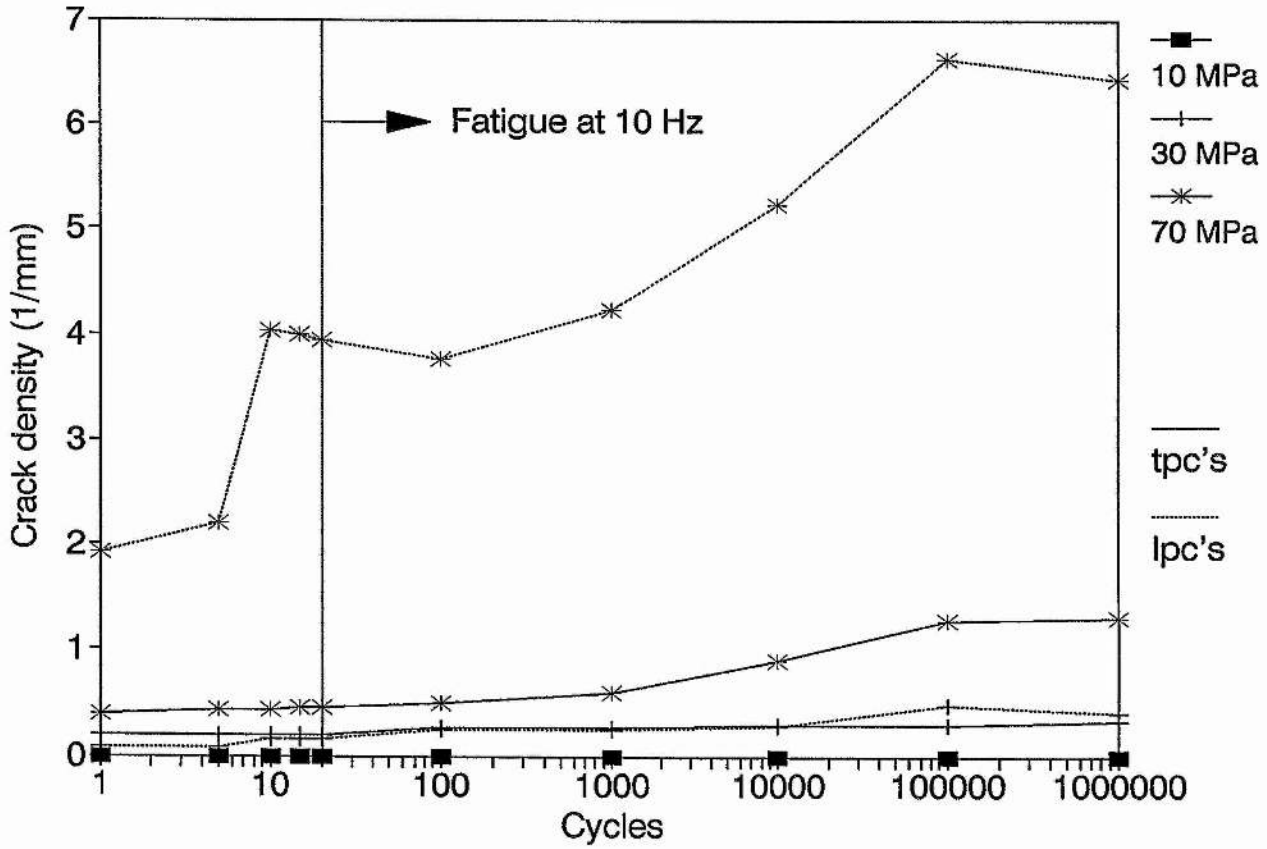

Figure 7.12 Transverse and longitudinal ply crack densities as a function of fatigue cycles for the $(0_2/90_4)_s$ laminates at three different maximum stress levels.

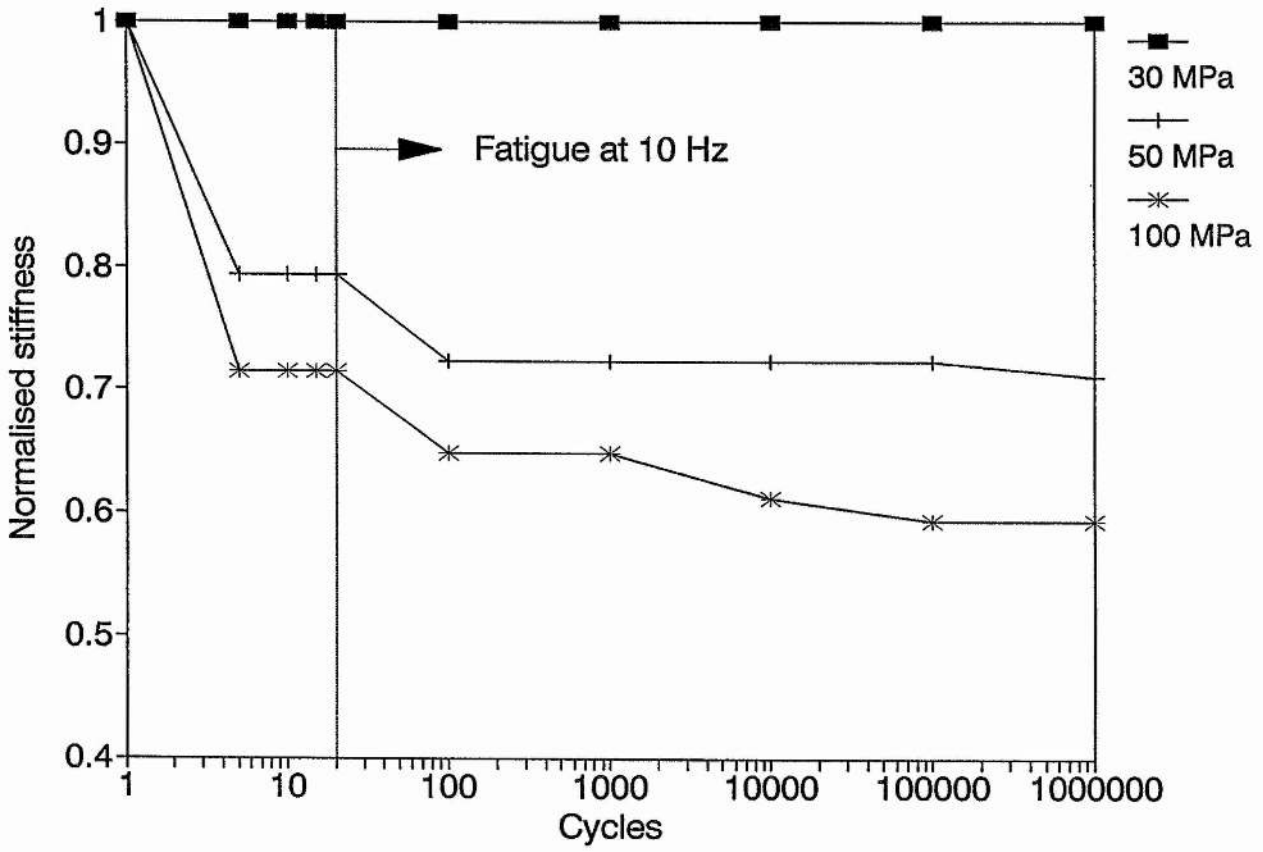

Figure 7.13 Normalised 0.02% secant stiffness vs cycles for the $(0/90)_s$ laminates.

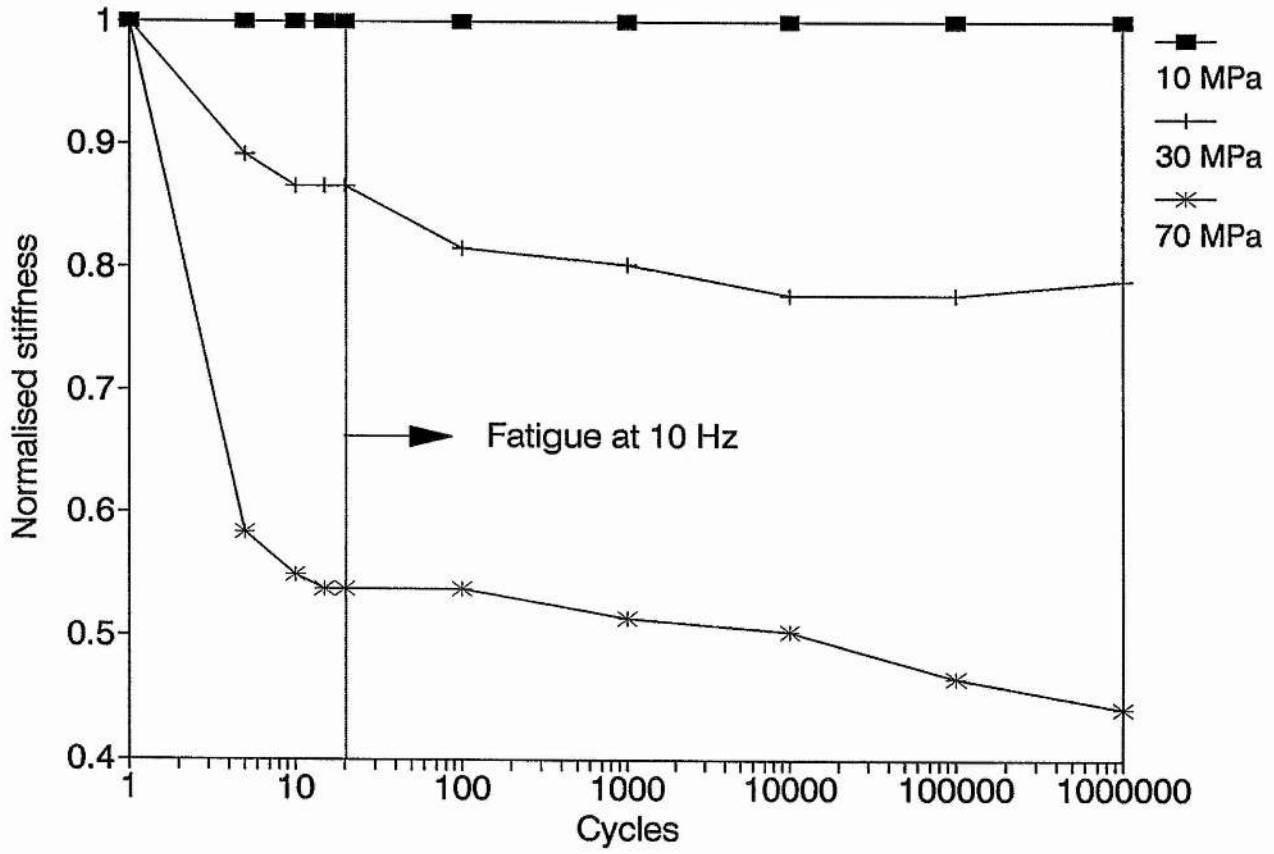

Figure 7.14 Normalised 0.02% secant stiffness vs cycles for the $(0_2/90_4)_s$ laminates.

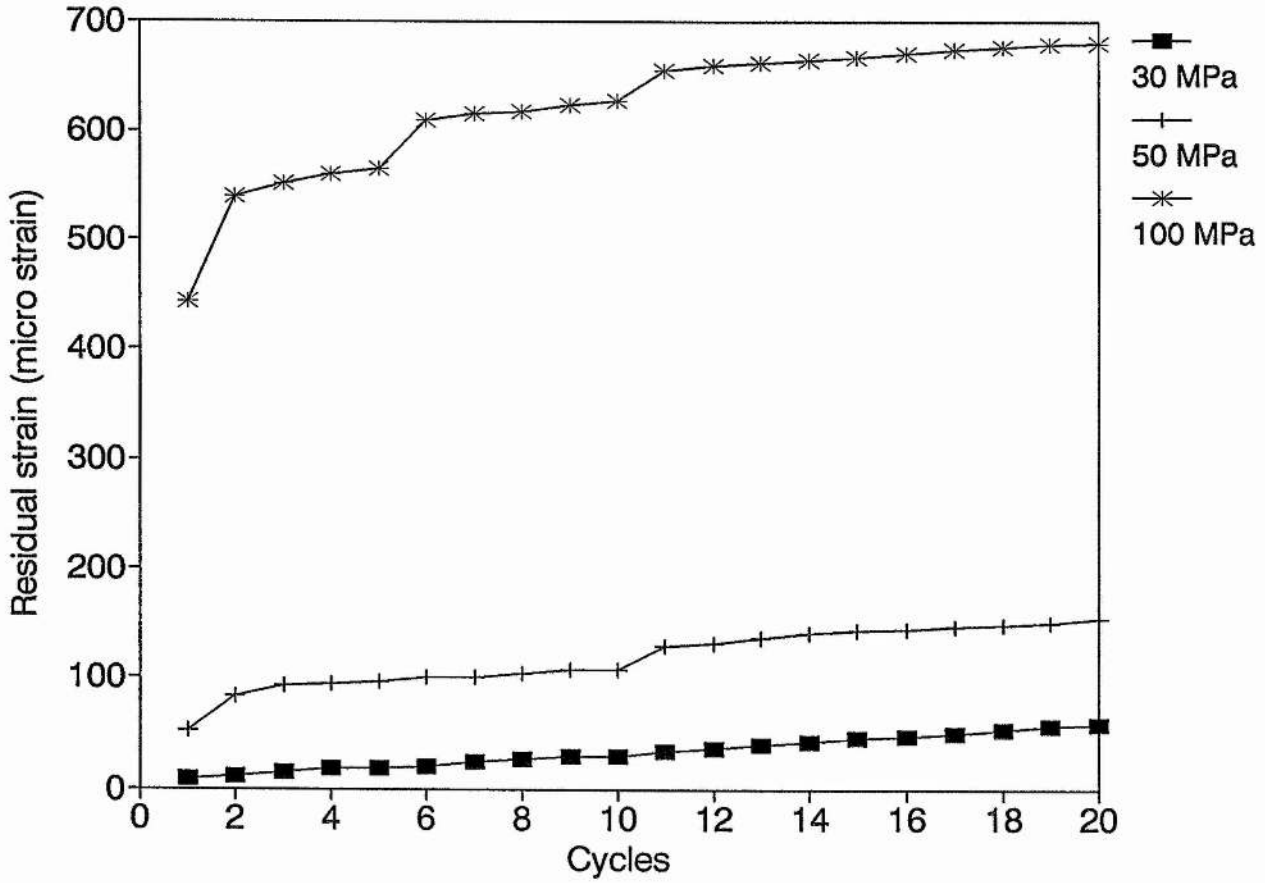

Figure 7.15 Cumulative residual strain vs low strain rate cycles for the $(0/90)_s$ laminates.

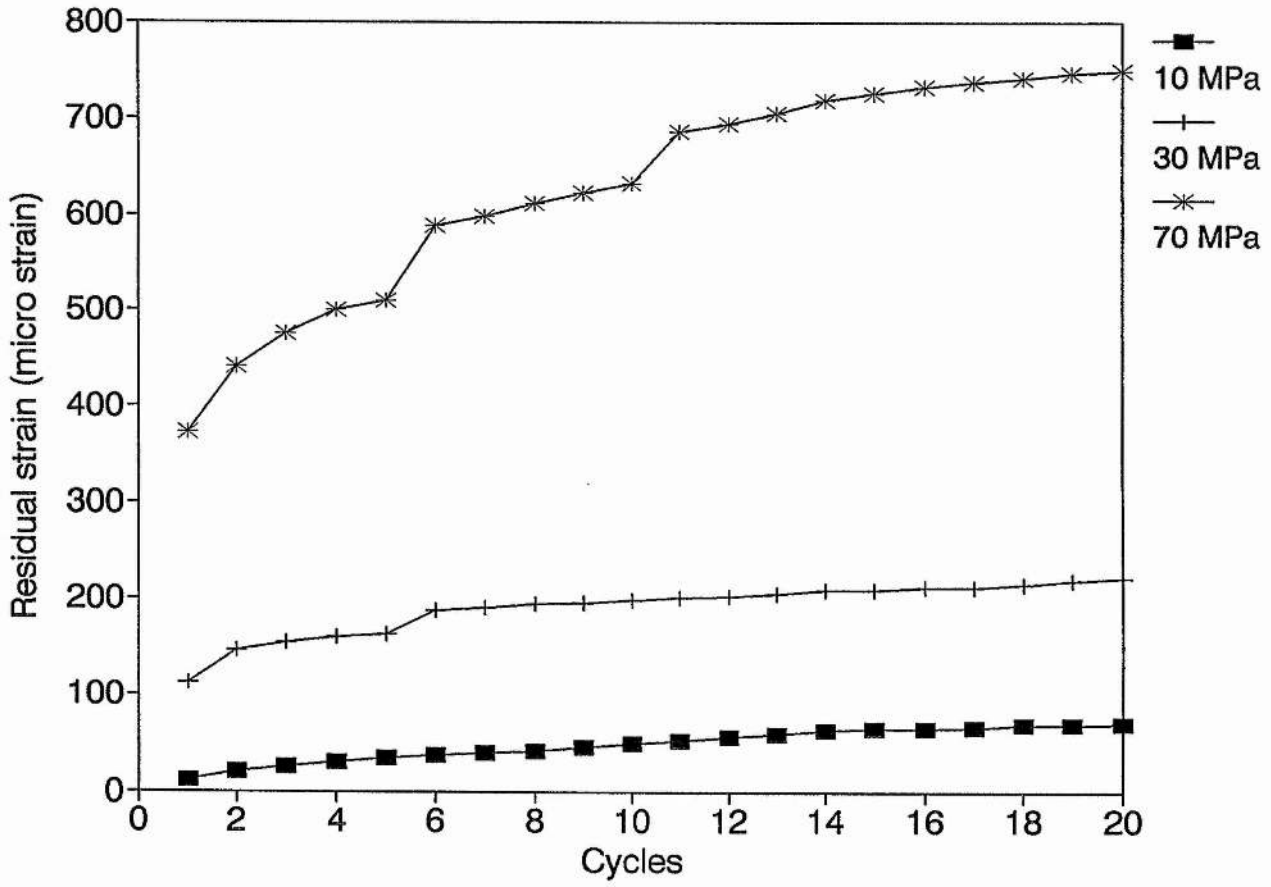

Figure 7.16 Cumulative residual strain vs low strain rate cycles for the $(0_2/90_4)_s$ laminates.

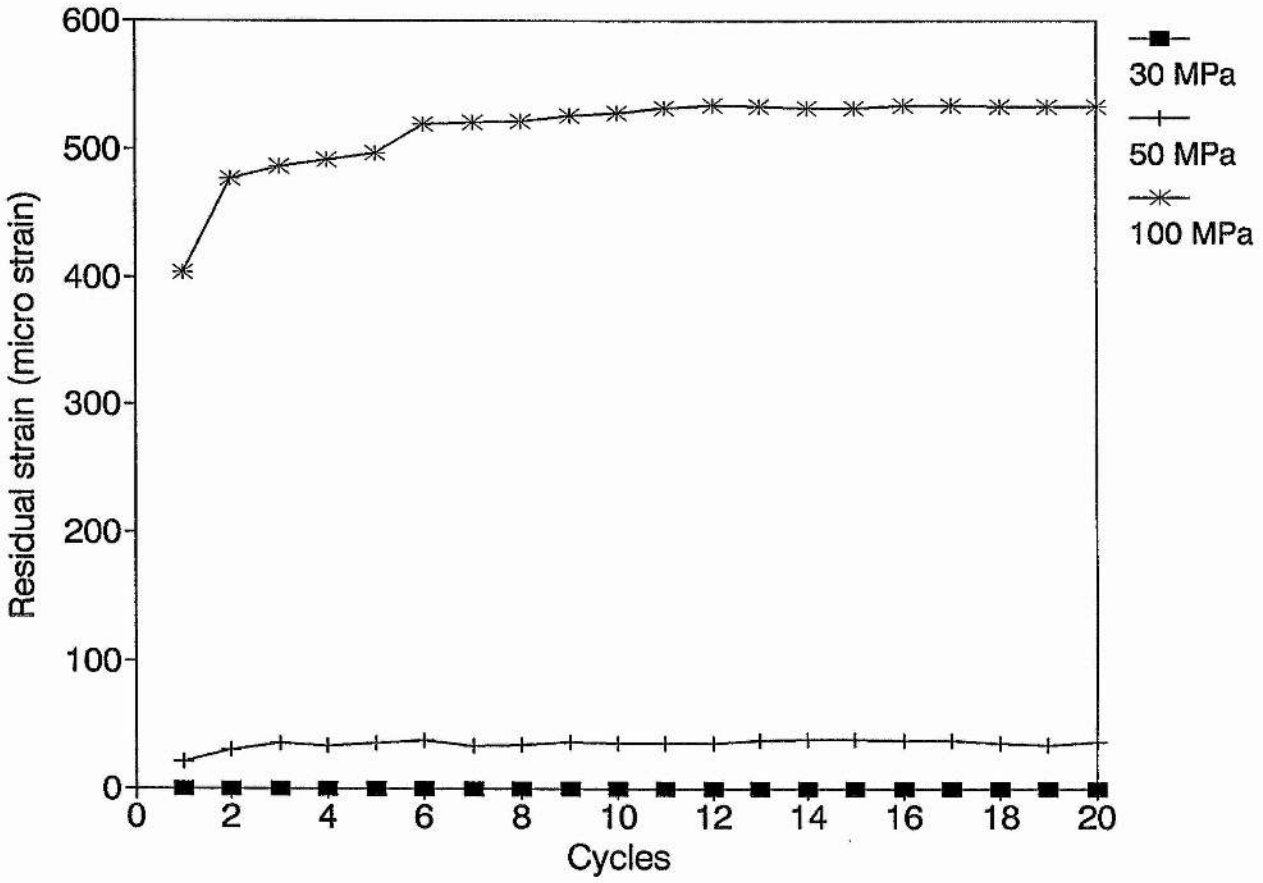

Figure 7.17 Cumulative residual strain vs low strain rate cycles for the $(0/90)_s$ laminates corrected for thermal drift and grip misalignment.

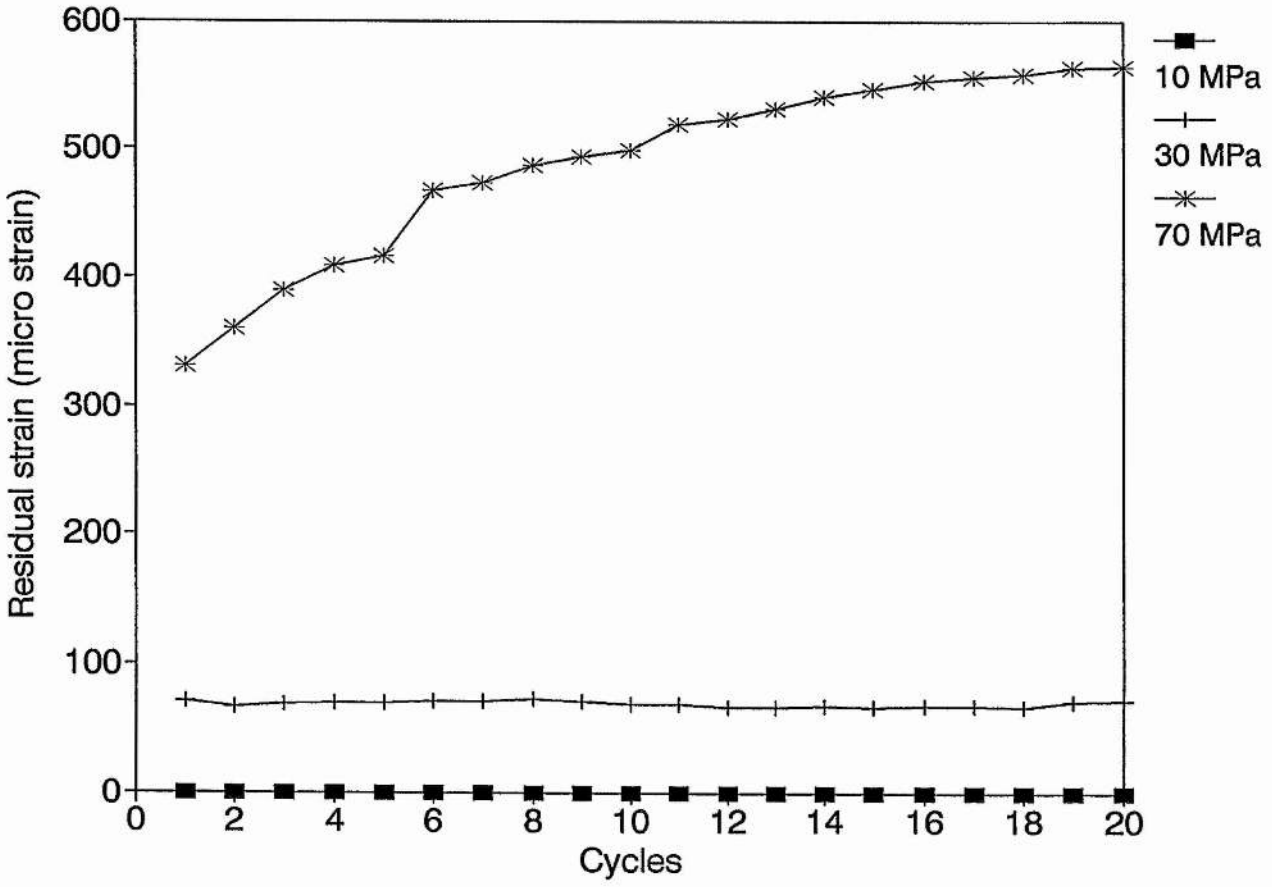

Figure 7.18 Cumulative residual strain vs low strain rate cycles for the $(0_2/90_4)_s$ laminates corrected for thermal drift and grip misalignment.

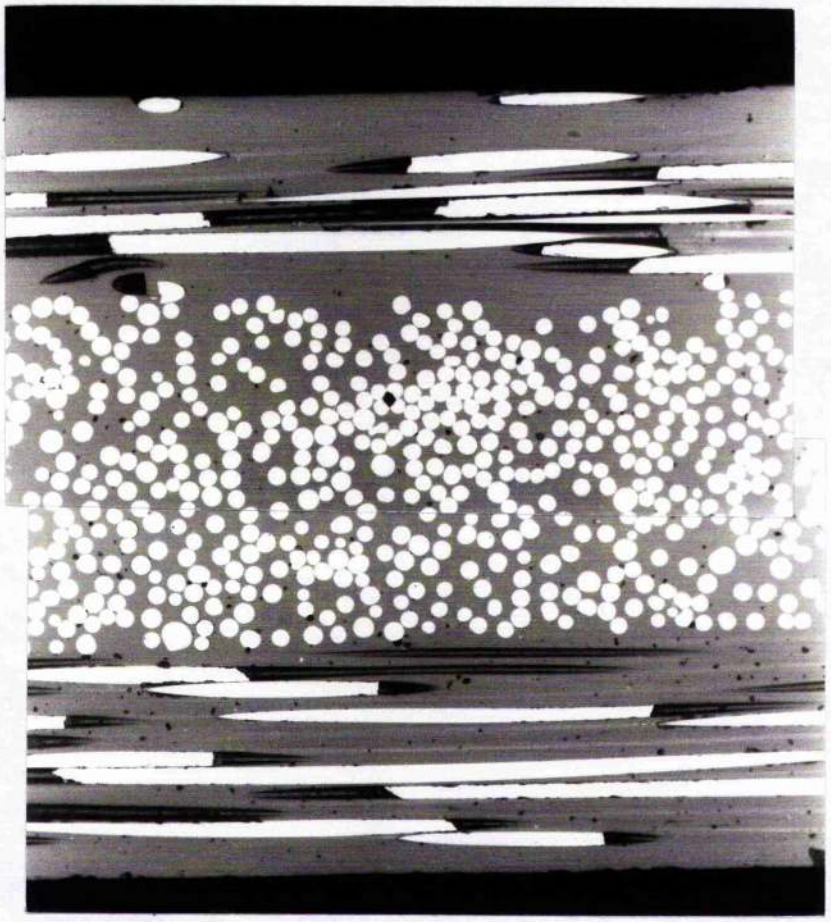

Figure 7.19 Optical micrograph of a crossply $(0/90)_s$ specimen after 20 low strain rate fatigue cycles at a maximum stress of 50 MPa.

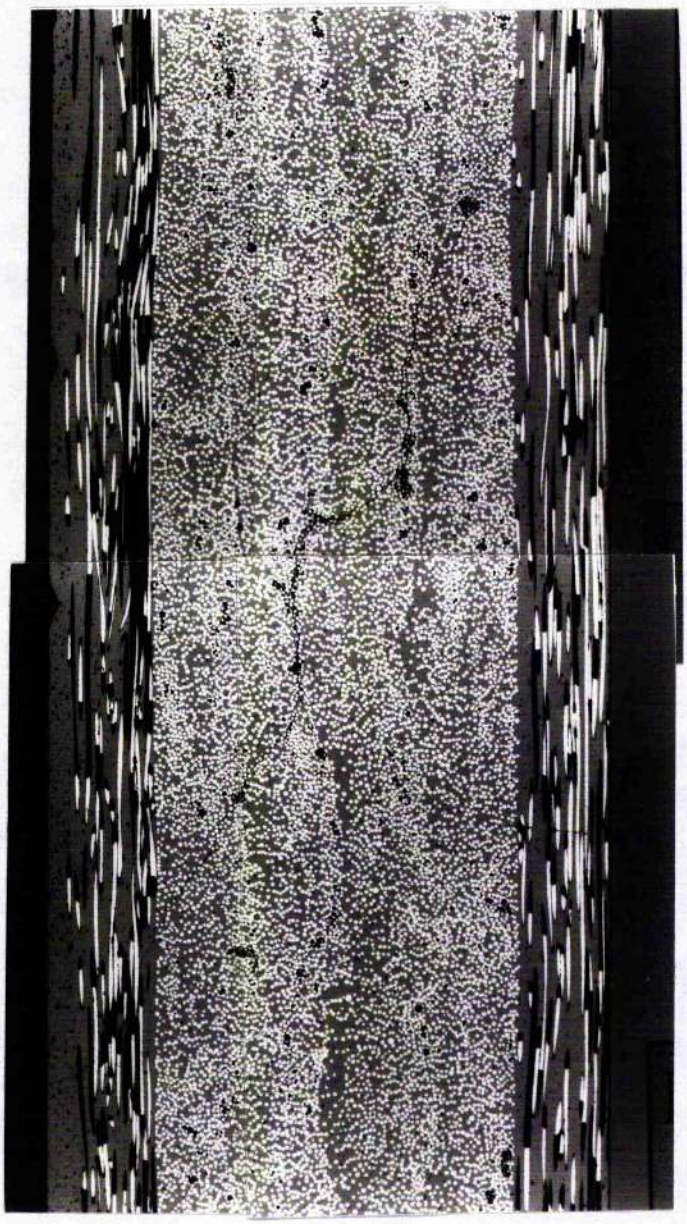

Figure 7.20 Optical micrograph of a crossply $(0_2/90_4)_s$ specimen after 20 low strain rate cycles at a maximum stress of 30 MPa.

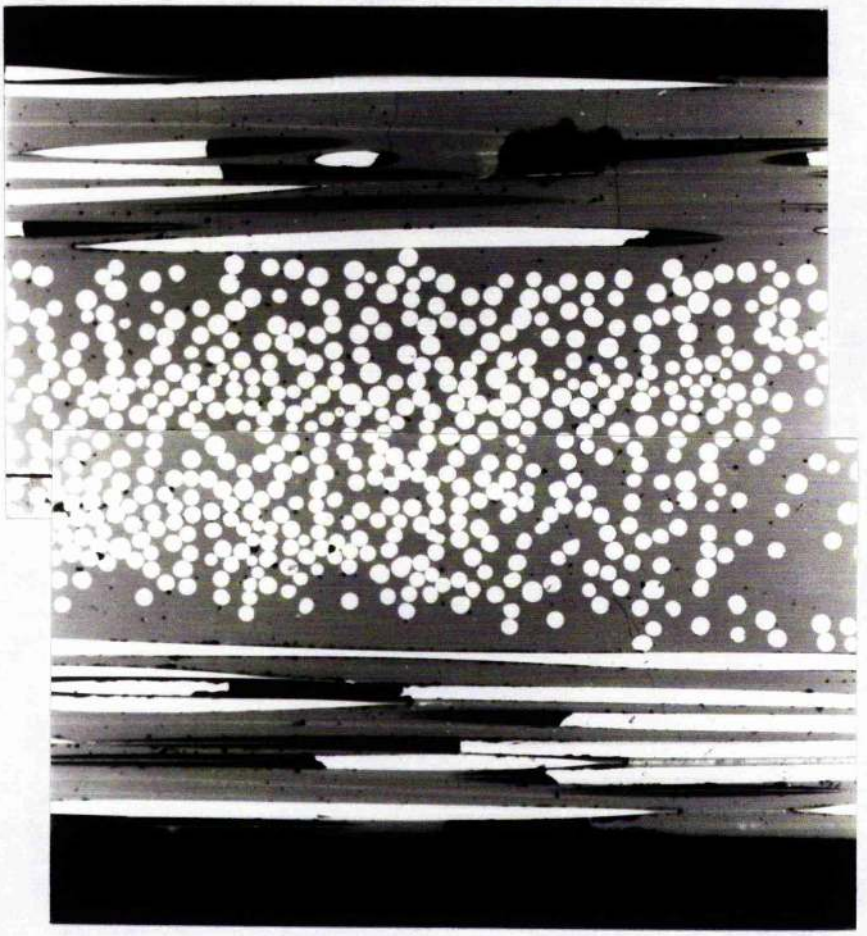

Figure 7.21 Optical micrograph of a crossply $(0/90)_s$ specimen after 20 low strain rate cycles at a maximum stress of 100 MPa.

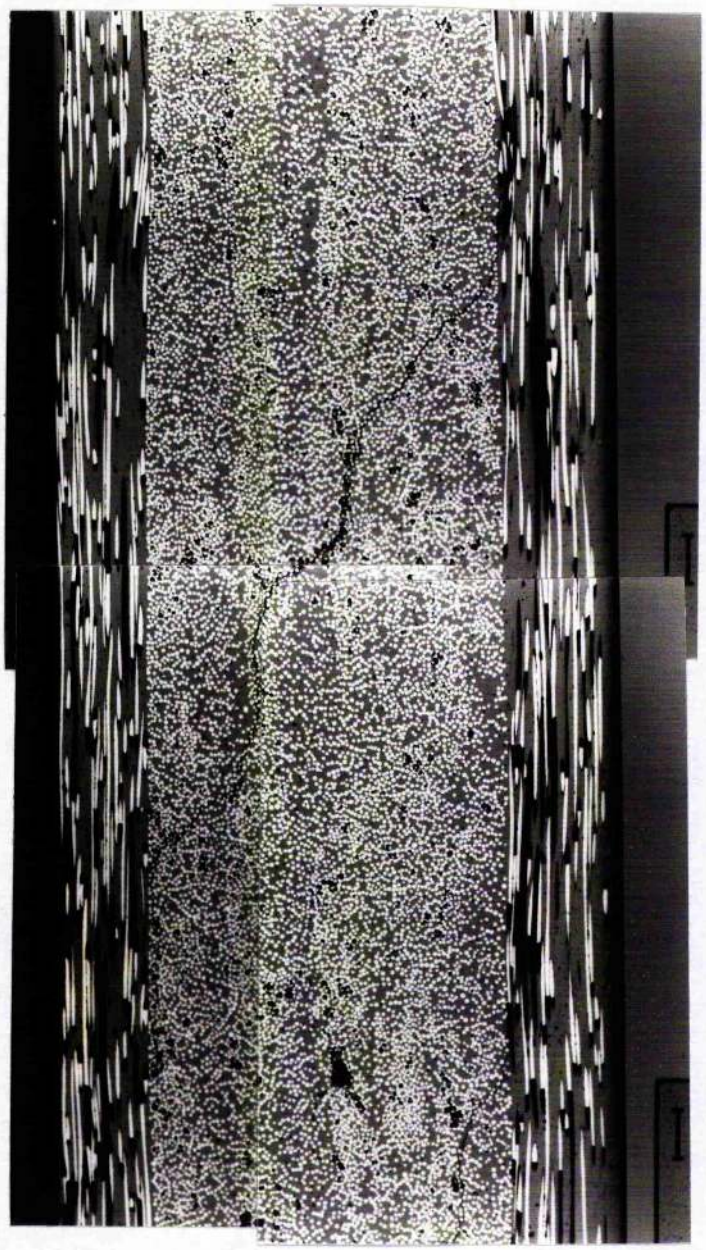

Figure 7.22 Optical micrograph of a crossply $(0_2/90_4)_s$ specimen after 20 low strain rate cycles at a maximum stress of 70 MPa.

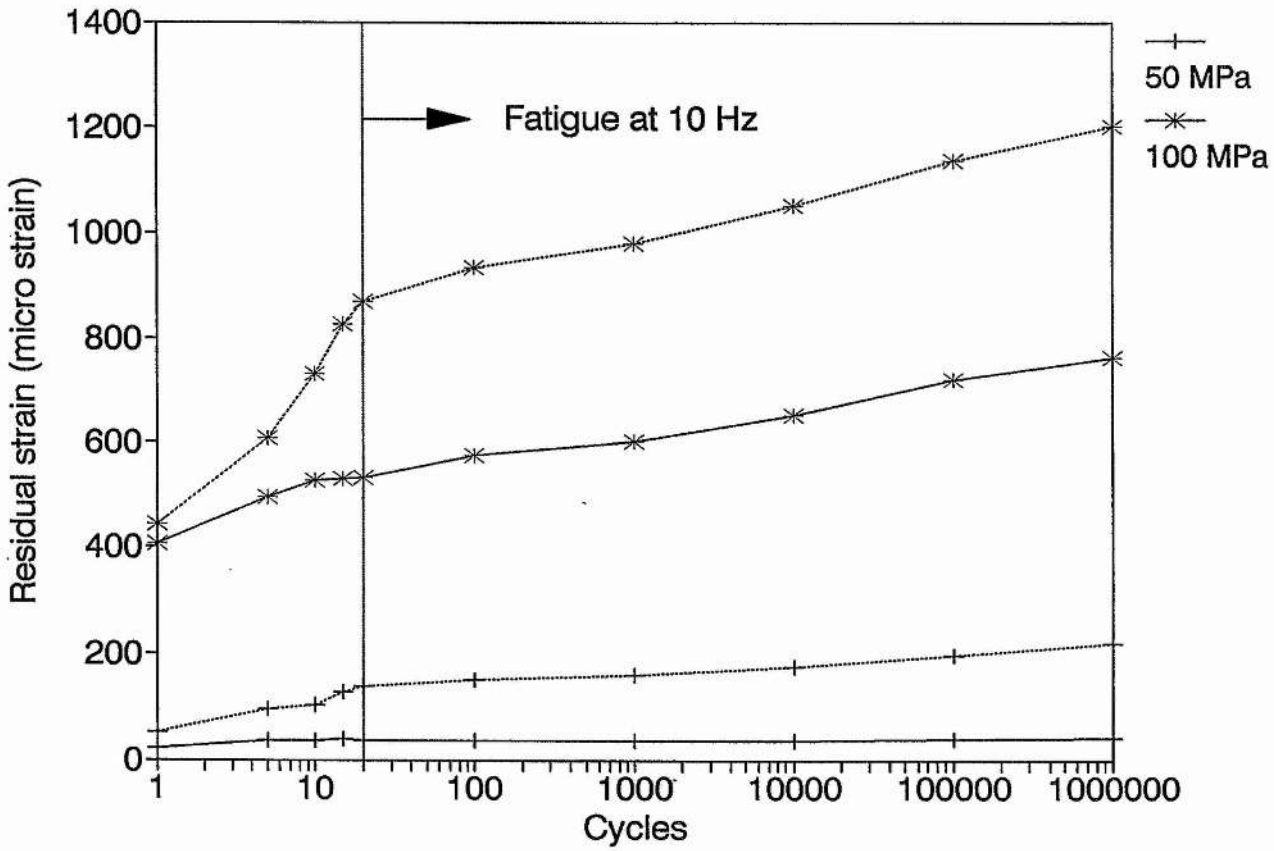

Figure 7.23 Residual strain vs cycles for the $(0/90)_s$ laminates.
Original data - broken lines.
Data corrected for thermal drift and grip misalignment - solid lines.

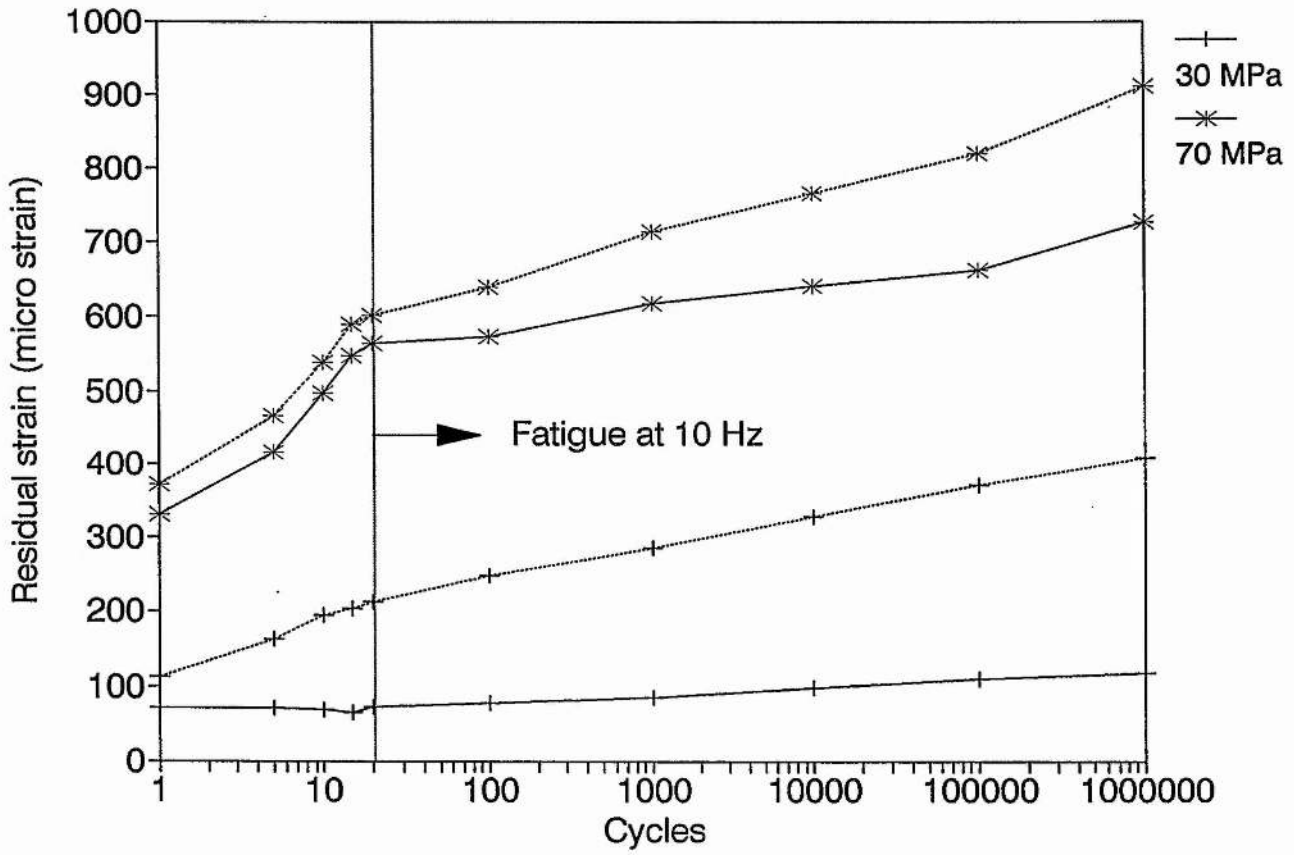

Figure 7.24 Residual strain vs cycles for the $(0_2/90_4)_s$ laminates.
Original data - broken lines.
Data corrected for thermal drift and grip misalignment - solid lines.

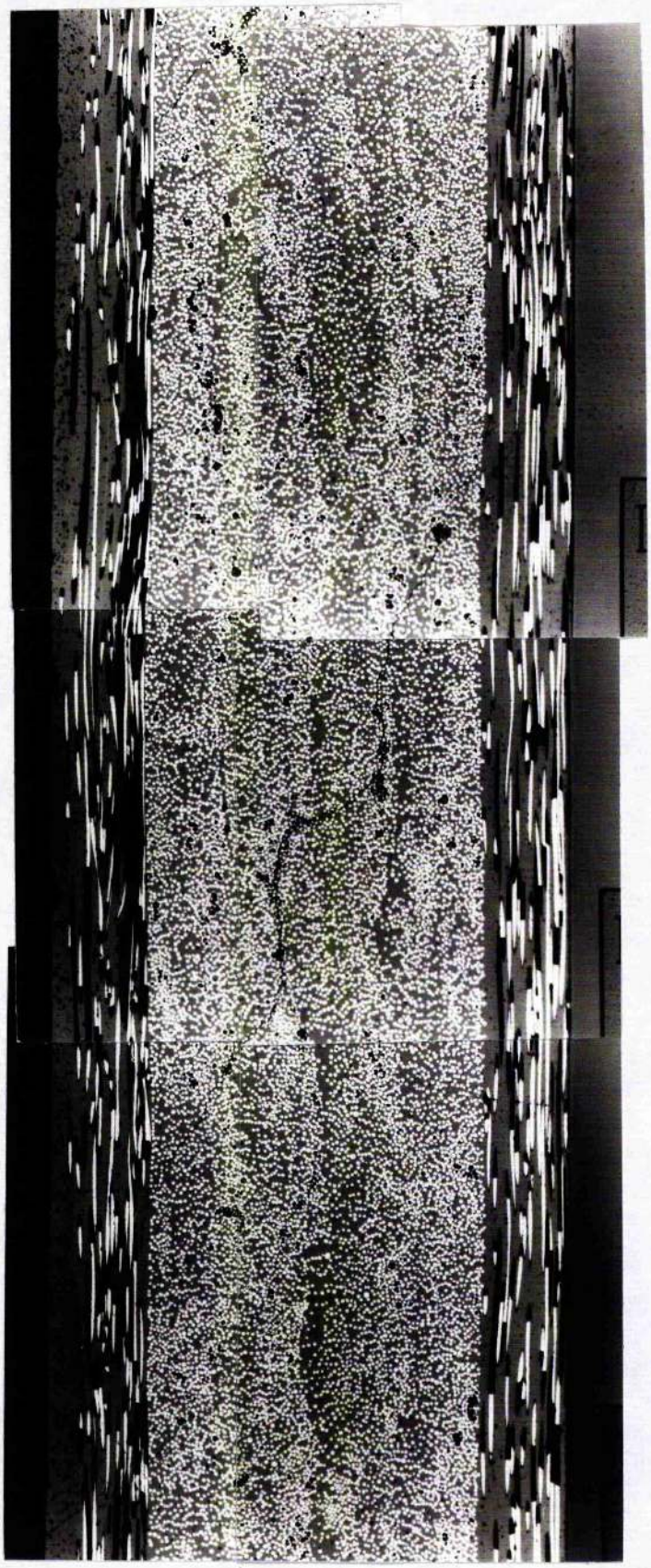

Figure 7.25 Optical micrograph of the crossply $(0_2/90_4)_s$ 30 MPa specimen after one million cycles.

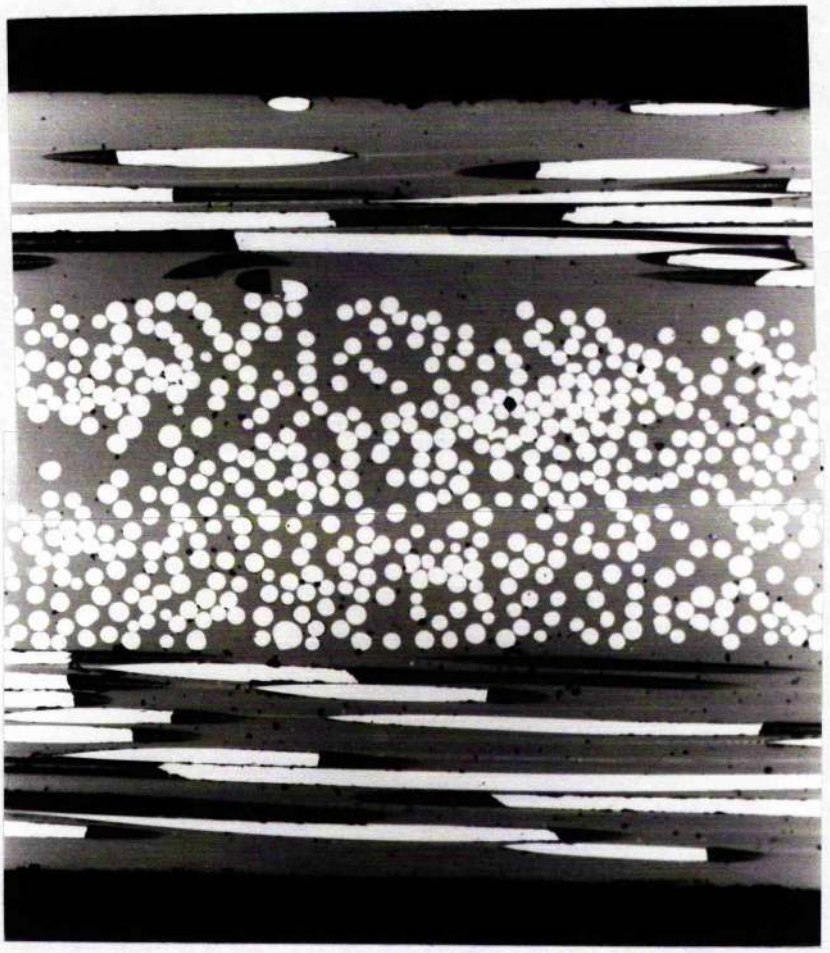

Figure 7.26 Optical micrograph of the crossply $(0/90)_s$ 50 MPa specimen after one million cycles.

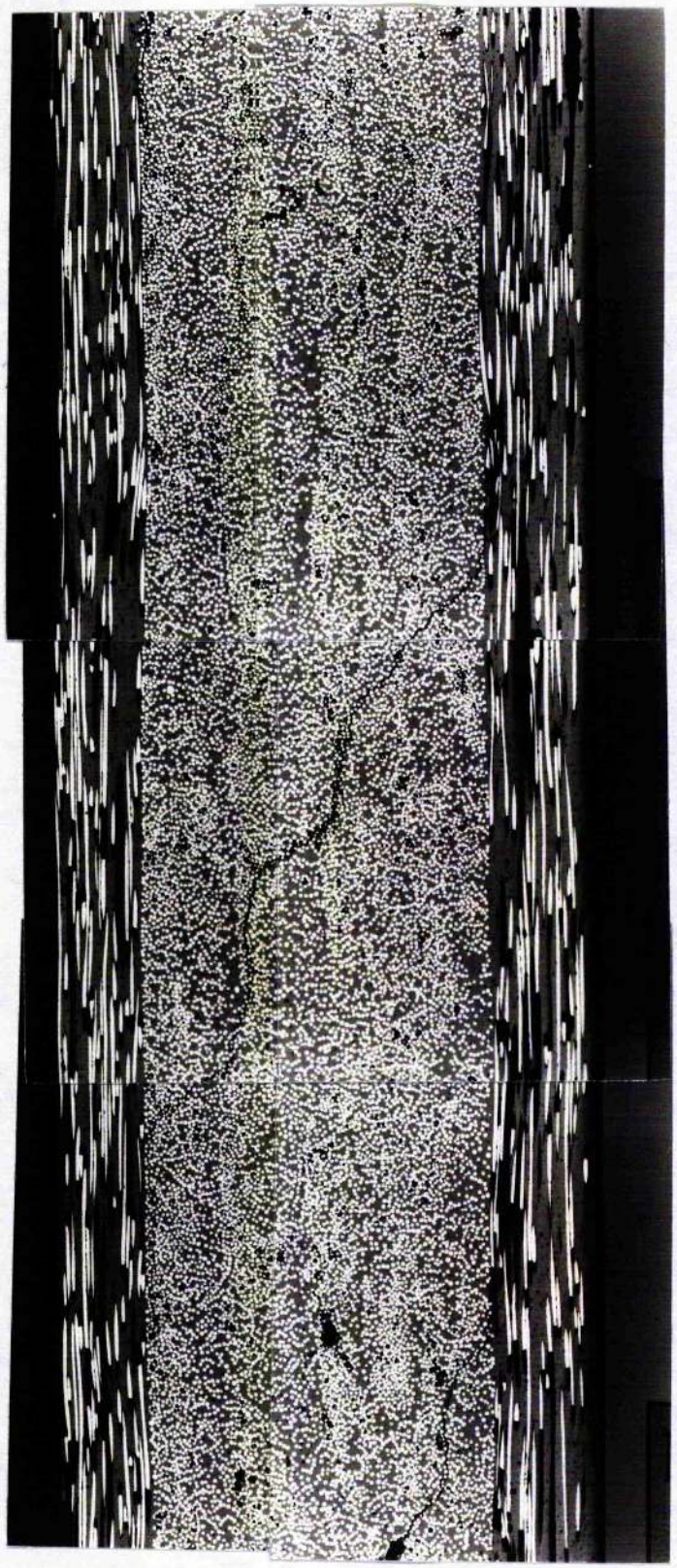

Figure 7.27 Optical micrograph of the crossply $(0_2/90_4)_s$ 70 MPa specimen after one million cycles.

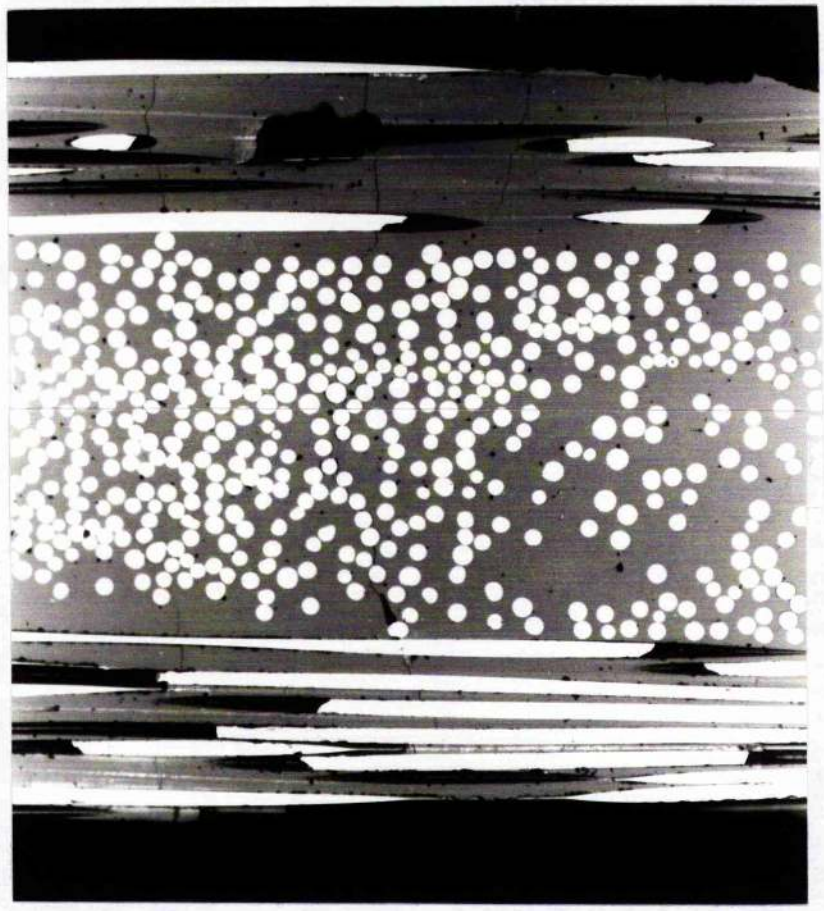

Figure 7.28 Optical micrograph of the crossply $(0/90)_s$ 100 MPa specimen after one million cycles.

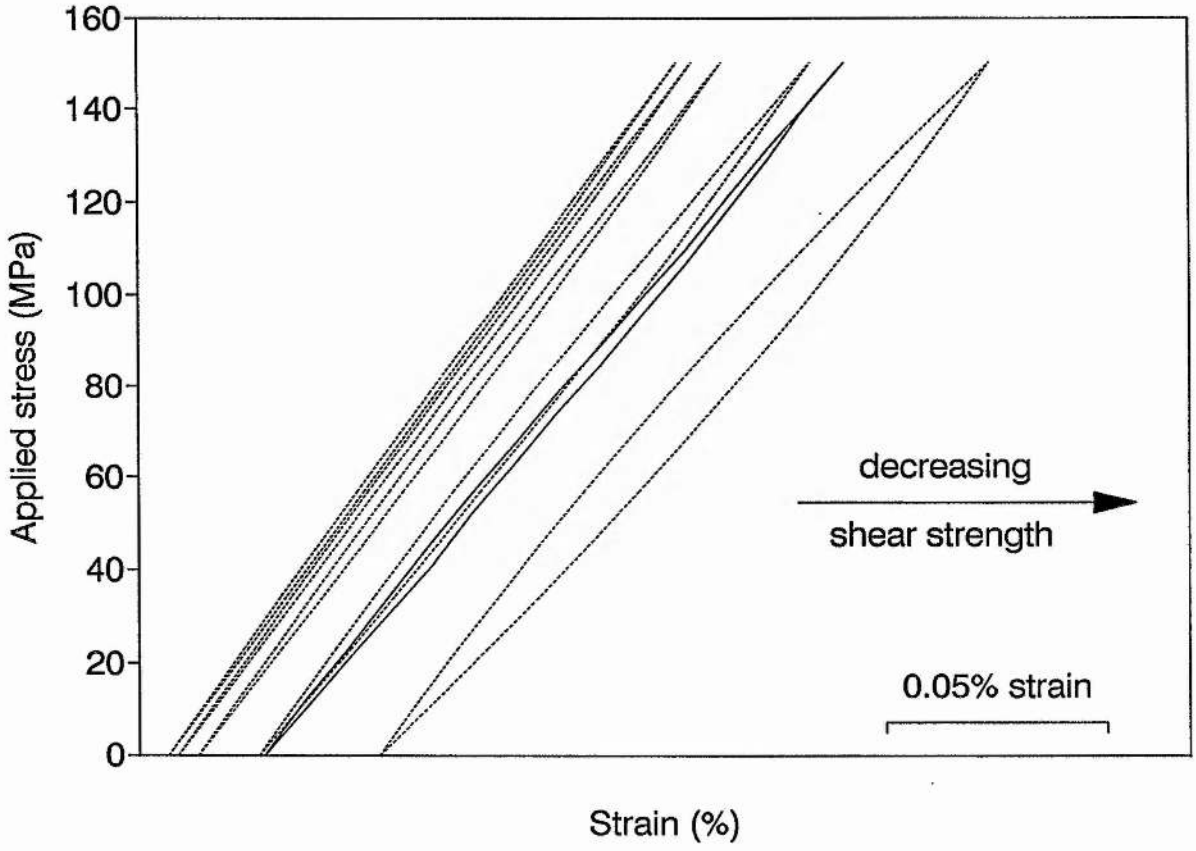

Figure 7.29 Experimental loading and unloading data for the specimen cycled to a maximum stress of 150 MPa (solid lines) compared with predictions using equations 6.15 and 6.17 for a constant value of -50 MPa for the initial thermal stress in the fibres and varying values of 8, 6, 4, 2, and 1 MPa for the interfacial shear strength (broken lines).

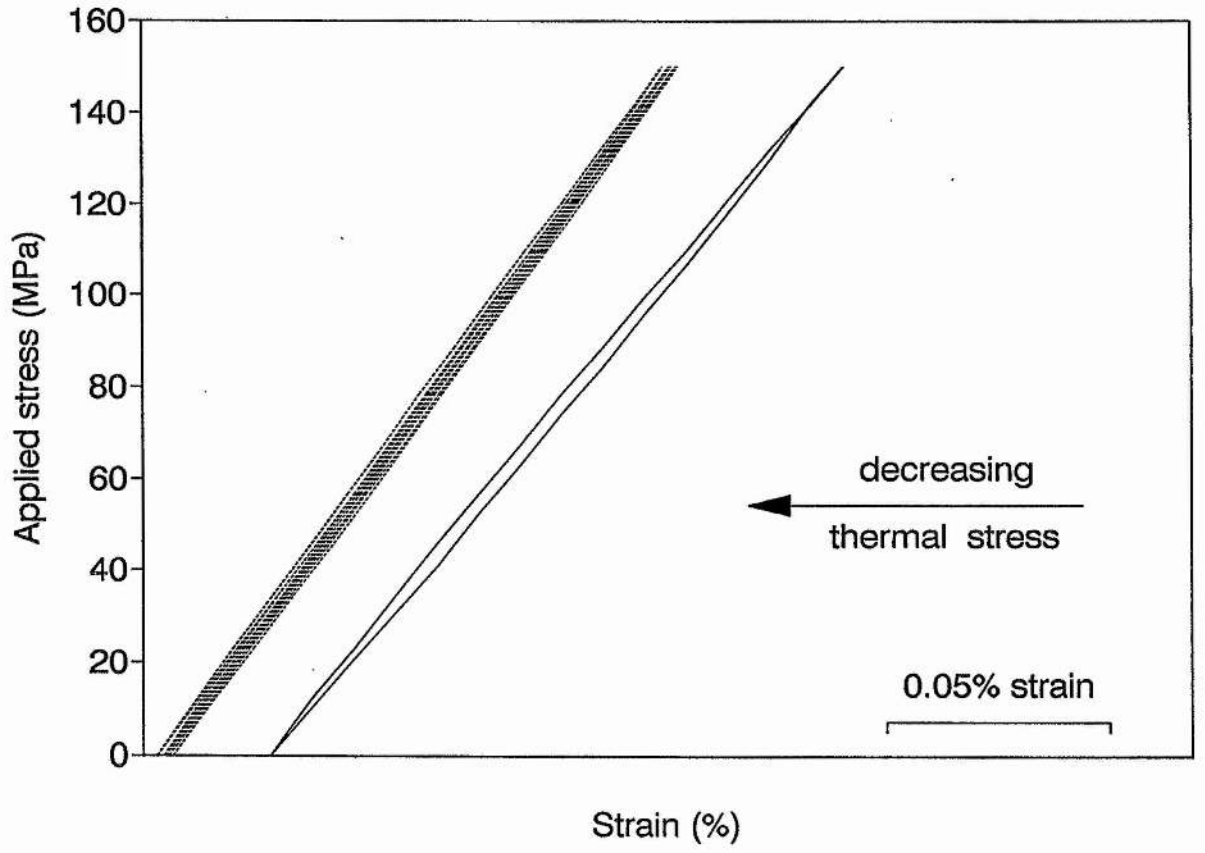

Figure 7.30 Experimental loading and unloading data for the specimen cycled to a maximum stress of 150 MPa (solid lines) compared with predictions using equations 6.15 and 6.17 for a constant interfacial shear strength of 8 MPa and varying values of -50, -40, -30, -20, and 0 MPa for the initial interfacial shear strength in the fibres (broken lines).

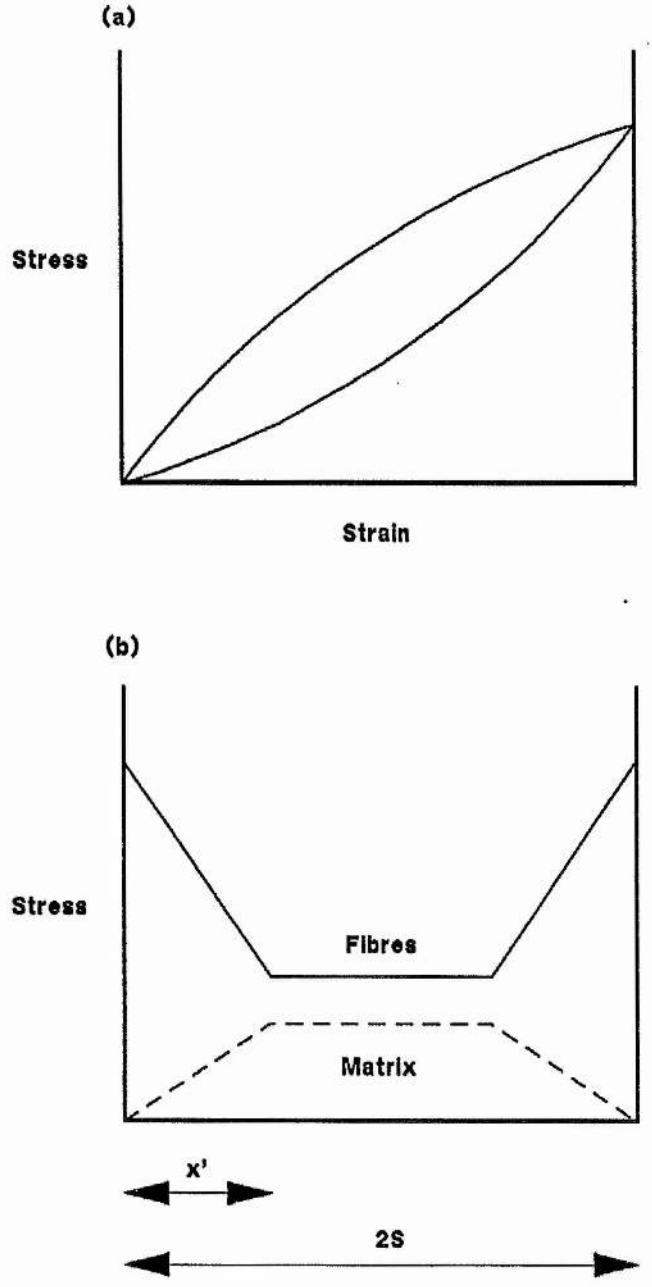

Figure 7.31 Specimen fatigued at a maximum stress such that $x' < s$

(a) stress/strain behaviour

(b) stress distribution in the fibres and matrix at peak stress.

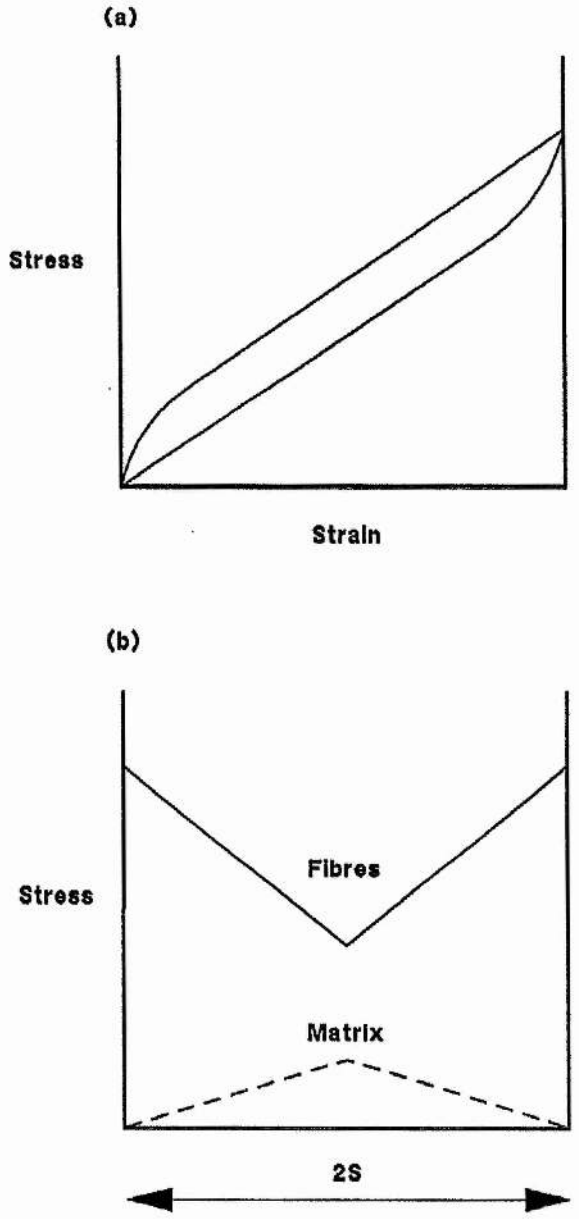

Figure 7.32 Specimen fatigued at a maximum stress such that $x' > s$

(a) stress/strain behaviour

(b) stress distribution in the fibres and matrix at peak stress.

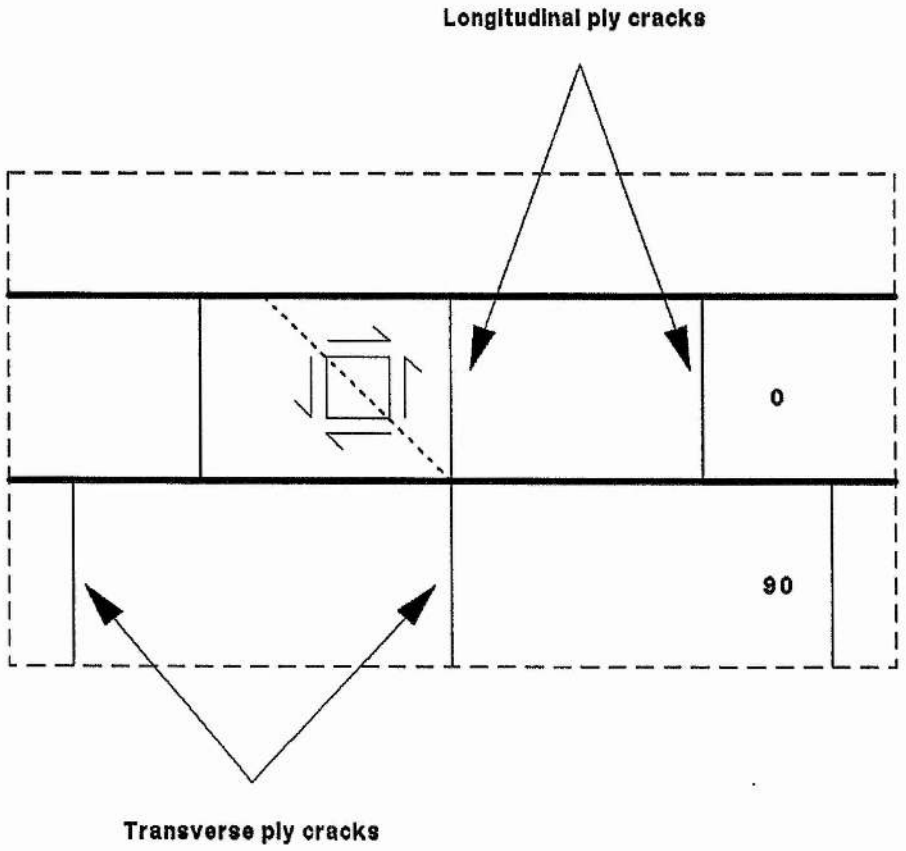

Figure 7.33 Schematic diagram of a crossply laminate showing the formation of longitudinal ply cracks oriented at an angle of 45° to the loading axis.

CHAPTER 8

CONCLUDING REMARKS

As indicated in the introduction of this thesis the development of ceramic matrix composite materials for use in engineering applications requires an understanding of the damage processes which occur during loading similar to that which exists for polymer matrix composites. The work presented here is an attempt to quantify matrix damage in Nicalon reinforced glass and glass ceramic matrix laminates under the simple loading modes of uniaxial quasi-static tension and tension/tension fatigue.

In Chapter 4 a number of Nicalon/Pyrex laminates of different lay-ups were examined and matrix damage quantified under quasi-static tension. Laminate stiffness properties are strongly influenced by the amount of matrix crystallisation which occurs during laminate processing due to the matrix microcracking around crystalline particles. Clearly, from a mechanical properties point of view, matrix crystallisation is undesirable in these laminates and processing conditions must therefore be tailored in order to prevent this.

The development of matrix damage was examined in Chapter 5 for unidirectional and crossply Nicalon/CAS laminates under quasi-static loading. For unidirectional laminates the ACK theory of multiple fracture is applied but is unable to describe accurately the accumulation of matrix cracks as a function of applied stress. This is because the data of the present work indicate that matrix cracks accumulate over a range of applied stress, corresponding to flaws of a different size propagating at different stresses. Fracture mechanics based models such as those proposed by Marshall and co-workers (1985) and McCartney (1987) are able to describe multiple fracture of the matrix over a range of applied stress. However, to apply these models a knowledge is required of the laminate toughness, size of individual flaws (perhaps, an impractical task given the size of the relevant flaws) and probably the local fibre geometry. The important feature of this work is that the control of initial flaw sizes will lead to a modification of the crack density as a function of applied stress. Elimination of the larger flaws will result in an improvement in the matrix cracking stress, the parameter likely to be the design limit for any practical CMC component.

In crossply Nicalon/CAS laminates distinct cracking thresholds are observed for the transverse and longitudinal plies under quasi-static loading. In both plies cracks

accumulate as a function of applied stress. A calculation of the critical flaw sizes indicate that cracking occurs in the transverse plies of $(0/90)_s$ and $(0_2/90_4)_s$ laminates in an unconstrained manner; slow crack growth across the ply width is not observed. The simple shear-lag analysis applied to predict progressive transverse ply cracking in both cases severely underestimates the laminate stress to produce a given crack density. If multiple cracking is to be modelled more accurately then not only does longitudinal ply cracking have to be accounted for (perhaps using the analysis of Chapter 6) but also, due to the unconstrained manner of crack propagation, the variability of the transverse ply strength. In polymer matrix composites the transverse ply strength has been described using a statistical (Weibull) distribution e.g. Fukanaga et al (1984). A similar approach could be adopted for the CMC crossply laminates considered here.

Using the crack density as a function of applied stress data (presented in Chapter 5) the stress/strain behaviour of unidirectional and (0/90) crossply Nicalon/CAS laminates is modelled in Chapter 6. For unidirectional laminates the stress analysis of Aveston et al (1971) is extended for continuous (accumulating damage) and discontinuous (constant damage) loading. The model describes the data using values of 8 MPa for the interfacial shear strength, τ, and 50 MPa (compression) for the initial thermal stress in the fibres, σ_f^T. The value of τ appears consistent with those measured by other, more direct methods such as fibre indentation. The initial thermal stress in the fibres is compressive in nature and is therefore consistent, though smaller in magnitude, to that calculated by considering the mismatch in fibre and matrix thermal expansion coefficients over the maximum possible temperature change (ceraming temperature to room temperature). Further study is required in order to identify the temperature at which elastic stresses begin to be generated which determine the initial laminate thermal stresses.

The model of Chapter 6 is useful in that the values of τ and σ_f^T are based on the analysis of bulk laminate stiffness properties where a uniform stress state in the fibres and matrix is a reasonable assumption. It is not clear whether this assumption is permissible for other, more direct techniques to measure τ such as fibre indentation methods. Further work is required to correlate the different techniques.

The continuous stress/strain behaviour of (0/90) crossply laminates is predicted with reasonable accuracy using a modified shear-lag analysis. The modification accounts for the damage occurring in the longitudinal plies by incorporating the unidirectional laminate analysis of Chapter 6 to describe the longitudinal ply modulus (and hence composite modulus) as a function of applied stress (and damage). However, the analysis does not include laminate thermal stresses. This is because of the extremely complex nature of the interaction between stress fields in the cracked longitudinal and transverse plies. Clearly, the model needs to be developed further.

A fundamental assumption of the models which predict stress/strain behaviour for both unidirectional and (0/90) crossply laminates is that the longitudinal fibres remain intact over the range of applied stress considered. This assumption is questionable at high stresses; the continuous stress/strain response for all laminates indicate that fibre breakages may occur (see Chapter 5). In order to describe accurately the stress/strain data over the entire stress range, i.e. up to laminate failure, a microstructural study is required in order to identify the fibre breakage threshold(s) and quantify fibre breakages as a function of applied stress.

The quasi-static cycling and high frequency fatigue of unidirectional and (0/90) crossply Nicalon/CAS laminates is examined in Chapter 7. The data indicate that quasi-static cycling or high frequency fatigue below the static cracking thresholds does not result in any matrix damage. As a result there is no loss in laminate stiffness properties.

In the case of unidirectional laminates, quasi-static cycling above the static matrix cracking threshold gives rise to stable stress/strain hysteresis loops which correspond to a stable matrix damage state. Slight increases in crack density are observed during high frequency fatigue as a result of the rapid propagation of a few cracks; slow crack growth is not observed. Stress/strain hysteresis loops recorded during high frequency fatigue are analyzed using the model proposed in Chapter 6. They indicate that high frequency fatigue has the effect of reducing the interfacial shear strength, possibly, by the wearing down of asperities at the fibre/matrix interface which inhibit the slippage process. Microstructural studies of the interface are required to elucidate these findings.

The increases in crack density with high frequency fatigue observed to occur in the transverse and longitudinal plies of (0/90) crossply laminates is explained in terms of the complex stress distribution between the cracked plies. However, the mechanisms responsible for these increases are only speculated upon, further, more specific studies must be carried out on fatigue crack growth behaviour in fibre reinforced ceramic matrix laminates.

LIST OF TABLES AND FIGURES

Chapter 1 page 4.

Chapter 2 pages 42 to 55.

Chapter 5 pages 111 to 137.

Chapter 7 pages 196 to 229.

Figure 7.31 Specimen fatigued at a maximum stress such that $x' < s$ (a) stress/strain behaviour (b) stress distribution in the fibres and matrix at peak stress.

Figure 7.32 Specimen fatigued at a maximum stress such that $x' > s$ (a) stress/strain behaviour (b) stress distribution in the fibres and matrix at peak stress.

Figure 7.33 Schematic diagram of a crossply laminate showing the formation of longitudinal ply cracks oriented at an angle of 45° to the loading axis.

REFERENCES

Agarwal, B. D. and Broutman, L. J. (1980). Analysis and Performance of Fibre Composites (John Wiley and Sons).

Aveston, J., Cooper, G. A. and Kelly, A. (1971). "Paper II - Single and multiple fracture". Conference proceedings of National Physical Laboratory (IPC Science and Technology Press Ltd), Guildford, Surrey. 15-26.

Aveston, J. and Kelly, A. (1973). "Theory of multiple fracture of fibrous composites". J. Comp. Mater. vol.8. 325-362.

Bacon, J. F. and Prewo, K. M. (1978). Proc. 2nd. Int. Conf. on Composite Materials, Toronto. 753-769.

Bader, M. G., Bailey, J. E., Curtis, P. T. and Parvizi, A. (1979). "The mechanisms of initiation and development of damage in multiaxial fibre reinforced plastics laminates". Proc. 3rd Int. Conf. on Mechanical Behaviour of Materials. vol.3. 227-239.

Bailey, J. E., Curtis, P. T. and Parvizi, A. (1979). "On transverse cracking and longitudinal splitting behaviour of glass and carbon fibre-reinforced epoxy crossply laminates and the effect of poisson and thermally generated strain". Proc. Roy. Soc. London A 366. 599-623.

Bailey, J. E. and Parvizi, A. (1981). "On fibre debonding effects and the mechanism of transverse-ply failure in crossply laminates of glass fibre/thermoset composites". J. Mater. Sci. vol.16. 649-659.

Batdorf, S. B. and Ghaffarian, R. (1982a). "Tensile strength of unidirectionally reinforced composites - Part I". J. Rein. Plas. Comp. vol.1. 153-164.

Batdorf, S. B. and Ghaffarian, R. (1982b). "Tensile strength of unidirectionally reinforced composites - Part II". J. Rein. Plas. Comp. vol.1. 165-175.

Bischoff, E., Rühle, M., Sbaizero, O. and Evans, A. G. (1989). "Microstructural studies on the interfacial zone of a SiC-fibre-reinforced lithium aluminium silicate glass ceramic". J. Am. Ceram. Soc. vol.72(2). 741-745.

Bleay, S. M. (1991). Private communication.

Bleay, S. M. and Scott, V. D. (1991). "Microstructure property relationship in Pyrex glass composites reinforced with Nicalon fibres". J. Mater. Sci. vol.26. 2229-2239.

Brennan, J. J. (1986). Tailoring of Multiphase and Ceramic Composites (Plenum Press, New York). 549-560.

Brennan, J. J. and Prewo, K. M. (1982). "Silicon carbide fibre-reinforced glass-ceramic matrix composites exhibiting high strength and toughness". J. Mater. Sci. vol.17. 2371-2383.

Budiansky, B., Hutchinson, J. W. and Evans, A. G. (1986). "Matrix fracture in fibre-reinforced ceramics". J. Mech. Phys. Solids. vol.34(2). 167-189.

Budiansky, B. and Amazigo, J. C. (1989). "Toughening by aligned frictionally constrained fibres". J. Mech. Phys. Solids. vol.37(1). 93-109.

Cao, H. C., Bischoff, E., Sbaizero, O., Rühle, M. and Evans, A. G. (1990). "The effect of interfaces on the mechanical performance of fibre reinforced brittle materials". J. Am. Ceram. Soc. vol.73(6). 1691-1699.

Caslini, M., Zanotti, C. and O'Brien, T. K. (1987). "Study of matrix cracking delamination in glass/epoxy laminates". J. Comps. Tech and Research. vol.9(4). 121-130.

Cooper, G. A. and Sillwood, J. M. (1972). "Multiple fracture in a steel reinforced epoxy resin composite". J. Mater. Sci. vol.7. 352-333.

Davidge, R. W. (1987). "Fibre reinforced ceramics". Composites. vol.18(2). 92-98.

Davidge, R. W. and Briggs, A. (1989). "The tensile failure of brittle matrix composites reinforced with unidirectional continuous fibres". J. Mater. Sci. vol.24. 2815-2819.

Dawson, D. M., Preston, R. F. and Purser, A. (1987). "Fabrication and materials evaluation of high performance aligned ceramic fibre-reinforced glass matrix composite". Ceram. Eng. Proc. vol.8. 815-821.

Dvorak, G. J. and Laws. N. (1987). "Analysis of progressive matrix cracking in composite laminates: II First ply failure". J. Comp. Mater. vol.21. 309-329.

Evans, A. G. (1980) "Fatigue in ceramics". Int. J. Fract. vol.16(6). 485-498.

Evans, A. G. and Marshall, D. B. (1989). "The mechanical behaviour of ceramic matrix composites". Acta Metall. vol.37. 1567-2583.

Evans, A. G. (1990). "Perspective on the development of high-toughness ceramics". J. Am. Ceram. Soc. vol.73(2). 187-206.

Ewart, L. and Suresh, S. (1987). "Crack propagation in ceramics under cyclic loads". J. Mater. Sci. vol.22. 1187-1192.

Fett, T., Martin, G., Munz, D. and Thun, G. (1991). "Determination of da/dN-ΔK_I curves for small cracks in alumina in alternating bending tests". J. Mater. Sci. vol.26. 3320-3328.

Flaggs, D. L. and Kural, M. H. (1982). "Experimental determination of in situ transverse lamina strength in graphite/epoxy laminates". J. Comp. Mater. vol.16. 103-116.

Ford, B., Cooke, R. G. and Newsam, S. (1987). "Failure mechanisms in silicon carbide fibre reinforced borosilicate glass". Proc. Brit. Ceram. vol.39. 229-234.

Fukanaga, H., Chou, T. W., Peters, P. W. M. and Schulte, K. (1984). "Probabilistic failure strength analyses of graphite/epoxy crossply laminates". J. Comp. Mater. vol.18. 339-356.

Garrett, K. W. and Bailey, J. E. (1977). "Multiple transverse fracture in 90° crossply laminates of a glass fibre-reinforced polyester". J. Mater. Sci. vol.12. 157-168.

Guiu, F., Reece, M. J. and Vaughan, D. A. J. (1991). "Cyclic fatigue of ceramics". J. Mater. Sci. vol.26. 3275-3286.

Habib, F. A., Cooke, R. G. and Harris, B. (1990). "Cracking in brittle matrix composites". Br. Ceram. Trans. J. vol.89. 115-124.

Hahn. H. T. and Tsai. S. W. (1974). "On the behaviour of composite laminates after initial failures". J. Comp. Mater. vol.8. 288-305.

Hahn, H. T. and Johannesson, T. (1983). "Fracture of unidirectional composites; theory and applications". "Mechanics of Composite Materials" ASME AMD. vol.58. 135-142.

Han. Y. M., Hahn, H. T. and Croman, R. B. (1988). "A simplified analysis of transverse ply cracking in crossply laminates". Comp. Sci and Tech. vol.31. 165-177.

Harrison, R. P. and Bader, M. G. (1981). "The micromechanics of carbon fibre composites damage initiation and development under quasi static and fatigue loading". Final report A93B/25. Surrey University.

Hertzberg, R. W. (1989). Deformation and fracture mechanics of engineering materials-third edition. (John Wiley and Sons).

Highsmith, A. L. and Reifsnider, K. L. (1982). "Stiffness reduction mechanisms in composite laminates". "Damage in Composite Materials" ASTM STP 775. 103-117.

Horibe, S. and Hirahara, R. (1991). "Cyclic fatigue of ceramic materials: Influence of crack path and fatigue mechanisms". Acta Metall. vol.39(6). 1309-1317.

Hull, D. (1988). An Introduction To Composite Materials (Cambridge Solid State Series), Cambridge University Press. 75-77.

Jeal, R. H. (1989). "Meeting the high temperature challenge - the non-metallic aero engine". Metals and Materials. vol.4(9). 539-542.

Jones, R. M. (1975). "Mechanics of composite materials". Scripta-McGraw Hill, Washington D.C.

Kerans, R. J., Hay, R. S. Pagano, N. J. and Parthasarathy, T. A. (1989). "The role of the fibre-matrix interface in ceramic composites". Ceram. Bull. vol.68(2). 429-442.

Kerans, R. J. and Parthasarathy, T. A. (1991). "Theoretical analysis of the fibre pull-out and push-out tests". J. Am. Ceram. Soc. (in press).

Kies, J. A. (1962). "Maximum strains in the resin of fibre-glass composites". US Naval Research Lab. Report 5752.

Kimber, A. C. and Keer, J. G. (1982). "On the theoretical average crack spacing in brittle matrix composites containing continuous aligned fibres". J. Mater. Sci. Lett. vol.1. 353-354.

Knott, J. F. (1973). Fundamentals of fracture mechanics, Butterworths.

Krohn, D. A. and Hasselman, D. P. H. (1972). "Static and cyclic fatigue behaviour of a polycrystalline alumina". J. Am. Ceram. Soc. vol.55(4). 208-211.

Laws, N. and Dvorak. G. J. (1988). "Progressive transverse ply cracking in composite laminates". J. Comp. Mater. vol.22. 900-916.

Lewis, V. D. (1983). Ceramic Engineering and Science Proceedings. vol.4. 9-10.

Levitt, S. R. (1973). "High-strength graphite fibre/lithium aluminosilicate composites". J. Comp. Mater. vol.8. 793-806.

Mah, T., Mendiratta, M. G., Katz, A. P., Ruh, R. and Mazdiyasni, K. S. (1985a). "Room temperature mechanical behaviour of fibre-reinforced ceramic-matrix composites". J. Am. Ceram. Soc. vol.68. C27-C30.

Mah, T., Mendiratta, M. G., Katz, A. P., Ruh, R. and Mazdiyasni, K. S. (1985b). "High temperature mechanical behaviour of fibre-reinforced glass-ceramic matrix composites". J. Am. Ceram. Soc. vol.68(9). C248-C251.

Manders, P. W., Chou, T. W., Jones, F. R. and Rock, J. W. (1983). "Statistical analysis of multiple fracture in 0°/90°/0° glass fibre/epoxy resin laminates". J. Mater. Sci. vol.18. 2876-2889.

Marshall, D. B. (1984). "An indentation method for measuring matrix-fibre frictional stresses in ceramic composites". Comm. Am. Ceram. Soc. December. c259-c260.

Marshall, D. B., Cox, B. N. and Evans, A. G. (1985). "The mechanics of matrix cracking in brittle matrix fibre composites". Acta. Metall. vol.33(11). 2013-2021.

Marshall, D. B. and Oliver, W. C. (1987). "Measurement of the interfacial mechanical properties in fibre-reinforced ceramic composites". J. Am. Ceram. Soc. vol.70(8). 452-548.

Masters, J. E. and Reifsnider, K. L. (1982). "An investigation of cumulative damage development in quasi-isotropic graphite/epoxy composites". Damage in Composite Materials' ASTM STP 775. 40-62.

McCartney, L. N. (1987). "Mechanics of matrix cracking in brittle matrix fibre-reinforced composites". Proc. Roy. Soc. London A 409. 329-350.

McMillan, P. W. (1979). Glass ceramics, Academic Press (London).

Minford, E. and Prewo, K. M. (1985). "Fatigue behaviour of silicon carbide fibre reinforced lithium-alumino-silicate glass ceramics". Proc 21st Univ Conf on Ceramic Science. 561-570.

Murty, V. S. R. and Lewis, M. H. (1989). "Interface structure and matrix crystallization in SiC (Nicalon)-Pyrex composites". J. Mater. Sci. Lett. vol.8. 571-572.

Nairn, J. A. (1989). "The strain energy release rate of composite microcracking: A variational approach". J. Comp. Mater. vol.23. 1107-1129.

Ogin. S. L., Smith, P. A. and Beaumont, P. W. R. (1984). "Transverse ply crack growth and associated stiffness reduction during the fatigue of a simple crossply laminate". Technical report CUED/C/MATS/TR105. Cambridge University Engineering Department.

Ogin, S. L. and Smith, P. A. (1985). "Fast fracture and fatigue growth of transverse ply cracks in composite laminates". Scripta Met. vol.19. 779-784.

Ogin, S. L. and Smith, P. A. (1987). "A model for matrix cracking in crossply laminates". ESA Journal. vol.11. 45-60.

Okamura, K. (1987). "Ceramic fibres from polymer precursors". Composites. vol.18(2). 107-120.

Parvizi, A. and Bailey, J. E. (1978). "On multiple transverse cracking in glass fibre epoxy crossply laminates". J. Mater. Sci. vol.13. 2131-2136.

Parvizi, A., Garrett, K. W. and Bailey, J. E. (1978). "Constrained cracking in glass fibre reinforced epoxy crossply laminates". J. Mater. Sci. vol.13. 195-201.

Peters, P. W. M. (1983). "The strength of 0/90 graphite-epoxy laminates with cracked 90° layers". Int. Conf. on Testing, Evaluation and Control of Composites, Surrey University.

Peters, P. W. N. (1984). "The strength distribution of 90° plies in 0/90/0 graphite-epoxy laminates". J. Comp. Mater. vol.18. 545-556.

Peters, P. W. M. and Chou, T. W. (1987). "On crossply cracking in glass and carbon-reinforced epoxy laminates". Composites. vol.18(1). 40-46.

Phillips, D. C., Sambell, R. A. J. and Bowen, D. H. (1972). "The mechanical properties of carbon fibre reinforced Pyrex glass". J. Mater. Sci. vol.7. 1454-1464.

Porter, D. L. and Heuer, A. H. (1979). "Microstructural development in MgO-partially stabilized zirconia (Mg-PSZ)". J. Am. Ceram. Soc. vol.62. 298-305.

Prewo, K. M. and Brennan, J. J. (1980). "High strength silicon carbide fibre-reinforced glass-matrix composites". J. Mater. Sci. vol.15. 463-468.

Prewo, K. M. and Brennan, J. J. (1982). "Silicon carbide yarn reinforced glass matrix composites". J. Mater. Sci. vol.17. 1201-1206.

Prewo, K. M. (1986). "Tension and flexural strength of silicon carbide fibre-reinforced glass ceramics". J. Mater. Sci. vol.21. 3590-3600.

Prewo,, K. M. (1987). "Fatigue and stress rupture of silicon carbide fibre-reinforced glass-ceramics". J. Mater. Sci. vol.22. 2695-2701.

Prewo, K. M., Johnson, B. and Starrett, S. (1989). "Silicon carbide fibre-reinforced glass-ceramic composite tensile behaviour at elevated temperature". J. Mater. Sci. vol.24. 1373-1379.

Reece, M. J., Guiu, F. and Sammur, M. F. R. (1989). "Cyclic fatigue crack propagation in alumina under direct tension-compression loading". J. Am. Ceram. Soc. vol.72(2). 348-352.

Reifsnider, K. L. and Stinchcomb, W. W. (1986). "A critical-element model of the strength and life of fatigue-loaded composite coupons". ASTM STP 907. 298-313.

Sambell, R. A. J., Briggs, A., Phillips, D. C. and Bowen, D. H. (1972a). "Carbon fibre composites with ceramic and glass matrices: Part I Discontinuous fibres". J. Mater. Sci. vol.7. 663-675.

Sambell, R. A. J., Briggs, A., Phillips, D. C. and Bowen, D. H. (1972b). "Carbon fibre composites with ceramic and glass matrices: Part II Continuous fibres". J. Mater. Sci. vol.7. 676-681.

Sbaizero, O. and Evans, A. G. (1986). "Tensile and shear properties of laminated ceramic matrix composites". J. Am. Ceram. Soc. vol.69. 481-486.

Seerat un Nabi, A. and Derby, B. (1988). "Mechanical properties of laminated Pyrex matrix composites". Proc 9th Risϕ Int. Symp. on Metallurgy and Materials Science. 463-468.

Shin, D. W. and Knowles, K. M. (1990). "Microstructure-property relationships in SiC fibre-reinforced borosilicate glass composites". Proc 4th Int. Conf. of the Institute of Mechanical Engineers, Liverpool. 163-168.

Simon, R. W. and Bunsell, A. R. (1984). "Mechanical and structural characterisation of the Nicalon silicon carbide fibre". J. Mater. Sci. vol.19. 3649-3657.

Smith, P. A. and Wood, J, R. (1990). "Poisson's ratio as a damage parameter in the static tensile loading of simple crossply laminates". Comp. Sci and Tech. vol.38. 85-93.

Steif, P. S. (1984). "Parabolic shear lag analysis of a $(0/90)_s$ laminate". Appendix to Ogin et al (1984).

Talreja, R. (1984) "Residual stiffness properties of cracked composite laminates". Proc 6th Int. Conf. on Fracture. vol.4. 3013-3020.

Talreja, R. (1985). "Transverse cracking and stiffness reduction in composite laminates". J. Comp. Mater. vol.19. 355-375.

Thompson, E. R. and Prewo, K. M. (1980). "Glass reinforced by graphite, silicon carbide and alumina fibres". Proc 21st Structures, Dynamics and Materials Conf. 539-543.

Thouless, M. D., Sbaizero, O., Sigl, L. S. and Evans, A. G. (1989). "Effect of interface mechanical properties on pullout in a SiC-fibre-reinforced lithium aluminium silicate glass-ceramic". J. Am. Ceram. Soc. vol.72(4). 525-532.

Wang, A. S. D. and Crossman, F. W. (1980). "Initiation and growth of transverse cracks and edge delamination in composite laminates: I An energy method". J. Comp. Mater. Supplement. vol.14. 71-87.

Wang, A. S. D., Chou, P. C. and Lei, S. C. (1984). "A stochastic model for the growth of matrix cracks in composite laminates". J. Comp. Mater. vol.18. 239-254.

Wang, A. S. D., Kishore, N. N. and Li, C. A. (1985). "Crack development in graphite-epoxy crossply laminates under uniaxial tension". Comp. Sci and Tech. vol.24. 1-31.

Wang, Y. R. and Chou, T. W. (1991). "Thermal shock resistance of laminated ceramic matrix composites". J. Mater. Sci. vol.26. 2961-2966.

Wiederhorn, S. M., Freiman, S. W., Fuller Jr, E. R. and Simmons, C. J. (1982). "Effects of water and other dielectrics on crack growth". J. Mater. Sci. vol.17. 3460-3478.

Yajima, S., Okamura, K., Hayashi, J. and Omori, M. (1976). "Synthesis of continuous SiC fibres with high tensile strength". J. Am. Ceram. Soc. vol.59. 324-327.

APPENDICES

APPENDIX 1 TECHNIQUE FOR THE PREPARATION OF COUPON EDGES.

1) GRINDING

BASE:	Struers 20μm metal bonded diamond disc
LUBRICATION:	Water
TIME:	Till plane
WEIGHT*:	2

OR

BASE:	Buehler Metlap 10
LUBRICATION:	Metadi 30μm slurry
TIME:	Till plane
WEIGHT:	2

2) INTERMEDIATE

BASE:	Metlap 4
LUBRICATION:	Metardi 6μm slurry
TIME:	20 minutes
WEIGHT:	2

BASE:	Metlap 2
LUBRICATION:	Metardi 6μm slurry
TIME;	10 minutes
WEIGHT:	2

3) POLISH

BASE:	Metlap 1
LUBRICATION:	Metardi 1μm slurry
TIME:	20 minutes
WEIGHT:	2

* weight refers to Struers Planopol 2 machine.

APPENDIX 2 IMAGE ANALYSIS ROUTINE FOR FIBRE VOLUME FRACTION AND FIBRE DIAMETER MEASUREMENTS

The routine printed below was written and run on a Cambridge Instruments Quantimet 970 image analysis routine using a Zeiss optical microscope.

The routine is noteworthy for the two "amend" statements (erode and invert skeleton) which separates touching fibres by one pixel and hence is able to make accurate fibre diameter measurements.

Example data are shown below for a Nicalon/CAS unidirectional laminate, giving the fibre area fraction in the matrix (c.f. volume fraction) and average fibre diameter for seventeen measurements.

```
Cambridge Instruments QUANTIMET 970 QUIPS/MX: V05.01MX    USER :
ROUTINE : ANDY2    DATE :                    RUN :   0   SPECIMEN :

        Scanner       ( No. 1 Newvicon AUTO-BRIGHTNESS  SENS= 1.22 PAUSE )
        Calibrate Microscope      (Calibration Value = 0.9010 microns      per pixel)
                                  (Optics Turret     = Transmitted)
                                  (Objective Lens Id.= x  8.0, Projection Lens Id.= x  2.0)
        CALL STANDARD
        For FIELD
        Binary Input A is DETECTED
        Binary Input B is DETECTED
        Binary Output goes to DETECTED
        Detect 2D     ( Lighter than  55  PAUSE )
        Edit (pause)
        Binary Output goes to TOUCH
        Amend         ( ERODE by   0 PAUSE )
        Binary Input A is TOUCH
        Amend         ( INVERSE SKELETON - Sub mode = None PAUSE )
        Edit (pause)
        Binary Output goes to DETECTED
        Image Transfer from A (AND) B to Binary Output
        Binary Input A is DETECTED
        Edit (pause)
        Measure field - Parameters into array FIELD
        Distribute FIELD.AREAFRACT vs FIELDNUM
             into GRAPH from     1.00 to    20.00, differential
        Measure feature      AREA           X.FCP          Y.FCP          LENGTH
                             BREADTH
            using  56 ferets
            into array FEATURE ( of 1000 features and   6 parameters )
        FEATURE   SHAPE      :=  ( LENGTH + BREADTH ) / 2.
        Distribution of COUNT v LENGTH (Units MICRONS   )
            from FEATURE in LENGTH from 7.000 to 24.00
             in  64 bins (LIN)
        Distribution of COUNT v SHAPE (Units MICRONS   )
            from FEATURE in SHAPE from 7.000 to 24.00
             in  64 bins (LIN)
        Pause
        Next FIELD
        Display Histogram GRAPH  (LIN) differential PAUSE
        Display Histogram LENGTH  (LIN) differential PAUSE
        Display Histogram SHAPE  (LIN) differential PAUSE
        END OF PROGRAM
```

Cambridge Instruments QUANTIMET 970 QUIPS/MX: V07.00 - USER :
ROUTINE : ANDY2 DATE : RUN : 17 SPECIMEN :

DISTRIBUTION OF FIELD AREAFRACT vs FIELDNUM

Total FIELD AREAFRACT = 3.09333 Mean = 0.344 Std Dev = 0.0381

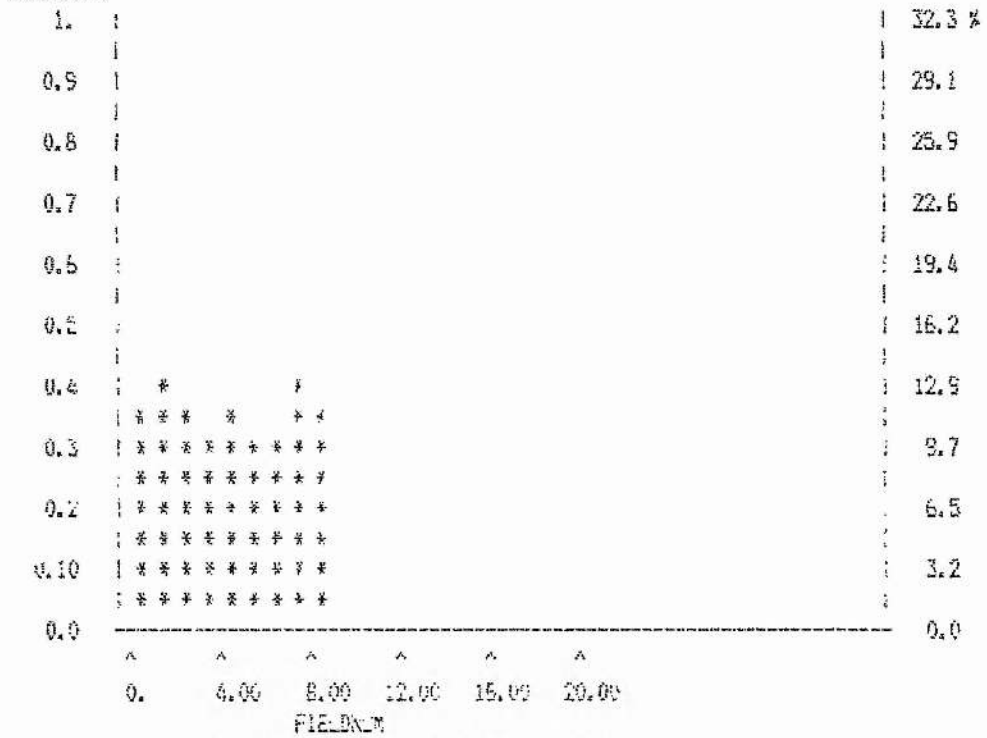

Cambridge Instruments QUANTIMET 970 QUIPS/MX: V07.00 - USER :
ROUTINE : ANDY2 DATE : RUN : 17 SPECIMEN :

DISTRIBUTION OF FIELD AREAFRACT vs FIELDNUM

Total FIELD AREAFRACT = 3.09333 Mean = 0.344 Std Dev = 0.0381

FIELDNUM LIMITS		AREAFRACT	
0. -	1.00	0.320313	!************
1.00 -	2.00	0.402302	!****************
2.00 -	3.00	0.358114	!**************
3.00 -	4.00	0.291823	!***********
4.00 -	5.00	0.329929	!************
5.00 -	6.00	0.321099	!************
6.00 -	7.00	0.315342	!************
7.00 -	8.00	0.335059	!**************
8.00 -	9.00	0.341281	!**************
9.00 -	10.00	0.	!
10.00 -	11.00	0.	!
11.00 -	12.00	0.	!
12.00 -	13.00	0.	!
13.00 -	14.00	0.	!
14.00 -	15.00	0.	!
15.00 -	16.00	0.	!
16.00 -	17.00	0.	!
17.00 -	18.00	0.	!
18.00 -	19.00	0.	!
19.00 -	20.00	0.	!

Cambridge Instruments QUANTIMET 570 QUIPS/MX: V07.00 - USER :
ROUTINE : ANDY2 DATE : RUN : 17 SPECIMEN :

DISTRIBUTION OF FEATURE COUNT vs LENGTH

Total FEATURE COUNT = 6770. Mean = 16.7 Std Dev = 2.61
Undersize Count = 59. Oversize Count = 135.

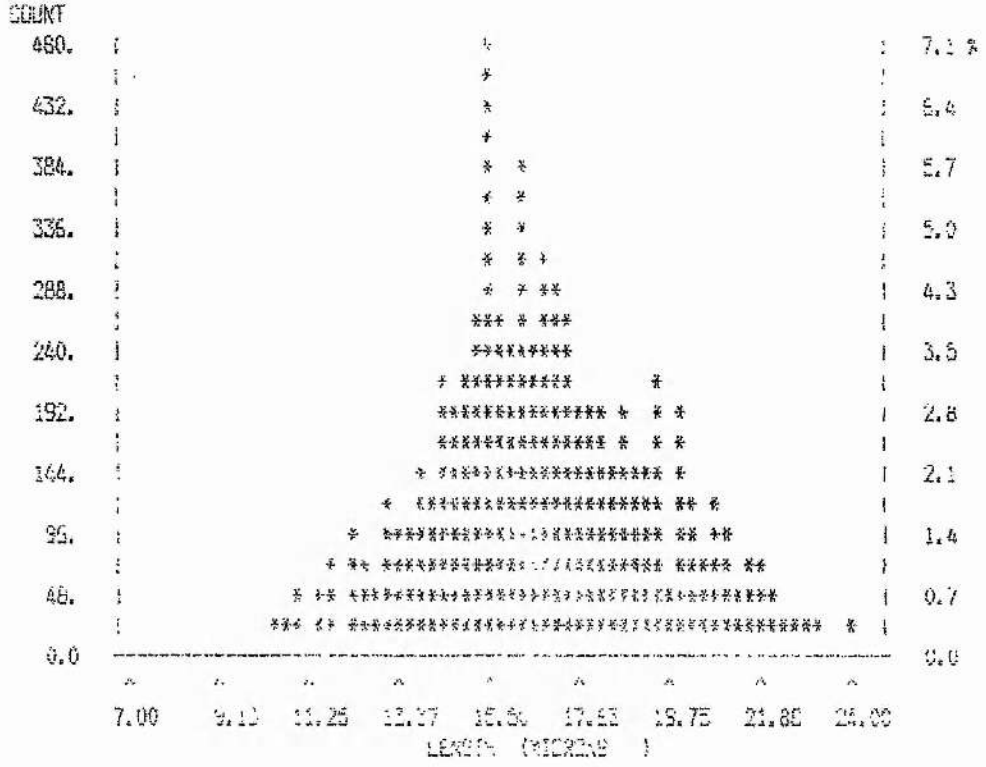

Cambridge Instruments QUANTIMET 970 QUIPS/MX: V07.00 - USER :
ROUTINE : ANDY2 DATE : RUN : 17 SPECIMEN :

DISTRIBUTION OF FEATURE COUNT vs LENGTH

Total FEATURE COUNT = 6770. Mean = 16.7 Std Dev = 2.61
Undersize Count = 59. Oversize Count = 135.

LENGTH (MICRONS) LIMITS		COUNT	
7.00 -	7.27	0.	:
7.27 -	7.53	0.	:
7.53 -	7.80	0.	:
7.80 -	8.06	0.	:
8.06 -	8.33	1.	:
8.33 -	8.59	0.	:
8.59 -	8.86	0.	:
8.86 -	9.13	0.	:
9.13 -	9.39	2.	:
9.39 -	9.66	1.	:
9.66 -	9.92	5.	:
9.92 -	10.19	2.	:
10.19 -	10.45	18.	:*
10.45 -	10.72	25.	:*
10.72 -	10.98	38.	:***
10.98 -	11.25	9.	:
11.25 -	11.52	55.	:****
11.52 -	11.78	66.	:*****
11.78 -	12.05	5.	:
12.05 -	12.31	107.	:********
12.31 -	12.58	74.	:*****
12.58 -	12.84	37.	:**
12.84 -	13.11	126.	:**********
13.11 -	13.37	87.	:******
13.37 -	13.64	90.	:*******
13.64 -	13.91	139.	:**********
13.91 -	14.17	119.	:*********
14.17 -	14.44	207.	:****************
14.44 -	14.70	194.	:***************
14.70 -	14.97	208.	:****************
14.97 -	15.23	254.	:********************
15.23 -	15.50	480.	:**************************************
15.50 -	15.77	260.	:********************
15.77 -	16.03	232.	:******************
16.03 -	16.30	392.	:******************************
16.30 -	16.56	236.	:******************
16.56 -	16.83	318.	:************************
16.83 -	17.09	296.	:**********************
17.09 -	17.36	268.	:********************
17.36 -	17.63	189.	:**************
17.63 -	17.89	200.	:***************
17.89 -	18.16	201.	:***************
18.16 -	18.42	144.	:**********
18.42 -	18.69	186.	:**************
18.69 -	18.95	151.	:**********
18.95 -	19.22	132.	:**********
19.22 -	19.48	224.	:*****************
19.48 -	19.75	55.	:****
19.75 -	20.02	194.	:***************
20.02 -	20.28	109.	:********
20.28 -	20.55	65.	:*****
20.55 -	20.81	108.	:********
20.81 -	21.08	87.	:*******
21.08 -	21.34	41.	:***
21.34 -	21.61	70.	:*****
21.61 -	21.88	62.	:****
21.88 -	22.14	40.	:***
22.14 -	22.41	34.	:**
22.41 -	22.67	29.	:**
22.67 -	22.94	26.	:**
22.94 -	23.20	33.	:**
23.20 -	23.47	7.	:
23.47 -	23.73	11.	:
23.73 -	24.00	21.	:*

APPENDIX 3 STRAIN ASSOCIATED WITH EXPOSED FIBRES BETWEEN MATRIX CRACKS IN UNIDIRECTIONAL LAMINATES

Figure A3.1 shows the stress distribution along the fibres from the mid point between two matrix cracks (B) to the mid point of the exposed fibres between the crack faces (A). The mean composite strain is obtained from Figure A3.1 by rewriting Equation 6.6 to include the contribution made by the exposed fibres. This gives

$$\bar{\epsilon} = \left(\frac{\Delta}{s+\Delta}\right)\frac{\sigma_c}{E_f V_f} + \left(\frac{x'}{s+\Delta}\right)\bar{\epsilon}_f + \left(1 - \frac{x'+\Delta}{s+\Delta}\right)\left(\epsilon_c + \frac{\sigma_f^T}{E_f}\right) \quad (A3.1)$$

where

2Δ = length of exposed fibres

The length of exposed fibres (the crack opening displacement or COD) over the distance between two cracks is given by the difference in the average fibre strain and the average matrix strain. This is

$$\frac{\Delta}{s} = \frac{x'}{s}\left[\frac{1}{2E_f}\left(\frac{\sigma_c}{V_f} + \sigma_c\frac{E_f}{E_c} + \sigma_f^T\right)\right] - \frac{1}{2E_m}\left(\sigma_c\frac{E_m}{E_c} + \sigma_m^T\right) \quad (A3.2)$$

Note that between a distance x' and s from the crack plane $\epsilon_f = \epsilon_m$. Substituting Equation 6.3 into Equation A3.2 gives

$$\Delta = \frac{r}{4\tau}\left[\sigma_c\frac{E_m V_m}{E_c V_f} - \sigma_f^T\right]\left[\frac{\sigma_c}{E_f V_f} + \frac{\sigma_f^T}{E_f} - \frac{\sigma_m^T}{E_m}\right] \quad (A3.3)$$

Using σ_c = 190 MPa (when $x' = s$) the mean composite strain can be calculated (for the values of interfacial shear strength and initial thermal stresses obtained in Section 6.1.2) and corresponds to the case where the contribution made by the exposed fibres is a maximum. Proceeding this way $\Delta = 20\mu m$ and by substitution into Equation A3.1 $\bar{\epsilon}$ can be determined. When compared with the value of $\bar{\epsilon}$ obtained from equation 6.6 an error of <1% is observed if the contribution to the mean composite strain by the exposed fibres is neglected.

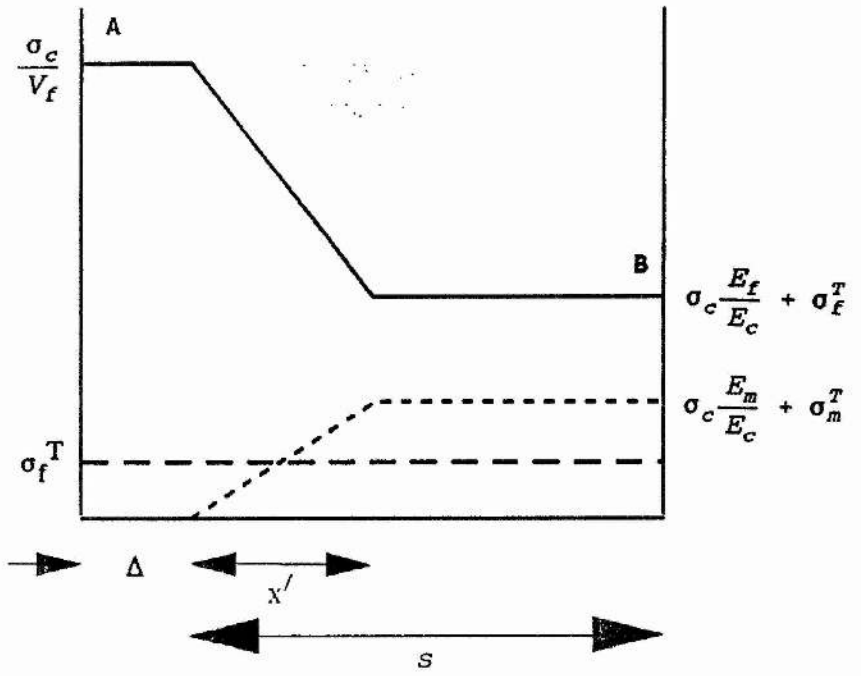

Figure A3.1. Stress profile in the fibres (solid line) and the matrix (dotted line) for a cracked unidirectional laminate at an applied stress of σ_c where σ_c>190 MPa.

APPENDIX 4 PUBLICATIONS

The following publications have been made during the course of this work.

Pryce, A. W., Hill, M. C. and Smith, P. A. (1990). "Damage development in glass matrix composite laminates". Proc 4th IMechE Int Conf (FRC'90 Fibre Reinforced Composites), Liverpool, U.K. 263-271.

Pryce, A. W. and Smith, P. A. (1991). "The behaviour of unidirectional and crossply ceramic matrix composites under quasi-static tensile loading". J. Mater. Sci. (in press).

Pryce, A. W. and Smith, P. A. (1991). "Modelling the stress/strain behaviour of unidirectional ceramic matrix composite laminates". Submitted to the Proc. Brit. Inst. Ceram.

Pryce, A. W. and Smith, P. A. (1991). "Matrix cracking in ceramic matrix composites under quasi-static tensile loading". Proc 8th Int Conf on Comp Mater. Hawaii. Section 22-29. 24A1-24A10.